Thermoplastic vulcanizates : the rubber particle size to control the properties-processing balance

Download date: 04. Oct. 2023

Thermoplastic vulcanizates

The rubber particle size to control the properties-processing balance

PROEFSCHRIFT

ter verkrijging van de graad van doctor aan de
Technische Universiteit Eindhoven, op gezag van de
Rector Magnificus, prof.dr.ir. C.J. van Duijn, voor een
commissie aangewezen door het College voor
Promoties in het openbaar te verdedigen
op dinsdag 21 april 2009 om 16.00 uur

door

Roy Martinus Adrianus l'Abee

geboren te Breda

Dit proefschrift is goedgekeurd door de promotor:

prof.dr. P.J. Lemstra

Copromotoren:
dr.ir. J.G.P. Goossens
en
dr.ir. M. van Duin

Table of contents

Thermoplastic vulcanizates

the rubber particle size to control the properties-processing balance

Summary

Thermoplastic vulcanizates (TPVs) are blends consisting of a large amount of cross-linked rubber particles dispersed in a thermoplastic matrix, which leads to a unique combination of elastic properties and melt (re)processability. Commercial TPVs are typically based on isotactic poly(propylene) (iPP) and ethylene-propylene-diene (EPDM) rubber and are prepared by dynamic vulcanization, where the rubber is selectively cross-linked during melt mixing with the thermoplastic. The increasing viscosity of the rubber phase during dynamic vulcanization affects the phase continuity by promoting phase inversion, which enables the cross-linked rubber to become the dispersed phase with dimensions in the μm-range. The dispersion of a large amount of cross-linked rubber into the thermoplastic matrix results in soft and highly elastic materials, while the continuous thermoplastic phase enables melt processability.

The main aim of the first part of this thesis was to obtain a more fundamental understanding of the influence of the rubber particle size on the mechanical and rheological properties of commercial iPP/EPDM-based TPVs. *In-situ* small-angle X-ray scattering (SAXS) measurements during tensile testing revealed that the deformation mechanism of the TPVs is dominated by yielding of the PP matrix. The formation of interlamellar voids, as occurs in unfilled PP during deformation, is more effectively suppressed with smaller rubber particles. Matrix crazing, internal rubber cavitation and particle/matrix debonding were not observed. The significant improvement of the tensile properties with decreasing rubber particle size ($\overline{D_n}$) is mainly attributed to the suppression of interlamellar void formation and subsequent coalescence of voids. Additionally, the chance of reaching the critical flaw size upon failure of a rubber particle decreases with $\overline{D_n}$. The decrease in $\overline{D_n}$ also leads to an enhancement of the elastic recovery, since the decrease in interparticle distance facilitates bending and buckling of the plastically deformed ligaments upon releasing the deformative stress. The decrease in interparticle distance and the increase in total surface area of the rubber phase upon decreasing $\overline{D_n}$ strengthens the physical network between the rubber particles in the melt, which leads to an increased viscosity upon decreasing $\overline{D_n}$. These results reveal the potential of TPVs with sub-μm rubber dispersions, since the rubber particle size can be used to control the properties-processing balance.

Since $\overline{D_n}$ of traditional iPP/EPDM-based TPVs prepared by dynamic vulcanization is limited to 1-3 μm, alternative approaches for the preparation of sub-μm were investigated, which are based on an increased compatibility between the thermoplastic and elastomer phases. The potential of highly compatible, yet immiscible thermoplastic/elastomer blends for the preparation of sub-μm TPVs was studied by dynamic vulcanization of copolymers of atactic polypropylene (aPP) and 5-ethylidene-2-norbornene (ENB) (aPP-*co*-ENB) in combination with iPP. The iPP/aPP-*co*-ENB blends show a very high compatibility, leading to a refinement of the morphology (both before and after dynamic vulcanization) in comparison to traditional blends based on iPP and EPDM. The aPP-*co*-ENB-based TPVs show improved tensile properties, but the relatively high glass transition temperature (T_g) of the rubber phase retards the elastic recovery after deformation at room temperature. Therefore, oil extension is required, since the oil decreases the T_g from 10 to -40 °C and significantly improves the elasticity of the TPVs. This study demonstrates the lower limit of the rubber particle size that is attainable via dynamic vulcanization of immiscible blends (~ 0.5 μm), since a further increase in blend compatibility would lead to initially miscible systems. Additionally, high rubber fractions of > 0.5 lead to larger rubber particles and to a (partially) co-continuous morphology due to incomplete phase inversion, which deteriorate the tensile and rheological properties.

The objective of the second part of this thesis was to explore the potential of reaction-induced phase separation (RIPS) as a new route for the preparation of sub-μm TPVs. The miscible systems that were studied are mainly based on poly(ε-caprolactone) and poly(ethylene) as the thermoplastic in combination with a low-molar-mass elastomer precursor containing epoxy or methacrylate end groups, which are all commercially available. Phase separation was induced by the increase in molar mass during selective cross-linking of the elastomer precursor, resulting in products with morphologies and properties typical for TPVs. This approach showed several advantages over the traditional dynamic vulcanization process of immiscible blends, the most important ones being (*i*) the small rubber particle size that is obtained (50 nm up to several μm's) over (*ii*) a very broad composition range (up to 80-90 wt% of cross-linked rubber was dispersed in the thermoplastic matrix) and (*iii*) the versatility of the approach. The latter is apparent from the different cross-linking mechanisms that can be applied (e.g. step-growth or chain-growth), the various elastomer precursors that can be chosen (fully amorphous or semi-crystalline, high/low T_g and high/low functionality) and the different thermoplastic/elastomer combinations that can be used (e.g. highly polar or apolar TPVs can be produced). It was shown that the occurrence of rubber particle connectivity, which originates from the interference of gelation of the elastomer precursor with the phase separation process under static cross-linking conditions, has a negative

influence on the tensile properties and the melt processability. Additionally, side reactions during *in-situ* cross-linking (e.g. grafting and/or cross-linking of the matrix) lead to changes in the crystallization behavior and the mechanical and rheological properties. These sub-µm TPVs showed an interesting combination of high hardness (Shore D range), good elasticity (compression set ranging from 10 to 40 %) and good tensile properties. Although it was shown that the viscosity of TPVs increases with decreasing $\overline{D_n}$, the absence of co-continuity in the sub-µm TPVs at high rubber contents leads to melt processable materials with viscosities similar to the commercially available iPP/EPDM-based TPVs. Additionally, oil extension enables a further optimization of the properties-processing balance.

Summarizing, the balance between the mechanical properties and the melt processability of TPVs strongly depends on the morphology, e.g. on the rubber particle size and the interparticle connectivity. The preparation of sub-µm TPVs via RIPS makes it possible to shift the properties-processing balance into areas that are not attainable with the currently available supra-µm TPVs.

Chapter 1

Introduction

1.1. (Thermoplastic) elastomers

Rubbers or, alternatively, elastomers are soft, flexible and highly elastic materials that are applied in a wide range of applications, such as tires, seals, tubes and gloves. Rubbers are composed of highly flexible, long chain molecules and have a glass transition temperature (T_g) below room temperature. Although *natural rubber* was already discovered as early as the 6th century B.C. by native Indians[1], the applications of rubber were limited because virgin rubbers are sticky, soluble and rather viscous materials with a low strength, since chain disentanglement readily occurs under stress, leading to viscous flow and permanent deformation[2,3]. The typical rubber properties as we know them from daily practice, such as elasticity, strength and solvent resistance, are only obtained after cross-linking, since this severely restricts the motion of the chain molecules. The invention of the sulfur-based cross-linking process (known as sulfur vulcanization) by Charles Goodyear in 1839 significantly extended the application area of natural rubber[1,4]. The spectacular expansion of the automotive industry in the beginning of the 20th century was the main driving force for the development of rubber technology. The shortage of natural rubber during the First and Second World Wars resulted in a major boost for the development of *synthetic rubbers*, such as poly(isoprene) rubber (IR), poly(butadiene) rubber (BR), styrene-butadiene rubber (SBR) and ethylene-propylene (EPM) rubber. Along with these advances in rubber technology came the industrial development of other cross-linking techniques, such as peroxide and phenolic curing[5], and of rubber additives, such as fillers (carbon black and minerals), plasticizers and stabilizers[1,2].

The formation of covalent cross-links between the chain molecules prevents melt (re)processing, which gives cross-linked rubbers a distinct disadvantage compared to thermoplastics. The relatively slow cross-linking process has to be performed when the rubber product is in its final shape, resulting in time-consuming and expensive multi-step processes. Additionally, simple recycling of scrap and waste material is not possible. In this respect, *thermoplastic elastomers* (TPEs) are an interesting class of materials, since they combine the good elastic properties of cross-linked rubbers with the melt (re)processability of thermoplastics[6-9]. TPEs can be classified as multiphase materials that consist of a rigid thermoplastic phase and a soft elastomer phase. Commercial TPEs are usually divided into two main classes, namely TPEs

based on block copolymers (either tri-block or multi-block copolymers) and TPEs based on polymer blends. Tri-block copolymers typically consist of a soft, flexible mid-block end-capped with two rigid end-blocks, such as poly(styrene)-poly(butadiene)-poly(styrene) (SBS). Multi-block copolymers are typically based on poly(esters), poly(amides) or poly(urethanes) as hard blocks and poly(ethers) as soft blocks. At service temperature, the rigid blocks cluster together to form small domains, which act as physical cross-links between the soft blocks, as is schematically shown for a tri-block copolymer in Fig. 1.1. Above the T_g or melting temperature (T_m) of the hard blocks, the physical cross-links disappear and the material becomes melt processable. This leads to materials with rubber-like properties at service temperature and (re)processability in the melt.

hard block   soft block
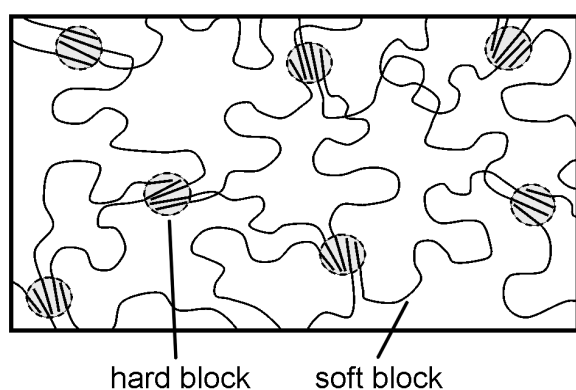
Fig. 1.1. Schematic representation of the morphology of a TPE based on a tri-block copolymer[8].

thermoplastic   elastomer
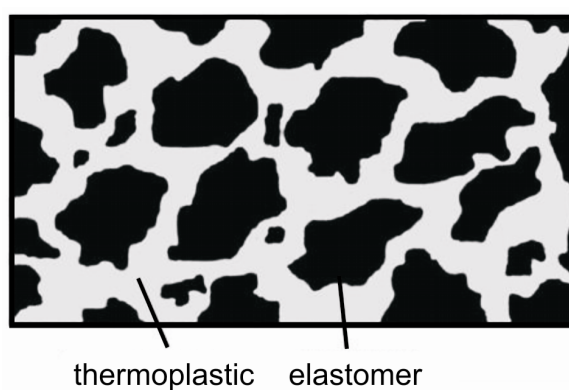
Fig. 1.2. Schematic representation of the morphology of a TPV.

TPEs based on heterogeneous polymer blends consist of a dispersion of elastomer particles in a semi-crystalline, thermoplastic matrix. *Thermoplastic polyolefins* (TPOs) typically contain a relatively small amount (< 40 wt%) of a non-cross-linked elastomer, which leads to materials with high toughness but a moderate elasticity and hardness. Commercial TPOs are mainly based on heterogeneous blends of poly(propylene) (PP) and EPM rubber. Since the elastomer phase is not cross-linked, the elastic properties of TPOs are inferior to those of cross-linked elastomers. However, the use of low-cost materials combined with the easy production process (simple melt blending or large-scale reactor blends) makes TPOs a suitable class of materials for many applications, especially in the automotive industry. Cross-linking of the elastomer phase leads to products known as *thermoplastic vulcanizates* (TPVs), which have superior elastic properties. Commercial TPVs typically consist of a large amount ($\geq$ 50 wt%) of cross-linked elastomer particles dispersed in a semi-crystalline thermoplastic matrix (Fig. 1.2). The dispersion of a large amount of cross-linked rubber into the thermoplastic matrix results in soft and highly elastic products, while the continuous thermoplastic phase enables melt processing[7-9]. Most commercial TPVs are based on heterogeneous blends of PP and ethylene-propylene-diene (EPDM) rubber

and are mainly applied in the automotive industry (tubing, sealing and airbag covers) and consumer applications (soft touch grips and wine corks).

Since the discovery of the elastic properties of plasticized PVC (which can be considered as a phase-separated, alternating block copolymer of crystalline syndiotactic blocks and soft atactic blocks) in 1926 [10], TPEs have gone through many academic and industrial developments, resulting in widespread applications. It was not until the 1960s, when poly(urethane) and styrene-butadiene-based block copolymers were developed, that TPEs became commercially attractive. Although TPEs as such, either based on block copolymers or blends, are relatively expensive, they are nowadays often applied as replacements for vulcanized rubbers. This replacement is largely driven by the cost-efficient, single-step fabrication process of finished parts via e.g. injection molding, extrusion or film blowing of ready-to-use TPE pellets. An additional cost-reduction of the products is achieved by compounding with large amounts of relatively cheap additives, such as oil and mineral fillers.

1.2. Production of TPVs

TPVs are produced by a process known as *dynamic vulcanization*, where the elastomer phase is selectively cross-linked during melt mixing with the thermoplastic. The morphology of immiscible polymer blends during melt mixing is mainly determined by the viscosity and composition ratio of the two blend components[11-13], as is schematically shown in Fig. 1.3. This basic model was slightly adjusted for TPVs[14, 15] and was used to qualitatively explain the morphology development of TPVs during the dynamic vulcanization process[16,17].
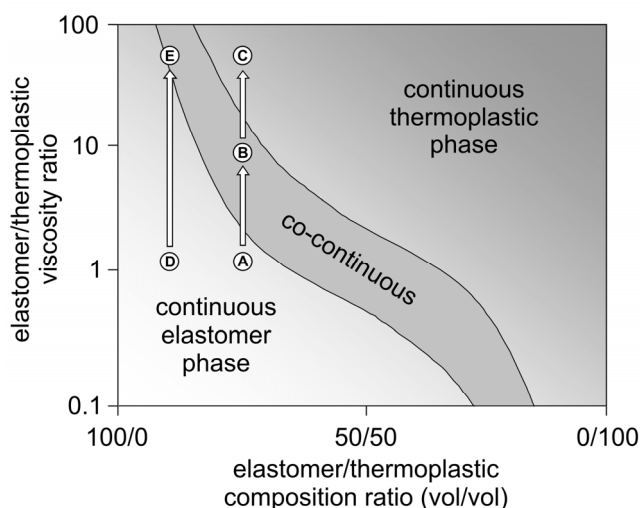
Fig. 1.3. Schematic representation of the morphology of elastomer/thermoplastic blends as a function of the composition and the viscosity ratio during melt blending.

At the starting situation, i.e. prior to cross-linking, the elastomer/thermoplastic ratio is high and the viscosity ratio is close to unity (A). It is assumed that the thermoplastic phase is fully molten and that the two immiscible phases have been mixed intimately. In this situation the

thermoplastic is dispersed in the elastomer matrix, since the component with the highest viscosity and/or the lowest volume fraction tends to be the dispersed phase[11,12]. Upon selective cross-linking of the elastomer phase, the viscosity ratio increases and the thermoplastic tends to become the continuous phase. Thus, cross-linking of the elastomer phase leads to a change in the morphology from a thermoplastic dispersion in an elastomer matrix (A) via a co-continuous morphology (B) to a dispersion of cross-linked elastomer particles in a thermoplastic matrix (C). This process is known as *phase inversion*, which enables the cross-linked elastomer to become the dispersed phase even when it is the majority phase. Fig. 1.3 shows that too high elastomer concentrations (D) will lead to incomplete phase inversion, which typically results in a co-continuous morphology (E) with inferior melt processability and tensile properties.

Although the general aspects of the morphology development during dynamic vulcanization are reasonably well understood, little is known about the actual kinetics of phase inversion as it occurs along the extruder axis. It was shown experimentally that phase inversion during dynamic vulcanization mainly occurs during the early stages of cross-linking and only takes place when the initial morphology is close to or in the co-continuous regime[17-21]. The influence of the compatibility of the blend components, i.e. the interfacial tension, on phase inversion of heterogeneous polymer blends is yet unclear. Some authors suggest a stabilization of the co-continuous morphology with decreasing interfacial tension and, thus, a broadening of the co-continuous regime[22], while others report a narrowing of the co-continuous regime[23-25] or only a minor influence of the interfacial tension on the phase inversion region[26,27].
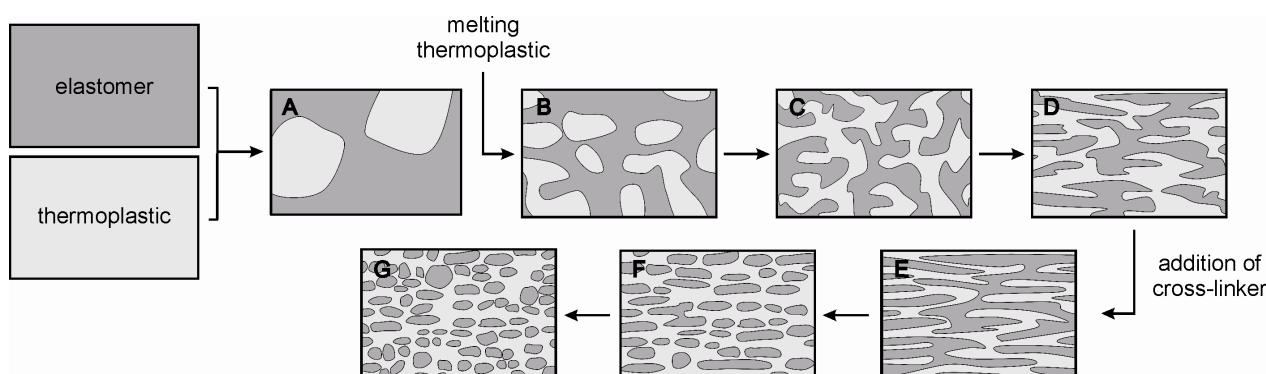
Fig. 1.4. Schematic representation of the morphology development during dynamic vulcanization of elastomer/thermoplastic blends.

Many studies have focused on the morphology of polymer blends during melt blending[11-13,23-27] and the influence of cross-linking on phase inversion[16-21]. Combining the results of these studies leads to the simplified representation of the morphology development during dynamic vulcanization as shown in Fig. 1.4. The early stage of the mixing process (A) is characterized by the presence of non-molten thermoplastic pellets that 'swim' in the elastomer matrix. After complete melting of the thermoplastic and intimate mixing of the two phases (B)

the morphology changes towards co-continuity (C). The combined shear and elongational forces that act on the viscous co-continuous phases during mixing deform the co-continuous morphology. This deformation leads to a refinement of the co-continuous strands, i.e. the strands become thinner but the co-continuity is preserved (D). Cross-linking leads to an increased viscosity of the elastomer phase, which results in a simultaneous increase in the shear and elongational forces acting on the system and, thus, to an increased deformation of the co-continuous structure (E). When a critical stress is achieved, the strands will break up into small particles, which results in a reduction of the stress and in a dispersion of cross-linked elastomer particles in a thermoplastic matrix (F). The dispersed elastomer phase will reach a final particle size (G) that depends on the deformation rate, the type of deformation, the composition, the viscosity (ratio) and the interfacial tension[28]. The final morphology of commercial TPVs usually consists of irregularly shaped elastomer particles with a broad size distribution and a rather heterogeneous distribution in space[7-9,17, 29]. For rubber-rich TPVs it is usually difficult to distinguish the separate particles, which is explained by the large volume content of the dispersed phase, microscopy artifacts (e.g. overlapping particles, lack of contrast and diffuse interfaces), actual interfacial contact and/or incomplete phase inversion.

1.3. Mechanical properties of TPVs

The most relevant mechanical properties of TPVs with respect to their applications are the elastic recovery and the tensile properties. The typical mechanical response of TPVs under tensile and compressive deformation will be discussed with the emphasis on the influence of the rubber particle size.

1.3.1. Elastic recovery

TPVs generally show a good elastic recovery after being subjected to a macroscopic deformation in either tension or compression. This elastic recovery is remarkable, since the matrix phase consists of a semi-crystalline thermoplastic polymer, which is expected to deform plastically via shear yielding. Thus, the question arises why the bulk properties of TPVs are not governed by the ductile character of the matrix but mostly by the elastic character of the dispersed phase. The physical origin of the elastic recovery of TPVs was first discussed by Kikuchi *et al.*[30,31], who modeled the deformation behavior of PP/EPDM-based TPVs under tensile conditions. They suggested that plastic deformation is concentrated in the thin PP ligaments in the equatorial region of the rubber particle. The ligaments in the direction perpendicular to the applied stress (polar region) remain below the yield stress, even at macroscopic strains of > 100 %. Since these undeformed ligaments maintain an equivalent stress

below the yield stress (i.e. within the elastic limit), they act as adhesion points between the rubber particles, thereby forming a pseudo-continuous elastic phase. The thicker parts of the matrix deform progressively at increasing overall strain and eventually the polar regions will also exceed the yield stress and will undergo plastic deformation as well. The validity of this two-dimensional model was later experimentally supported by combining infrared spectroscopy dichroism with tensile tests[32,33]. The importance of the presence of thin ligaments was illustrated by simulating the deformation behavior of TPVs in compression, where the elastic recovery increased significantly upon decreasing the ligament thickness[29,34]. Upon unloading, the micromechanical model predicts that the elastic forces of the stretched rubber particles pull back the highly plastically deformed thin ligaments via buckling and bending of the ligaments. Oderkerk et al.[35] convincingly showed the presence of buckled ligaments via microscopy studies on deformed TPVs based on poly(amide)-6 and anhydride-functionalized EPDM. Besides bending and buckling of the plastically deformed ligaments, the restoring forces that are exerted by the stretched rubber particles onto the deformed ligaments may be large enough to reach the yield stress in the ligaments, causing the ligaments to partially yield back to their original shape. The deformation and recovery mechanism of TPVs is schematically presented in Fig. 1.5, which shows (A) the undeformed state, (B) the deformed state at low macroscopic strain, (C) the deformed state at higher macroscopic strain and (D) the recovered morphology after releasing the stress. It is noted that, although the cross-linked rubber phase will show an almost instantaneous recovery after releasing the stress, deformation of the semi-crystalline matrix is governed by a viscoelastic component. Therefore, the experimentally determined value of the elastic recovery of TPVs, e.g. via tension set or compression set measurements, will show a significant dependence on both the deformation and recovery time and temperature.
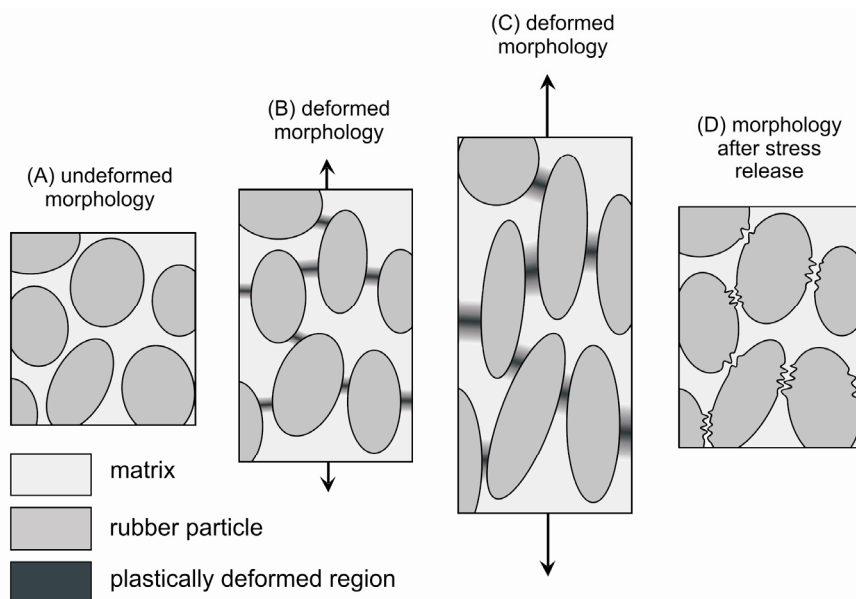
Fig. 1.5. Schematic representation of the deformation and recovery behavior of TPVs.

The final extent of permanent deformation depends on the ability of the stretched rubber particles to bend, buckle and/or yield the deformed matrix ligaments in order to recover the sample back to its original shape. As discussed, thinner matrix ligaments lead to a larger extent of elastic recovery, since lower restoring forces are required to bend, buckle and yield the ligaments after releasing the compressive stress. Since the matrix ligament thickness scales linearly with the rubber particle size at a constant volume content[36], an enhancement of the elastic recovery with decreasing rubber particle size is anticipated. However, no experimental studies on the effect of the rubber particle size on the elasticity of TPVs have been reported so far.

1.3.2. Tensile properties

The tensile properties of TPVs depend strongly on the blend composition, the cross-link density of the rubber phase, the state of the rubber dispersion and the rubber domain size[7]. The strong influence of the rubber particle size on the tensile properties was demonstrated by Coran *et al.*[37] and Araghi[38] for TPVs based on PP and EPDM. The variation in rubber particle size was accomplished by using pre-cross-linked EPDM milled to particles with different sizes[37] and by dynamic vulcanization of PP/EPDM blends at various screw speeds[38]. Both the elongation at break and the tensile strength increased by a factor of five upon decreasing the rubber particle size from 70 down to 1-2 μm (Fig. 1.6).
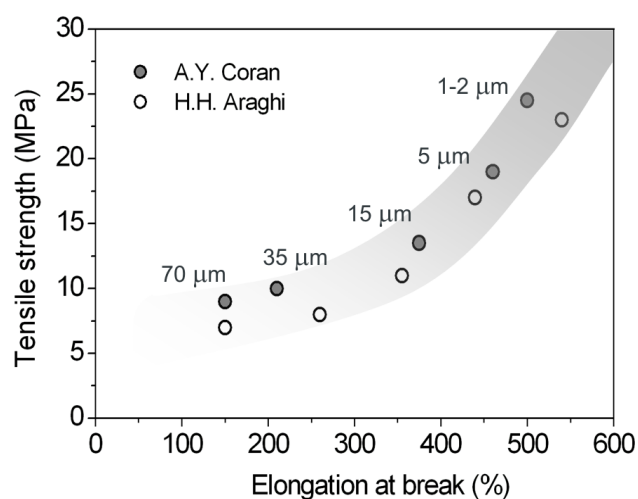
Fig. 1.6. Influence of rubber particle size on tensile strength and elongation at break of PP/EPDM-based TPVs containing 60 wt% EPDM. Redrawn from refs. 37 and 38.

Coran *et al.* attributed the improvement of the tensile properties to a decrease in the size of material flaws[37]. He thereby assumed that the rubber particles act as defects and initiate macroscopic failure of the sample. Araghi stated that the enhancement of the tensile properties originates from a more efficient control of craze development by the larger number of stress concentration points with decreasing particle size[38]. However, this is rather unlikely, since the

failure mechanism of PP under the applied conditions (room temperature and low strain rates) is known to be dominated by the ductile shear yielding mechanism rather than by crazing[39,40]. Although the data presented by Coran *et al.* and Araghi are convincing, no experimental evidence was provided to support their explanations of the particle size effect. Additionally, since the deformation behavior of TPVs has hardly been studied, the micromechanical deformation mechanisms of TPVs under tensile conditions are poorly understood.

1.4. Rubber particle size during melt blending

Based on the results presented by Coran *et al.*[37] and Araghi[38] it is envisioned that TPVs with sub-µm rubber dispersions have superior tensile properties. However, experimental studies on TPVs prepared via dynamic vulcanization showed that the lower limit of the rubber particle size is approximately 1-3 µm[7-9]. It has even been stated that the preparation of TPVs with smaller rubber particles via dynamic vulcanization is impossible[8]. The influence of various parameters on the rubber particle size during melt blending is discussed, first for polymer blends without cross-linking and subsequently for TPVs prepared by dynamic vulcanization.

1.4.1. Polymer blends

The particle size of the dispersed phase in polymers blends is determined by a complex interplay between the viscosity of the phases, the interfacial properties, the blend composition and the processing conditions. An elementary step in obtaining fine dispersions is the deformation and break-up of particles by the applied flow field during melt mixing[41]. Deformation of particles is promoted by the shear stress τ exerted on the particles by the flow field, but is counteracted by the concomitant increase in the interfacial area. The interfacial stress Γ/R (with Γ the interfacial tension and R the local radius) minimizes the interfacial energy, thus tending to a spherical shape. The ratio between these two stresses is called the capillary number Ca:

$$Ca = \frac{\tau R}{\Gamma} \tag{1.1}$$

If Ca exceeds the critical value Ca_{crit}, the shear stress overrules the interfacial stress, which leads to extension of the particle and finally to break-up into smaller particles. If $Ca < Ca_{crit}$, the shear stress applied to the particle is insufficient to overcome the interfacial stress, which leads to a slight deformation of the particle but not to break-up. The value of Ca_{crit} depends mostly on the type of shear flow and the particle-to-matrix viscosity ratio p. Generally, elongational flow is more efficient in particle break-up than simple shear flow, especially at high p[42]. Apart from the

deformation and break-up of coarse morphologies during mixing, a coarsening of the morphology may occur due to coalescence of the dispersed particles. The final morphology of a polymer blend will, therefore, be determined by the dynamic equilibrium between particle break-up and coalescence.

The potential of polymer melt blending to create sub-μm rubber dispersions in the absence of cross-linking can be estimated by relations based on the balance between particle break-up and coalescence. Although the interplay between particle break-up and coalescence during melt mixing complicates the prediction of particle sizes in concentrated polymer blends, several easily applicable models have been reported for (semi-)dilute systems[28,43]. These models are generally empirical in nature and relate the number-averaged dispersed particle size ($\overline{D_n}$) to p, Γ, the matrix viscosity (η_m) and the shear rate ($\dot{\gamma}$) via:

$$\overline{D_n} = \frac{k\,\Gamma(p)^n}{\eta_m \dot{\gamma}} \qquad (1.2)$$

The constants k and n increase with increasing volume fraction of the dispersed phase (ϕ_d), where Everaert *et al.*[43] reported $k = 1.2$ and $n = 0.45$ for very dilute blends ($\phi_d = 0.01$) and Wu[28] reported $k = 4.0$ and $n = 0.84$ for semi-dilute blends ($\phi_d = 0.15$). This relation covers the general trend of decreasing $\overline{D_n}$ with increasing η_m and $\dot{\gamma}$ and decreasing Γ and p. The increase in $\overline{D_n}$ that is typically observed with increasing ϕ_d[44] is covered by the scaling parameters k and n. Applying equation 1.2 at $\phi_d = 0.15$ to PP/EPDM blends with $\Gamma = 0.58$ mN/m[45-47], $p = 2.5$, $\eta_m = 300$ Pa·s and $\dot{\gamma} = 50$ s^{-1} as representative values leads to $\overline{D_n} = 0.33$ μm. Since ϕ_d is low in comparison to the typical values for TPVs ($\phi_d > 0.50$), the value of 0.33 μm can be interpreted as the lower limit of the attainable rubber particle size in the physical blend. To evaluate the relevance of this calculated particle size, a comparison has to be made with experimentally obtained values. The experimentally obtained $\overline{D_n}$ of PP/EPDM blends is generally found to be somewhat higher than the calculations, i.e. $\overline{D_n}$ in the order of 0.3 to 2.0 μm is typically obtained at $\phi_d = 0.10$ to 0.20[45,48-53]. Due to the increasing influence of coalescence on the blend morphology with increasing ϕ_d[54], an increase in $\overline{D_n}$ is generally observed with increasing ϕ_d up to the formation of a co-continuous morphology when ϕ_d approaches 0.50[46,52,53,55]. The relative variations in the experimentally obtained $\overline{D_n}$ increase with ϕ_d, which may be attributed to the increasing influence of the preparation conditions on the morphology[56].

Compatibilization of blends of dissimilar polymers is an efficient route to decrease the dispersed phase dimensions in traditional polymer blends, where particle dispersions as small as 50-100 nm were reported for highly incompatible polymer pairs after compatibilization[57-60]. Pre-formed block or graft copolymers are frequently used as compatibilizers. Several experimental

studies showed that the main role of the copolymers is not to decrease the interfacial tension, but to inhibit the coalescence of droplets in shear-induced collisions[44,61-64]. The lack of economically viable routes for their synthesis and the high probability of the formation of micelles[65] have limited the application of pre-formed compatibilizers. A good alternative is to generate the compatibilizer via a chemical reaction between suitable functionalized polymers at the interface during melt mixing, a process known as *in-situ* compatibilization or reactive blending.

1.4.2. Thermoplastic vulcanizates

The calculations and experimental studies indicate that the particle size of PP/EPDM blends with low EPDM contents ($\phi_d < 0.2$) is typically in the order of 1 μm and increases with the EPDM content. Whereas the balance between particle break-up and coalescence is determinative for the particle size in PP/EPDM blends, coalescence of the rubber particles is limited by cross-linking and the final morphology of TPVs is, therefore, mainly determined by the break-up process. Despite these different characteristics, the general trend for polymer blends as indicated by equation 1.2 is also applicable to TPVs, since it has been reported that $\overline{D_n}$ decreases with increasing η_m and $\dot{\gamma}$[38] and decreasing Γ[66,67] and p[68]. Additionally, the typical μm-sized rubber dispersions in PP/EPDM blends imply that the preparation of TPVs with rubber dispersions in the sub-μm range is not straightforward. Rubber particle sizes in the range of 1-3 μm are typically observed for TPVs and sub-μm rubber particles have indeed not been achieved so far[7-9]. This limited rubber particle size may be explained by the fact that further break-up of the μm-sized particles into smaller particles is suppressed at high viscosity ratios[42].

A significant particle size reduction of TPVs based on highly incompatible thermoplastic/rubber blends via compatibilization was reported by Radusch *et al.*[20,69]. However, the effectiveness of compatibilization in order to prepare TPVs with reduced rubber particle sizes is generally limited[27,70]. Several studies indicated that compatibilization of TPVs is only effective when the rubber is already the dispersed phase at the beginning of the dynamic vulcanization process, e.g. at high viscosity ratios and/or relatively low rubber contents[71,72]. As soon as phase inversion occurs, compatibilization hardly contributes to the refinement of the TPV morphology[73], which is due to the fact that break-up of the rubber particles rather than coalescence is the limiting factor for the minimum attainable rubber particle size.

1.5. TPVs prepared via reaction-induced phase separation

Since dynamic vulcanization of immiscible polymer blends leads to μm-sized rubber dispersions, an alternative approach to produce TPVs will be discussed in this thesis, which

potentially leads to sub-μm rubber dispersions over a broad composition range. This alternative approach is based on reaction-induced phase separation (RIPS) of initially miscible blends of a semi-crystalline thermoplastic in combination with a low-molar-mass elastomer precursor, where phase separation is induced by the increase in molar mass during the selective cross-linking of the elastomer precursor. The motivation to apply RIPS in order to obtain sub-μm morphologies is based on the fundamental difference between the changes in the morphological length scale during phase separation in comparison to dynamic vulcanization, as illustrated in Fig. 1.7. During dynamic vulcanization, the initial morphological length scale is in the order of mm's, e.g. during the stage where the partially molten thermoplastic pellets are mixed with the elastomer (Fig. 1.4A). During dynamic vulcanization, large shear and elongational forces in combination with selective cross-linking of the elastomer are required to decrease the morphological length scale down to the μm range (Fig. 1.4G). The development of the morphological length scale during RIPS is essentially different. The starting system is a blend that is miscible on the molecular scale and could therefore be described by a characteristic length scale in the order of Ångstroms. Selective cross-linking of the elastomer precursor induces phase separation, which starts at the nm scale and may eventually proceed into the μm regime. It is expected that large forces as applied during dynamic vulcanization and additional compatibilization of the system are no longer required to obtain fine rubber dispersions. The phase separation process is now determining the state of the rubber dispersion and the rubber particle size.

Fig. 1.7. Comparison of the morphological length scales involved during the preparation of TPVs via reaction-induced phase separation and dynamic vulcanization.

The RIPS process can be explained in more detail on the basis of Fig. 1.8, which shows the Upper Critical Solution Temperature (UCST) phase diagram of a binary mixture, where β represents the ratio between the molar mass of the elastomer phase and the thermoplastic phase. For polymer blends ($\beta = 100/100$) the miscibility gap is generally symmetric with the critical point, i.e. the point where the binodal and spinodal curves intersect, positioned at $\Phi \sim 0.5$. When a homogeneous solution prepared at (Φ_1,T_1) is thrust into the meta-stable, two-phase region by a drop in temperature from T_1 to T_2, the solution will phase separate via the nucleation and growth mechanism, typically leading to a dispersion of the minority component into a matrix of the majority component. A rapid decrease in temperature from T_1 to the unstable two-phase region at T_3 will lead to phase separation by the spinodal decomposition mechanism, typically leading to a co-continuous morphology during the early stages of phase separation, which may break up into a matrix-droplet morphology during the later stages of phase separation.
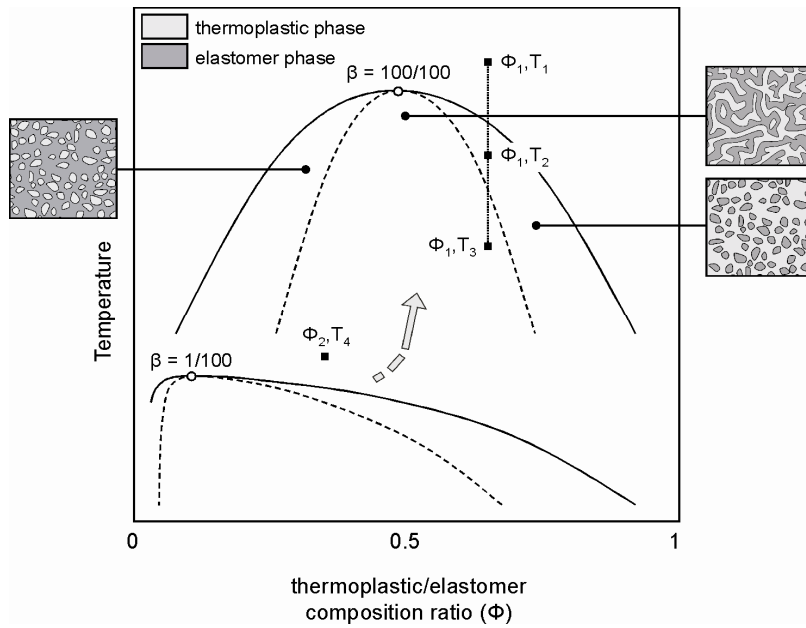
Fig. 1.8. Schematic representation of the phase diagram of thermoplastic/elastomer blends with β = 100/100 and 1/100. Solid and dashed lines represent binodal and spinodal conditions, respectively. Three typical morphologies are presented for the case of β = 100/100.

A decrease in the molar mass of the elastomer will increase the entropy gain upon mixing with the thermoplastic, leading to an enhanced miscibility. This is schematically shown in Fig. 1.8 for a decrease in β from 100/100 to 1/100, which leads to a shift of the miscibility gap towards lower T. Additionally, the difference in chain lengths between the two blend components causes the critical point and the phase boundaries to shift towards lower Φ. Accordingly, increasing the molar mass of the elastomer precursor, e.g. by polymerization and/or cross-linking, leads to a shift of the miscibility gap to higher T and Φ, indicated by the arrow in Fig. 1.8. Cross-linking of the elastomer precursor in the homogeneous thermoplastic/elastomer mixture at (Φ_2, T_4) will lead to phase separation into a (partially) cross-linked elastomer phase and a thermoplastic phase as soon as the phase boundaries have reached (Φ_2, T_4)[74]. A schematic representation of the morphology development during RIPS is shown in Fig. 1.9, which covers (A) melting of the thermoplastic, (B) the formation of a homogeneous mixture, (C,D) phase separation via
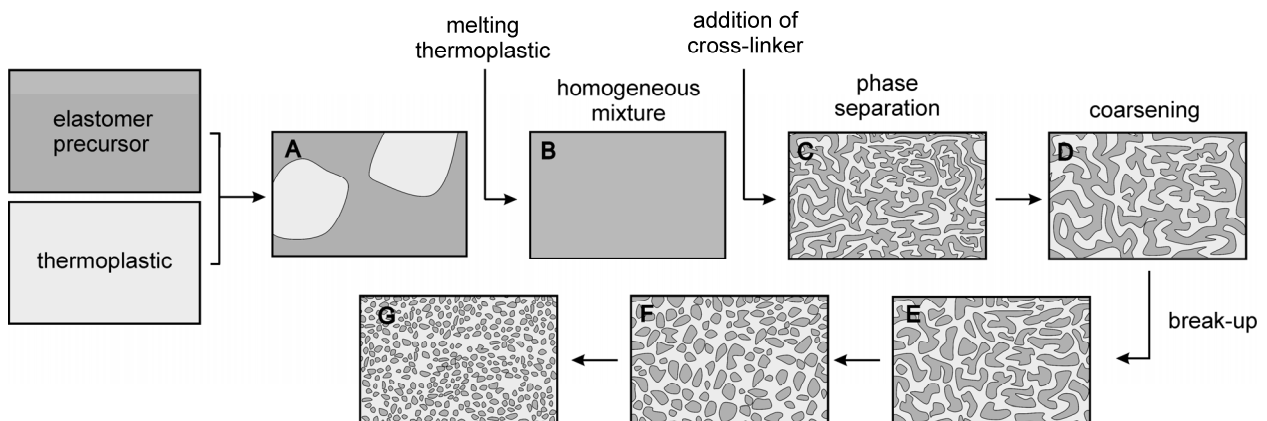
Fig. 1.9. Schematic representation of the morphology development during RIPS via spinodal decomposition.

spinodal decomposition as induced by cross-linking and (E-G) break-up of the co-continuous structure into a dispersion of cross-linked rubber particles.

Inoue et al.[75] showed that TPVs can be prepared by dynamic vulcanization of miscible blends based on poly(vinylidene fluoride) (PVDF) and acrylic rubber (ACM). Dynamic vulcanization led to a complex morphology of both supra-μm and a small number of nano-sized ACM particles in a PVDF matrix, where well-developed PVDF crystalline lamellae were visible in the supra-μm ACM particles. However, the application of RIPS based on polymer blends for the preparation of TPVs is restricted by the very limited number of thermoplastic/elastomer blends that are known to be miscible and the use of a low-molar-mass elastomer precursor is, therefore, preferred. Additionally, the concomitant shift of the critical point and phase boundaries towards higher elastomer contents suggests that the dispersion of larger amounts of cross-linked rubber in the thermoplastic matrix, without forming a co-continuous structure, is facilitated. Poly(ε-caprolactone) (PCL) is a semi-crystalline thermoplastic known to be miscible with many monomers and oligomers and is, therefore, a convenient polymer to study the preparation of sub-μm TPVs via RIPS. However, since PCL has a relatively low T_m of ~ 60 °C the temperature window for applications of the resulting TPVs is limited. In the final chapter of this thesis the thermoplastic component is changed to poly(ethylene) and syndiotactic poly(propylene), which have a higher T_m of ~ 130 °C.

1.6. Scope and outline of the thesis

Although fine rubber dispersions are generally aspired during the production of TPVs, the influence of the rubber particle size on the mechanical properties of TPVs is not well understood. The main objective of the first part of this thesis is, therefore, to study the influence of the rubber particle size of conventional PP/EPDM-based TPVs on the tensile properties and to obtain a more fundamental understanding of the primary deformation mechanism. Additionally, the work is extended towards other equally important properties, such as the elastic recovery and the melt processability. Based on the obtained results it is concluded that the rubber particle size is an important parameter to control the balance between properties and processing of TPVs. Since the preparation of sub-μm morphologies is not feasible for conventional PP/EPDM-based TPVs prepared by dynamic vulcanization, an alternative approach is used to prepare sub-μm TPVs. This approach is based on reaction-induced phase separation (RIPS) of initially miscible blends of a semi-crystalline thermoplastic and a low-molar-mass elastomer precursor. The (dis)advantages, limitations and versatility of RIPS for the preparation of TPVs are discussed for several miscible systems, based on the relation between the morphology, the chemical composition and the properties. In order to be able to relate the morphology to the mechanical

properties of TPVs, the relevant deformation mechanisms under compression and tensile conditions are discussed. The thesis is structured as follows:

In **Chapter 2** the influence of the rubber particle size on the mechanical and rheological properties and the deformation mechanisms under compressive and tensile deformation are discussed for conventional PP/EPDM-based TPVs.

In **Chapter 3** the lower limit of the rubber particle size as attainable via dynamic vulcanization of immiscible blends is investigated. Therefore, the EPDM rubber is replaced by an atactic poly(propylene) rubber functionalized with 5-ethylidene-2-norbornene (ENB) groups. The morphology and properties before and after dynamic vulcanization of these highly compatible, yet immiscible blends are discussed.

Chapter 4 describes the preparation of TPVs via RIPS based on miscible blends of poly(ε-caprolactone) (PCL) and bisepoxide-terminated poly(propylene oxide) (PPOn-epoxy), where triethylene tetramine (TETA) is used as the cross-linker. Based on the morphology and properties of statically and dynamically cured blends, it is demonstrated that TPVs can indeed be prepared by RIPS, although the rubber particle size remains in the range of 0.5 to 3.0 μm. **Chapter 5** provides a more detailed insight on the phase separation behavior of these blends and discusses structure-properties relations.

In **Chapter 6** the cross-linking mechanism is changed from the step-growth reaction of the epoxy/amine system to the chain-growth reaction of elastomer precursors based on difunctional methacrylates, leading to rubber particle sizes in the range of 80 to 900 nm. An overview is given on the morphology and the thermal, mechanical and rheological properties. **Chapter 7** provides a detailed study on the crystallization behavior of these systems.

Chapter 8 deals with RIPS of miscible mixtures based on polyolefins, alkyl methacrylates and divinylbenzene, which leads to TPVs with particle sizes in the range of 70 to 500 nm. These TPVs combine excellent tensile properties with a good elastic recovery and melt processability.

The **technology assessment** evaluates the influence of the rubber particle size on the properties-processing balance of TPVs and discusses the advantages and disadvantages of the newly developed approach for the preparation of TPVs. Finally, several considerations on the economical relevance and the possible scale-up of the approach are discussed.

1.7. References

[1] *Rubber: Natural and Synthetic*; Stern, H. J., Ed.; Palmerton Publishing Co.: New York, 1967.
[2] *Rubber Technology Handbook*; Hofmann, W., Ed.; Hanser Publishers: Munich, 1989.
[3] *Engineering with Rubber: How to Design Rubber Components*; Gent, A. N., Ed.; Hanser Publishers: Munich, 1992.

[4] Coran, A.Y. *J. Appl. Polym. Sci.* **2003**, *87*, 24-30.

[5] *Vulcanization of Elastomers*; Alliger, G.; Sjothun, I.J., Eds.; Reinhold Publishing Co.: New York, 1963.

[6] Radar, C.P. In *Basic Elastomer Technology*; Baranwal, K.C.; Stephens, H.L., Eds.; The Rubber Division, American Chemical Society: Akron, 2001.

[7] *Thermoplastic Elastomers: A Comprehensive Review*; Holden, G.; Legge, N.R.; Quirk, R.P., Eds.; Hanser Publishers: Munich, 1996.

[8] *Thermoplastic Elastomers*; Holden, G.; Kricheldorf, H.R.; Quirk, R.P., Eds.; Hanser Publishers: Munich, 2004.

[9] *Thermoplastic Elastomers from Rubber-Plastic Blends*; De, S.K.; Bhowmick, A.K., Eds.; Ellis Horwood: New York, 1990.

[10] Semon, W.L. US Patent 1,929,453 to B.F. Goodrich Co. (1933).

[11] Avgeropoulos, G.N.; Weissert, F.C.; Biddison, P.H.; Böhm, G.G.A. *Rubber Chem. Technol.* **1976**, *49*, 93-104.

[12] Jordhamo, G.M.; Manson, J.A.; Sperling, L.H. *Polym. Eng. Sci.* **1986**, *26*, 517-524.

[13] Utracki, L.A. *J. Rheol.* **1991**, *35*, 1615-1637.

[14] Paul, D.R.; Barlow, J.W. *J. Macromol. Sci., Rev. Macromol. Chem.* **1980**, *C18*, 109-168.

[15] Miles, I.S.; Zurek, A. *Polym. Eng. Sci.* **1988**, *28*, 796-805.

[16] Romanini, D.; Garagnani, E.; Marchetti, E. *New Polym. Mat., Proc. Int. Semin.* **1987**, 56-87.

[17] Machado, A.V.; van Duin, M. *Polymer* **2005**, *46*, 6575-6586.

[18] Goharpey, F.; Katbab, A. A.; Nazockdast, H. *J. Appl. Polym. Sci.* **2001**, *81*, 2531-2544.

[19] Abdou-Sabet, S; Patel, R.P. *Rubber Chem. Technol.* **1991**, *64*, 769-779.

[20] Radusch, H.-J. In *Micro- and Nanostructured Multiphase Polymer Blend Systems: Phase Morphology and Interfaces*; Harrats, C.; Thomas, S.; Groeninckx, G., Eds.; CRC Press: London, 2006.

[21] Radusch, H.-J.; Pham, T. *Kaut. Gummi Kunstst.* **1996**, *49*, 249-257.

[22] Veenstra, H.; van Lent, B.J.J.; van Dam, J.; de Boer, A.P. *Polymer* **1999**, *40*, 6661-6672.

[23] Dedecker, K.; Groeninckx, G. *Polymer* **1998**, *39*, 4985-4992.

[24] Bourry, D.; Favis, B.D. *J. Polym. Sci.: Part B: Polym. Phys.* **1998**, *36*, 1889-1899.

[25] Chuai, C.Z.; Almdal, K.; Lyngaae-Jørgensen, J. *Polymer* **2003**, *44*, 481-493.

[26] Hietaoja, P.T.; Holsti-Miettinen, R.M.; Seppälä, J.V.; Ikkala, O.T. *J. Appl. Polym. Sci.* **1994**, *54*, 1613-1623.

[27] Martin, P.; Maquet, C.; Legras, R.; Bailly, C.; Leemans, L.; van Gurp, M.; van Duin, M. *Polymer* **2004**, *45*, 5111-5125.

[28] Wu, S. *Polym. Eng. Sci.* **1987**, *27*, 335-343.

[29] Sabet, A.S.; Kear, K.E.; Boyce, M.C.; Shaw, K.D. US Patent 6,579,944 to Advanced Elastomer Systems LP (2003).

[30] Kikuchi, Y.; Fukui, T.; Okada, T.; Inoue, T. *Polym. Eng. Sci.* **1991**, *31*, 1029-1032.

[31] Kikuchi, Y.; Fukui, T.; Okada, T.; Inoue, T. *J. Appl. Polym. Sci.: Appl. Polym. Symp.* **1992**, *50*, 261-271.

[32] Huy, T.A.; Lüpke, T.; Radusch, H.-J. *J. Appl. Polym. Sci.* **2001**, *80*, 148-158.

[33] Oderkerk, J.; Groeninckx, G.; Soliman, M. *Macromolecules* **2002**, *35*, 3946-3954.

[34] Boyce, M.C.; Socrate, S.; Kear, K.; Yeh, O.; Shaw, K. *J. Mech. Phys. Solids* **2001**, *49*, 1323-1342.

[35] Oderkerk, J.; de Schaetzen, G.; Goderis, B.; Hellemans, L.; Groeninckx, G. *Macromolecules* **2002**, *35*, 6623-6629.

[36] Wu, S. *Polymer* **1985**, *26*, 1855-1863.

[37] Coran, A.Y.; Patel, R.P. *Rubber Chem. Technol.* **1980**, *53*, 141-150.

[38] Araghi, H.H. Proceedings of the International Rubber Conference, Birmingham, United Kingdom, 2001.

[39] Jang, B.Z.; Uhlmann, D.R.; Vander Sande, J.B. *J. Appl. Polym. Sci.* **1984**, *29*, 3409-3420.

[40] Gensler, R.; Plummer, C.J.G.; Grein, C.; Kausch, H.H. *Polymer* **2000**, *41*, 3809-3819.

[41] Janssen, J.M.H.; Meijer, H.E.H *Polym. Eng. Sci.* **1995**, *35*, 1766-1780.

[42] Grace, H.P. *Chem. Eng. Commun.* **1982**, *14*, 225-277.

[43] Everaert, V.; Aerts, L.; Groeninckx, G. *Polymer* **1999**, *40*, 6627-6644.

[44] Sundararaj, U.; Macosko, C.W. *Macromolecules* **1995**, *28*, 2647-2657.

[45] Shariat Panahi, H.; Nazokdast, H.; Dabir, B.; Sadaghiani, K.; Hemmati, M. *J. Appl. Polym. Sci.* **2002**, *86*, 3148-3159.

[46] Bhadane, P.A.; Champagne, M.F.; Huneault, M.A.; Tofan, F.; Favis, B.D. *Polymer* **2006**, *47*, 2760-2771.

[47] Hemmati, M.; Nazokdast, H.; Shariat Panahi, H. *J. Appl. Polym. Sci.* **2001**, *82*, 1129-1137.

[48] Karger-Kocsis, J.; Kalló, A.; Kuleznev, V.N. *Polymer* **1984**, *25*, 279-286.

[49] Pukánszky, B.; Fortelný, I.; Kovár, J.; Tüdõs, F. *Plast. Rubber Comp. Proc. Appl.* **1991**, *15*, 31-38.

[50] Jang, B.Z.; Uhlmann, D.R.; Vander Sande, J.B. *J. Appl. Polym. Sci.* **1985**, *30*, 2485-2504.

[51] Oksman, K.; Clemons, C. *J. Appl. Polym. Sci.* **1998**, *67*, 1503-1513.

[52] Van der Wal, A.; Gaymans, R.J. *Polymer* **1999**, *40*, 6045-6055.

[53] Jain, A.K.; Nagpal, A.K.; Singhal, R.; Gupta, N.K. *J. Appl. Polym. Sci.* **2000**, *78*, 2089-2103.

[54] González-Nuñez, R.; Arellano, M.; Moscoso, F.J.; González-Romero, V.M.; Favis, B.D. *Polymer* **2001**, *42*, 5485-5489.

[55] Feng, W.; Isayev, A.I. *Polymer* **2004**, *45*, 1207-1216.

[56] Hoppner, D.; Wendorff, J.H. *Colloid Polym. Sci.* **1990**, *268*, 500-512.

[57] Koning, C.; van Duin, M.; Pagnoulle, C.; Jerome, R. *Prog. Polym. Sci.* **1998**, *23*, 707-757.

[58] Teng, J.; Otaigbe, J.U.; Taylor, E.P. *Polym. Eng. Sci.* **2004**, *44*, 648-659.

[59] Tol, R.T.; Mathot, V.B.F.; Groeninckx, G. *Polymer* **2005**, *46*, 383-396.

[60] Madbouly, S.A.; Otaigbe, J.U. *Polymer* **2007**, *48*, 4097-4107.

[61] Macosko, C.W.; Guégan, P.; Khandpur, A.K.; Nakayama, A.; Marechal, P.; Inoue, T. *Macromolecules* **1996**, *29*, 5590-5598.

[62] Beck Tan, N.C.; Tai, S.-K.; Briber, R.M. *Polymer* **1996**, *37*, 3509-3519.

[63] Milner, S.T.; Xi, H. *J. Rheol.* **1996**, *40*, 663-687.

[64] Milner, S.T. *Mat. Res. Sci. Bull.* **1997**, *22*, 38-42.

[65] Fayt, R.; Jerome, R.; Teyssie, P. *J. Polym. Sci., Part C: Polym. Lett.* **1981**, *19*, 79-84.

[66] Coran, A.Y.; Patel, R.P. *Rubber Chem. Technol.* **1981**, *54*, 892-903.

[67] Coran, A.Y.; Patel, R.P. In *Reactive Modifiers for Polymers*; Al-Malaika, S., Ed.; Blackie Academic & Professional: London, 1997.

[68] Katbab, A.A.; Nazockdast, H.; Bazgir, S. *J. Appl. Polym. Sci.* **2000**, *75*, 1127-1137.

[69] Corley, B.; Radusch. H.-J. *J. Macromol. Sci., Part B: Phys.* **1998**, 37, 265-273.

[70] Huang, H.; Ikehara, T.; Nishi, T. *J. Appl. Polym. Sci.* **2003**, *90*, 1242-1248.

[71] Oderkerk, J.; Groeninckx, G. *Polymer* **2002**, *43*, 2219-2228.

[72] Moffett, A.J.; Dekkers, M.E.J. *Polym. Eng. Sci.* **1992**, *32*, 1-5.

[73] Naskar, K.; Noordermeer, J.W.M. *J. Appl. Polym. Sci.* **2006**, *100*, 3877-3888.

[74] Inoue, T. *Prog. Polym. Sci.* **1995**, *20*, 119-153.

[75] Li, Y.; Oono, Y.; Kadowaki, Y.; Inoue, T.; Nakayama, K.; Shimizu, H. *Macromolecules* **2006**, *39*, 4195-4201.

The influence of the rubber particle size on the tensile properties, elastic recovery and rheological behavior of thermoplastic vulcanizates

Thermoplastic vulcanizates (TPVs) based on isotactic poly(propylene) (PP) and ethylene-propylene-diene (EPDM) rubber with a constant rubber content and cross-link density and a variation in the number-averaged rubber particle size ($\overline{D_n}$) from 1 to 70 μm were prepared by dynamic vulcanization. Time-resolved small-angle X-ray scattering (SAXS) measurements during tensile testing revealed that the deformation mechanism of the TPVs is dominated by yielding of the PP matrix. The formation of interlamellar voids, as occurs in unfilled PP during deformation, is more effectively suppressed with smaller rubber particles. Matrix crazing, internal rubber cavitation and particle/matrix debonding were not observed during tensile testing. The significant improvement of the tensile properties with decreasing $\overline{D_n}$ is mainly attributed to the suppression of interlamellar void formation and subsequent coalescence of voids. Additionally, the decreasing probability of reaching the critical crack size upon internal fracture of the rubber particle may contribute to the enhanced tensile properties. The decrease in $\overline{D_n}$ also leads to an enhancement of the elastic recovery, since the decrease in interparticle distance facilitates bending and buckling of the plastically deformed ligaments upon releasing the deformative stress. The trends in tensile properties and elastic recovery are independent of the particle size distribution. The decrease in interparticle distance and the increase in total surface area of the rubber phase upon decreasing $\overline{D_n}$ strengthens the physical network between the rubber particles in the melt, which leads to an increase in the viscosity and the storage modulus with decreasing $\overline{D_n}$.

2.1. Introduction

Polymers are rarely used as such in practical applications. Instead, polymeric products usually consist of mixtures of several components, such as polymers, fillers, plasticizers and stabilizers. Blending two or more polymers is a convenient route to develop new polymeric materials, since synergy between the blend components can lead to materials with enhanced properties, especially in the case of phase-separated blends[1,2]. Many synergetic blends combine (semi-)ductile thermoplastics with soft elastomers, yielding rubber-toughened plastics (5-20 wt% rubber) or thermoplastic vulcanizates (TPVs; 40-80 wt% rubber). As described in Chapter 1, TPVs are produced by a process known as dynamic vulcanization, where the elastomer phase is selectively cross-linked during melt mixing with the thermoplastic[3,4]. The increasing viscosity of the elastomer phase upon cross-linking affects the phase continuity by promoting phase inversion, which enables the cross-linked elastomer to become the dispersed phase even when it is the majority phase. A too high rubber content and/or a too low elastomer/thermoplastic viscosity ratio (e.g. resulting from a low molar mass of the rubber or insufficient cross-linking) leads to incomplete phase inversion, which typically results in a co-continuous morphology with inferior properties. The dispersion of a large amount of cross-linked rubber into the thermoplastic matrix results in soft and elastic materials, while the continuous thermoplastic phase enables melt processing[3,4].

The material properties of polymer blends are the result of a complex interplay between the properties of the individual components and the blend morphology. Thermoplastic/rubber blends with a matrix-droplet morphology often show an enhancement of the mechanical properties upon decreasing the dimensions of the dispersed phase. The most prominent example of this size effect can be found in the area of rubber-toughening, where a reduction of the particle size typically leads to a significant increase in the impact toughness of the rubber/thermoplastic blend[5-9]. An improvement of the ultimate tensile properties of TPVs upon decreasing the rubber particle size has also been reported[10,11]. The deformation behavior of rubber-toughened polymers has been studied extensively over the past decades and the micromechanical deformation mechanisms responsible for rubber-toughening are relatively well understood. Although the structure-properties relationships of TPVs have hardly gained attention, the primary deformation mechanisms may be expected to resemble those of rubber-toughened polymers. Therefore, a short overview on the micromechanical deformation behavior of rubber-toughened polymers is presented here, after which the influence of the rubber particle size on the properties of TPVs is discussed.

The toughness of polymers is governed by a competition between plastic deformation and a terminal process leading to fracture. The key to obtain a tough macroscopic behavior is based on delocalization of the strain over the sample volume in such a way that the local stress levels do not exceed the critical values that will lead to brittle failure[12]. The precise mechanism responsible for the toughness enhancement largely depends on the properties of the thermoplastic matrix. For brittle polymers, for which crazing is the main local deformation mechanism, the rubber particles delocalize the deformation by acting as stress concentrators, thereby initiating a great number of small energy-absorbing crazes, which is known as the multiple crazing mechanism. Decreasing the rubber particle size at a constant rubber content leads to a more effective use of the rubber phase and an increased toughness, although it has been shown that rubber particles smaller than ~ 1 μm are not able to initiate crazes and, consequently, do not contribute to the toughness of the system[13-15].

For (semi-)ductile matrices, e.g. many semi-crystalline polymers, shear yielding is known to be the main local deformation mechanism. The most widely accepted toughening mechanism for rubber-modified, semi-crystalline polymers is based on the delocalization of the strain by internal cavitation of the rubber particles and the subsequent formation of shear bands[6,16]. The role of the rubber particles in the rubber-toughened polymer subjected to a triaxial (hydrostatic) stress is to cavitate internally or to debond from the matrix. This leads to a local release of the hydrostatic stress and the stress state in the ligaments between the rubber particles is converted from triaxial to uniaxial, thereby initiating shear yielding. Although the formation of cavities absorbs a small part of the applied deformation energy, the toughness enhancement is mainly achieved by the dissipation of energy through shear yielding[16, 17]. Internal cavitation of the particles is a prerequisite for toughness enhancement and becomes more difficult with decreasing rubber particle size[18-20] and with increasing shear modulus of the rubber (e.g. due to cross-linking)[18,21]. Decreasing the rubber particle size at a constant rubber content typically leads to an improvement of the toughness[22-25]. However, rubber particles smaller than approximately < 200 nm are not able to cavitate, since the build up of the hydrostatic stress inside the particle does not reach the energy that is required to create a new surface by cavitation[18,19,22] and, therefore, do not contribute to the toughness enhancement. The improved toughness of polyamide/rubber blends upon decreasing the rubber particle size was explained empirically by Wu[8]. He proposed that the particle-induced stress fields interact if the rubber particles are sufficiently close to each other. In other words, when the interparticle ligament thickness Λ is smaller than the critical ligament thickness Λ_c, matrix yielding is enhanced and, concomitantly, a significant improvement of the toughness is observed. Λ_c is often considered as an intrinsic property of the thermoplastic matrix,

independent of the size and the nature of the particles. Similar interparticle distance effects were later reported for a large variety of polymer/rubber combinations, with typical values for Λ_c of 0.3 μm for isotactic poly(propylene) (PP)[23-25], poly(amide)-6,6[8,26,27] and poly(butylene terephthalate) (PBT)[28], 0.6 μm for high-density poly(ethylene) (HDPE)[29] and 2.0 μm for poly(amide)-12[30]. The physical origin of Λ_c is still a subject of discussion. Muratoğlu et al.[26] attributed the absolute length scale of Λ_c to a layer of transcrystallized material with a reduced resistance to plastic flow surrounding the rubber particles, which is formed due to a nucleating effect of the rubber particles. However, this explanation is controversial[30], since the original study of Muratoğlu et al. is based on thin films[26] and the influence of the processing conditions on the crystalline organization was neglected. The conclusion of Muratoğlu et al. was invalidated by Corté et al.[30], who showed that the improved toughness originated from a strong lamellar orientation perpendicular to the flow direction as induced by the processing conditions. The oriented matrix has a lower shear yield stress due to the easy chain slippage in the direction perpendicular to the crystalline lamellae[31]. Re-crystallization of the samples led to the disappearance of a specific lamellar orientation and to a significant reduction of the toughness[30]. More recently, Corté and Leibler provided a fresh view on the toughening of semi-crystalline thermoplastics by means of a more general model[32]. Their reasoning starts with the work of Kuksenko and Tamusz[33], who showed that during deformation of semi-crystalline polymers, sub-μm-sized voids or cracks accumulate and coalesce in avalanche at a critical crack concentration, leading to brittle fracture. In order for toughening to be successful, matrix yielding around the rubber particles must bring sufficient confinement to shield interactions between the cracks formed in the elastic regions and to inhibit their coalescence[32]. Corté and Leibler stated that the critical confinement length depends on matrix properties (such as yield stress and stress at break), the cavitation process, the critical distance between cracks above which cracks will coalesce, and the rubber particle size.

As mentioned above, very few studies on the influence of the rubber particle size on TPV properties have been reported. Coran et al.[10] and Araghi[11] demonstrated that the tensile properties of TPVs based on PP and ethylene-propylene-diene (EPDM) rubber are strongly influenced by the rubber particle size. The variation in rubber particle size was accomplished by using pre-cross-linked EPDM, milled to particles with different sizes[10], and by dynamic vulcanization of PP/EPDM blends at various screw speeds[11], respectively. Both the elongation at break and the tensile strength increased by a factor of five upon decreasing the rubber particle size from 70 down to 1 μm. Coran et al. assumed that the rubber particles act as defects that initiate macroscopic failure of the sample and attributed the improvement to a decrease in the size of material flaws[10]. Araghi assumed that macroscopic failure of the TPVs is mainly determined by

the multiple crazing mechanism and stated that the enhancement of the tensile properties originates from a more efficient suppression of craze growth by the larger number of stress concentration points[11]. However, the failure of PP under the applied conditions (room temperature and low strain rates) is known to be dominated by the shear yielding mechanism[34,35].

Even though the experimental data presented by Coran *et al.*[10] and Araghi[11] are convincing, they should be interpreted with care for several reasons. Both studies do not discuss several important factors that are known to influence the tensile behavior of TPVs, such as the state of rubber dispersion. Coran *et al.* prepared 4 out of 5 TPVs by mixing pre-cross-linked EPDM particles into a PP matrix on a batch mixer. This is a very different approach than dynamic vulcanization, which was applied to prepare the fifth sample only. The origin of the significantly lower elastic modulus of the dynamically vulcanized sample (58 MPa) as compared to the other TPVs (97-105 MPa) was not discussed. Additional experimental details, such as the preparation conditions, the cross-link density and the elastic moduli of the TPVs, are missing in the study performed by Araghi. Unfortunately, both studies do not provide any additional experimental evidence to support the proposed deformation mechanisms. Additionally, the influence of the rubber particle size on the elasticity and the melt processability of the TPVs is not discussed. It is for these reasons that this chapter provides a more detailed study on the influence of the rubber particle size on the properties of PP/EPDM-based TPVs. Although commercial TPVs typically contain a large amount of extender oil to decrease the hardness, the viscosity and the material costs, the TPVs prepared in this study do not contain oil, since the addition of oil may affect the physicochemical phenomena that occur during dynamic vulcanization and, thus, may influence the structure and properties of the TPVs.

The variation in the rubber particle size, as determined by transmission electron microscopy (TEM) and optical microscopy (OM), is achieved by varying the shear rate during dynamic vulcanization on a batch mixer. At similar degrees of cross-linking, determined by selective solvent extraction and swelling experiments, the influence of the rubber particle size on the tensile behavior is correlated to the micromechanical deformation mechanism, which is studied by *in-situ* small-angle X-ray scattering experiments (SAXS) during tensile deformation. The influence of the particle size is not only studied for the tensile properties, but also for other equally important properties, such as the elastic recovery and the melt rheology. Finally, the influence of the rubber particle size distribution on the mechanical properties of the TPVs is discussed.

2.2. Experimental

2.2.1. Materials

PP (MFI = 2.0 g/10 min, ρ = 0.905 g/cm^3) was supplied by Sabic Europe (The Netherlands). 5-Ethylidene-2-norbornene-(ENB)-containing EPDM rubber (ENB content = 9 wt%, ethylene content = 48 wt%, ML(1+8) 150 °C = 60) was supplied by DSM Elastomers (The Netherlands). The phenolic-based anti-oxidant Irganox 1010 was supplied by Ciba Specialty Chemicals (Switzerland). The phenolic resin R7530 (resol; Arkema, France) and tin chloride dihydrate (SnCl$_2$·2H$_2$O; Evonik, Germany) were used as curatives. Fully amorphous atactic PP was synthesized in-house. Cyclohexane was obtained from Aldrich and used as received.

2.2.2. Blend preparation

TPVs were prepared by dynamic vulcanization of 50/50 wt/wt PP/EPDM blends without oil on a Haake Rheomix OS kneader equipped with Roller rotors. The total batch size was approximately 40 g and consisted of 100 parts per hundred rubber (phr) PP, 0.3 phr stabilizer, 1.5 phr SnCl$_2$·2H$_2$O and 3.0 phr resol. The details of the mixing sequences are shown in Fig. 2.1, including the temperatures (T$_1$ and T$_2$) and the rotor speeds (RS$_1$ and RS$_2$). Most of the TPVs were prepared by Method A, in which the initial rotor speed during blending of the various ingredients before cross-linking (RS$_1$) was varied. Several additional samples were prepared by Method B, in which a pre-mixed masterbatch of EPDM and SnCl$_2$·2H$_2$O was used and the rotor speed RS$_2$ was varied just before the addition of the EPDM/SnCl$_2$·2H$_2$O (100/1.5 phr) masterbatch. The EPDM/SnCl$_2$·2H$_2$O masterbatch was prepared by mixing the two components for 6 min at 80 rpm and 110 °C.
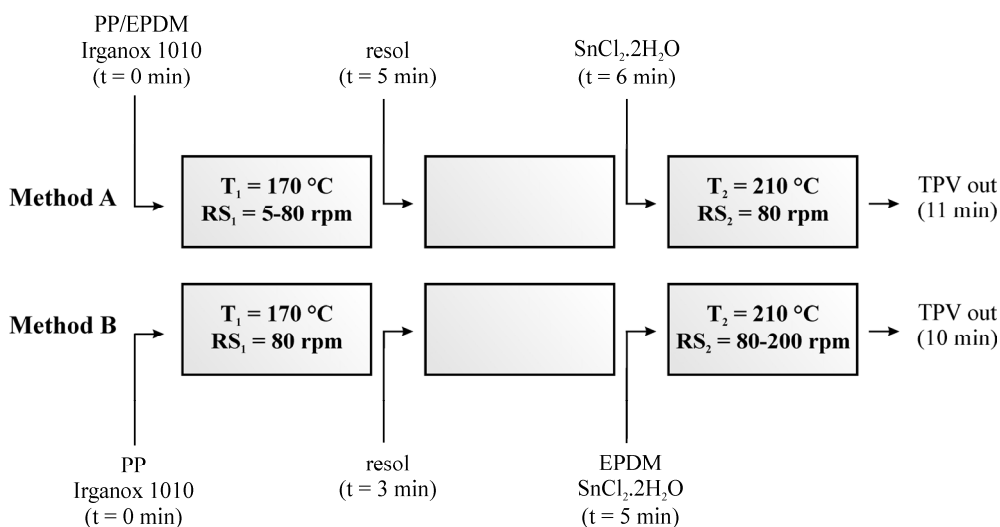
Fig. 2.1. Preparation conditions for TPVs.

2.2.3. Characterization techniques

Cross-link density. To determine the rubber gel content (*%gel*) and the degree of swelling (*%swell*), 1 mm thick compression-molded films of the TPVs were extracted and swollen in cyclohexane at room temperature for 48 hrs and were subsequently dried for 5 hrs at 100 °C under vacuum. The *%gel* and *%swell* are calculated by the following equations:

$$\%gel = \frac{m_{residue} - (m \times \phi_{insol})}{m \times \phi_{rubber}} \times 100\% \tag{2.1}$$

$$\%swell = \frac{m_{swollen} - (m \times \phi_{insol})}{m \times \phi_{rubber} \times (\%gel/100)} \times 100\% \tag{2.2}$$

where $m_{residue}$ is the weight of the dried sample after extraction, m is the weight of the sample before extraction, ϕ_{insol} is the mass fraction of insoluble components (e.g. PP and resol), ϕ_{rubber} is the mass fraction of rubber and $m_{swollen}$ is the weight of the swollen sample.

Transmission electron microscopy (TEM). Morphological investigations were performed with a Tecnai 20 transmission electron microscope operated at 200 kV. Samples were trimmed at -130 °C and subsequently vapour-stained for 30 min with a ruthenium tetroxide (RuO$_4$) solution prepared according to Montezinos *et al.*[36]. Ultrathin sections (70 nm) were obtained at -120 °C by using a Leica UltracutS/FCS microtome. The sections were placed on a 200 mesh copper grid with a carbon support layer. The rubber particle size and the particle size distribution were determined with the Image Pro Plus 4.5 software. The number-averaged diameter ($\overline{D_n}$), the volume-averaged diameter ($\overline{D_v}$) and the polydispersity index (*PDI*) were calculated according to:

$$\overline{D_n} = \frac{\sum_i n_i \overline{D_n}_i}{\sum_i n_i} \tag{2.3}$$

$$\overline{D_v} = \frac{\sum_i n_i \overline{D_n}_i^4}{\sum_i n_i \overline{D_n}_i^3} \tag{2.4}$$

$$PDI = \frac{\overline{D_v}}{\overline{D_n}} \tag{2.5}$$

The interparticle distance (*ID$_{mono}$*) was calculated from the relation proposed by Wu[9] for monodisperse, spherical particles:

$$ID_{mono} = \overline{D_n} \left[\left(\frac{k\pi}{6\phi} \right)^{1/3} - 1 \right] \tag{2.6}$$

where k is a geometric constant ($k = 2$ for body-centred cubic) and ϕ is the volume fraction of rubber. To account for the effect of a distribution of particle sizes, equation 2.6 was modified by Wu[9] to obtain:

$$ID_{poly} = \overline{D_n} \left[\left(\frac{k\pi}{6\phi} \right)^{1/3} - 1 \right] e^{(\ln^2 \sigma)} \tag{2.7}$$

where the particle size distribution parameter (σ) can be calculated by the log-normal distribution[37]:

$$\ln \sigma = \sqrt{\frac{\sum_{i=1}^{N} n_i \left(\ln \overline{D_{n\,i}} - \ln \overline{D_n} \right)^2}{\sum_{i=1}^{N} n_i}} \qquad (2.8)$$

For a monodisperse particle size distribution, σ is equal to 1, while for polydispersity, σ is larger than 1.

Optical microscopy (OM). For the coarser TPV morphologies, optical microscopy under crossed polarizers on a Zeiss Axioplan 2 microscope equipped with a Zeiss Axiocam camera was used to study the morphology. Thin sections (5-10 μm) were obtained at -100 °C by using a Leica RM2165 microtome and were sandwiched between two thin glass slides. The images were analyzed with the accompanying AxioVision v3.0.6 software and the particle size (distribution) was calculated as previously described.

Wide-angle X-ray diffraction (WAXD) and small-angle X-ray scattering (SAXS). WAXD measurements and time-resolved SAXS measurements during tensile testing were performed at the Dutch-Belgian (DUBBLE) beamline BM26 of the European Synchrotron Radiation Facility (ESRF) in Grenoble, France. The size of the X-ray beam was approximately 200 x 200 μm^2 with a wavelength of 1.203 Å. For the WAXD measurements a FRELON detector was used with 2048 x 2048 pixels and a pixel size of 97.6 x 97.6 μm^2 at a sample-detector distance of 70.34 mm. For the SAXS measurements a 2D multiwire gas-filled detector was used with 512 x 512 pixels and a pixel size of 260 x 260 μm^2 at a sample-detector distance of 3200 mm.

Tensile testing. Films with a thickness of 1 mm were compression molded at 180 °C and 100 bar from which dumbbell-shaped tensile bars (15 x 5 x 1 mm) were punched. Tensile tests were performed at a cross-head speed of 20 mm/min using a 10 kN force cell on a Zwick Z010 tensile tester according to ASTM D412[38]. The equipment was controlled with the TestXpert v7.11 software. Each sample was tested in at least 7-fold and average values are presented.

Compression set. The compression set (*CS*) was measured on cylindrical samples with a diameter of 13 mm and a thickness of 6 mm at 25% compressive deformation for 22 hrs and a relaxation time of 30 min (all at room temperature), according to ASTM D395[39]. The *CS* was calculated as follows:

$$CS = \frac{(t_i - t_o)}{(t_i - t_n)} \times 100\% \qquad (2.9)$$

where t_i is the initial thickness of the sample, t_o the final thickness of the sample and t_n the thickness of the spacer. The relative standard deviation in *CS* is 1-2%.

Rheological measurements. Dynamic shear measurements were performed on a strain-controlled AR-G2 rheometer (TA Instruments) by using a 8 mm parallel-plate geometry and disk-shaped specimens (8 mm diameter; 0.5 mm thick). Frequency sweeps from 10^2 to 10^{-2} rad/s were performed at 210 °C with a strain of 0.1%, which is in the linear viscoelastic regime. Creep measurements were performed on a stress-controlled AR-G2 rheometer (TA Instruments). A range of shear stresses was applied to the samples for 10 min at 210 °C.

2.3. Results and discussion

2.3.1. Sample preparation and characterization

In order to ensure full dispersion of the cross-linked EPDM phase in the PP matrix, a relatively low amount (50 wt%) of a high molar mass EPDM with a high third monomer content (9 wt%) was applied. Two representative examples of the morphologies of TPVs with fine and coarse rubber dispersions are shown in Figs. 2.2a and b, respectively. The TEM image in Fig. 2.2a shows a fine dispersion of EPDM particles (dark phase) in the PP matrix (light phase). The relatively large dimension of the rubber particles in most of the TPVs in this study makes OM the preferred technique to study the morphology. An example is shown in Fig. 2.2b, where the contrast is achieved by the use of crossed polarizers, which enables the distinction between crystalline (light) and amorphous (dark) regions. The OM image shows the dispersion of amorphous rubber particles (dark) in a semi-crystalline matrix (light and dark areas corresponding to crystalline and amorphous regions, respectively). Both images clearly show a dispersion of EPDM particles in the PP matrix with a large variation in particle size. The rubber particles are not spherical in shape and have rather irregular surfaces, which is typical for TPVs. Although the occurrence of rubber connectivity cannot definitely be excluded on the basis of 2D microscopy images, both TEM and OM strongly indicate the absence of continuity of the rubber phase in the TPVs in this study. This was confirmed by full disintegration of the samples after extraction of the PP phase with boiling toluene, with the exception of the TPV with $\overline{D_n}$ = 1 μm, which showed only partial disintegration.
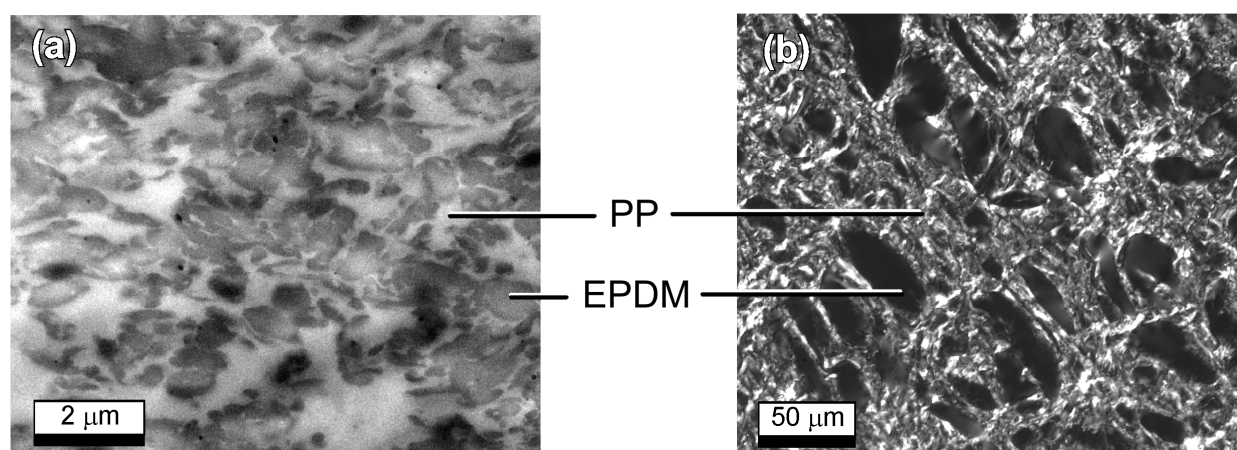
Fig. 2.2. Representative examples of the morphology of TPVs with varying particle sizes as observed by (a) transmission electron microscopy on a TPV with $\overline{D_n}$ = 1 μm and (b) optical microscopy under crossed polarizers on a TPV with $\overline{D_n}$ = 21 μm.

An overview of a selection of the TPVs used in this study is presented in Table 2.1, which is organized by increasing number-averaged rubber particle size ($\overline{D_n}$). Most of the TPVs collected

in Table 2.1 were prepared via Method A, i.e. by varying the rotor speed prior to cross-linking (RS_1) with a constant rotor speed during cross-linking (RS_2) of 80 rpm. $\overline{D_n}$ decreases rapidly with increasing RS_1 and levels off at a value of approximately 1 μm (Fig. 2.3). After mixing the PP/EPDM blends at RS_1, the rotor speed RS_2 was changed to 80 rpm directly after the addition of the curatives. Table 2.1 shows that variations in RS_2 hardly influence $\overline{D_n}$, which indicates that the shear rate prior to cross-linking determines the final morphology of the blend. The rapid decrease in $\overline{D_n}$ with increasing RS_1 and the constant $\overline{D_n}$ at various RS_2 indicate that the EPDM phase is already the dispersed phase prior to cross-linking and, thus, that phase inversion and break up of a co-continuous morphology during the dynamic vulcanization process does not occur for the particular TPV composition studied.
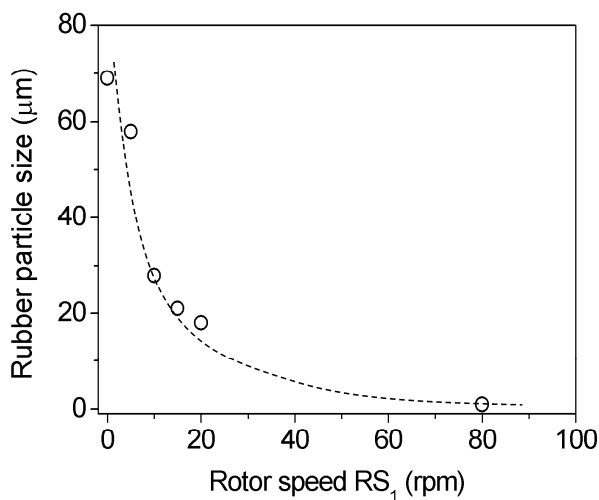
Fig. 2.3. Number-averaged rubber particle size $\overline{D_n}$ as a function of the rotor speed RS_1 (Method A) at $RS_2 = 80$ rpm.

Two additional TPVs in Table 2.1 were prepared by Method B, i.e. by first melt mixing PP, Irganox 1010 and resol, after which a masterbatch of EPDM and $SnCl_2 \cdot 2H_2O$ was added. Since cross-linking of the EPDM starts as soon as it is added to the PP melt, a final morphology with relatively large rubber particle sizes is obtained. Table 2.1 shows that an increase in $\overline{D_n}$ also leads to an increase in $\overline{D_v}$ and an increase in *PDI*. In accordance with equations 2.6 and 2.7, both ID_{mono} and ID_{poly} increase with increasing $\overline{D_n}$.

The extent of cross-linking of TPVs is typically characterized by the rubber gel content (*%gel*) and the degree of swelling (*%swell*). The high *%gel* of > 98 % (Table 2.1) indicates that high degrees of cross-linking were achieved. Generally, *%swell* is indicative for the cross-link density of the EPDM phase, since the equilibrium amount of solvent that can be absorbed by a cross-linked network decreases with increasing cross-link density. Table 2.1 shows a random variation in *%swell* between 350 and 470 %, which indicates similar cross-link densities for all

Table 2.1. Preparation method, degree of cross-linking and rubber particle size (distribution) of selected TPVs with increasing $\overline{D_n}$.

Preparation method	RS_1 (rpm)	RS_2 (rpm)	%gel (%)	%swell (%)	$\overline{D_n}$ (μm)	$\overline{D_v}$ (μm)	PDI (-)	ID_{mono} (μm)	ID_{poly} (μm)
A	80	80	99.8	365	1.1	1.5	1.5	0.1	0.1
A	20	80	100.2	390	18	43	2.4	2.5	4.0
A	20	20	100.0	351	21	78	3.7	3.0	5.2
A	15	80	99.4	403	21	122	5.8	3.0	6.0
A	10	80	99.1	418	28	267	9.6	3.9	7.0
B	80	80	98.2	469	38	123	3.2	5.4	9.8
B	80	200	98.5	459	49	249	5.1	6.8	13.9
A	5	80	100.0	384	58	272	4.7	8.1	15.6
A	0	80	101.1	405	69	280	4.1	9.6	24.7

TPVs. However, the ability of the EPDM phase to swell is limited in the case of a confined geometry, as may be imposed by the rigid PP phase. Due to this influence of the morphology on *%swell*, the values presented in Table 2.1 should be taken as an indicative rather than an absolute number.

The selection of TPVs prepared via Methods A and B shown in Table 2.1 provides a series of TPVs with a variation in $\overline{D_n}$ from 1 to 70 μm and a similar, high cross-link density, which is suitable to study the influence of $\overline{D_n}$ on the properties of TPVs.

2.3.2. Crystallinity and crystal structure

The crystallinity and the crystal structure of the PP phase in the TPVs were studied by WAXD on compression-molded samples. Fig. 2.4a shows an example of the one-dimensional (1D) WAXD pattern of a PP/EPDM-based TPV after circular integration of the two-dimensional diffraction pattern and a scaled subtraction of the amorphous EPDM diffraction pattern. The crystallinity (X_c) can be quantified according to

$$X_c = \frac{A_c}{A_{total}}$$ (2.10)

where $A_c = A_{total} - A_a$ is the area of the crystalline peaks, A_{total} is the total area and A_a is the area of the amorphous halo. The amorphous halo was measured on fully amorphous, atactic PP and was subtracted after scaling to the minimum between the α(110) and α(040) diffraction peaks, which leads to the WAXD pattern in Fig. 2.4b.
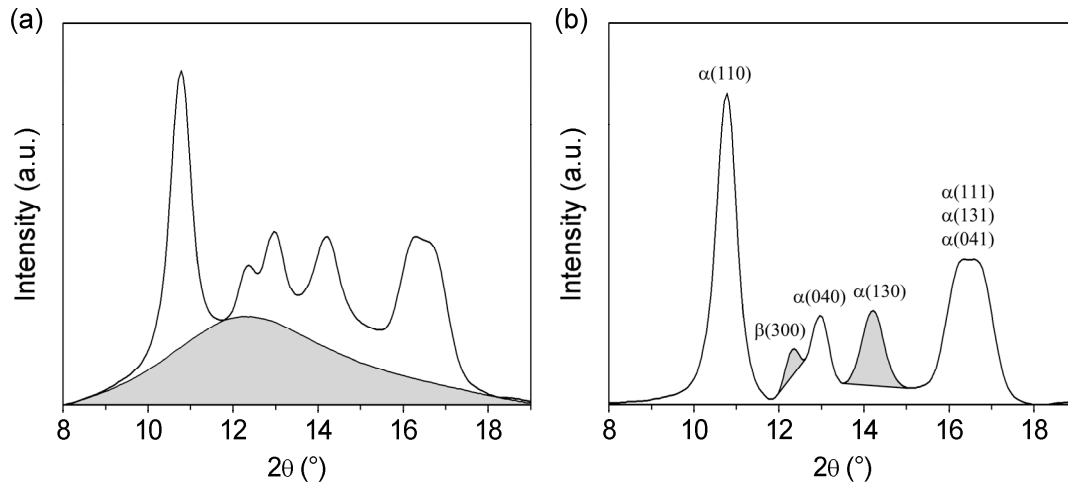
Fig. 2.4. (a) 1D WAXD pattern for a TPV with $\overline{D_n}$ = 1 μm. The shaded area is the underlying amorphous halo. (b) 1D WAXD pattern after subtraction of the amorphous halo. The shaded areas indicate the reflections of the α(130) and β(300) phases, which were used to quantify the fractions of α and β modifications.

PP can crystallize into different crystal modifications, of which the α, β and γ modifications are the most commonly observed. The α modification has a monoclinic unit cell and is formed under normal conditions[40], whereas the β modification has a hexagonal unit cell and is typically formed in the presence of nucleating agents or in the case of a strongly imposed orientation[41]. The typical WAXD peaks corresponding to the α and β modification in the range of $8° < 2\theta < 19°$ are indicated in Fig. 2.4b. The occurrence of the γ modification, with its orthorhombic unit cell, is determined by the molecular structure of the PP used, i.e. its stereo-regularity, molar mass and comonomer content[42]. The presence of the γ modification would lead to a characteristic diffraction peak γ(117) at a scattering angle $2\theta = 15.8°$, which is not observed in any of the TPVs. The fractions of α and β modifications can be quantified by

$$X_i = \frac{A_i}{A_\alpha + A_\beta} \tag{2.11}$$

with i the specific crystal structure (either α or β) and A_i the area of the corresponding WAXD peak. Fig. 2.4b illustrates the method used to determine A_α and A_β, following Van der Burgt *et al.*[43], and the calculated values are presented in Table 2.2. Where pure PP has an X_c of 57.6 % and consists solely of α type crystals, the PP phase in the various TPVs shows a lower X_c of ~ 50 %, which is independent of the EPDM particle size. A decrease in X_c was previously observed for non-cross-linked PP/EPDM blends and was explained by a decrease in the growth rate of the crystals due to topological confinements, which leads to a decrease in the perfection of the crystal structure as well[44]. The TPVs contain both α and β type crystals and the amount of β type crystals increases with decreasing $\overline{D_n}$. The formation of crystals with the β modification is attributed to the slight nucleating effect of the rubber particles[45] and orientation of the PP phase

between the rubber particles, originating from flow imposed on the system during compression molding. A decrease in $\overline{D_n}$ increases the surface area that is available for PP nucleation and increases the shear rate of the molten PP in between the particles during melt processing and, consequently, leads to an increase in X_β.

Table 2.2. Crystallinity and crystal structure of PP and PP/EPDM-based TPVs.

$\overline{D_n}$ (µm)	X_c (%)	X_α (%)	X_β (%)
1	50.1	42.8	7.3
18	51.0	47.9	3.1
28	51.4	51.2	0.2
38	49.9	49.4	0.5
Pure PP	57.6	57.6	0.0

2.3.3. Influence of rubber particle size on tensile properties

Figs. 2.5a and b show the influence of $\overline{D_n}$ and ID_{poly} on the elongation at break (*EB*) and the tensile strength (*TS*), respectively. It has to be noted that all the TPVs deform homogeneously, i.e. necking of the tensile bars was not observed. While *EB* improves in a linear fashion with decreasing $\overline{D_n}$ from 100 to 850 %, *TS* is initially rather low (~ 10 MPa) and independent of $\overline{D_n}$, but improves significantly at $\overline{D_n}$ < 30 µm up to ~ 25 MPa. Since the interparticle distance scales linearly with the rubber particle size at a constant rubber volume fraction, the same trend is observed when correlating *EB* and *TS* to either $\overline{D_n}$ or ID_{mono}. However, the particle size distribution is not the same for all TPVs and differences in the two correlations may, therefore, be expected. Figs. 2.5a and b show that the correlations between *EB* and *TS* with either $\overline{D_n}$ or ID_{poly} are rather similar, from which it can be concluded that polydispersity of the rubber particle size does not influence *EB* and *TS*.
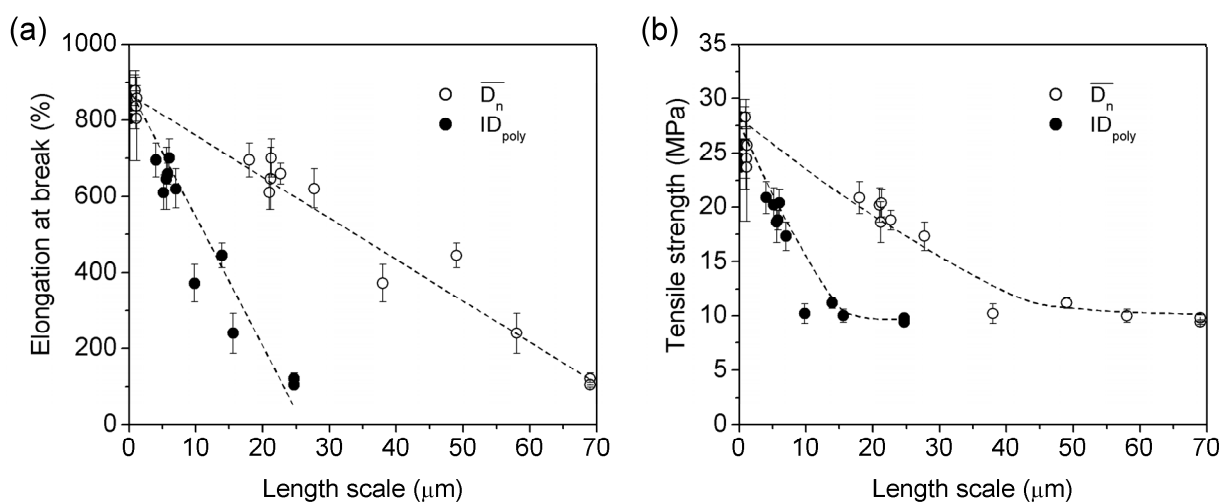
Fig. 2.5. (a) Elongation at break and (b) tensile strength as a function of $\overline{D_n}$ and ID_{poly}.

Combining the data from Figs. 2.5a and b leads to Fig. 2.6, in which the experimental data are represented in a similar fashion as presented by Coran *et al.*[10] and Araghi[11]. The data points of *TS* and *EB* for TPVs with varying $\overline{D_n}$ approximately coincide with the median tensile curve of the TPV with $\overline{D_n}$ = 1 µm (solid line in Fig. 2.6). This suggests that the macroscopic failure of the TPVs is simply shifted to higher extensions with decreasing $\overline{D_n}$ without significantly changing the stress/strain dependency of the materials, as was already shown by Coran *et al.*[10].
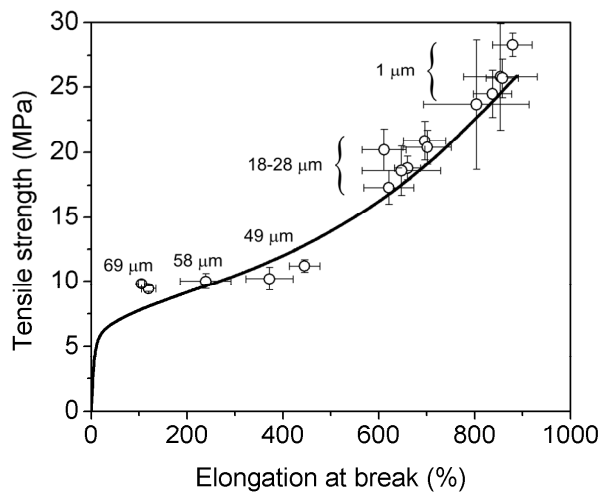
Fig. 2.6. Tensile strength and elongation at break for TPVs with various $\overline{D_n}$. The solid line represents the tensile curve of a TPV with $\overline{D_n}$ = 1 µm.
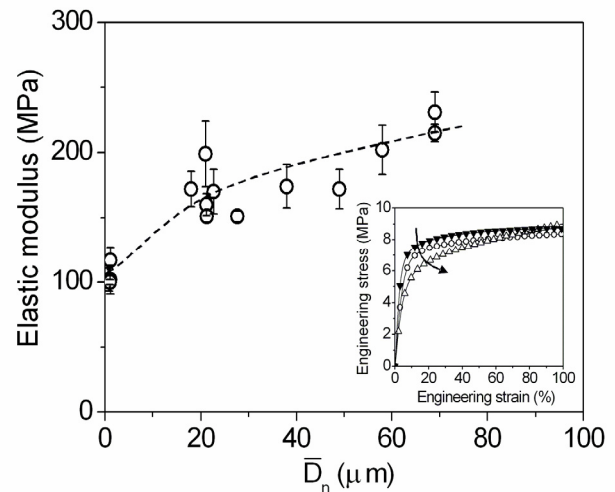
Fig. 2.7. Elastic modulus as a function of $\overline{D_n}$. The inset shows an enlargement of the tensile curves near the yield point of PP for TPVs with $\overline{D_n}$ = 69 µm (▼), 38 µm (O) and 1 µm (Δ).

However, a more careful examination of Fig. 2.6 shows that the data points deviate from the median tensile curve of the TPV with $\overline{D_n}$ = 1 µm, especially for the TPVs with large $\overline{D_n}$. This deviation is evident from a decrease in the elastic modulus (*E*) with decreasing $\overline{D_n}$, along with a slight decrease in the yield stress (σ_y) (Fig. 2.7). The decrease in *E* is not related to changes in the rubber content nor the crystallinity of the PP matrix, since these are constant for all samples. A decrease in *E* is expected with an increasing continuity of the rubber phase. Based on the microscopy and extraction experiments, the absence of rubber-connectivity was proven for all TPVs with the exception of the TPVs with $\overline{D_n}$ = 1 µm. Therefore, only the relatively low *E* of the TPVs with $\overline{D_n}$ = 1 µm may be related to partial rubber-connectivity. Since β type crystals of PP are known to have a lower *E* and a lower σ_y as compared to α type crystals[46], the decrease in *E* and σ_y may be partially ascribed to the increasing fraction of β crystals. Additionally, the crystalline order and orientation near the interface may be influenced, which will lead to changes in the interfacial properties[47-49]. Several authors have reported a particle size dependency of *E* in filled polymers[48,50-52]. For blends of polymers with rubbers, a decrease in *E* was observed with decreasing rubber particle size[52], while the opposite trend was observed for polymer composites

with rigid fillers[48,50,51], indicating that the influence of the filler on E becomes more pronounced with decreasing particle size.

Fig. 2.8 shows the morphology of a PP/EPDM-based TPV with $\overline{D_n}$ = 1 μm at high magnifications, where the contrast between EPDM (dark) and PP (light) was achieved by 24 hrs bulk staining with a RuO$_4$ solution. The images clearly demonstrate the presence of an interphase layer at the PP/EPDM interface, which originates from the high compatibility between PP and EPDM. The thickness of this interphase layer as estimated from the TEM images is in the order of 20 nm, which is very similar to the thickness of the interphase layer of PP/EPDM blends prior to cross-linking, as will be discussed in Chapter 3. The interphase layer is composed of amorphous EPDM and semi-crystalline PP and this mixing of PP with EPDM will induce a plasticizing effect in the interphase, leading to a decrease in E of the interphase. The amount of interphase material increases rapidly with decreasing rubber particle size, since the total volume of interphase in the sample is proportional to the third power of the particle size, which contributes to the decrease in E with decreasing $\overline{D_n}$ (Fig. 2.7). An additional conclusion that can be drawn from the TEM images in Fig. 2.8 is that the PP matrix is able to crystallize even in a confined space between rubber particles of < 50 nm, which is in agreement with previous crystallization studies on PS/PP multilayer systems[53].
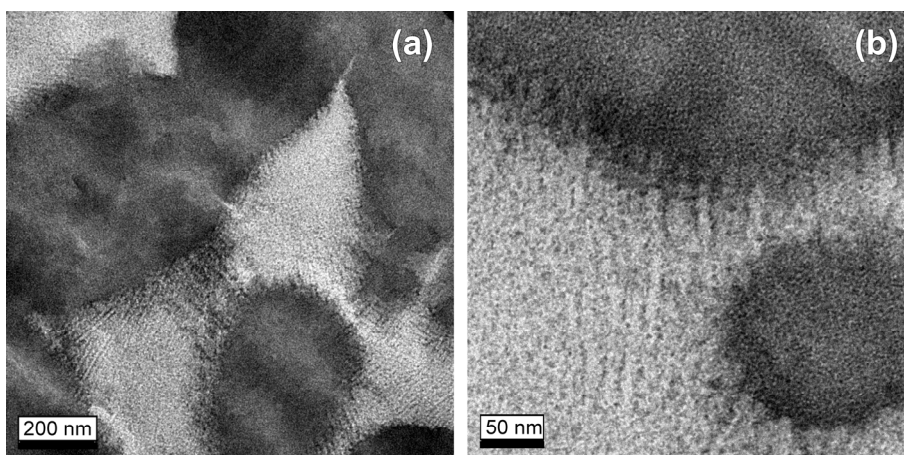
Fig. 2.8. TEM images of a TPV with $\overline{D_n}$ = 1 μm, showing the penetration of PP lamellae into the cross-linked EPDM particles at various magnifications.

2.3.4. Deformation mechanism under tensile conditions

SAXS can be used to study the structural changes that take place on a nanometer scale during the deformation of polymers. First, the deformation mechanism of pure PP, as derived from the development of the *in-situ* SAXS patterns in Fig. 2.9, is discussed in order to subsequently explain the deformation mechanism of PP/EPDM-based TPVs with $\overline{D_n}$ = 18 and 1 μm. It is important to note that pure PP deformed via localized yielding and subsequent necking, while all

the TPVs deformed homogeneously, i.e. necking was not observed. A schematic illustration of the changes in the semi-crystalline morphology and the accompanying SAXS patterns during tensile deformation is shown in Fig. 2.11.

The initial SAXS pattern of PP at a macroscopic strain (ε_{macro}) of 0 % (Fig. 2.9a) shows an isotropic scattering ring that originates from the long period of the PP. At ε_{macro} = 9 %, an intensification of the meridional scattering intensity is observed, which is caused by the orientation of lamellar stacks perpendicular to the stretching direction[54]. At the same time, the long period increases due to interlamellar separation. Microscopic localization of the stress at the yield point leads to the formation of a neck, which progresses through the sample. Since necking may initiate at any position in the tensile bar, the onset of necking most likely occurs outside the beam and upon further deformation the neck progresses into the beam at a certain ε_{macro}. As the neck moves into the X-ray beam (at ε_{macro} ~ 25 % in Fig. 2.9a), several distinct changes in the scattering pattern can be observed within a short range of ε_{macro}. Strong meridional scattering lobes appear close to the beam stop, which originate from the formation of voids in the amorphous phase between the lamellar stacks[54-60] (see also Fig. 2.11). The meridional and equatorial scattering intensities can be described by their respective invariants Q_m and Q_e, where Q is a measure for the total electron density difference in the sample and is defined by:

$$Q = \int\limits_{q=q_{min}}^{q=q_{max}} I(q)q^2 dq \qquad (2.12)$$

where q is the scattering vector defined by $q = (4\pi/\lambda)\sin(\theta)$, with λ the wavelength and θ the scattering angle. Q_m represents the meridional scattering intensity integrated over azimuthal angles (α) ranging from 45 to 135° and from 225 to 315°, whereas Q_e describes the equatorial scattering intensity integrated over α ranging from -45° to 45° and from 135 to 225°. The formation of the interlamellar voids upon yielding of PP leads to an increase in Q_m (Fig. 2.10), where the voids rapidly increase in number upon slightly increasing ε_{macro}. As schematically shown in Fig. 2.11, the voids are initially oriented perpendicular to the direction of the applied stress ($Q_m > Q_e$), but with increasing ε_{macro} they rapidly orient parallel to the direction of the applied stress ($Q_m < Q_e$), as indicated by the transition from intense meridional to equatorial scattering (Fig. 2.9a) and the concomitant decrease in Q_m and increase in Q_e at ε_{macro} ~ 30 % (Fig. 2.10). In this stage of deformation the long period disappears, since the order within the lamellar stacks is lost upon yielding. Due to the strong reduction of the sample thickness upon necking, a decrease in both Q_m and Q_e is observed at ε_{macro} > 40 % (Fig. 2.10). No changes in the SAXS pattern are observed as the neck progresses throughout the remainder of the sample.
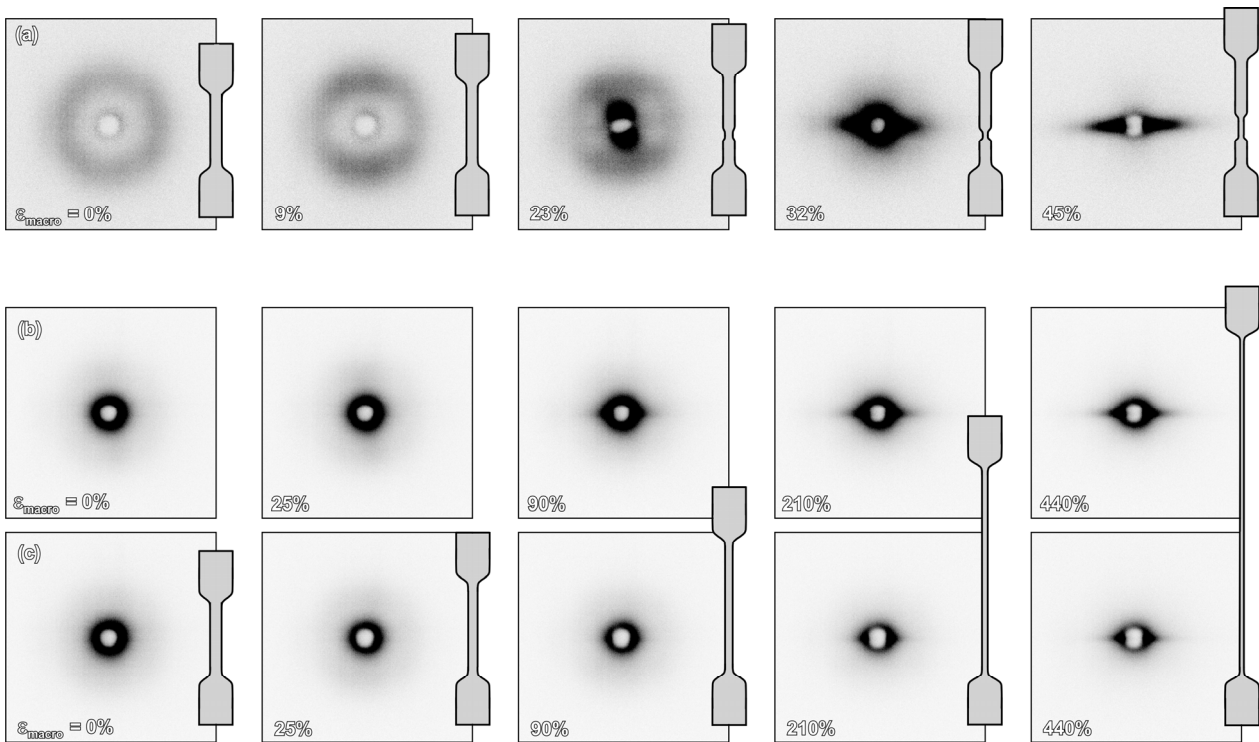
Fig. 2.9. Development of SAXS patterns of in-situ deformed (a) pure PP and TPVs with (b) $\overline{D_n}$ = 18 μm and (c) $\overline{D_n}$ = 1 μm at various macroscopic strains (ε_{macro}). The stress is applied in the vertical direction and the macroscopic shape of the tensile bars is schematically shown.

At ε_{macro} = 0 %, the TPVs show an isotropic scattering profile at very low q-values, which is mostly covered by the beam stop. Since this profile is not observed for pure PP, it can be attributed to scattering of the rubber particles. In comparison to pure PP, the long period of the PP phase in the TPVs is significantly less distinct, which indicates a wider distribution of the long period and less perfect lamellar stacks. This was confirmed by differential scanning calorimetry (DSC) experiments where a broader melting endotherm of the PP phase in TPVs was observed in comparison to pure PP (not shown here). Deformation of the TPV with $\overline{D_n}$ = 18 μm leads to the formation of equatorial streaks in the SAXS patterns (Fig. 2.9b), albeit with a significantly lower intensity and at higher ε_{macro} as compared to the case of pure PP. The reduced intensity of the streaks and the shift towards higher ε_{macro} indicate that the formation of interlamellar voids in the TPV is suppressed. This observation is supported by the development of Q_m and Q_e as a function of ε_{macro} in Fig. 2.10, where the increase in Q_m is directly followed by an increase in Q_e. Both Q_m and Q_e pass through a maximum at ε_{macro} = 60 and 150 %, respectively, and then decrease continuously at higher ε_{macro}.

It has to be noted that the extent of void formation is also related to the geometry of the tensile bars. Uniaxial deformation of very thick tensile bars will lead to a triaxial stress state and, inevitably, to the formation of voids in the matrix, in the rubber particles and/or at the rubber/matrix interface. The hydrostatic stress state originates from the absence of flow, which

limits the lateral contraction of the sample that is required to retain a constant total volume during deformation. For very thin samples this lateral contraction is not limited and the hydrostatic stress state is not reached and, therefore, voiding does not occur. Since the geometry of the tensile bars used in this study is constant (15 x 5 x 1 mm), the influence of the sample geometry on the deformation mechanism is not discussed. The suppression of interlamellar void formation in the TPV in comparison to pure PP is explained by (*i*) the absence of necking, *(ii)* the lower stress imposed on the PP matrix during deformation and *(iii)* stress localization at the equatorial regions between the rubber particles. The stress level required to deform a TPV to a certain strain decreases with increasing amount of rubber[61]. This indicates that, at a certain ε_{macro}, the PP phase in TPVs is subjected to a lower stress level as compared to pure PP, leading to a decrease in the extent of deformation of the PP phase. Kikuchi *et al.*[62,63] stated that plastic deformation of the matrix concentrates in the thinnest PP ligaments at the equatorial regions of the rubber particles, while the PP ligaments at the polar regions remain below the matrix yielding condition (see also Chapter 1.3.1). Thus, the deformation process of pure PP through lamellar orientation in the elastic regime and the subsequent interlamellar void formation and void orientation also occurs in the TPVs, but is localized in the PP ligaments at the equatorial regions of the rubber particles (Fig. 2.11). Upon increasing ε_{macro} the thicker parts of the matrix deform progressively and eventually the polar regions will exceed the yield stress and will undergo plastic deformation as well. Deformation of the TPV with $\overline{D_n}$ = 1 μm also leads to the formation of equatorial streaks in the SAXS patterns (Fig. 2.9c), but at an even lower intensity and higher ε_{macro} as compared to the TPV with $\overline{D_n}$ = 18 μm. This indicates that the formation of interlamellar voids is more effectively suppressed at lower $\overline{D_n}$. This is also supported by the development of Q_m and Q_e (Fig. 2.10), which do not pass through a maximum value as in the case of PP and the TPV with $\overline{D_n}$ = 18 μm, but show a continuous decrease with increasing ε_{macro}.
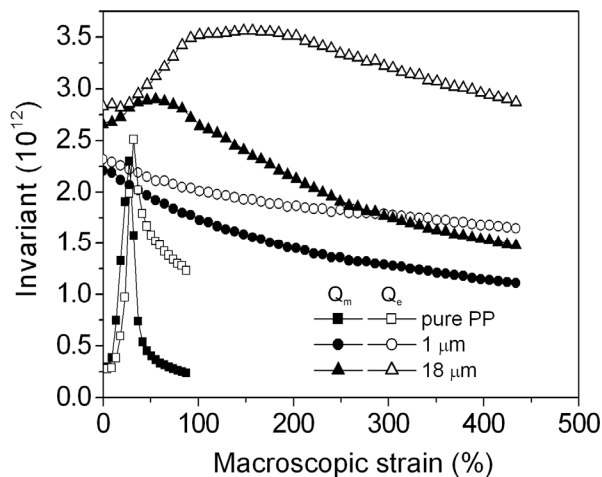
Fig. 2.10. Invariants Q_m and Q_e of in-situ deformed PP and TPVs with $\overline{D_n}$ = 1 and 18 μm in the equatorial (open symbols) and the meridional (closed symbols) direction.

Pure PP			TPVs		
			Equatorial region	Polar region	Combined
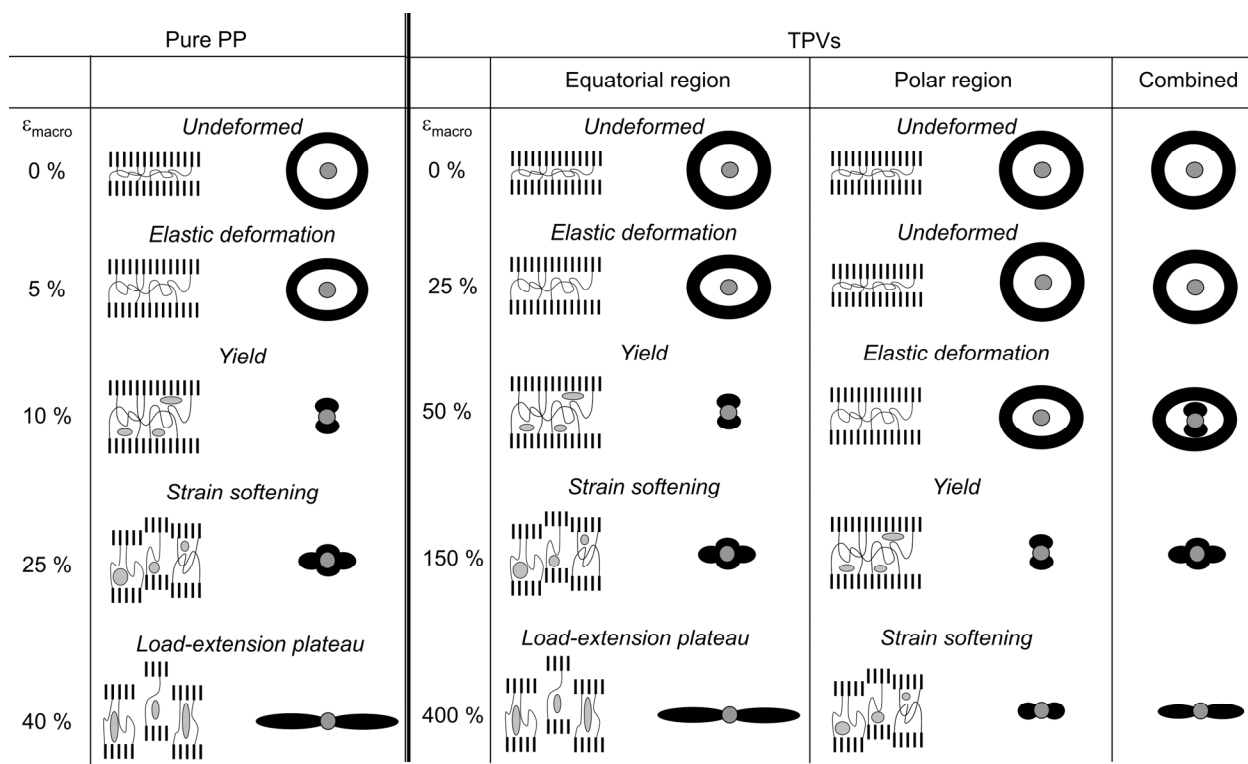
Fig. 2.11. Schematic representation of the development of voids in the interlamellar region and the accompanying SAXS patterns during tensile deformation of pure PP and TPVs. The approximate macroscopic stain (ε_{macro}) is given and the stress is applied in the vertical direction.

The formation of crazes would lead to a SAXS pattern in the form of a cross, with meridional streaks, originating from the reflection of the craze-bulk interface, and equatorial streaks, originating from the scattering of the fibrils and voids [64]. Internal rubber cavitation or particle/matrix debonding would lead to an increase in the isotropic scattering intensity, originating from the formed cavities. The SAXS patterns in Fig. 2.9 and the development of the invariants in Fig. 2.10 demonstrate that yielding of the PP matrix is the main deformation mechanism of the TPVs and that rubber cavitation and crazing both do not occur. The absence of crazing is as expected, since the local deformation behavior of PP changes from multiple crazing at high tensile speeds (> 10 mm/s) to shear yielding at lower tensile speeds (0.1 – 1 mm/s), which is related to the decrease in yield stress at lower deformation rates[35]. Although the occurrence of internal rubber cavitation is crucial for the enhancement of the impact toughness of rubber-toughened polymers[6,16], the results presented here indicate that cavitation is not required in order to obtain a high toughness for TPVs tested under tensile conditions. The absence of rubber cavitation for TPVs is explained by the facilitation of matrix yielding due to *(i)* a decrease in yield stress with decreasing deformation rate[35, 65], *(ii)* readily yielding of the thin matrix ligaments[63,66], *(iii)* a decrease in yield stress due to the loss in crystal perfection and decrease in lamellar thickness[44], *(iv)* a decrease in yield stress due to the increased fraction of β type crystals[46] and *(v)* the relatively high shear modulus of the cross-linked rubber in comparison to

the amorphous PP phase. Due to the facilitation of matrix yielding, the critical hydrostatic stress in the rubber particles is not reached and cavitation does, therefore, not occur. The absence of rubber cavitation was supported by TEM studies on the TPV with $\overline{D_n}$ = 1 μm after deformation to macroscopic strains of 50 and 800 % and by OM and TEM studies on the TPV with $\overline{D_n}$ = 18 μm during deformation (not shown here). The absence of rubber cavitation was also reported by Oderkerk et al.[66] for reactively compatibilized poly(amide)-6/EPDM-based TPVs and by Kikuchi et al.[63] for PP/EPDM-based TPVs.

It can be concluded that matrix yielding is the main deformation mechanism of PP/EPDM-based TPVs, where crazing and rubber cavitation do not occur during the deformation process. Sub-μm-sized interlamellar voids are formed in the matrix during deformation, which grow in amount and size and may, eventually, coalesce in avalanche, leading to macroscopic failure. Decreasing the rubber particle size leads to the suppression of void formation and to an improved confinement that shields the interactions between the voids and inhibits their coalescence, both of which lead to an increased *EB* and *TS* (Figs. 2.4 and 2.5). Although rubber cavitation is not observed during the tensile tests, voids in the rubber phase may, eventually, be formed by fracture of the rubber particle due to internal imperfections, such as variations in the network density. If such voids originate from large particles they are likely to form a critical crack, which will lead to macroscopic failure[67,68]. On the other hand, small particles may retard the void formation to higher stress levels and a large number of stable voids may be initiated, which permits further deformation of the matrix ligaments between the particles.

2.3.5. Influence of rubber particle size on elastic recovery

The compression set (*CS*) is a practical and direct measure for the elastic behavior of cross-linked rubbers and TPVs and is, therefore, widely used as an indication for the elastic performance. Low *CS* values indicate low permanent set, i.e. a high elastic recovery, while high *CS* values indicate poor elastic recovery. TPVs generally show a high elastic recovery, though not as good as thermoset cross-linked rubbers. This is remarkable as the matrix phase of TPVs consists of a semi-crystalline thermoplastic polymer, which is expected to deform plastically and, thus, irreversibly via shear yielding. The physical origin of the elastic recovery is explained by the stress localization in the thin PP ligaments at the equatorial regions of the EPDM rubber particles[62,63]. The PP ligaments in the polar region remain below the matrix yielding condition, i.e. within the elastic limit, and act as adhesion points between the rubber particles, thereby forming a pseudo-continuous elastic phase. Upon unloading, the elastic forces of the elongated

rubber particles pull back the plastically deformed thin ligaments via bending, buckling and yielding of the ligaments[62,63,66,69,70].
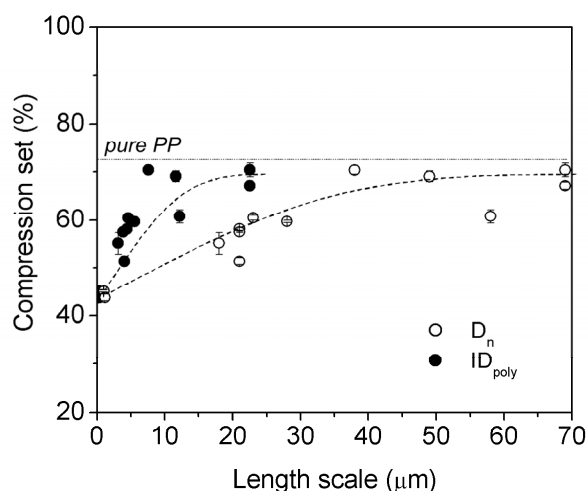
Fig. 2.12. CS as a function of $\overline{D_n}$ and ID_{poly}. The dotted line indicates the CS value of pure PP.

CS appears to be independent of the rubber particle size for $\overline{D_n} > 40$ µm, while a significant improvement of the elastic recovery is observed at smaller $\overline{D_n}$ (Fig. 2.12). A similar trend is observed for *CS* as a function of ID_{poly}, i.e. *CS* decreases significantly at ID_{poly} values below ~ 7 µm. The improvement of the elastic recovery with decreasing interparticle distance is in good agreement with the simulations performed by Boyce *et al.*[69,70]. The improvement can be explained by assessing the balance between the elastic energy that is stored in the rubber particles upon deformation and the stress that is required for the PP ligaments to bend or buckle. Since the elastic energy increases with decreasing rubber particle size[22] and lower stress levels are required to bend or buckle thin ligaments in comparison to thick ligaments, an improvement of the elastic recovery with decreasing $\overline{D_n}$ and/or ID_{poly} is expected. *CS* of the TPVs with coarse morphologies ($\overline{D_n} > 40$ µm) is constant and similar to *CS* of pure PP (*CS* = 73 %). This demonstrates the existence of a critical $\overline{D_n}$ and/or ID_{poly} above which the rubber particles do not contribute to the elastic recovery of the material.

2.3.6. Influence of bimodal rubber particle size distribution on properties

Sabet *et al.*[71] have claimed that TPVs containing a combination of large (1-5 µm) and small (< 0.1 µm) particles at a constant rubber content, i.e. TPVs with a bimodal particle size distribution, exhibit a better elastic recovery in comparison to TPVs with a unimodal particle size distribution. It is postulated that the presence of the small particles decreases the interparticle distance, which, according to the simulations of Boyce *et al.*[69,70], leads to an enhancement of the

elastic recovery. It is unclear whether the bimodality of the particle size distribution influences the elastic recovery in another way than by only changing the interparticle distance.

Fig. 2.5 already indicated that the polydispersity of the rubber particles does not influence *EB* and *TS*. Fig. 2.13 presents the tensile properties and *CS* of TPVs with unimodal and bimodal particle size distributions, where bimodal distributions were obtained by melt mixing two TPVs with varying $\overline{D_n}$ at different composition ratios. Although evaluation of the actual morphologies via OM and TEM is complicated by the large range of $\overline{D_n}$, TEM studies suggest intimate mixing of the small and large rubber particles (not shown here). Fig. 2.13 clearly shows that the trends in tensile properties and elastic recovery are covered by variations in $\overline{D_n}$ alone, independent of the modality of the particle size distribution. Therefore, it can be concluded that the tensile properties and elastic recovery are determined by the average rubber particle size and interparticle distance, independent of the particle size distribution. These results are in contrast with the claims of Sabet *et al.*[71], which may be due to the fact that Sabet *et al.* estimated the particle size and its distribution visually.
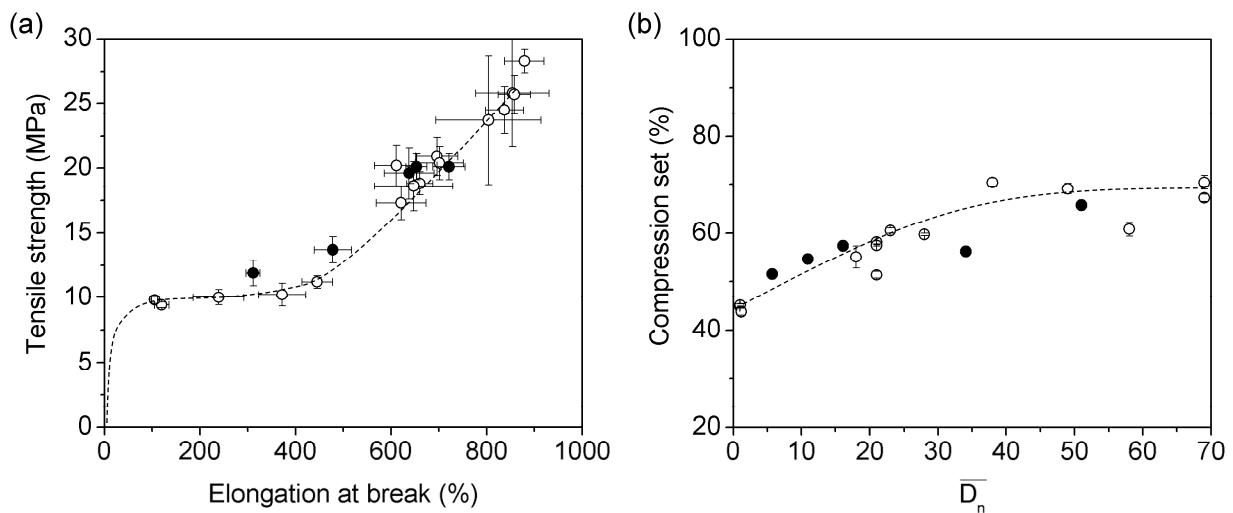
Fig. 2.13. (a) Tensile strength and elongation at break for TPVs with varying $\overline{D_n}$ and (b) CS as a function of $\overline{D_n}$ for (○) unimodal and (●) bimodal particle size distribution.

2.3.7. Influence of rubber particle size on rheological behavior

As the melt processability on standard thermoplastic processing techniques is an essential property of TPVs, the influence of $\overline{D_n}$ on the rheological behavior of the TPVs was also studied. Fig. 2.14 shows the complex viscosity (η^*) and the storage modulus (G') as a function of the applied frequency (ω) at 210 °C, where η^* is equivalent to the steady-shear viscosity when ω equals the shear rate $\dot{\gamma}$[72]. The slope of $\log(\eta^*)$ versus $\log(\omega)$ approaches -1 and that of $\log(G')$ versus $\log(\omega)$ approaches 0 at low frequencies, which indicates that the TPVs behave almost like an ideal elastic network under these conditions. This observation is consistent with previous

studies on PP/EPDM-based TPVs, in which it was suggested that physical clustering of the rubber particles at low shear rates leads to rheological co-continuous behavior, whereas high shear rates lead to break up of the clusters, resulting in a rheological behavior typical for a matrix/dispersion morphology[73-75]. A significant increase in both η^* and G' is observed with decreasing $\overline{D_n}$, especially at low frequencies, which suggests strengthening of the physical network with decreasing $\overline{D_n}$.
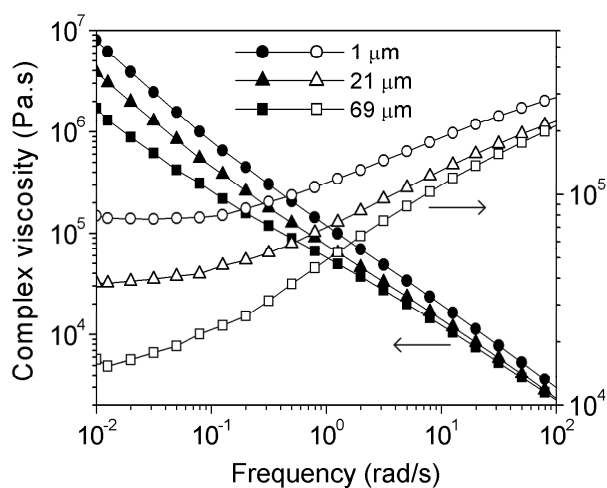
Fig. 2.14. Complex viscosity (η^*) and storage modulus (G') for TPVs with varying $\overline{D_n}$ at 210 °C.
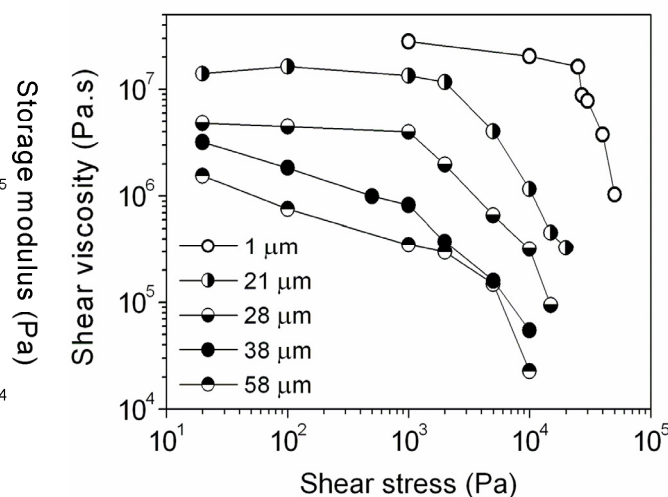
Fig. 2.15. Shear viscosity after 100 s creep for TPVs with varying $\overline{D_n}$ at 210 °C.

The influence of $\overline{D_n}$ on the strength of the physically interacting network formed by the rubber particles can be studied by measuring the stress that is required to break up the network. This critical stress or, alternatively, the yield stress can be studied by performing creep experiments at various shear stresses[74-76]. Fig. 2.15 shows the (non-steady) shear viscosity after 100 s creep as a function of the applied shear stress. At all stresses the viscosity increases with decreasing $\overline{D_n}$, which is consistent with the results presented in Fig. 2.14. The shear viscosity decreases with increasing shear stress and shows a significant drop at a certain critical shear stress. The value of the yield stress increases significantly with decreasing $\overline{D_n}$. The increase in η^*, G' and yield stress with decreasing $\overline{D_n}$ can be attributed to the increase in interfacial surface area and the decrease in interparticle distance, both of which increase the extent of physical contact between the particles and, thus, strengthens the physical network.

2.4. Conclusions

TPVs with a high cross-link density and a variation in rubber particle size were prepared by varying the preparation conditions during dynamic vulcanization. Increasing the shear rate during dynamic vulcanization led to a decrease in the rubber particle size from 70 down to 1 μm.

Decreasing the rubber particle size leads to a significant enhancement in the elongation at break and tensile strength, while a reduction in the elastic modulus is observed. The decrease in elastic modulus is explained by (*i*) an increasing contribution of the PP/EPDM interphase, *(ii)* an increasing content of β type crystals, *(iii)* an increasing influence of the dispersed rubber phase on the macroscopic behavior and *(iv)* an increased connectivity between the rubber particles for the TPVs with the smallest particle size of 1 μm. The criteria to obtain a high elongation at break and tensile strength for TPVs tested under low speed tensile conditions are very different than those for traditional rubber-toughened polymers. The latter typically require a fine dispersion of easily cavitating rubber particles to allow for shear yielding of the matrix to occur and, thus, to obtain tough behavior. The deformation behavior of TPVs is dominated by localized yielding of the PP matrix in the thin ligaments at the equatorial regions of the rubber particles and by the formation of interlamellar voids. Matrix crazing, internal rubber cavitation and particle/matrix debonding were not observed. The improvement of the tensile properties with decreasing rubber particle size is mainly attributed to the suppression of interlamellar void formation and the improved confinement that prevents the coalescence of voids. Additionally, the suppression of rubber particle cavitation and the decreasing probability of reaching the critical crack size upon internal fracture of the rubber particle may contribute to the enhanced tensile properties.

Since lower stress levels are required to bend or buckle thin ligaments in comparison to thick ligaments, decreasing the rubber particle size leads to an improved elastic recovery. In fact, for large interparticle distances the cross-linked rubber phase hardly contributes to the elastic recovery. The trends in tensile properties and elastic recovery appeared to be independent of the particle size distribution.

The increase in interfacial area and the decrease in interparticle distance upon decreasing rubber particle size lead to an increased physical interaction between the rubber particles, which explains the increase in viscosity, storage modulus and yield stress in the molten state. It is, therefore, concluded that the melt processability of the TPVs deteriorates with decreasing particle size.

The results demonstrate that the rubber particle size is an important parameter that can be used to control the balance between mechanical properties and melt processability of TPVs. Since particle cavitation is not the driving force behind the improvement of the tensile properties, no limitations on the minimum rubber particle size are expected, which is in sharp contrast to conventional rubber-toughened thermoplastics. This conclusion reveals the potential of TPVs with sub-μm rubber particle sizes, which could be used to control the properties-processing balance into a range that is not achievable with the currently available supra-μm TPVs.

2.5. References

1 *Polymer Blends*; Paul, D.R.; Bucknall, C.B., Eds.; Wiley: New York, 2000.
2 *Polymer Blends Handbook*; Utracki, L.A., Ed.; Kluwer Academic Publishers: Dordrecht, 2002.
3 *Thermoplastic Elastomers: A Comprehensive Review*; Holden, G.; Legge. N.R.; Quirk, R.P., Eds.; Hanser: Munich, 1996.
4 *Thermoplastic Elastomers*; Holden, G.; Kricheldorf, H.R.; Quirk, R.P., Eds.; Hanser Publishers: Munich, 2004.
5 *Toughening of Plastics: Advances in Modeling and Experiments*; Pearson, R.A.; Sue, H.-J.; Yee, A.F., Eds.; American Chemical Society: Washington DC, 2000.
6 *Toughened Plastics*; Bucknall, C.B., Ed.; Applied Science: London, 1977.
7 *Toughened Plastics I: Science and Engineering*; Riew, C.K.; Kinloch, A.J., Eds.; American Chemical Society: Washington DC, 1993.
8 Wu, S. *Polymer* **1985**, *26*, 1855-1863.
9 Wu, S. *J. Appl. Polym. Sci.* **1988**, *35*, 549-561.
10 Coran, A.Y.; Patel, R.P. *Rubber Chem. Technol.* **1980**, *53*, 141-150.
11 Araghi H.H. Proceedings of the International Rubber Conference, Birmingham, United Kingdom, 2001.
12 Argon, A.S.; Cohen, R.E. *Polymer* **2003**, *44*, 6013-6032.
13 Bucknall, C.B.; Davies, P.; Partridge, I.K. *J. Mat. Sci.* **1987**, *22*, 1341-1346.
14 Donald, A.M.; Kramer, E.J. *J. Mat. Sci.* **1982**, *17*, 1765-1772.
15 Donald, A.M.; Kramer, E.J. *J. Mat. Sci.* **1982**, *17*, 2351-2358.
16 Pearson, R.A.; Yee, A.F. *J. Mat. Sci.* **1991**, *26*, 3828-3844.
17 Magalhães, A.M.L.; Borggreve, R.J.M. *Macromolecules* **1995**, *28*, 5841-5851.
18 Dompas, D.; Groeninckx, G. *Polymer* **1994**, *35*, 4743-4749.
19 Dijkstra, K.; van der Wal, A.; Gaymans, R.J. *J. Mat. Sci.* **1994**, *29*, 3489-3496.
20 *Predictive Modeling of the Properties and Toughness of Rubber-Toughened Epoxies*; Kinloch, A.J.; Guild, F.J. In *Toughened Plastics II: Novel Approaches in Science and Engineering, Advances in Chemistry 252*; Riew, C.K.; Kinloch, A.J., Eds.; American Chemical Society: Washington DC, 1996.
21 Gent, A.N.; Tompkins, D.A *J. Polym. Sci., Part A-2: Polym. Phys.* **1969**, *7*, 1483-1488.
22 Dompas, D.; Groeninckx, G.; Isogawa, M.; Hasegawa, T.; Kadokura, M. *Polymer* **1994**, *35*, 4750-4759.
23 Stricker, F.; Thomann, Y.; Mülhaupt, R. *J. Appl. Polym. Sci.* **1998**, *68*, 1891-1901.
24 Jiang, W.; Tjong, S.C.; Li, R.K.Y. *Polymer* **2000**, *41*, 3479-3482.
25 Huang, L.; Pei, Q.; Yuan, Q.; Li, H.; Cheng, F.; Ma, J.; Jiang, S.; An, L.; Jiang, W. *Polymer* **2003**, *44*, 3125-3131.
26 Muratoğlu, O.K.; Argon, A.S.; Cohen, R.E.; Weinberg, M. *Polymer* **1995**, *36*, 921-930.
27 Muratoğlu, O.K.; Argon, A.S.; Cohen, R.E. *Polymer* **1995**, *36*, 2143-2152.
28 Aróstegui, A.; Gaztelumendi, M.; Nazábal, J. *Polymer* **2002**, *43*, 6993-7001.
29 Bartczak, Z.; Argon, A.S.; Cohen, R.E.; Weinberg, M. *Polymer* **1999**, *40*, 2331-2346.
30 Corté, L.; Beaume, F.; Leibler, L. *Polymer* **2005**, *46*, 2748-2757.
31 Lin, L.; Argon, A.S. *Macromolecules* **1994**, *27*, 6903-6914.
32 Corté, L.; Leibler, L. *Macromolecules* **2007**, *40*, 5606-5611.
33 Kuksenko, V.S.; Tamusz, V.P. In *Fracture Micromechanics of Polymer Materials*; Sih, G.C., Ed.; Martinus Nijhoff Publishers: Boston, 1981; pp 61-163.
34 Jang, B.Z.; Uhlmann, D.R.; Van der Sande, J.B. *J. Appl. Polym. Sci.* **1984**, *29*, 3409-3420.
35 Gensler, R.; Plummer, C.J.G.; Grein, C.; Kausch, H. H. *Polymer* **2000**, *41*, 3809-3819.
36 Montezinos, D.; Wells, B.G.; Burns, J.L. *J. Polym. Sci., Polym. Lett. Ed.* **1985**, *23*, 421-425.
37 Premphet, K.; Paecharoenchai, W. *J. Appl. Polym. Sci.* **2001**, *82*, 2140-2149.

2

[38] ASTM Standard D412 "Standard Test Methods for Vulcanized Rubber and Thermoplastic Elastomers – Tension", 1986.

[39] ASTM Standard D395 "Standard Test Methods for Rubber Property – Compression Set", 1989.

[40] Norton, D.R.; Keller, A. *Polymer* **1985**, *26*, 704-716.

[41] Varga, J.; Karger-Kocsis, J. *J. Polym. Sci., Part B: Polym. Phys.* **1996**, *34*, 657-670.

[42] Lotz, B.; Graff, S.; Straupé, C.; Wittmann, J.C. *Polymer* **1991**, *32*, 2902-2910.

[43] van der Burgt, F.P.T.J.; Rastogi, S.; Chadwick, J.C.; Rieger, B. *J. Macromol. Sci., Part B: Phys.* **2002**, *B41*, 1091-1104.

[44] Bieliński, D.M.; Ślusarski, L.; Włochowicz, A.; Ślusarczyk, A.; Douillard, A. *Polym. Int.* **1997**, *44*, 161-173.

[45] Inoue, T.; Suzuki, T. *J. Appl. Polym. Sci.* **1996**, *59*, 1443-1450.

[46] Karger-Kocsis, J.; Varga, J. *J. Appl. Polym. Sci.* **1996**, *62*, 291-300.

[47] Amitay-Sadovsky, E.; Cohen, S.R.; Wagner, H.D. *Macromolecules* **2001**, *34*, 1252-1257.

[48] Vollenberg, P.H.T.; Heikens, D. *Polymer* **1989**, *30*, 1656-1662.

[49] Wenig, W.; Fiedel, H.-W. *J. Mat. Sci.* **1991**, *26*, 3253-3256.

[50] Wang, M.; Joseph, R.; Bonfield, W. *Biomaterials* **1998**, *19*, 2357-2366.

[51] Vollenberg, P.T.H.; Heikens, D. *J. Mat. Sci.* **1990**, *25*, 3089-3095.

[52] Pukánszky, B.; Fortelný, I.; Kovář, J.; Tüdõs, F. *Plast. Rubber Comp. Proc. Appl.* **1991**, *15*, 31-38.

[53] Jin, Y.; Rogunova, M.; Hiltner, A.; Baer, E.; Nowacki, R.; Galeski, A.; Piorkowska, E. *J. Polym. Sci., Part B: Polym. Phys.* **2004**, *42*, 3380-3396.

[54] Schneider, K.; Trabelsi, S.; Zafeiropoulos, N.E., Davies, R.; Riekel, C.; Stamm, M. *Macromol. Symp.* **2006**, *236*, 241-248.

[55] Lee, H.S.; Yoo, S.R.; Seo, S.W. *J. Polym. Sci.: Part B: Polym. Phys.* **1999**, *37*, 3233-3245.

[56] Zhang, X.C.; Butler, M.F.; Cameron, R.E. *Polymer* **2000**, *41*, 3797-3807.

[57] Butler, M.F.; Donald, A.M.; Ryan, A.J. *Polymer* **1997**, *38*, 5521-5538.

[58] Li, X.; Schneider, K.; Kretzschmar, B.; Stamm, M. *Macromolecules* **2008**, *41*, 4371-4379.

[59] Sugimoto, M.; Ishikawa, M.; Hatada, K. *Polymer* **1995**, *36*, 3675-3682.

[60] Baltá-Calleja, F.J.; Peterlin, A. *J. Mat. Sci.* **1969**, *4*, 722-729.

[61] Boyce, M.C.; Kear, K.; Socrate, S.; Shaw, K. *J. Mech. Phys. Solids* **2001**, *49*, 1073-1098.

[62] Kikuchi, Y.; Fukui, T.; Okada, T.; Inoue, T. *J. Appl. Polym. Sci.: Appl. Polym. Symp.* **1992**, *50*, 261-271.

[63] Kikuchi, Y.; Fukui, T.; Okada, T.; Inoue, T. *Polym. Eng. Sci.* **1991**, *31*, 1029-1032.

[64] Mills, P.J.; Kramer, E.J.; Brown, H.R. *J. Mat. Sci.* **1985**, *20*, 4413-4420.

[65] Fond, C *J. Polym. Sci., Part B: Polym. Phys.* **2001**, *39*, 2081-2096.

[66] Oderkerk, J.; de Schaetzen, G.; Goderis, B.; Hellemans, L.; Groeninckx, G. *Macromolecules* **2002**, *35*, 6623-6629.

[67] Kausch, H.H.; Béguelin, Ph.; Fischer, M. *Mech. Comp. Mat.* **2000**, *36*, 177-184.

[68] Kausch, H.H,; Béguelin, Ph. *Macromol. Symp.* **2001**, *169*, 79-87.

[69] Boyce, M.C.; Socrate, S.; Kear, K.; Yeh, O.; Shaw, K. *J. Mech. Phys. Solids* **2001**, *49*, 1323-1342.

[70] Boyce, M.C.; Yeh, O.; Socrate, S.; Kear, K.; Shaw, K. *J. Mech. Phys. Solids* **2001**, *49*, 1343-1360.

[71] Sabet, A.S.; Kear, K.E.; Boyce, M.C.; Shaw, K.D. US Patent 6,579,944 to Advanced Elastomer Systems LP (2003).

[72] Gleissle, W.; Hochstein, B. *J. Rheol.* **2003**, *47*, 897-910.

[73] Goharpey, F.; Nazockdast, H.; Katbab, A.A. *Polym. Eng. Sci.* **2005**, *45*, 84-94.

[74] Han, P.K.; White, J.L. *Rubber Chem. Technol.* **1995**, *68*, 728-738.

[75] Araki, T.; White, J.L. *Polym. Eng. Sci.* **1998**, *38*, 590-595.

[76] Steeman, P.; Zoetelief, W. *ANTEC* **2000**, 3297-3302.

Thermoplastic vulcanizates based on highly compatible blends of isotactic poly(propylene) and ENB-containing atactic poly(propylene)

The potential of highly compatible thermoplastic/elastomer blends for the preparation of thermoplastic vulcanizates (TPVs) with refined morphologies and improved mechanical properties was studied. Copolymers of atactic polypropylene (aPP) and 5-ethylidene-2-norbornene (ENB) (aPP-co-ENB) were prepared via metallocene catalysis. Blends of isotactic poly(propylene) (iPP) and the aPP-co-ENB rubbers show a very high compatibility before cross-linking, which leads to a refinement of the morphology after dynamic vulcanization in comparison to traditional TPVs based on iPP and ethylene-propylene-diene (EPDM) rubber. The aPP-co-ENB-based TPVs show improved tensile properties, while the relatively high glass transition temperature (T_g) of the rubber phase retards the elastic recovery after deformation at room temperature. Oil extension broadens the temperature window for applications, since the T_g decreases from ~ 10 down to ~ -40 °C, and improves the elasticity of the TPVs.

3.1. Introduction

The tensile properties of thermoplastic vulcanizates (TPVs) are strongly influenced by the rubber particle size, as was first demonstrated by Coran et al.[1] and Araghi[2] for TPVs based on isotactic poly(propylene) (iPP) and ethylene-propylene-diene (EPDM) rubber. The variation in rubber particle size was accomplished by using pre-cross-linked EPDM milled to particles with different sizes[1] and by dynamic vulcanization of iPP/EPDM blends at various screw speeds[2], respectively. Both the elongation at break (EB) and the tensile strength (TS) increased by a factor of five upon decreasing the rubber particle size from 70 down to 1 μm. As discussed in Chapter 2, this substantial improvement originates mainly from the suppression of interlamellar void formation in the iPP matrix and the higher efficiency of smaller rubber particles to bring sufficient confinement to shield interactions between the formed microcracks and, thus, inhibit their coalescence. Additionally, the resistance against cavitation within the rubber phase increases with decreasing particle size, whereas the chance of reaching the critical crack size upon internal void formation decreases. In addition to the improved tensile properties, an enhancement of the elastic recovery and an increase in the melt viscosity were observed with decreasing rubber particle size. Based on these results, it is envisioned that TPVs with sub-μm rubber dispersions have superior solid state properties.

Commercial TPVs are usually based on blends of iPP and EPDM rubber and are prepared via dynamic vulcanization, where the elastomer is selectively cross-linking during melt mixing with the thermoplastic, typically leading to rubber particle sizes in the μm-range[1-4]. It has even been stated that the preparation of TPVs with sub-μm-sized rubber particles is impossible[4]. The potential of melt blending in order to obtain sub-μm rubber dispersions can be estimated by relations based on the dynamic equilibrium between particle break up and coalescence. Although the interplay between particle break up and coalescence during melt mixing complicates the prediction of particle sizes in concentrated polymer blends, several easily applicable models have been reported for (semi-)dilute blends[5,6]. These models are generally empirical in nature and relate the dispersed particle size ($\overline{D_n}$) to the matrix viscosity (η_m), the dispersed phase to matrix viscosity ratio (p), the shear rate ($\dot{\gamma}$) and the interfacial tension (Γ):

$$\overline{D_n} = \frac{k\Gamma(p)^n}{\eta_m\dot{\gamma}} \tag{3.1}$$

The constants k and n increase with increasing volume fraction of the dispersed phase (ϕ_d), where Everaert et al.[5] reported $k = 1.2$ and $n = 0.45$ for very dilute blends ($\phi_d = 0.01$) and Wu[6] reported $k = 4.0$ and $n = 0.84$ for semi-dilute blends ($\phi_d = 0.15$). This relation covers the general trend of

decreasing $\overline{D_n}$ with increasing η_m and $\dot{\gamma}$ and decreasing Γ and p for polymer blends in the absence of cross-linking. Applying equation 3.1 for $\phi_d = 0.15$ with $\Gamma = 0.58$ mN/m[7-9], $p = 2.5$, $\eta_m = 300$ Pa.s and $\dot{\gamma} = 50$ s^{-1} as representative values for melt blending of iPP/EPDM in an extruder leads to $\overline{D_n} = 0.33$ μm. Upon increasing ϕ_d, extensive coalescence of the particles typically results in an increased $\overline{D_n}$ and to the formation of a co-continuous morphology if ϕ_d approaches 0.50[10-12]. Since ϕ_d is low in comparison to the typical values for TPVs with relatively low hardness and high elasticity ($\phi_d > 0.50$), the value of 0.33 μm is considered as the lower limit of the attainable rubber particle size in the physical blend. As discussed in Chapter 1, the morphology development of TPVs prepared by dynamic vulcanization is mainly determined by the break-up process, since coalescence of the rubber particles is suppressed by the cross-linking reactions. Nevertheless, the general trend for polymer blends as indicated by equation 3.1 is also applicable to TPVs, since it has been reported that $\overline{D_n}$ decreases with increasing η_m and $\dot{\gamma}$ [2] and decreasing Γ [13,14] and p [15].

This chapter discusses the potential of highly compatible thermoplastic/elastomer combinations for the preparation of sub-μm TPVs via dynamic vulcanization. The increased blend compatibility is achieved by replacing the EPDM rubber in traditional iPP/EPDM-based TPVs by an atactic PP (aPP) rubber, which contains ENB groups to enable cross-linking. The chemical similarity between the aPP-*co*-ENB rubber (which was prepared via metallocene catalysis) and iPP results in a very small Γ and, therefore, the system is not only highly compatible but may even be partially miscible in the melt. Besides the expected refinement of the morphology after dynamic vulcanization, the improved interfacial adhesion may also contribute to an enhancement of the mechanical properties.

First, the physical properties of the aPP-*co*-ENB rubbers are discussed. The influence of the ENB content on the thermal stability, the T_g and the molar mass of the rubber (in comparison to a commercial EPDM rubber) are studied via thermogravimetric analysis (TGA), differential scanning calorimetry (DSC) and size exclusion chromatography (SEC). Transmission electron microscopy (TEM), small-angle X-ray scattering (SAXS) and isothermal crystallization studies with DSC are used to explain the differences in compatibility between the iPP/aPP-*co*-ENB and iPP/EPDM blends. Subsequently, the morphology, the cross-link density and the mechanical properties of the corresponding TPVs are discussed.

3.2. Experimental

3.2.1. Materials

iPP (MFI = 2.0 g/10 min, ρ = 0.905 g/cm^3) was supplied by Sabic Europe, the Netherlands. ENB-containing EPDM rubber (ENB content = 8.9 wt%, ethylene content = 48 wt%, M_w = 245 kg/mol, M_w/M_n = 3.4, ML(1+4) 125 °C = 65) was supplied by DSM Elastomers, the Netherlands. The phenolic-based anti-oxidant Irganox 1010 was supplied by Ciba Specialty Chemicals, Switzerland. The phenolic resin R7530 (resol; Arkema, France) and tin chloride dihydrate (SnCl$_2$·2H$_2$O; Evonik, Germany) were used as curatives and a white, aliphatic oil was used for oil extension. Cyclohexane, methanol (MeOH), diethylether, ethanol and hydrochloric acid (HCl) (all from Aldrich) were used as received. *N,N'*-bis(2,6-dimethylphenyl)ethylenediamine, 1,3-bis-(2,6-dimethylaniline)-2-imino-imidazolidin and the pre-catalyst Cp*[1,3-(2,6-Me$_2$C$_6$H$_3$)$_2$C$_2$H$_4$N$_2$C=N]TiCl$_2$ were prepared according to procedures reported earlier[16-18]. Toluene (Aldrich) was dried over an alumina column. ENB (Aldrich) was purified over neutral alumina, degassed and poured over molecular sieves prior to use. 2,6-di-*tert*-butyl-4-methylphenol (BHT; Aldrich), Cp*TiCl$_3$ (Strem) and methylaluminoxane (MAO; Chemtura, USA) were used as received.

3.2.2. Synthesis of aPP-*co*-ENB

aPP-*co*-ENB was prepared by titanium-catalyzed olefin copolymerization. A 250 mL three-necked round-bottom flask was placed under an atmosphere of propylene (1 bar) and charged with toluene (150 mL), MAO (Al/Ti = 500 mol/mol), BHT (Al/BHT = 2/1 mol/mol) and the desired amount of ENB. The solution was mechanically stirred at 750 rpm for 15 min at room temperature. The precatalyst (100 μmol) in toluene (15 mL) was added to the mixture and the reaction was allowed to proceed for 30 min. The obtained polymer was precipitated with a MeOH/HCl (550/50 v/v) mixture, was dissolved in toluene (200 mL) and was precipitated into MeOH/HCl. Further purification was performed by dissolution in diethylether (300 mL), followed by precipitation, washing with ethanol (600 mL) and drying at 60 °C for 18 hrs under reduced pressure before the final mass was weighed. The rubbers are coded as aPP-*co*-ENB[x], where x indicates the ENB content in the rubber in wt%.

3.2.3. Blend preparation

Physical blends of iPP and rubber were prepared by mixing the blend components in a home-built, recirculating, twin-screw micro-extruder with an internal volume of 5 cm^3. TPVs were prepared by dynamic vulcanization of iPP/rubber blends in the micro-extruder (Fig. 3.1). The total batch size was approximately 6 g and the formulation of the TPVs consists of 100 phr (part per hundred rubber) of rubber, 43 or 100 phr iPP, 0.3 phr stabilizer, 3.0 phr resol and 2.0 phr SnCl$_2$·2H$_2$O. Some of the TPVs were extended with 100 phr oil, i.e. an oil-to-rubber ratio of 1. In the remainder of the study, the iPP, rubber and oil contents in the TPVs are indicated in wt%.
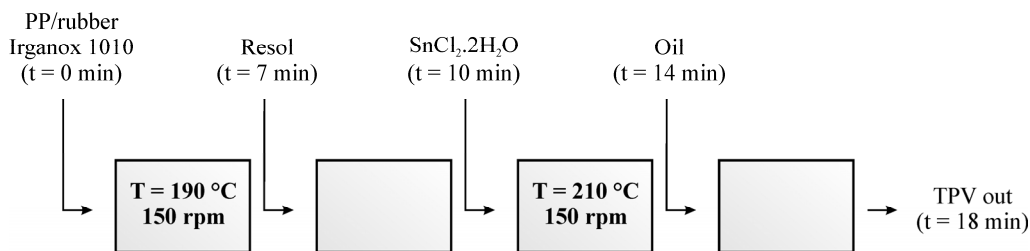
Fig. 3.1. Preparation conditions of TPVs.

3.2.4. Characterization techniques

[1]H nuclear magnetic resonance (^{1}H NMR) spectroscopy. To quantify the ENB content of the rubbers, solution ^{1}H NMR spectra were recorded on a Varian 400 MHz spectrometer at 25 °C and at a resonance frequency of 400.164 MHz. 15 mg of polymer was dissolved in 0.8 mL deuterated chloroform (CDCl$_3$; Aldrich), which contained 0.03 vol% tetramethylsilane (TMS) as internal standard. The spectra were acquired using 32 scans, a delay time of 5 s and a total number of data points of 64 k. The ENB content is calculated according to equation 3.2:

$$ENB\ (wt\%) = \frac{M_{ENB}}{\left(\dfrac{\alpha}{\left[(4 \times m_e) + (6 \times m_p)\right]\beta}\right) \times \left[(M_e \times m_e) + (M_p \times m_p)\right] + M_{ENB}} \times 100\% \qquad (3.2)$$

where M_{ENB}, M_p and M_e are the molar masses of ENB (120 g/mol), propylene (42 g/mol) and ethylene (28 g/mol), respectively. m_e and m_p are the molar ratios of ethylene and propylene in the rubber, viz. respectively 0.58 and 0.42 for EPDM and 0 and 1 for aPP-*co*-ENB. α is the integral of the aliphatic region ($\delta = 0.5 - 1.7$ ppm) and β is the integral of the ENB region ($\delta = 5.0 - 5.5$ ppm).

Thermogravimetric analysis (TGA). To determine the thermal stability of the non-stabilized aPP rubbers, thermogravimetric analysis (TGA) was performed on a TA Q500 instrument (TA Instruments). Samples with a typical weight of 5 mg were heated with 10 °C/min to 700 °C in an air atmosphere.

Differential scanning calorimetry (DSC). The thermal behavior of the rubbers was studied using a TA Instruments Q1000 calorimeter. Hermetically sealed aluminum pans were used with a typical sample weight of 5 mg. The samples were first heated to 140 °C and equilibrated for 5 min in order to remove the thermal history. Subsequently, they were cooled at a rate of 10 °C/min to -90 °C, where they were kept for 5 min, and then reheated to 140 °C at a rate of 10 °C/min. The glass transition temperature (T_g) was determined from the inflection point observed during the second heating run.

Size exclusion chromatography (SEC). The molar mass distribution of the rubbers was determined relative to poly(styrene) (PS) standards by using a Waters model 510 pump and a Waters 712 WISP chromatograph with PL-gel mix D columns (300 x 7.5 mm, Polymer Laboratories). THF was used as eluent with a flow rate of 1 mL/min. The samples were diluted to 1 mg/mL and filtered by using 0.2 μm syringe filters.

Transmission electron microscopy (TEM). Morphological investigations were performed with a Tecnai 20 transmission electron microscope operated at 200 kV. Samples were trimmed at -100 °C and

subsequently bulk-stained for 24 hrs with a ruthenium tetroxide (RuO$_4$) solution prepared according to Montezinos *et al.*[19]. Ultrathin sections (70 nm) were obtained at -100 °C by using a Leica UltracutS/FCS microtome. The sections were placed on a 200 mesh copper grid with a carbon support layer.

Small-angle X-ray scattering (SAXS). Single-shot SAXS measurements were performed during tensile testing at the Dutch-Belgian (DUBBLE) beamline BM26 of the European Synchrotron Radiation Facility (ESRF) in Grenoble, France. The size of the X-ray beam was approximately 200 x 200 μm^2 with a wavelength of 1.203 Å. A 2D multiwire gas-filled detector was used with 512 x 512 pixels and a pixel size of 260 x 260 μm^2 at a sample-detector distance of 3200 mm.

Cross-link density. The rubber gel content (*%gel*) and the degree of swelling (*%swell*) where used as measured for the cross-link density of the rubber phase of the TPVs. Compression-molded films of the TPVs were extracted and swollen in cyclohexane at room temperature for 48 hrs and were subsequently dried for 5 hrs at 100 °C under vacuum. The *%gel* and *%swell* are calculated by the following equations:

$$\%gel = \frac{m_{residue} - (m \times \phi_{insol})}{m \times \phi_{rubber}} \times 100\% \tag{3.3}$$

$$\%swell = \frac{m_{swollen} - (m \times \phi_{insol})}{m \times \phi_{rubber} \times (\%gel/100)} \times 100\% \tag{3.4}$$

where $m_{residue}$ is the weight of the dried sample after extraction, m is the weight of the sample before extraction, ϕ_{insol} is the mass fraction of insoluble components (e.g. PP and resol), ϕ_{rubber} is the mass fraction of rubber and $m_{swollen}$ is the weight of the swollen sample.

Dynamic mechanical thermal analysis (DMTA). Compression-molded samples (10.0 x 3.0 x 0.5 mm) were measured on a TA Instruments DMA Q800 with a film tension setup. Temperature sweeps from -100 to 200 °C were performed with a heating rate of 3 °C/min at a frequency of 1 Hz. A pre-load force of 0.01 N, an amplitude of 10 μm and a force track of 110 % were used. The glass transition temperature (T_g) was determined from the maximum in the loss modulus (E'').

Tensile testing. Films with a thickness of 1 mm were compression molded at 180 °C and 100 bar from which dumbbell-shaped tensile bars (15 x 5 x 1 mm) were punched. Tensile tests were performed at a cross-head speed of 20 mm/min using a 100 N force cell on a Zwick Z010 tensile tester according to ASTM D412[20]. The equipment was controlled with the TestXpert v7.11 software. Each sample was tested in at least 5-fold and average values are presented.

Compression set. The compression set (*CS*) was measured on cylindrical samples with a diameter of 13 mm and a thickness of 6 mm at 25 % compressive deformation for 22 hrs and a relaxation time of 30 min (all at room temperature), according to ASTM D395[21]. The *CS* was calculated as follows:

$$CS = \frac{(t_i - t_o)}{(t_i - t_n)} \times 100\% \tag{3.5}$$

where t_i is the initial thickness of the sample, t_o the final thickness of the sample and t_n the thickness of the spacer.

3.3. Results and discussion

3.3.1. Characterization of aPP-*co*-ENB rubber

The quantification of the ENB content in the aPP-*co*-ENB rubbers is performed by ^{1}H NMR spectroscopy. A commercial EPDM rubber with an ENB content of 8.9 wt% is measured as a control sample. Fig. 3.2a depicts the ^{1}H NMR spectra of EPDM, aPP and two aPP-*co*-ENB rubbers, where the resonances of the aliphatic CH, CH_2 and CH_3 units are clearly visible at $\delta =$ 0.5 – 1.7 ppm. Fig. 3.2b shows the magnification of the ^{1}H NMR spectra in the $\delta =$ 4.5 – 5.5 ppm range. The H-atom at C8 of the ENB unit shows two resonances at $\delta =$ 5.3 and 5.1 ppm in a 3:1 ratio, reflecting the *E:Z* conformational ratio of the methyl group in the ENB monomer. The diene concentration can be calculated by evaluation of the integrated intensities of the aliphatic region at $\delta =$ 0.5 – 1.7 ppm and the ENB region, according to equation 3.2. The ENB content of the reference EPDM was calculated to be 9.3 wt%, which is in good agreement with the value of 8.9 wt% as indicated by the supplier. The ENB content in the aPP-*co*-ENB rubbers increases linearly from 0 to 10.2 wt% upon increasing the ENB/toluene volume ratio from 0 to $1.2 \cdot 10^{-2}$ during the metallocene-catalyzed copolymerization. Since no resonances are observed at $\delta \sim$ 6.3
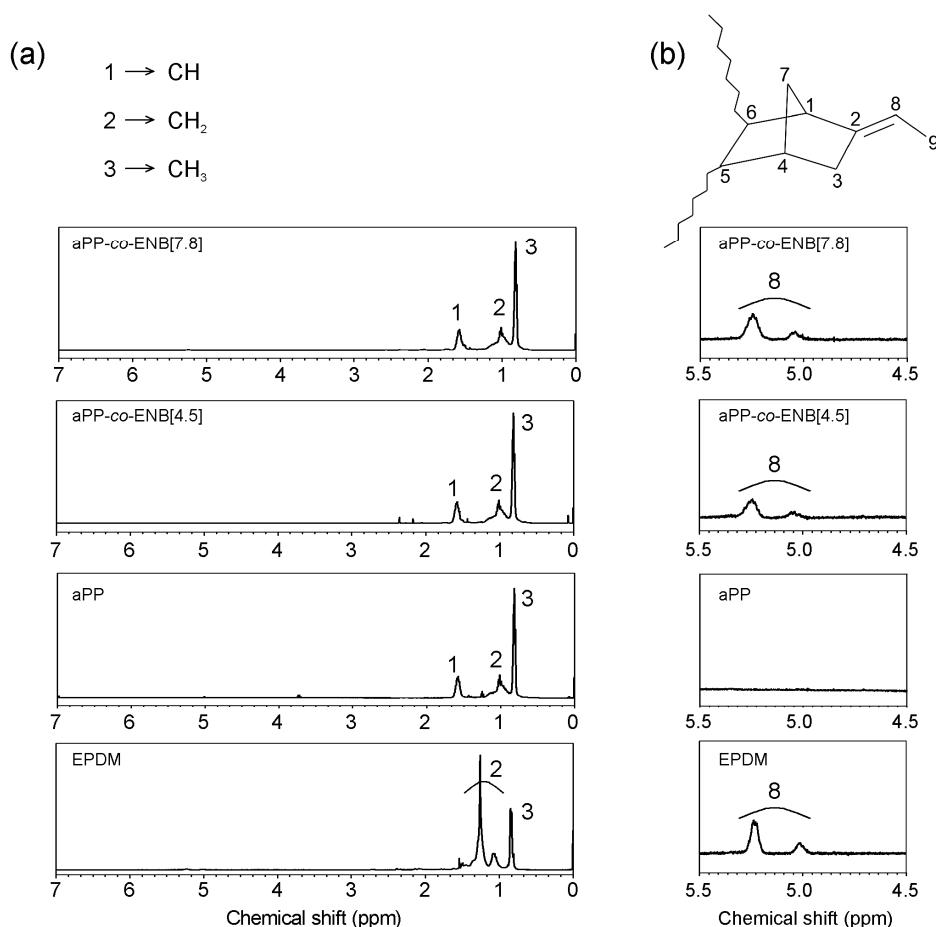
Fig. 3.2. ^{1}H NMR spectra of EPDM, aPP and aPP-co-ENB rubbers.

ppm (H-atoms of C5 and C6 of ENB), it can be concluded that the ENB monomer is incorporated into the aPP polymer chain only via the norbornene unsaturation.

T_g of the rubbers was determined by DSC (Fig. 3.3 and Table 3.1). Incorporation of the relatively rigid ENB groups into the aPP backbone leads to an increase in T_g from -2.4 °C for aPP up to 6.8 °C for aPP-*co*-ENB[10.2]. Obviously, these T_g's are substantially higher than that of EPDM (-49.2 °C). The absence of a melting endotherm upon heating from -90 to 140 °C indicates that all rubbers are fully amorphous. This was supported by wide-angle X-ray diffraction (WAXD) measurements, which only showed an amorphous halo.
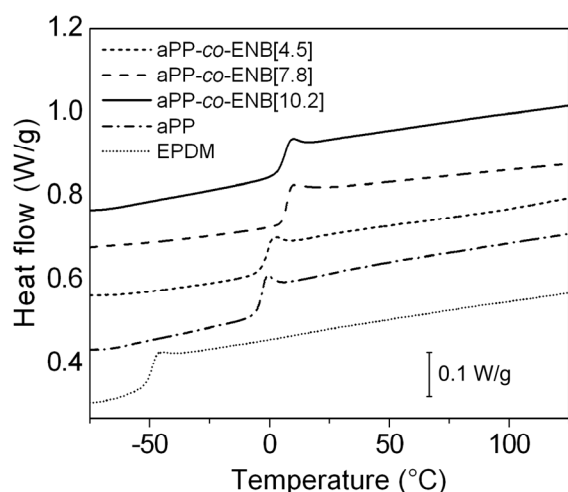
Fig. 3.3. DSC curves of EPDM, aPP and aPP-co-ENB rubbers.
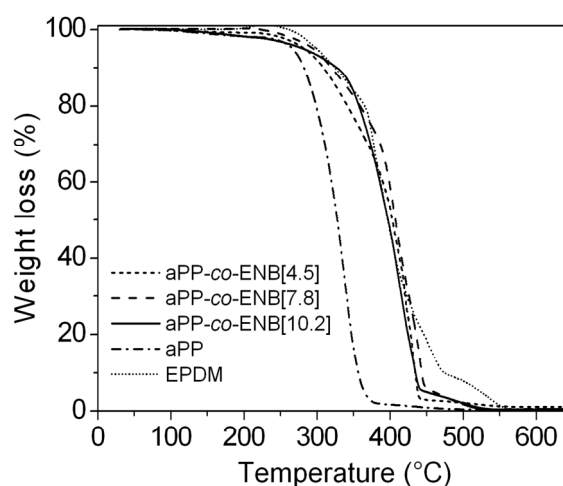
Fig. 3.4. TGA curves of EPDM, aPP and aPP-co-ENB rubbers.

The thermal stability of the aPP rubbers was determined by TGA and was compared to the thermal stability of the commercial EPDM rubber (Fig. 3.4 and Table 3.1). It is noted that the EPDM rubber contains stabilizers, while the aPP rubbers are not stabilized. The temperature at which a weight loss of 1 % is reached ($T_{1\%}$) exceeds 200 °C for all rubbers, indicating that only a minute amount of residual volatiles from the polymerization process, such as ENB, water, methanol and/or toluene, are present. Although TGA analysis only allows for the determination of the degradation temperature at which volatiles start to be formed (which may be significantly higher than the temperature where actual break-down of the molar mass starts), the temperature at which a weight loss of 5 % is reached ($T_{5\%}$) can be used as a measure for the thermal stability of the polymers. $T_{5\%}$ equals 299 °C for the commercial EPDM rubber and 267 °C for the aPP rubber and increases with the ENB content up to 296 °C for the aPP-*co*-ENB[10.2] rubber. Based on these results, no complications with degradation of the rubbers are expected during melt blending with iPP at temperatures ≤ 210 °C, especially since an anti-oxidant is added.

The number-averaged and weight-averaged molar masses (M_n and M_w, respectively) relative to PS standards and the polydispersity index (*PDI*) of the rubbers, as determined by SEC, are summarized in Table 3.1, together with the results of the DSC and TGA measurements. M_w

decreases with increasing ENB content from 258 kg/mol for aPP to 167 kg/mol for aPP-*co*-ENB[10.2]. A similar trend is observed for M_n, resulting in an approximately constant *PDI*. A similar decrease in molar mass was reported for metallocene-catalysed co-polymerization of ethylene and ENB, which was related to the termination by chain transfer coming from a species in which ENB is the last-inserted species[22]. The molar masses of the aPP-*co*-ENB copolymers are in the same range as that of the EPDM.

Table 3.1. Properties of EPDM, aPP and aPP-co-ENB rubbers.

Sample	T_g (°C)	5% weight loss temperature (°C)	M_n (kg/mol)	M_w (kg/mol)	PDI (-)
EPDM	-49.2	299	142	380	2.7
aPP	-2.4	267	128	258	2.0
aPP-*co*-ENB[4.5]	0.3	270	142	302	2.1
aPP-*co*-ENB[7.8]	6.0	296	104	219	2.1
aPP-*co*-ENB[10.2]	6.8	282	89	167	1.9

The results presented in Figs. 3.2-3.4 and Table 3.1 show that the aPP-*co*-ENB rubbers have physical properties that are similar to the commercial EPDM rubber, with the exception of T_g. The EPDM rubbers that are used in commercial PP/EPDM-based TPVs typically contain 4-9 wt% ENB and have a M_w of 200-500 kg/mol. Based on the ENB content and the molar masses, the aPP-*co*-ENB[4.5] and aPP-*co*-ENB[7.8] rubbers are most similar to the EPDM rubbers used in commercial TPVs and are, therefore, used during the remainder of this study.

3.3.2. Compatibility of iPP/aPP-*co*-ENB blends

Although iPP/EPDM blends are generally considered as being compatible, yet immiscible[23], several authors demonstrated a (partial) miscibility of iPP/EPDM blends in the melt[24,25]. The origin of this disagreement can be explained by the small region of miscibility, which is located above T_m of iPP and below the thermodynamic miscibility gap of the blend (gray area in Fig. 3.5), the latter being characterized by a Lower Critical Solution Temperature (LCST) at a composition ratio close to unity[24,25]. Since the binodal conditions of the miscibility gap cross T_m (i.e. LCST < T_m) over a broad composition range, miscibility can only be observed at low and high iPP contents. Additionally, the miscibility gap is highly dependent on the molecular structure of EPDM (e.g. ENB content, ethylene/propylene ratio and branching content) and the molar mass (distribution) of both blend components. Therefore, miscibility of iPP/EPDM blends is rarely observed in practice under standard processing conditions.
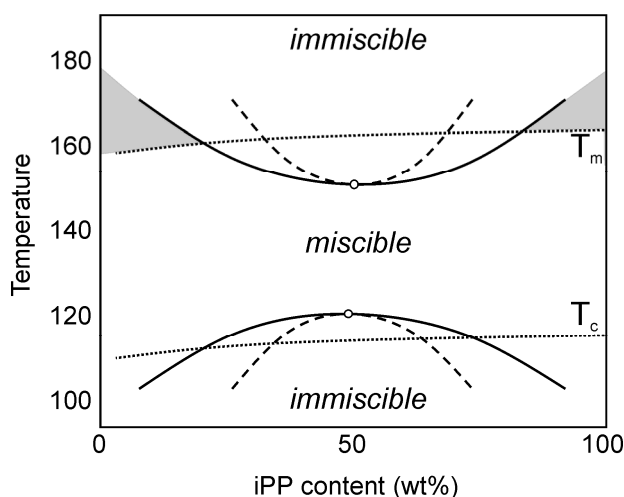
Fig. 3.5. Schematic phase diagram of iPP/EPDM blends (partially reproduced from refs. 24 and 25), where the gray area represents the miscible region. Solid and dashed lines represent binodal and spinodal conditions, respectively and dotted lines represent T_m and T_c of iPP in the blend.

The compatibility and miscibility of PP of varying stereoregularity has recently gained attention because of the tremendous developments in the field of synthesis of stereoregular polymers by the introduction of single-site metallocene catalysts[26]. Although it may be expected that polymers with a similar chemical structure are fully miscible in the melt, it was shown that small changes in the microstructure, molar mass and *PDI* of the blend components may lead to demixing[27-30]. This probably explains why iPP/aPP blends have been reported to be miscible[27], partially miscibile[30,31] or immiscibile[29]. It is noted that the aPP that is reported to be miscible with iPP is often obtained as the heptane-soluble fraction of iPP, which also contains isotactic sequences[32]. Additionally, it is difficult to study the miscibility of iPP/aPP blends, since the blend components possess similar physical properties, such as electron density, scattering length density, refractive index and T_g.

Fig. 3.6 compares the influence of the type of rubber on the morphology of iPP/rubber blends containing 50 wt% of rubber, where the dark regions represent the rubber phase and the light regions the iPP phase. For both blends, the TEM images show a co-continuous morphology after crystallization from the melt, which is typical for 50/50 blends of polymers with similar viscosities[33,34]. The iPP/EPDM blend shows a coarse, co-continuous morphology with a characteristic length scale in the order of 1 μm. The iPP/aPP-*co*-ENB blend, on the other hand, shows a much finer co-continuous morphology with a characteristic length scale in the order of 100 nm. Very similar morphologies were obtained for ENB contents of 4.5 and 7.8 wt%. The refinement of the morphology is a direct result of the higher compatibility of iPP with aPP-*co*-ENB in comparison to EPDM. Cross-hatched lamellae, which are typically observed for iPP, are clearly visible in Fig. 3.6c, which also shows that the crystalline lamellae penetrate into the rubber phase. Although this is also observed for the iPP/EPDM blend, it is more distinct for the

iPP/aPP-*co*-ENB blends. The interphase material that consists of both iPP and aPP-*co*-ENB is not formed due to co-crystallization of the rubber with the iPP, as will be discussed further on. This observation supports the earlier conclusion on the increased compatibility of the iPP/aPP-*co*-ENB blend, since the thickness of the interface layer (λ) scales with the blend compatibility via $\lambda \propto (\chi)^{-1/2}$, with χ the Flory-Huggins interaction parameter[35]. A very rough estimation of λ from the TEM images indicates $\lambda \sim 20$ nm for the iPP/EPDM blend and $\lambda \sim 35$ nm for the iPP/aPP-*co*-ENB blend. The corresponding Flory-Huggins interaction parameter (χ) can then be calculated according to ref. 35 and is $1.4 \cdot 10^{-3}$ for iPP/EPDM and $0.6 \cdot 10^{-3}$ for iPP/aPP-*co*-ENB, when using $b = 0.8$ nm and $N_A = N_B = 4000$.
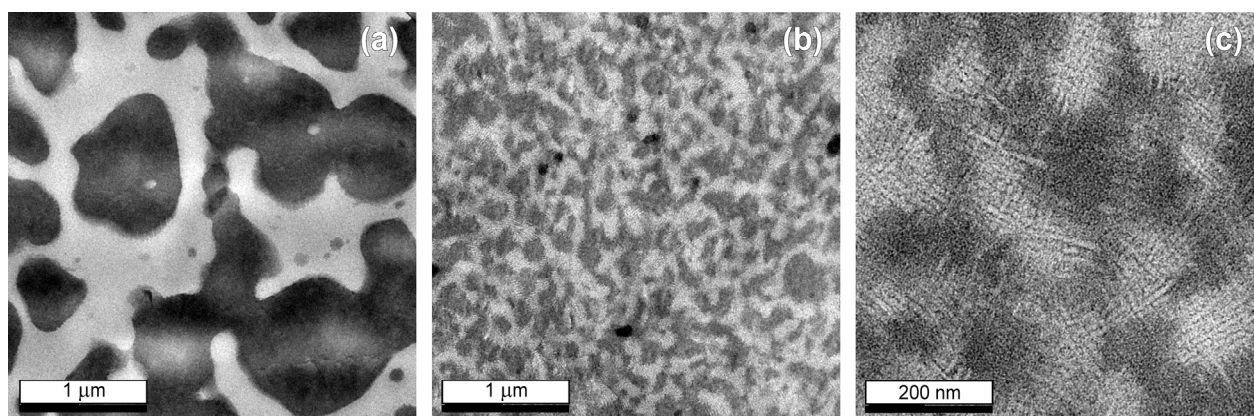
Fig. 3.6. TEM images of blends based on (a) iPP/EPDM and (b,c) iPP/aPP-co-ENB[4.5], all containing 50 wt% rubber.

The observation of a two-phase morphology does not necessarily mean that the iPP/aPP-*co*-ENB blends are immiscible in the molten state, since phase separation may be induced by crystallization of iPP upon cooling. Small-angle X-ray scattering (SAXS) studies on iPP/aPP and iPP/aPP-*co*-ENB blends prepared under similar crystallization conditions showed a constant long period (L) of 16.2 ± 0.7 nm over the whole composition range and for ENB contents ranging from 0 to 10.2 wt%. The constant L is indicative for immiscibility of the iPP/aPP and iPP/aPP-*co*-ENB blends in the molten state. Crystallization of the iPP phase in a miscible blend with aPP-*co*-ENB would lead to incorporation of the aPP-*co*-ENB into the amorphous iPP phase[31], leading to an increased L.

Shanks *et al.*[36] demonstrated that the miscibility of blends based on iPP and poly(ethylene) (PE) is conveniently determined by studying the crystallization kinetics of iPP in the blend at temperatures below T_m of iPP, but above T_c of PE. For immiscible blends, the crystallization half-time ($\tau_{1/2}$) of iPP is similar to that of pure iPP. Crystallization of iPP from a miscible blend, however, showed a dramatic increase in $\tau_{1/2}$, since the iPP now crystallizes from a (semi-)dilute solution/melt. The $\tau_{1/2}$ for pure iPP and blends of iPP/aPP-*co*-ENB[4.5], as determined from the Avrami analysis[37] of isothermal crystallization experiments, does not increase with the aPP-*co*-

ENB[4.5] content (Fig. 3.7). In fact, $\tau_{1/2}$ decreases slightly with increasing rubber content, which may be attributed to nucleating effects of aluminum-based residuals ($\sim$ 0.1-0.2 wt% as determined by X-ray photoelectron spectroscopy). Additionally, similar values for the rate constant $K(T)$ and the constant n, which depends on the mechanism of nucleation and the geometry of crystal growth, were obtained..

It can be concluded that the iPP/aPP-*co*-ENB blends, as used for the preparation of TPVs show an improved compatibility in comparison to iPP/EPDM blends, but immiscible, since the blends show *(i)* a two-phase morphology at room temperature, *(ii)* no changes in the crystalline long period, and *(iii)* no changes in crystallization kinetics.
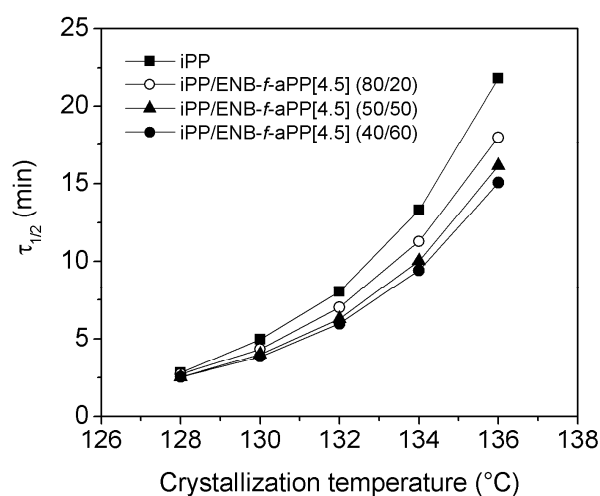
Fig. 3.7. iPP crystallization half-time ($\tau_{1/2}$) as a function of the crystallization temperature for iPP and blends of iPP/aPP-co-ENB[4.5] with varying blend compositions.

3.3.3. Preparation of TPVs based on iPP and aPP-*co*-ENB

Fig. 3.8 shows the morphologies of TPVs based on EPDM and aPP-*co*-ENB[7.8] rubber, where the dark regions represents the rubber phase and the light regions the iPP phase. The elongational and shear forces applied to the blends containing 50 wt% of rubber (Figs. 3.6a and b) during dynamic vulcanization lead to break-up of the rubber phase and to a dispersion of cross-linked rubber particles in the iPP matrix (Figs. 3.7a and c). It is difficult to determine the absolute particle size ($\overline{D_n}$) and its distribution of the TPVs at these high rubber contents, since the separate particles may appear connected or overlap[38] and have an irregular shape and large size distribution without a sharp interface. However, a refinement of the morphology can clearly be observed for the iPP/aPP-*co*-ENB[7.8]-based TPVs ($\overline{D_n}$ $\sim$ 300 nm) in comparison to the iPP/EPDM-based TPVs ($\overline{D_n}$ $\sim$ 1 μm). The characteristic length scale of the iPP/aPP-*co*-ENB blend increases from $\sim$ 100 nm (Figs. 3.6b and c) up to $\sim$ 300 nm after dynamic vulcanizations (Fig. 3.8c), which may be attributed to irreversible coalescence of the particles, i.e. reacting particles coalesce and form covalent bonds, limiting their subsequent break-up[39]. Partial co-

continuity is observed for the blends with a rubber content of 70 wt% (Figs. 3.7b and d), indicating that break up of the rubber phase during dynamic vulcanization was not complete, which is quite common for rubber-rich TPVs.
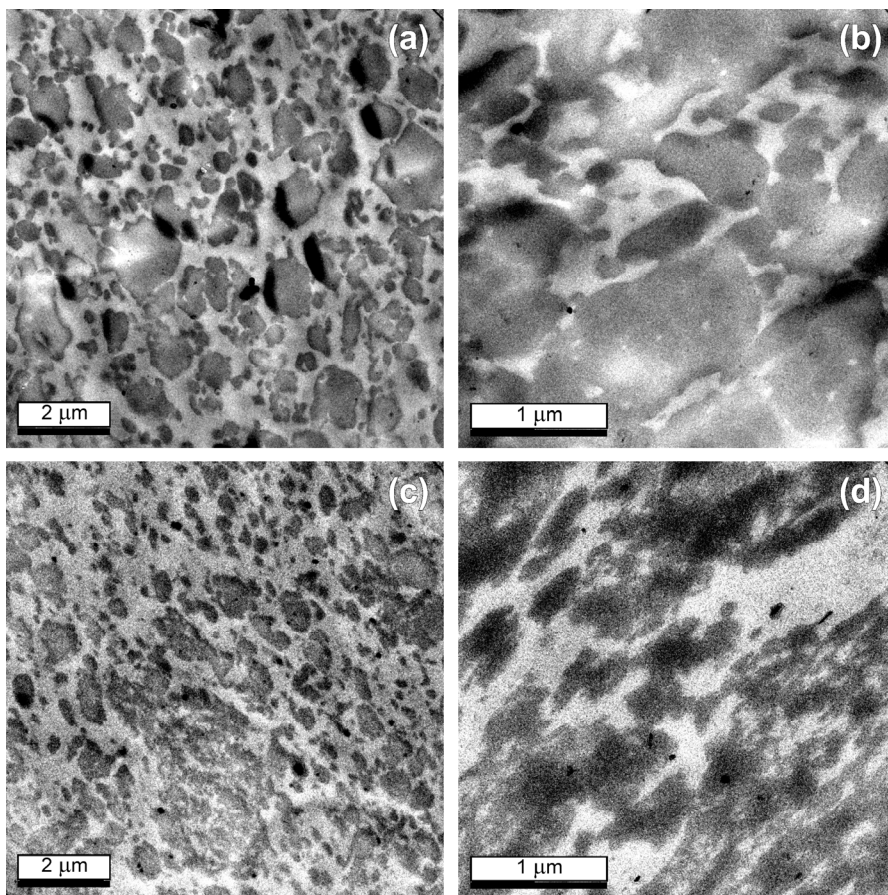
Fig. 3.8. TEM images of (a) iPP/EPDM-based TPV with 50 wt% rubber and (b) 70 wt% rubber and (c) iPP/aPP-co-ENB[7.8]-based TPVs with 50 wt% rubber and (d) 70wt% rubber.

The extent of cross-linking of TPVs is typically characterized by the rubber gel content (*%gel*) and the degree of swelling (*%swell*). The high *%gel* of close to 100 % (Table 3.2) indicates that hardly any EPDM chains can be extracted from the sample, indicating that high degrees of cross-linking were achieved. Generally, *%swell* is indicative for the cross-link density of the EPDM phase, since the equilibrium amount of solvent that can be absorbed by a cross-linked network decreases with cross-link density. The slightly lower *%gel* and higher *%swell* of the aPP-*co*-ENB-based TPVs suggests a slightly lower cross-link density in comparison to the EPDM-based TPVs. The cross-link density of the rubber phase is determined by the total number of chemical cross-links and trapped chain entanglements, with the latter depending on the entanglement density of the rubber during cross-linking. Since the molar mass between entanglements (M_e) of aPP (3.5-5.8 kg/mol[40,41]) is reported to be higher than the M_e of ethylene-propylene rubber (1.8-2.9 kg/mol[41]), a somewhat lower overall cross-linking density of the aPP-based rubbers is expected in comparison to the EPDM rubber at a similar ENB content. However, comparison of %swell of EPDM and aPP-*co*-ENB-based TPVs should be done with care, since χ

of EPDM/cyclohexane may be slightly different from that of aPP-*co*-ENB/cyclohexane, which may lead to differences in the equilibrium *%swell* at constant cross-link densities.

Table 3.2. %gel and %swell of EPDM and aPP-co-ENB[7.8]-based TPVs.

Type of rubber	iPP content (wt%)	Rubber content (wt%)	%gel (%)	%swell (%)
EPDM	50	50	98.3	381
EPDM	30	70	97.1	405
aPP-*co*-ENB[7.8]	50	50	97.3	406
aPP-*co*-ENB[7.8]	30	70	96.4	453

3.3.4. Mechanical properties

Fig. 3.9 shows the storage and loss moduli (*E'* and *E''*, respectively) as a function of temperature for the EPDM and aPP-*co*-ENB[7.8]-based TPVs, which clearly shows the difference in the glass transition temperature (T_g) between EPDM and aPP-*co*-ENB[7.8]. The EPDM-based TPVs show a T_g at approximately -47 and 3 °C corresponding to the EPDM and the amorphous iPP phase, respectively. The aPP-*co*-ENB[7.8]-based TPVs show a single T_g at approximately 10 °C, which originates from the overlapping, individual T_g's of the aPP-*co*-ENB[7.8] rubber and the amorphous iPP phase at ~ 6 and ~ 10 °C, respectively. The somewhat higher *E'* of the EPDM-based TPVs above room temperature is explained by the slightly higher cross-link density in comparison to the aPP-*co*-ENB[7.8]-based TPVs at equal rubber contents.
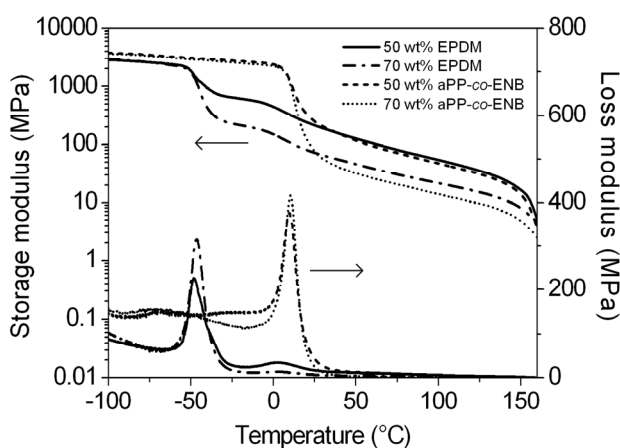
Fig. 3.9. DMTA curves of EPDM and aPP-co-ENB[7.8]-based TPVs.
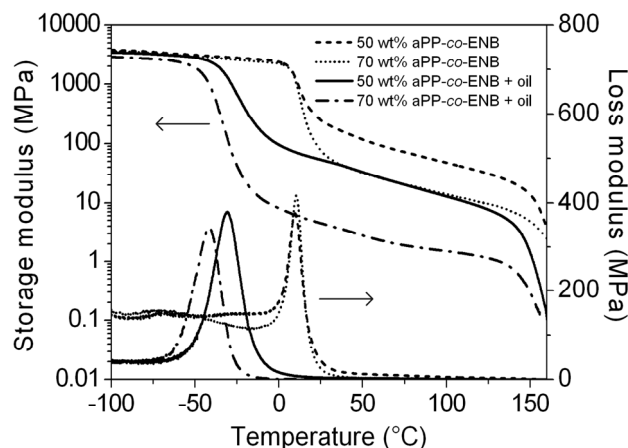
Fig. 3.10. DMTA curves of aPP-co-ENB[7.8]-based TPVs with and without oil.

The temperature window for TPV applications is typically limited to temperatures between the T_g of the rubber and/or thermoplastic phases at the lower side and the T_m of the thermoplastic matrix at the higher side. A decrease in elasticity is typically observed below T_g due to the

decrease in mobility. Upon approaching T_m, the TPV will lose its dimensional stability due to softening and, eventually, melting of the thermoplastic matrix resulting in a decreased elasticity. The relatively high T_g of the aPP-*co*-ENB rubbers, therefore, narrows the temperature window for applications of the corresponding aPP-*co*-ENB-based TPVs. However, the addition of processing oil, which is usually added to commercial TPVs to reduce the melt viscosity, the hardness and the materials costs, leads to a significant decrease in the T_g of the aPP-*co*-ENB[7.8]-based TPVs (Fig. 3.10 and Table 3.3). A decrease in the overlapping iPP and rubber T_g from 10 °C down to -30 °C and -41 °C is observed after oil extension at rubber contents of 50 and 70 wt%, respectively. This indicates that the oil resides in the amorphous iPP phase as well as in the cross-linked rubber phase, similar to the case of conventional PP/EPDM-based TPVs[42]. Obviously, oil extension results in softening, leading to a decrease in the storage modulus above T_g.

Table 3.3. Glass transition temperature (T_g) of rubber and iPP phases in TPVs.

Type of rubber	*iPP content (wt%)*	*Rubber content (wt%)*	*Oil content (wt%)*	*T_g rubber (°C)*	*T_g iPP (°C)*
EPDM	50	50	0	-48.1	2.2
EPDM	30	70	0	-46.3	3.9
aPP-*co*-ENB[7.8]	50	50	0	9.9	
aPP-*co*-ENB[7.8]	30	70	0	10.3	
aPP-*co*-ENB[7.8]	33	33	33	-30.5	
aPP-*co*-ENB[7.8]	18	41	41	-41.4	

Previous research indicated an enhancement of the tensile properties with decreasing rubber particle size[1,2] and increasing interfacial adhesion[13]. So the refinement of the morphology of the aPP-*co*-ENB-based TPVs in comparison to the EPDM-based TPVs may lead to an improved tensile behavior. Fig. 3.11 compares the tensile curves of the various TPVs and Table 3.4 summarizes their mechanical properties. A decrease in hardness, *EB* and *TS* is observed with increasing rubber content from 50 to 70 wt%, which is a trend typically observed for TPVs. Partial co-continuity of the TPVs containing 70 wt% rubber may contribute to the significant decrease in *E* upon increasing the rubber content from 50 to 70 wt%. The aPP-*co*-ENB-based TPVs show a lightly lower E in comparison to the EPDM-based TPVs, which is in agreement with the DMTA results (Fig. 3.9). A clear improvement of the tensile properties is indeed observed for the aPP-*co*-ENB[7.8]-based TPVs, which show a higher *EB* and *TS* in comparison to the EPDM-based TPVs. Oil extension leads to a decrease in hardness, *E*, *EB* and *TS*, which is in good agreement with the work presented by Medintseva *et al.*[43].
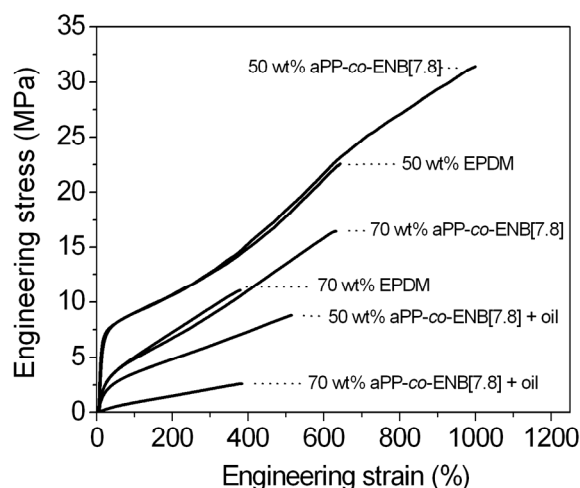
Fig. 3.11. Tensile curves of EPDM and aPP-co-ENB[7.8]-based TPVs before and after oil extension.

The compression set (*CS*) is a practical measure for the elastic behavior of cross-linked rubbers and TPVs. Low *CS* values indicate low permanent set, i.e. a good elastic recovery, while high *CS* values indicate poor elastic recovery. A low *CS* is obtained when little plastic deformation occurs during the compression step and a good recovery occurs after unloading. *CS* decreases with increasing rubber content (Table 3.4), since the increasing amount of the elastic rubber phase in the TPVs promotes the elastic recovery of the TPV as a whole. The results presented in Chapter 2.3.5 showed an improvement of *CS* with decreasing rubber particle size. However, lower CS values are obtained for the EPDM-based TPVs in comparison to the aPP-*co*-ENB[7.8]-based TPVs as measured after 30 min of relaxation (*CS$_{30}$*). These higher values are explained by the relatively high *T$_g$* of the aPP-*co*-ENB[7.8] close to the temperature of the *CS* measurement, which retards the strain recovery of the TPVs after releasing the compressive strain due to the low mobility of the rubber phase. As the strain relaxation process proceeds with time, *CS* of both the EPDM and aPP-*co*-ENB[7.8]-based TPVs decreases. After a relaxation time of ~ 20 days (*CS$_\infty$*), the changes in *CS* with time are marginal and approach the experimental error. After such long relaxation times, similar *CS* values are obtained for the EPDM and aPP-*co*-ENB[7.8]-based TPVs, which only depend on the amount of rubber. This supports the hypothesis that the higher *CS$_{30}$* of the aPP-*co*-ENB[7.8]-based TPVs originates from a retardation of the recovery process. In addition, the slightly lower cross-link density of the aPP-*co*-ENB-based TPVs contribute to a higher *CS* value in comparison to the EPDM-based TPVs. Oil extension of the TPVs leads to significantly lower *CS*, which is attributed to an increased relaxation rate. Additionally, the stress level required to deform a TPV to a certain macroscopic strain decreases with increasing oil content, which means that the PP phase in the TPV is subjected to a lower stress level. This leads to a decrease in the extent of plastic deformation of the PP phase during the compression step and, consequently, to lower *CS* values.

Table 3.4. Mechanical properties of EPDM and aPP-co-ENB-based TPVs.[a]

Type of rubber	iPP (wt%)	Rubber (wt%)	Oil (wt%)	E (MPa)	EB (%)	TS (MPa)	Hardness (Shore D)	CS_{30} (%)	CS_∞ (%)
EPDM	50	50	0	109	650	22.9	50	53.8	28.7
EPDM	30	70	0	31	359	10.9	38	30.4	9.4
aPP-co-ENB[7.8]	50	50	0	98	940	30.8	50	57.0	29.9
aPP-co-ENB[7.8]	30	70	0	24	631	16.8	40	36.4	9.2
aPP-co-ENB[7.8]	33	33	33	23	510	8.5	30	34.4	19.4
aPP-co-ENB[7.8]	18	41	41	3	369	2.6	14	18.4	7.6

[a] *The relative standard deviation is 4-17% for E, 4-16% for EB, 4-14% for TS, 1-5% for hardness and 1-2% for CS.*

3.4. Conclusions

ENB-containing aPP rubbers can be prepared by titanium-catalyzed copolymerization of ENB and propylene, where the ENB content of the rubbers correlates linearly with the amount of ENB that is used during the copolymerization. These aPP-co-ENB rubbers have a similar thermal stability and molar mass as commercial EPDM rubbers typically used to the prepare TPVs.

The iPP/aPP-co-ENB blends are immiscible in the melt, since the blends show *(i)* a two-phase morphology at room temperature, *(ii)* no changes in crystalline long period, and *(iii)* no changes in crystallization kinetics. Nevertheless, the iPP/aPP-co-ENB blends show an increased compatibility in comparison to iPP/EPDM blends. This increased compatibility led to a refinement of the dispersed rubber particle size after dynamic vulcanization and to an improvement of the tensile properties. The relatively high T_g of the aPP rubber limits the elastic recovery of the aPP-based TPVs, leading to higher *CS* values in comparison to EPDM-based TPVs. A significant decrease in T_g was achieved by oil extension of the aPP-based TPVs, leading to a significant improvement of the elastic recovery and to a decrease in hardness, *E*, *EB* and *TS*.

3.5. References

[1] Coran, A.Y.; Patel, R. P. *Rubber Chem. Technol.* **1980**, *53*, 141-150.
[2] Araghi H.H. Proceedings of the International Rubber Conference, Birmingham, United Kingdom, 2001.
[3] *Thermoplastic Elastomers: A Comprehensive Review*; Holden, G.; Legge. N.R.; Quirk, R.P., Eds.; Hanser: Munich, 1996.
[4] *Thermoplastic Elastomers*; Holden, G.; Kricheldorf, H.R.; Quirk, R.P., Eds.; Hanser Publishers: Munich, 2004.
[5] Everaert, V.; Aerts, L.; Groeninckx, G. *Polymer* **1999**, *40*, 6627-6644.
[6] Wu, S. *Polym. Eng. Sci.* **1987**, *27*, 335-343.

7   Shariat Panahi, H.; Nazokdast, H.; Dabir, B.; Sadaghiani, K.; Hemmati, M. *J. Appl. Polym. Sci.* **2002**, *86*, 3148-3159.

8   Bhadane, P.A.; Champagne, M.F.; Huneault, M.A.; Tofan, F.; Favis, B.D. *Polymer* **2006**, *47*, 2760-2771.

9   Hemmati, M.; Nazokdast, H.; Shariat Panahi, H. *J. Appl. Polym. Sci.* **2001**, *82*, 1129-1137.

10 Van der Wal, A.; Gaymans, R.J. *Polymer* **1999**, *40*, 6045-6055.

11 Jain, A.K.; Nagpal, A.K.; Singhal, R.; Gupta, N.K. *J. Appl. Polym. Sci.* **2000**, *78*, 2089-2103.

12 Feng, W.; Isayev, A.I. *Polymer* **2004**, *45*, 1207-1216.

13 Coran, A.Y.; Patel, R.P. *Rubber Chem. Technol.* **1981**, *54*, 892-903.

14 Coran, A.Y.; Patel, R.P. In *Reactive Modifiers for Polymers*; Al-Malaika, S., Ed.; Blackie Academic & Professional: London, 1997.

15 Katbab, A.A.; Nazockdast, H.; Bazgir, S. *J. Appl. Polym. Sci.* **2000**, *75*, 1127-1137.

16 Mimoun, H.; de Saint Laumer, J.Y.; Giannini, L.; Scopelliti, R.; Floriani, C. *J. Am. Chem. Soc.* **1999**, *121*, 6158-6166.

17 Toldy, L.; Kurti, M.; Schafer, I. **1979**, *DE 2916140.*

18 Kretschmer, W.P. **2002**, *WO 02/070569 A1.*

19 Montezinos, D.; Wells, B.G.; Burns, J.L. *J. Polym. Sci., Polym. Lett. Ed.* **1985**, *23*, 421-425.

20 ASTM Standard D412 – Standard Test Methods for Vulcanized Rubber and Thermoplastic Elastomers – Tension, 1986.

21 ASTM Standard D395 – Standard Test Methods for Rubber Property – Compression Set, 1989.

22 Yoshida, Y.; Mohri, J.; Ishii, S.; Mitani, M.; Saito, J.; Matsui, S.; Makio, H.; Nakano, T.; Tanaka, H.; Onda, M.; Yamamoto, Y.; Mizuno, A.; Fujita, T. *J. Am. Chem. Soc.* **2004**, *126*, 12023-12032.

23 Coran, A.Y. In *Handbook of Elastomers. New Developments and Technology*; Bhowmick, A.K.; Stephens, H.L., Eds.; Marcel Dekker: New York, 1988, p. 249.

24 Chen, C.-Y.; Yunus, W.M.Z.W.; Chiu, H.-W.; Kyu, T. *Polymer* **1997**, *38*, 4433-4438.

25 Ramanujam, A.; Kim, K.J.; Kyu, T. *Polymer* **2000**, *41*, 5375-5383.

26 Brintzinger, H.-H.; Fischer, D.; Mülhaupt, R.; Rieger, B.; Waymouth, R. *Angew. Chemie* **1995**, *107*, 1255-1283.

27 Lohse, D.J. *Polym. Eng. Sci.* **1986**, *26*, 1500-1509.

28 Maier, R.-D.; Thomann, R.; Kressler, J.; Mülhaupt, R.; Rudolf, B. *J. Polym. Sci., Part B: Polym. Phys.* **1997**, *35*, 1135-1144.

29 Silvestri, R.; Sgarzi, P. *Polymer* **1998**, *39*, 5871-5876.

30 Phillips, R.A. *J. Polym. Sci., Part B: Polym. Phys.* **2000**, *38*, 1947-1964.

31 Wang, Z.-G.; Phillips, R.A.; Hsiao, B.S. *J. Polym. Sci., Part B: Polym. Phys.* **2000**, *38*, 2580-2590.

32 Moore, W.R.; Boden, G.F. *J. Appl. Polym. Sci.* **1965**, *9*, 2019-2029.

33 Avgeropoulos, G.N.; Weissert, F.C.; Biddison, P.H.; Böhm, G.G.A. *Rubber Chem. Technol.* **1976**, *49*, 93-104.

34 Jordhamo, G.M.; Manson, J.A.; Sperling, L.H. *Polym. Eng. Sci.* **1986**, *26*, 517-524.

35 Yukioka, S.; Inoue, T. *Polymer* **1993**, *34*, 1256-1259.

36 Shanks, R.A.; Li, J.; Yu, L. *Polymer* **2000**, *41*, 2133-2139.

37 Avrami, M. *J. Chem. Phys.* **1939**, *7*, 1103-1112.

38 Sengupta, P.; Noordermeer, J.W.M. *Macromol. Rapid Commun.* **2005**, *26*, 542-547.

39 Meynie, L.; Fenouillot, F.; Pascault, J.-P. *Polymer* **2004**, *45*, 1867-1877.

40 Fetters, L.J.; Lohse, D.J.; Colby, R.H. In *Physical Properties of Polymers Handbook*; Mark, J.E.; Press, A.I.P., Eds.; Woodbury: New York, 1996, p. 335.

41 Lohse, D.J. *J. Macromol. Sci., Part C: Polymer Rev.* **2005**, *45*, 289-308.

42 Sengers, W.G.F.; Wübbenhorst, M.; Picken, S.J.; Gotsis, A.D. *Polymer* **2005**, *46*, 6391-6401.

43 Medintseva, T.; Erina, N.; Prut, E. *Macromol. Symp.* **2001**, *176*, 49-53.

Chapter 4[*]

Thermoplastic vulcanizates obtained by reaction-induced phase separation of miscible poly(ε-caprolactone)/epoxy systems

A new method for the preparation of thermoplastic vulcanizates (TPVs) was successfully developed. Starting from a miscible system of a semi-crystalline thermoplastic polymer and an elastomer precursor, phase separation was induced by the increase in molar mass during selective cross-linking of the elastomer precursor. As a model system, the semi-crystalline thermoplastic poly(ε-caprolactone) (PCL) was used in combination with a rubbery epoxy resin based on poly(propylene oxide) (PPOn-epoxy). This approach enables the dispersion of up to 80 wt% of cross-linked rubber in a thermoplastic matrix, providing morphologies that are typical for TPVs. A range in rubber particle size of 0.5 to 3.0 μm was obtained by this approach without the need of blend compatibilization or dynamic processing. The materials exhibit mechanical and rheological properties that are typical for TPVs and the rubber particles have a high cross-link density. Connectivity between the rubber particles is observed at high curing temperatures, which has a negative influence on the mechanical properties and the rheological behavior.

4.1. Introduction

Commercial thermoplastic vulcanizates (TPVs) are usually based on blends of poly(propylene) (PP) and ethylene-propylene-diene (EPDM) rubber and are prepared via dynamic vulcanization, which typically leads to rubber particle sizes in the μm-range[1-3]. Chapter 2 showed a significant improvement of the mechanical properties of PP/EPDM-based TPVs upon decreasing the rubber particle size ($\overline{D_n}$) from 70 to 1 μm, where the variation in $\overline{D_n}$ was achieved by varying the shear rate during dynamic vulcanization. It was previously stated that the preparation of TPVs with sub-μm-sized rubber particles via dynamic vulcanization of PP/EPDM blends is impossible[3]. This statement is in agreement with the results presented in Chapter 2, where a minimum $\overline{D_n}$ of ~ 1 μm was observed at high shear rates. Chapter 3 showed that an increased compatibility of the blend components leads to a refinement of the morphology after dynamic vulcanization, although real sub-μm morphologies were not obtained. Additionally, high rubber contents typically lead to (partially) co-continuous morphologies due to incomplete phase inversion, which leads to a deterioration of the tensile and rheological properties[1-3]. It is, therefore, concluded that the preparation of sub-μm TPVs with high rubber contents cannot be achieved by dynamic vulcanization of immiscible blends.

Compatibilizers, such as pre-synthesized block or graft copolymers, are often used for the refinement of blend morphologies[4]. The compatibilizer lowers the interfacial tension and suppresses coalescence[5,6], which leads to finer dispersions and an improved interfacial adhesion[7]. Although pre-formed copolymers can be effectively used as compatibilizers, the lack of economically viable routes for their synthesis and the high probability of the formation of micelles[8] have limited their applications. A good alternative is to generate the compatibilizer via a chemical reaction between suitable functionalized polymers at the interface during melt mixing, a process known as *in-situ* compatibilization or reactive blending[4]. A major disadvantage of *in-situ* compatibilization is that chemical functionalization of the blend components is often required[9,10]. Although particle dispersions as small as 50-100 nm were reported for highly incompatible polymer pairs after compatibilization[11-13], the effectiveness of compatibilization in order to prepare TPVs with reduced rubber particle sizes is generally limited[14,15]. This may be explained by the fact that compatibilizers reduce the particle size mainly by preventing the occurrence of coalescence, while break-up of the rubber particles is mostly determinative for the final rubber particle size during dynamic vulcanization.

In this chapter, an alternative route for the preparation of TPVs, with the potential of sub-μm morphologies at high rubber contents, is discussed. Phase separation of a miscible system based on a semi-crystalline thermoplastic polymer and an elastomer precursor is induced by selective

cross-linking of the elastomer precursor. This method, which is known as reaction-induced phase separation (RIPS), can be applied to a wide variety of thermoplastic polymers in combination with an elastomer or a low-molar-mass elastomer precursor. Inoue *et al.*[16] showed that TPVs can be prepared by dynamic vulcanization of miscible blends based on poly(vinylidene fluoride) (PVDF) and acrylic rubber (ACM). Dynamic vulcanization led to complex morphologies, since a dispersion of both supra-µm as well as a small amount of nano-sized ACM particles in a PVDF matrix were obtained, where the supra-µm ACM particles contained well-developed PVDF crystal lamellae. Since miscible thermoplastic/elastomer blends are rare due to their low gain in entropy upon mixing, the use of a low-molar-mass elastomer precursor in combination with a semi-crystalline thermoplastic is advantageous. This chapter deals with miscible blends of poly(ε-caprolactone) (PCL) and an epoxy resin based on poly(propylene oxide) (PPOn-epoxy) as a model system to study the potential of RIPS for the preparation of (sub-µm) TPVs. It is expected that by starting with a miscible system, large shear forces during dynamic vulcanization and compatibilization of the system are no longer required to obtain a fine rubber dispersion. Now the phase separation process is crucial, since it determines the final morphology of the blend and, thus, its properties.

The aliphatic epoxy resin based on poly(propylene oxide) has been chosen because of its rubbery character, i.e. low T_g, after curing. Additionally, the telechelic character of the epoxy resin and the high reactivity of the oxirane rings make the material particularly suitable for cross-linking, preferably by means of multifunctional amines. PCL has been chosen as the thermoplastic phase because of its miscibility with the aliphatic epoxy and its semi-crystalline character, since it has been shown that the best TPV properties are obtained by using semi-crystalline thermoplastics[17]. The highly reactive curing agent triethylene tetramine (TETA) is used in order to achieve relatively fast cross-linking. The goal of this chapter is to explore the potential of RIPS for the preparation of TPVs and not the optimization of the process and the final properties of the TPVs. Therefore, additives that are often used to improve the properties and processability of TPVs, such as fillers, oil and stabilizers, are not used.

The approach of RIPS is principally different from the conventional dynamic vulcanization process. For dynamic vulcanization, two immiscible polymers have to be subjected to high shear rates during the vulcanization process to enable a reduction of the characteristic morphological length scale from several mm's (e.g. pellet size) down to the µm-range (final rubber particle size). For RIPS, the starting system is a blend that is miscible on the molecular scale and could, therefore, be described by a structural dimension in the order of a few nanometers. Upon cross-

linking of the elastomer precursor, phase separation is induced by the increase in molar mass, increasing the morphological length scale up to the sub-μm (or in some cases supra-μm) range.

The influence of the initial composition and the curing temperature on the morphology of cured PCL/PPOn-epoxy blends is studied by scanning electron microscopy (SEM). The chemical composition, i.e. the extent of cross-linking and the amount of grafted PCL, is characterized by determination of the gel content via solvent extractions and Fourier transform infrared (FTIR) spectroscopy on the residue. The tensile properties and elastic recovery are studied and related to the blend morphology. The melt processability of the materials is studied by dynamic shear measurements.

4.2. Experimental

4.2.1. Materials

PCL having M_n = 20 kg/mol and M_w = 37 kg/mol (CAPA 6400) was supplied by Solvay Caprolactones, UK. Two different poly(propylene oxide)-based liquid epoxy resins (Aldrich) were used with a PPO block length of 5 (PPO5-epoxy) and 9 (PPO9-epoxy) repeating units and an epoxy equivalent weight (EEW) of 190 and 320 g/eq, respectively. Triethylene tetramine (TETA; Huntsman, Belgium) was used as the curing agent, having an amino equivalent weight (AEW) of 27 g/eq. The chemical structures of PPOn-epoxy, PCL and TETA are shown in Fig. 4.1. Tetrahydrofuran (THF; Aldrich) was used as received.
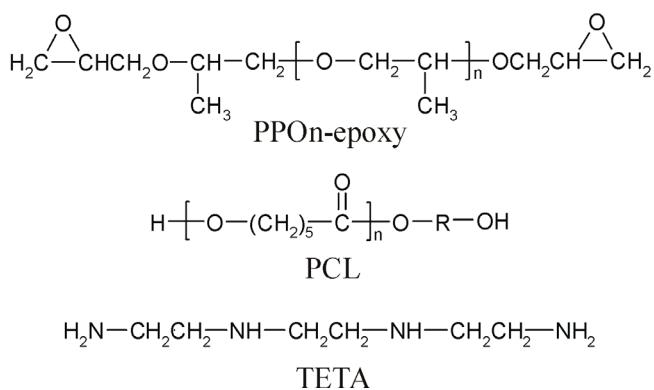
Fig. 4.1. Chemical structures of PPOn-epoxy, PCL and TETA.

4.2.2. Blend preparation

Homogeneous blends were prepared by dissolving PCL in the liquid epoxy resin at temperatures above 60 °C in a round-bottom flask by using a mechanical stirrer. The curing agent was added to the solution under continuous stirring at 250 rpm until a homogeneous mixture was obtained, after which the stirring was stopped during the actual curing process (static curing). Alternatively, the blend preparation and curing process were carried out in a home-built, recirculating, twin-screw micro-extruder with an internal volume of 5 cm^3 at 150 rpm (dynamic curing). Based on the results obtained from infrared studies on the curing reaction of the PPOn-epoxy resin with TETA (see Chapter 5.3.1), an appropriate curing time

was chosen to allow for maximum curing of the epoxy resin. The curing temperature was varied between 80 °C and 160 °C. Unless stated otherwise, the epoxy resin and amine were used in equivalent amounts.

4.2.3. Characterization techniques

Solvent extractions. The gel content (*%gel*) of the cured blends was determined by extraction with boiling THF for 24 hrs using cellulose extraction thimbles in a Soxlet HT2 1045 extraction unit. The *%gel* is defined as the percentage of rubber not dissolved in the solvent.

Fourier transform infrared (FTIR) spectroscopy. Infrared experiments were performed on a BioRad Excalibur 3000 spectrometer equipped with a diamond Specac Golden Gate attenuated total reflection (ATR) setup over a spectral range of 650 to 5000 cm^{-1}. Fifty spectra at a resolution of 4 cm^{-1} were signal-averaged and the resulting spectra were analyzed by using the BioRad Merlin 3.0 software. The grafted PCL content was determined by evaluating the ratio of the integrated intensities of the C=O stretching band of PCL at 1721 cm^{-1} and the asymmetric C-O-C stretching band of the propylene oxide repeat unit of positioned at 1094 cm^{-1}.

Scanning electron microscopy (SEM). Morphological investigations were performed with a Scanning Electron Microscope (SEM) (model XL30 FEG, FEI) at an acceleration voltage of 10 kV. The cured samples were fractured in liquid nitrogen and the fracture surfaces were etched with THF in order to remove the soluble PCL. After drying overnight under vacuum, the samples were sputter-coated with a thin layer of gold to improve the electric conductivity. The number-averaged size of the rubber particles ($\overline{D_n}$) was determined with the Image Pro Plus 4.5 software.

Dynamic mechanical thermal analysis (DMTA). Compression-molded samples (10.0 x 3.0 x 0.5 mm) were measured on a TA Instruments DMA Q800 with a film tension setup. Temperature sweeps from -100 to 100 °C were performed with a heating rate of 3 °C/min at a frequency of 1 Hz. A preload force of 0.01 N, an amplitude of 10 μm and a force track of 110 % were used. The glass transition temperature (T_g) was determined from the maximum in the loss modulus (E'').

Tensile testing. Tensile tests were performed on dumbbell-shaped tensile bars (32 x 2 x 1 mm) at 12 mm/min using a 2.5 kN force cell on a Zwick Z010 tensile tester according to ASTM D412[18]. Films with a thickness of 1 mm were compression molded at 100 bar and 100 °C, from which the tensile bars were punched. The equipment was controlled with the TestXpert v7.11 software. Each sample was tested in at least 10-fold and average values are presented.

Compression set. The compression set (*CS*) was measured on cylindrical samples with a diameter of 13 mm and a thickness of 6 mm for 22 hrs at 25 % compressive strain and a subsequent relaxation time of 30 min (all at room temperature), according to ASTM D395[19] and ISO 815[20]. The *CS* was calculated as follows:

$$CS = \frac{(t_i - t_o)}{(t_i - t_n)} \times 100\% \tag{4.1}$$

where t_i is the initial thickness of the sample, t_o the final thickness of the sample and t_n the thickness of the spacer. The relative standard deviation in *CS* is 1-2 %

Rheological measurements. Dynamic shear measurements were conducted by using a strain-controlled RMS 800 rheometer (Rheometrics) with a 25 mm parallel-plate geometry on disk-shaped specimens (25 mm diameter; 1 mm thick). Frequency sweeps from 10^2 to 10^{-1} rad/s were performed over a temperature range of 80 to 120 °C at 10 % strain, which corresponds to the linear viscoelastic regime. Time-temperature superposition was applied by using the TA Rheology Advantage v5.2.18 software.

4.3. Results and discussion

4.3.1. Morphology

DSC measurements on PCL/PPOn-epoxy mixtures with a varying composition demonstrated a clear melting temperature (T_m) depression of PCL with increasing epoxy concentration (not shown here), indicating miscibility of the mixtures over the whole composition range at temperatures above T_m PCL (~ 60 °C). The morphology of the cured PCL/PPO5-epoxy blends was studied by SEM after removal of the PCL phase, so the SEM images in Figs. 4.2-4.4 only show the cross-linked epoxy phase. Static curing of PCL/PPO5-epoxy at 140 °C leads to a coarse, co-continuous structure for a PCL content of 10 wt% (Fig. 4.2a), which indicates that the initial composition is close to the critical concentration (i.e. the concentration where the binodal and spinodal curves intersect). The occurrence of secondary phase separation is also observed, i.e. small epoxy particles are observed in the PCL-rich phase and small PCL particles are found in the epoxy-rich phase.

(a)   (b)

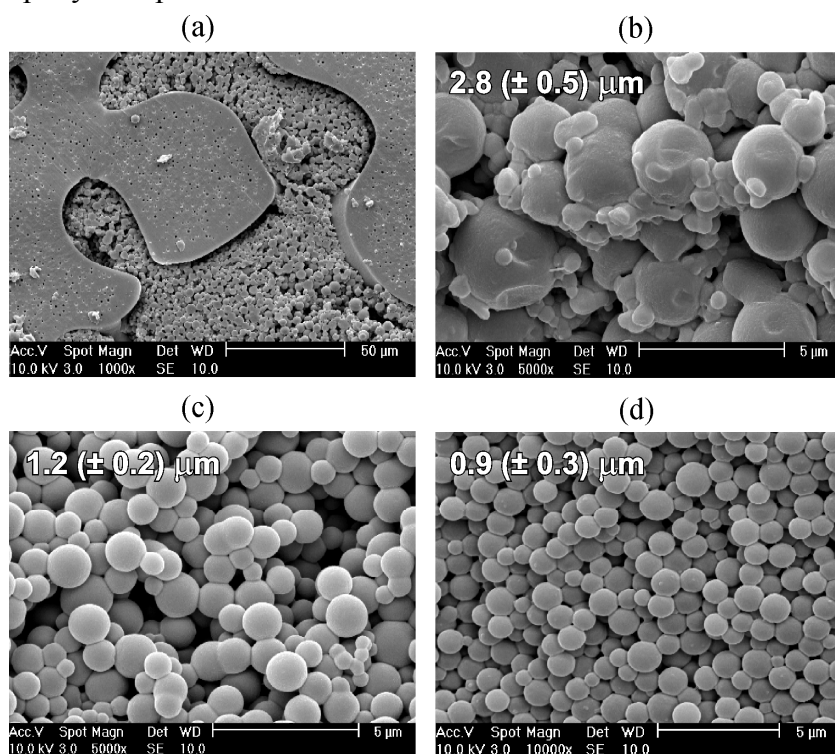(c)   (d)

Fig. 4.2. Morphology of PCL/PPO5-epoxy blends after static curing at 140 °C, containing (a) 10 wt% PCL, (b) 20 wt% PCL, (c) 40 wt% PCL and (d) 60 wt% PCL. The average rubber particle size and its standard deviation are shown in the figures.

Upon increasing the PCL content, the composition deviates further from the critical concentration and the morphology changes from a co-continuous structure to a dispersion of cross-linked epoxy particles in the thermoplastic PCL matrix. At a PCL content of 20 wt%, relatively large epoxy particles are observed, indicating that the initial composition is not far from critical (Fig. 4.2b). As the PCL content is further increased, the viscosity of the mixture during cross-linking increases, which leads to a reduction of the epoxy particle size to 1.2 μm at 40 wt% PCL and 0.9 μm at 60 wt% PCL. The rather uniform particle size distribution suggests that phase separation has proceeded via spinodal decomposition. The PCL/PPO9-epoxy blends showed very similar morphologies after static curing, with the exception of a PCL content of 20 wt%, where a co-continuous structure was observed. This difference is explained by the shift of the miscibility gap with increasing molar mass of the elastomer precursor, as discussed in Chapter 1.5. These results show that by RIPS of PCL/PPOn-epoxy blends, a fine dispersion of cross-linked rubber particles in a thermoplastic matrix can be obtained over a very broad composition range.
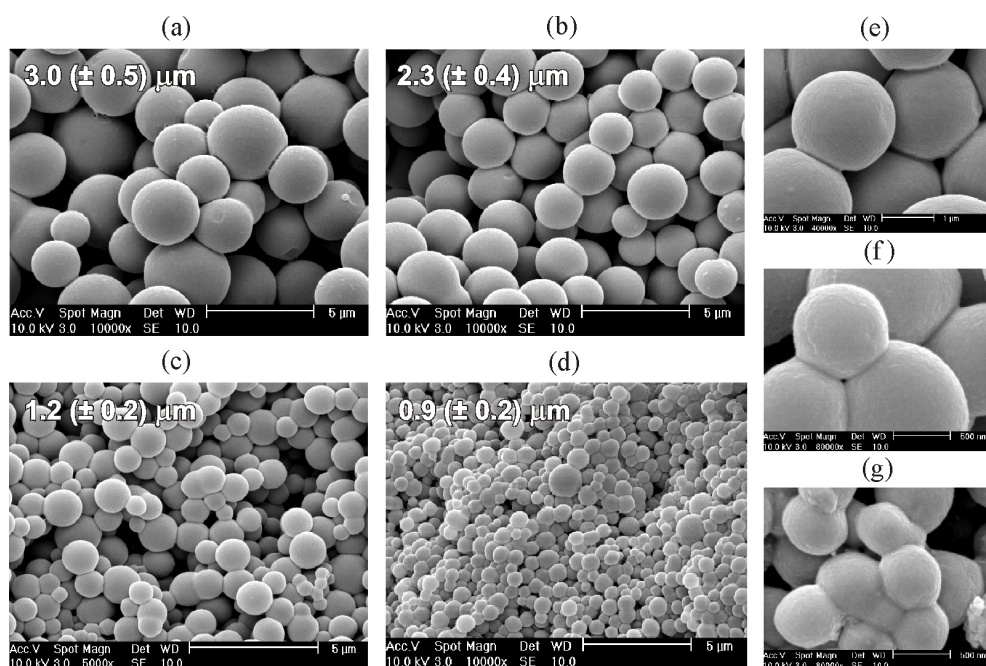
Fig. 4.3. Morphology of PCL/PPO5-epoxy blends containing 40 wt% PCL after static curing at (a) 80 °C, (b) 100 °C, (c) 140 °C and (d) 160 °C. The average rubber particle size and its standard deviation are mentioned in the figures. Magnifications of the morphology are shown for the same blends after curing at (e) 80 °C, (f) 140 °C and (g) 160 °C.

Generally, the rubber particles decrease in size upon increasing the PCL concentration, due to the increased viscosity. Increasing T_{cure} leads to an additional reduction of the rubber particle size (Fig. 4.3). This reduction is caused by the increase in quench rate, i.e. an increase in thermodynamic quench depth with time, with increasing T_{cure}, which suppresses structure coarsening prior to reaching the gel point of the system[21,22]. At high T_{cure} and high PCL contents, sub-μm rubber dispersions are obtained. However, a more detailed look at the obtained

morphologies shows that with increasing T_{cure}, the rubber particles become connected to each other (Figs. 4.3e-g). This phenomenon was previously described by Inoue and Yamanaka and was recognized to be related to the phase separation process of thermoplastic/epoxy systems[21,23], which will be discussed in more detail in the next chapter. An overview of $\overline{D_n}$ as a function of composition and T_{cure} is presented in Table 4.1. Comparison of the morphologies presented in Fig. 4.2 with TEM studied (not shown here) proved that the extraction process of the soluble PCL with THF did not alter the morphology.

Table 4.1. Number-averaged rubber particle size of PCL/PPO5-epoxy blends after curing.

PCL content (wt%)	Number-averaged rubber particle size $\overline{D_n}$ $(\mu m)^a$					
	$T_{cure} =$ 80 °C	$T_{cure} =$ 100 °C	$T_{cure} =$ 120 °C	$T_{cure} =$ 140 °C	$T_{cure} =$ 150 °C	$T_{cure} =$ 160 °C
20				2.8 (0.5)		
40	3.0 (0.5)	2.3 (0.4)	2.2 (0.4)	1.2 (0.2)		0.9 (0.2)
60	2.1 (0.5)	1.3 (0.3)	1.2 (0.2)	0.9 (0.3)	0.7 (0.2)	0.5 (0.1)
80				0.7 (0.2)		

^{a} The value between brackets represents the standard deviation.

So far, PCL/PPO5-epoxy systems prepared by static curing have been discussed. The typical morphology of PCL/PPO5-epoxy blends as obtained by dynamic curing is presented in Fig. 4.4, showing that a much coarser morphology with a characteristic length scale of 5-15 μm is obtained. Additionally, the shape of the epoxy particles appears irregular in comparison to the spherical particles obtained by static curing (Fig. 4.2c). Coarsening of the structure can be attributed to the promotion of coalescence by the shear forces during extrusion. Due to the reactive nature of the epoxy/amine phase, irreversible coalescence of the epoxy particles may occur, i.e. multiple particles coalesce and react with each other, forming a larger, cross-
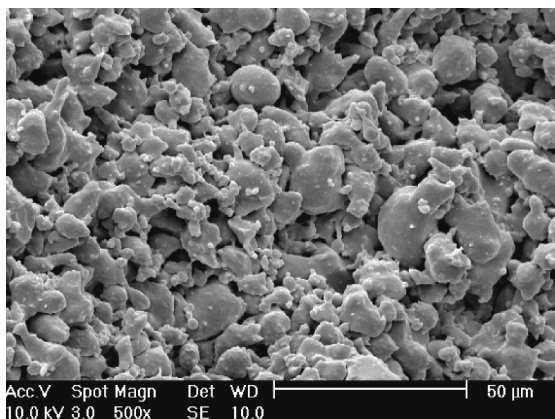

Fig. 4.4. Morphology of a PCL/PPO5-epoxy blend with 40 wt% PCL after dynamic curing at 140 °C.

linked rubber particle[24,25]. At conversions close to or above the gel point, break-up and shape relaxation of the particles is limited. These phenomena explain the coarser morphology and the irregular shape of the cross-linked rubber phase.

4.3.2. Chemical composition

The gel content (*%gel*) is commonly used to express the state of cross-linking of rubber networks, where *%gel* quantifies the amount of rubber that is incorporated into the covalently cross-linked network. The gel content of the PCL/PPO5-epoxy blends was determined by extraction with THF, which is a good solvent for PCL, the non-cross-linked epoxy resin and the residual curing agent. FTIR spectroscopy on the residue showed that after full extraction of the blends, a small amount of PCL (typically 0.5-2.0 wt% based on the total weight of the sample) could not be extracted. It is known that the hydroxyl end groups of PCL are able to react with the oxirane rings of the epoxy resin[26], by which part of the PCL is chemically grafted onto the epoxy network and can, therefore, not be extracted from the blend. Additionally, transesterification and amidation reactions may occur during the curing reaction, which may also lead to PCL grafting[26, 27]. The amount of grafted PCL in the statically and dynamically cured samples decreases with increasing PCL content and is independent of the preparation conditions (Fig. 4.5). The gel content of the epoxy phase was corrected for the amount of grafted PCL. Increasing the PCL content leads to a decrease in *%gel* for both the statically and dynamically cured samples, indicating a decrease in cross-link density. Up to 60 wt% PCL, reasonable gel contents of > 80 % are obtained, but the gel content decreases to < 60 % at a PCL concentration of 80 wt%. These results suggest that a certain amount of amine is unavailable for reaction with the epoxy, which can be explained by residual amine in the PCL phase and by partial amidation of the amine. Additionally, the increased viscosity of the system at higher PCL contents leads to slower diffusion of the components during the curing process and the presence of PCL in the blend decreases the probability for epoxy/amine reaction to occur due to a dilution effect. The gel content was found to be very sensitive to small changes in the epoxy/amine ratio, and gel contents of 100 % could easily be reached by slightly decreasing the epoxy/amine ratio.

Upon increasing the curing temperature, more PCL chains are grafted to the epoxy network (Fig. 4.6), indicating that the side-reactions that lead to PCL grafting are dependent on the curing temperature. The curing temperature hardly affects the gel content of the cross-linked epoxy phase. Therefore, it can be concluded that the morphology can be altered by varying the curing temperature (Fig. 4.3), while the gel content of the cross-linked epoxy phase remains constant.
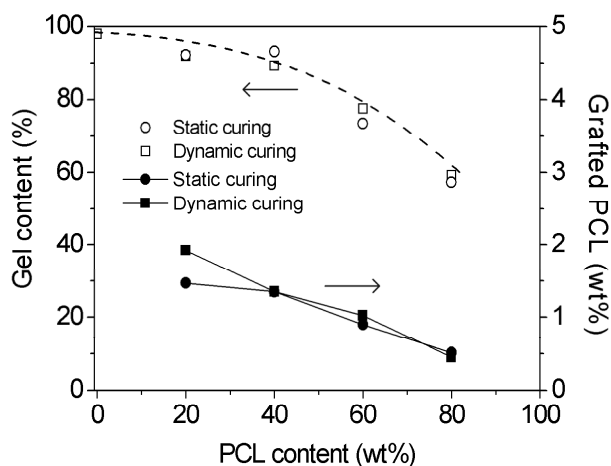
Fig. 4.5. Influence of PCL content on the gel content and the amount of grafted PCL (based on the total weight of the sample) for PCL/PPO5-epoxy blends cured at 140 °C.
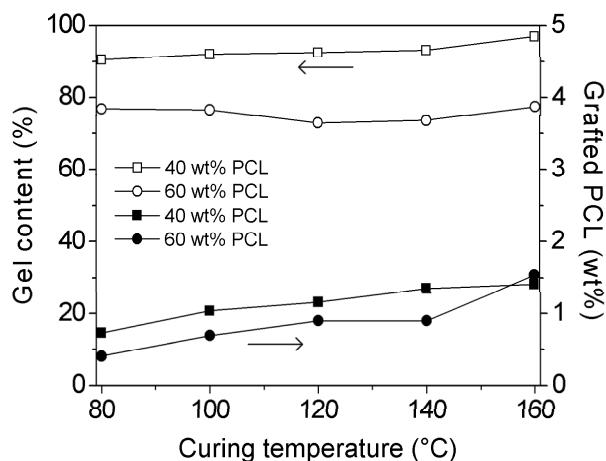
Fig. 4.6. Influence of curing temperature on the epoxy gel content and the amount of grafted PCL (based on the total weight of the sample) for PCL/PPO5-epoxy blends containing 40 and 60 wt% PCL.

4.3.3. Mechanical properties

As shown by SEM and extraction studies, RIPS of PCL/PPOn-epoxy blends yields products with a dispersion of up to 80 wt% of cross-linked rubber particles in the thermoplastic PCL matrix. Consequently, the cured PCL/PPOn-epoxy blends are expected to provide melt processable materials with good elastic properties.

Fig. 4.7 shows the storage and loss moduli (E' and E'', respectively) as a function of temperature for PCL/PPO9-epoxy blends after static curing. The T_g of the cross-linked PPO9-epoxy is determined from the maximum in E'' and equals -29 °C, independent of the composition. The cross-linked PPO5-epoxy showed a T_g of ~ 0 °C (not shown here). A weak transition is observed around -55 °C, which corresponds to the T_g of PCL. As expected, the storage modulus of the cured blends at room temperature decreases with increasing epoxy content.

Fig. 4.8 shows the influence of the composition on the tensile properties for PCL/PPO5-epoxy TPVs, cured statically and dynamically at 140 °C. Upon increasing the rubber content, both the elastic modulus (E) and elongation at break (EB) decrease, which is a trend typical for TPVs. Surprisingly, dynamic curing leads to a higher EB and TS in comparison to static curing at equal compositions. Microscopy studies showed that static curing leads to finely dispersed rubber particles, whereas dynamic curing leads to much coarser structures (Figs. 4.2-4.4). In line with the work presented by Coran et al.[28] and Araghi[29] and the results presented in Chapter 2, it may be expected that the finer rubber dispersion of statically cured TPVs would lead to better tensile
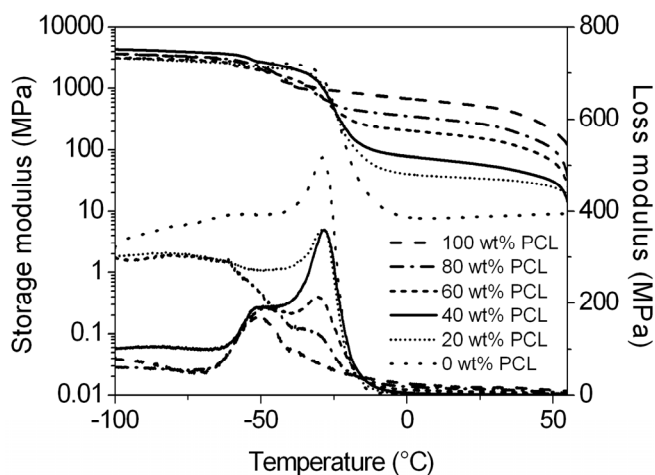
Fig. 4.7. Storage and loss moduli as a function of temperature for PCL/PPO9-epoxy blends with a variation in PCL content after static curing at 140 °C.
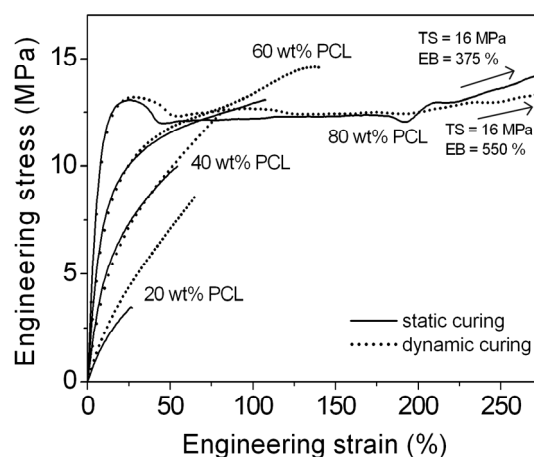
Fig. 4.8. Effect of composition and preparation method on tensile properties of PCL/PPO5-epoxy blends cured at 140 °C.

properties, but Fig. 4.8 shows the opposite behavior. Extraction experiments showed that the gel content and the amount of grafted PCL of dynamically cured samples are similar to that of statically cured samples (Fig. 4.5). The connection of the rubber particles in statically cured blends (as seen in Figs. 4.3e-g) causes the morphology to change from a dispersed droplet-like structure towards a co-continuous structure, thereby decreasing *EB* and *TS*. The enhancement of the tensile properties by dynamic curing relative to static curing may, therefore, be attributed to the disruption of the connectivity between the rubber particles. These results indicate that, although an improvement of the tensile properties is expected with decreasing rubber particle size, the positive effect of the smaller particle size on the tensile properties is overruled by the negative influence of the rubber connectivity.

The compression set (*CS*) is a practical and direct measure for the elastic behavior of a material and is, therefore, widely used as an indication for the elastic performance of TPVs. Fig. 4.9 shows the compression set at 23 °C for PCL/PPOn-epoxy blends after static and dynamic curing at 140 °C. As expected, *CS* decreases upon increasing the amount of cross-linked rubber in the system. Although significant differences are observed between the tensile properties of statically and dynamically cured blends, it appears that the *CS* is rather insensitive to small changes in the morphology, since similar results are obtained for the statically and dynamically cured samples. Traditional TPVs prepared by dynamic vulcanization typically show an improvement of the elasticity upon increasing the cross-link density of the dispersed rubber phase. However, *CS* of the blends based on PCL and PPOn-epoxy increases only slightly upon decreasing the cross-link density, where the decrease in cross-link density is achieved by increasing the number of repeating PPO units from 5 to 9. In case of full cross-linking, the molar mass between cross-links of the epoxy phase in the cured PCL/PPOn-epoxy blends is calculated to be 204 and 262 g/mol for PPO5-epoxy and PPO9-epoxy, respectively. The cross-link density

of the rubber phase in traditional PP/EPDM TPVs prepared by dynamic vulcanization is typically in the order of 2000 g/mol[30]. Although the PCL/PPOn-epoxy systems will generally not be fully cross-linked (for reasons discussed earlier), the cross-link density of traditional PP/EPDM-based TPVs is significantly lower in comparison to the TPVs based on PCL/PPOn-epoxy. It is known that *CS* is improved with increasing cross-link density, but eventually levels off to a value which depends only on the total rubber content in the TPV[31]. Therefore, it can be concluded that the PCL/PPOn-epoxy TPVs have such high cross-link densities that an increase in the epoxy chain length from 5 to 9 repeating PPO units hardly affects *CS*. These results indicate that there is room for optimization of the mechanical properties of these TPVs: *CS* will hardly be affected by a certain decrease in cross-link density (e.g. by increasing the epoxy chain length or changing the functionality of the epoxy resin and/or curing agent), while *EB* will be increased. It has to be mentioned that the PCL/PPO9-epoxy blend containing 20 wt% of PCL showed a co-continuous morphology after static curing (comparable to the 10 wt% PCL/PPO5-epoxy blend in Fig. 4.2a), rather than a dispersion of rubber particles.
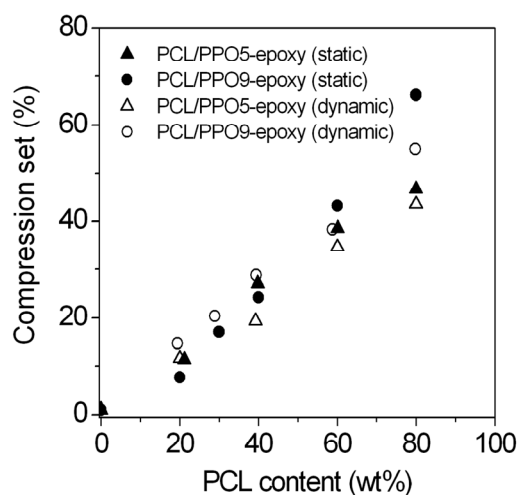
Fig. 4.9. Compression set of PCL/PPO5-epoxy and PCL/PPO9-epoxy blends prepared by static and dynamic curing at 140 °C.

4.3.4. Rheological behavior

Since most of the cured PCL/PPO5-epoxy blends consist of a thermoplastic matrix containing a dispersion of cross-linked rubber particles, it is expected that the cured blends are processable above T_m of PCL. Fig. 4.10 shows complex viscosity (η^*) master curves for pure PCL and PCL/PPO5-epoxy blends after static curing, which were obtained by horizontal shifting of the storage modulus (G') to a reference temperature of 100 °C. While pure PCL exhibits full terminal flow (i.e. η^* independent of frequency) at low frequencies, the terminal flow region is not reached for the TPVs. Although all materials are easily processable by compression molding at 100 °C, a pronounced viscosity upturn at low shear rates is observed with increasing rubber

content. At higher rubber contents, the slope of $\log(\eta^*)$ versus $\log(\omega_r)$ (where ω_r is the reduced frequency) approaches -1, which indicates that the material behaves almost like an ideal elastic network.

Fig. 4.11 shows the effect of the composition on the storage modulus (G'). This figure again shows that the terminal flow region is reached for pure PCL (indicated by a slope of 2) but not for the TPVs. Compared to pure PCL, the addition of rubber particles leads to a strong increase in G', especially at low shear rates. These observations are consistent with previous studies on PP/EPDM-based TPVs, in which it was suggested that physical clustering of the rubber particles at low shear rates leads to rheological co-continuous behavior, whereas high shear rates lead to break up of the clusters, resulting in rheological behavior typical for a matrix/dispersion morphology[32-34]. The chemical connectivity between the rubber particles as observed in Figs. 4.3e-g will also contribute to an increase in the viscosity and storage modulus[32]. The TPVs with 40-60 wt% cross-linked rubber show a η^* of 300-800 Pa·s at $\omega = 100$ rad/s and $T = 110$ °C ($= T_m + 50$ °C). This value is somewhat lower than η^* of the conventional PP/EPDM-based TPVs discussed in Chapter 2.3.7, which showed a η^* of ~ 3000 Pa·s at $\omega = 100$ rad/s and $T = 210$ °C ($= T_m + 50$ °C).
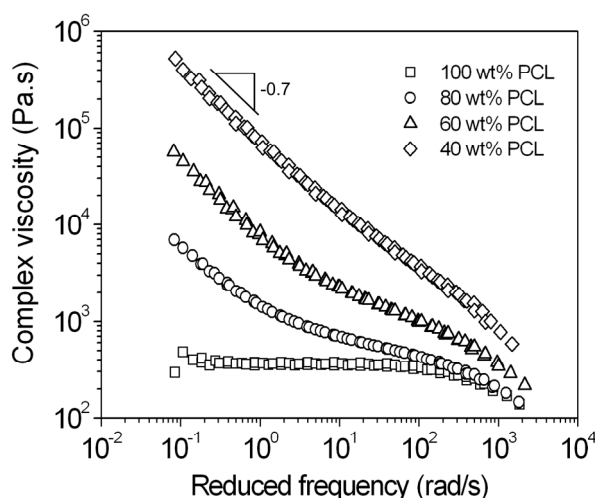
Fig. 4.10. Influence of PCL content on the complex viscosity (η^*) of PCL/PPO5-epoxy blends after static curing at 140 °C. Time-temperature superposition was applied by shifting G' to a reference temperature of 100 °C.
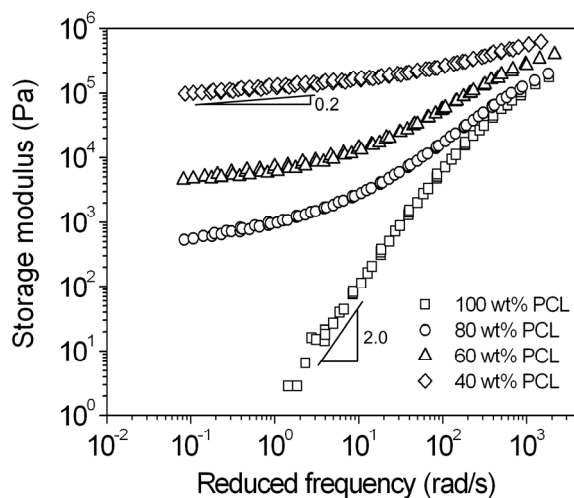
Fig. 4.11. Influence of PCL content on the storage modulus (G') of PCL/PPO5-epoxy blends after static curing at 140 °C. Time-temperature superposition was applied by shifting G' to a reference temperature of 100 °C.

4.4. Conclusions

A new method for the preparation of TPVs was introduced. Reaction-induced phase separation was successfully applied to prepare materials with typical TPV morphologies, i.e. a dispersion of cross-linked rubber particles in a semi-crystalline thermoplastic matrix. Fine rubber dispersions with particle sizes in the range of 0.5 to 3.0 μm were obtained over a broad

composition range, where the rubber particle size decreases with increasing PCL content and increasing curing temperature. The gel content appeared to be very sensitive to the stoichiometry of the epoxy/amine reaction. The presence of PCL in the PPOn-epoxy/TETA mixture induces changes in the stoichiometry, e.g. via side-reactions with the epoxy and amine groups and the distribution of the amine curing agent over the PCL and epoxy phases, which leads to a significant decrease in the gel content.

It was shown that the materials exhibit mechanical and rheological properties that are typical for TPVs and that there is still room for optimization of the properties by increasing the cross-link density of the cross-linked epoxy phase. At high curing temperatures and low PCL contents, connectivity between the rubber particles was observed, which results in a deterioration of the tensile properties and the melt processability. The presence of connected rubber particles in the final blend is probably related to the phase separation process as induced by the cross-linking reaction. The next chapter presents a more detailed study of the phase separation behavior of PCL/PPO5-epoxy blends in order to be able to prevent the rubber particles from connecting, which is expected to lead to enhanced properties.

4.5. References

1. *Thermoplastic Elastomers: A Comprehensive Review*; Holden, G.; Legge. N.R.; Quirk, R.P., Eds.; Hanser: Munich, 1996.
2. *Thermoplastic Elastomers from Rubber-Plastic Blends*; De, S.K.; Bhowmick, A.K., Eds.; Ellis Horwood: New York, 1990.
3. *Thermoplastic Elastomers*; Holden, G.; Kricheldorf, H.R.; Quirk, R.P., Eds.; Hanser Publishers: Munich, 2004.
4. Koning, C.; van Duin, M.; Pagnoulle, C.; Jerome, R. *Prog. Polym. Sci.* **1998**, *23*, 707-757.
5. Sundararaj, U.; Macosko, C.W. *Macromolecules* **1995**, *28*, 2647-2657.
6. Tan, N.C.; Tai, S.K.; Briber, R.M. *Polymer* **1996**, *37*, 3509-3519.
7. Hudson, S.D.; Jamieson, A.M. In *Polymer Blends, Vol. 1: Formulations*; Paul, D.R.; Bucknall, C.B., Eds.; J. Wiley & Sons: New York, 2000.
8. Fayt, R.; Jerome, R.; Teyssie, P. *J. Polym. Sci., Part C: Polym. Lett.* **1981**, *19*, 79-84.
9. Liu, N.C.; Baker, W.E. *Adv. Polym. Technol.* **1992**, *11*, 249-253.
10. Xanthos, M. *Polym. Eng. Sci.* **1988**, *28*, 1392-1399.
11. Teng, J.; Otaigbe, J.U.; Taylor, E.P. *Polym. Eng. Sci.* **2004**, *44*, 648-659.
12. Tol, R.T.; Mathot, V.B.F.; Groeninckx, G. *Polymer* **2005**, *46*, 383-396.
13. Madbouly, S.A.; Otaigbe, J.U. *Polymer* **2007**, *48*, 4097-4107.
14. Huang, H.; Ikehara, T.; Nishi, T. *J. Appl. Polym. Sci.* **2003**, *90*, 1242-1248.
15. Naskar, K.; Noordermeer, J.W.M. *J. Appl. Polym. Sci.* **2006**, *100*, 3877-3888.
16. Li, Y.; Oono, Y.; Kadowaki, Y.; Inoue, T.; Nakayama, K.; Shimizu, H. *Macromolecules* **2006**, *39*, 4195-4201.
17. Coran, A.Y.; Patel, R.P.; Williams, D. *Rubber Chem. Technol.* **1982**, *55*, 116-136.
18. ASTM Standard D412 "Standard Test Methods for Vulcanized Rubber and Thermoplastic Elastomers – Tension", 1986.

[19] ASTM Standard D395 "Standard Test Methods for Rubber Property – Compression Set", 1989.

[20] International Standard ISO 815 "Rubber, Vulcanized or Thermoplastic – Determination of Compression Set at Ambient, Elevated or Low Temperatures", 1991

[21] Inoue, T. *Prog. Polym. Sci.* **1995**, *20*, 119-153.

[22] Williams, R.J.J.; Rozenberg, B.A.; Pascault, J.P. *Adv. Polym. Sci.* **1997**, *128*, 95-156.

[23] Yamanaka, K.; Inoue, T. *Polymer* **1989**, *30*, 662-667.

[24] Meynie, L.; Fenouillot, F.; Pascault, J.-P. *Polymer* **2004**, *45*, 1867-1877.

[25] Meynie, L.; Fenouillot, F.; Pascault, J.-P. *Polymer* **2004**, *45*, 5101-5109.

[26] Chen, J.; Huang, H.; Li, M.; Chang, F. *J. Appl. Polym. Sci.* **1999**, *71*, 75-82.

[27] Chen, J.; Chang, F. *Macromolecules* **1999**, *32*, 5348-5356.

[28] Coran, A.Y.; Patel, R.P. *Rubber Chem. Technol.* **1980**, *53*, 141-150.

[29] Araghi H.H. Proceedings of the International Rubber Conference, Birmingham, United Kingdom, 2001.

[30] Litvinov, V.M. *Macromolecules* **2006**, *39*, 8727-8741.

[31] Radar, C.P. In *Handbook of Thermoplastic Elastomers*; Walker, B.M.; Radar, C.P., Eds.; Van Nostrand Reinhold: New York, 1988.

[32] Goharpey, F.; Nazockdast, H.; Katbab, A.A. *Polym. Eng. Sci.* **2005**, *45*, 84-94.

[33] Han, P.K.; White, J.L. *Rubber Chem. Technol.* **1995**, *68*, 728-738.

[34] Araki, T.; White, J.L. *Polym. Eng. Sci.* **1998**, *38*, 590-595.

4

Thermoplastic vulcanizates obtained by reaction-induced phase separation: interplay between phase separation dynamics, morphology and properties

Reaction-induced phase separation (RIPS) of miscible blends of poly(ε-caprolactone) (PCL) and an epoxy resin based on poly(propylene oxide) (PPO5-epoxy) was used to prepare thermoplastic vulcanizates (TPVs) with fine rubber dispersions. Scanning electron microscopy (SEM) confirmed the formation of cross-linked rubber particles dispersed in the thermoplastic matrix at PCL contents $\geq$ 20 wt%. The morphology development during phase separation was studied by time-resolved small-angle light scattering (SALS) and optical microscopy (OM). It was shown that higher curing temperatures lead to a decrease in rubber particle size, but at the same time to an increase in the extent of particle connectivity. At high curing temperatures, gelation of the PPO5-epoxy-rich phase limits full structure development, which leads to extensive connectivity between the dispersed rubber particles and a deterioration in tensile properties.

5.1. Introduction

A new approach for the preparation of TPVs was introduced in Chapter 4, with the potential of obtaining sub-µm rubber dispersions over a broad composition range. Phase separation of a miscible system based on the semi-crystalline thermoplastic poly(ε-caprolactone) (PCL) and an aliphatic epoxy resin based on poly(propylene oxide) (PPOn-epoxy) was induced by selective cross-linking of the elastomer precursor with a multifunctional amine. This method, which is known as reaction-induced phase separation (RIPS), can be applied to a wide variety of thermoplastic polymers in combination with a low-molar-mass elastomer precursor.

The concept of RIPS based on miscible blends of epoxy resins and thermoplastic polymers has already been explored since the late 1960s and has successfully been applied in various industrial processes, which include the preparation of high-impact poly(styrene), the toughening of epoxy thermoset resins and the processing of intractable polymers. The application of RIPS to toughen brittle epoxies with a secondary rubbery phase has gained much attention since the late 1960s, when RIPS was applied to produce an epoxy matrix with a high glass transition temperature (T_g) containing 10 to 20 wt% of well-dispersed rubber particles, which are often chemically grafted to the epoxy matrix[1-5]. This increasing interest was followed up in the early 1980s, when RIPS was used to toughen epoxies with thermoplastic polymers, generally by using less than 20 wt% of thermoplastic polymer[7-9]. More recently, miscible thermoplastic/epoxy systems proved to be useful for the processing of intractable polymers[10,11]. Also the miscibility and phase separation behavior[12-15] and crystallization kinetics[16,17] of PCL/epoxy systems have been studied in detail. However, all these studies deal with a thermoset matrix based on an aromatic epoxy resin with a high T_g, e.g. the diglycidyl ether of bisphenol-A (DGEBA). For these systems vitrification will occur, which drastically suppresses the reaction and concurrent diffusional processes associated with phase separation. Although RIPS of miscible blends of thermoplastics and epoxy resins is said to be reasonably well understood, it is still a subject of in-depth studies because of the complexity that arises from the many parameters that influence the phase separation mechanism and the corresponding kinetics and, thus, the final morphology. The chemistry in miscible blends of thermoplastics and epoxy resins is complicated, since it involves chain extension, grafting and cross-linking, together with a redistribution of the reactive components during phase separation.

Preliminary miscibility studies on the PCL/PPO5-epoxy system used for the preparation of TPVs in Chapter 4 have shown a clear melting temperature (T_m) depression of PCL with increasing PPO5-epoxy concentration, which indicates miscibility of the mixture over the whole composition range at temperatures above T_m of PCL. RIPS enabled the dispersion of up to 80

wt% of cross-linked PPO5-epoxy rubber in the thermoplastic PCL matrix. Fine rubber dispersions were obtained without applying blend compatibilization or dynamic shear forces during cross-linking. At high curing temperatures (T_{cure}), morphologies with a sub-μm rubber dispersion were obtained under quiescent conditions (static curing), while applying shear forces during the curing process (dynamic curing) led to coarser morphologies. Extrapolation of the work of Coran *et al.*[18] and Araghi[19] and the results presented in Chapter 2 indicate that TPVs with a refined rubber dispersion provide enhanced tensile properties. However, the dynamically-cured PCL/PPO5-epoxy-based TPVs showed a higher elongation at break and tensile strength than the statically-cured TPVs (Chapter 4.3.3). Based on electron microscopy studies, it was proposed that the inferior tensile properties of the statically-cured TPVs are related to connectivity of the rubber particles. A similar observation was made by Ratna[20], who showed that rubber-toughened brittle epoxy resins prepared by RIPS initially demonstrate an enhancement of the toughness upon increasing T_{cure}, followed by a strong decrease in toughness upon a further increase of T_{cure}. Ratna proposed that at higher T_{cure} phase separation starts after the epoxy resin has formed a three-dimensional cross-linked network, i.e. after reaching the gel point. Gelation of the epoxy resin induces diffusional restrictions, which limits the full development of a phase-separated morphology. Although no experimental proof was given, it is plausible that particle connectivity in reaction-induced phase-separated blends is related to the coarsening behavior and leads to deteriorated mechanical behavior.

In this chapter a more detailed study on RIPS of PCL/PPO5-epoxy systems is presented, which provides a better insight in the potential of RIPS for the preparation of (sub-μm) TPVs. Vitrification of the epoxy resin does not occur, since the fully cured PPO5-epoxy/TETA system has a T_g below room temperature. The curing reaction of PPO5-epoxy, both neat and in the blends with PCL, is studied by Fourier transform infrared (FTIR) spectroscopy. Optical microscopy (OM) and scanning electron microscopy (SEM) are used to study the later stages of RIPS and the final morphology, respectively, whereas small-angle light scattering (SALS) is used to study the phase separation dynamics. Finally, the morphology development during RIPS is related to the tensile properties of the TPVs.

5.2. Experimental

5.2.1. Materials

PCL having M_n = 20 kg/mol and M_w = 37 kg/mol (CAPA 6400) was supplied by Solvay Caprolactones, UK. A poly(propylene oxide)-based liquid epoxy resin (Aldrich) having a PPO block length of 5 (PPO5-epoxy) was used with an equivalent weight (EEW) of 190 g/eq. Triethylene tetramine

(TETA, Huntsman, Belgium) was used as the curing agent, having an amino equivalent weight (AEW) of 27 g/eq. Tetrahydrofuran (THF, Aldrich) was used as received.

5.2.2. Blend preparation

Homogeneous blends were prepared by dissolving PCL in the liquid PPO5-epoxy at temperatures above 60 °C in a round-bottom flask by using a mechanical stirrer. The curing agent was added to the solution under continuous stirring at 250 rpm until a homogeneous mixture was obtained, after which the stirring was stopped during the remainder of the experiment. TETA was used in stoichiometric epoxy/amine ratios and curing temperatures ranged from 80 to 160 °C.

5.2.3. Characterization techniques

Fourier transform infrared (FTIR) spectroscopy. The curing reaction of PPO5-epoxy, both neat and in the blends with PCL, was studied by FTIR spectroscopy. Spectra were obtained by placing (PCL/)PPO5-epoxy/TETA mixtures on the diamond crystal of a Specac Golden Gate attenuated total reflection (ATR) setup placed in a BioRad Excalibur 3000 spectrometer. Fifty spectra at a resolution of 4 cm^{-1} over a spectral range of 600 to 5000 cm^{-1} were signal-averaged and the resulting spectra were analyzed using the BioRad Merlin 3.0 software. The intensity of the absorption band assigned to the symmetric ring deformation of the epoxy group at 843 cm^{-1} (A) was used to calculate the epoxy conversion (α) by the following equation:

$$\alpha = \frac{A_0 - A_t}{A_0 - A_\infty} \tag{5.1}$$

where A_0 and A_∞ represent the initial and final intensity, respectively, while A_t represents the intensity at curing time t. The anti-symmetric C-O-C stretching vibration of the propylene oxide repeat unit at 1069 cm^{-1} was used as reference peak to correct for changes in the penetration depth of the evanescent wave, which is approximately 1 μm. For the PCL/PPO5-epoxy mixtures, the spectrum of amorphous, molten PCL was subtracted to obtain the spectra of PPO5-epoxy.

Optical microscopy (OM). The later stages of the phase separation behavior upon curing were studied by OM using a Zeiss Axioplan 2 microscope equipped with a Zeiss Axiocam camera. The images were analyzed with the accompanying AxioVision v3.0.6 software. Samples were sandwiched between two thin glass slides and fixed on a Linkam THMS-600 hot-stage for temperature control.

Scanning electron microscopy (SEM). Morphological investigations were performed with a scanning electron microscope (SEM) (model XL30 FEG, FEI) at an acceleration voltage of 10 kV. The fully cured samples were fractured in liquid nitrogen and the fractured surfaces were etched with THF in order to remove all soluble PCL. After drying overnight under vacuum, the samples were sputter-coated with a thin layer of gold to improve the electrical conductivity. The number-averaged size of the rubber particles ($\overline{D_n}$) was determined with the Image Pro Plus 4.5 software.

Small-angle light scattering (SALS). The phase separation dynamics was studied by small-angle light scattering (SALS). A 1 mW-intensity stabilized HeNe laser was used as incident light source. The light was guided through a pinhole and then through the sample, which was fixed between two glass

slides. The temperature was controlled by a Linkam THMS-600 hot-stage. The scattered light was projected on a semi-transparent poly(propylene) screen. The scattering patterns were captured with a 16-bit 512 x 512 CCD camera (Versarray:512B Princeton CCD with a ST-133 controller), equipped with a Rodenstock Rodagon 50mm f 1:2,8 lens with a variable focal distance. The CCD camera was linked to a personal computer for data acquisition and analysis. The scattering angles were calibrated with a 300 lines/mm grid. The usable span of scattering vector (q) magnitudes was in the range of 0.7 μm^{-1} < q < 3.0 μm^{-1}. The data acquisition time was typically 1000 ms per image and was controlled by a home-made script running under V++ for Windows (version 4.0, Digital Optics Ltd)[21].

Size exclusion chromatography (SEC). The molar mass distribution of PCL was determined by using a Waters model 510 pump and a Waters 712 WISP chromatograph with PL-gel mix D columns (300 x 7.5 mm, Polymer Laboratories). THF was used as eluent with a flow rate of 1 mL/min. All samples were diluted to 1 mg/mL and filtered by using 0.2 μm syringe filters. The absolute molar mass of PCL was calculated using poly(styrene) standards, applying the universal calibration principle with the Mark-Houwink parameters K = 0.00109 dL/g and α = 0.6[22].

Tensile testing. Films with a thickness of 1 mm were compression molded at 100 bar and 100 °C from which dumbbell-shaped tensile bars (32 x 2 x 1 mm) were punched. Tensile tests were performed at 12 mm/min using a 2.5 kN force cell on a Zwick Z010 tensile tester according to ASTM D412[23]. The equipment was controlled with the TestXpert v7.11 software. Each sample was tested in at least 10-fold and average values are presented.

5.3. Results and discussion

5.3.1. PPO5-epoxy/TETA reaction

First, the reaction kinetics of the neat PPO5-epoxy cured with TETA as measured by FTIR spectroscopy are discussed, after which the influence of PCL on the reaction kinetics in the miscible blends will be addressed. Fig. 5.2 shows that the conversion rate of the neat PPO5-epoxy increases with increasing T_{cure}. The final epoxy conversion is only slightly influenced by T_{cure} and is almost complete (> 95 %). Auto-catalytic effects, which arise from the formation of hydroxyl groups during the curing process, are commonly observed for epoxy/amine reactions and are characterized by S-shaped conversion-versus-time profiles[24,25]. However, such auto-catalytic effects seem to be absent in our systems (Fig. 5.2). This may be attributed to the fast reaction kinetics, which makes it difficult to determine the starting point of the reaction accurately. The activation energy ($E_α$) of the curing reaction was calculated by evaluating the slope of the plot of ln($t_α$) against 1/T, where $t_α$ is the time t required to reach a specific epoxy conversion α at an isothermal curing temperature T[26]. The calculated $E_α$ ranges from 68 to 79 kJ/mol for conversions ranging from 40 to 80 %. The dependency of $E_α$ on α is a well-known phenomenon in

epoxy/amine reactions and is generally attributed to the multi-step reaction mechanism that results in complex kinetics[26,27].
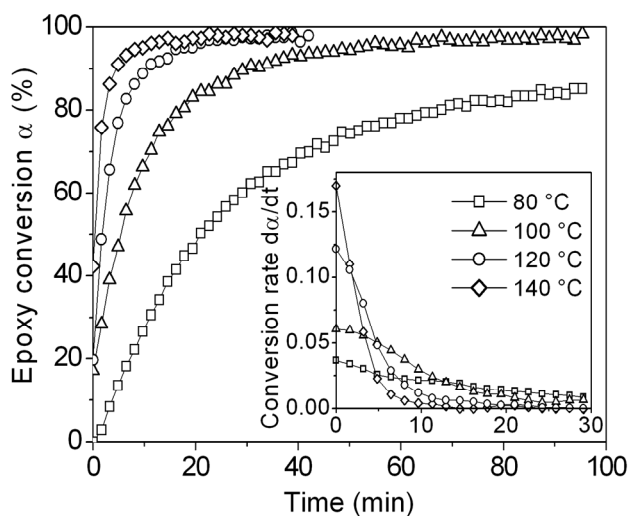
Fig. 5.2. Epoxy conversion upon curing of neat PPO5-epoxy as measured by FTIR spectroscopy. The inset shows the conversion rate as a function of time.
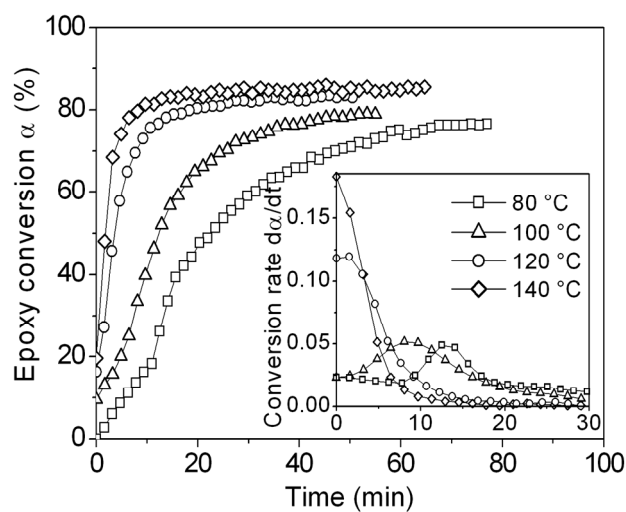
Fig. 5.3. Epoxy conversion upon curing of PPO5-epoxy in a PCL/PPO5-epoxy mixture containing 50 wt% PCL as measured by FTIR spectroscopy. The inset shows the conversion rate as a function of time.

Fig. 5.3 shows that the addition of 50 wt% PCL to the PPO5-epoxy slows down the initial conversion rate. The concentration of the reactive epoxy and amine groups is decreased by the addition of PCL, which decreases the probability of the epoxy/amine reaction to occur. Fig. 5.3 shows that the final epoxy conversion is somewhat decreased by the addition of PCL. Previous studies on blends of thermoplastic polymers with aromatic epoxy resins showed that the addition of 20-40 wt% of thermoplastic polymer decreased the final epoxy conversion from > 95 % down to < 60 %[28,29]. This significant decrease in final epoxy conversion was attributed to vitrification of the system, occurring when T_g of the partially reacted epoxy resin becomes equal to T_{cure}. Since the PPO5-epoxy/TETA system used in this study has a T_g of ~ 0 °C after full conversion, vitrification of the system does not occur. The rubber gel content of the blends was measured by extraction with THF, which dissolves PCL and non-cross-linked PPO5-epoxy and TETA (Chapter 4). A decrease in the rubber gel content was observed upon increasing the PCL concentration, which is consistent with the FTIR measurements. The gel content appeared to be fairly constant over a range of T_{cure} from 80 to 160 °C. FTIR spectroscopy showed that a small amount of PCL (typically in the range of 0.5-2.0 wt%) could not be extracted from the blends. The decrease in final epoxy conversion in the PCL/PPO5-epoxy system is, therefore, explained by a redistribution of the amine curing agent over the PPO5-epoxy and PCL phases after phase separation, as a result of which part of the amine is no longer available for the cross-linking reaction[29]. Partial amidation of PCL with the amine will also lead to grafting of PCL onto the epoxy network and to a lower final epoxy conversion. Previous studies showed that the hydroxyl

end groups of PCL may react with the oxirane rings of the epoxy resin, which leads to grafting of PCL chains onto the cross-linked particles[12]. Additionally, traces of water in the system may lead to partial hydrolysis of the PCL under the formation of hydroxyl and carboxylic acid end groups. The carboxylic acid end groups readily react with the oxirane rings of the epoxy resin, as proven by solution ^{1}H nuclear magnetic resonance (^{1}H NMR) spectroscopy on low-molar-mass model components (not shown here).

In contrast to the neat PPO5-epoxy, which shows a continuous decrease in conversion rate as a function of time (inset of Fig. 5.2), the PCL/PPO5-epoxy blends show a distinct maximum in the conversion rate (inset of Fig. 5.3), which shifts to shorter reaction times upon increasing T_{cure}. The acceleration of the conversion rate is not related to an auto-catalytic effect, but can be explained by phase separation of the PCL/PPO5-epoxy blends during curing, as will be discussed in the next section. The reaction time at which the conversion rate shows a maximum value is close to the onset of phase separation as determined by SALS (Fig. 5.8). As stated earlier, the presence of PCL in the blend decreases the local concentration of epoxy and amine groups, thereby decreasing the conversion rate. After phase separation, PPO5-epoxy-rich and PCL-rich phases are formed. In the PPO5-epoxy-rich phase the epoxy concentration is higher than before phase separation, which increases the conversion rate[30]. When T_{cure} is increased, phase separation sets in earlier (Fig. 5.8) and, concomitantly, the maximum in conversion rate shifts towards shorter curing times.

The molar mass build-up of the reacting PPO5-epoxy/TETA system can be calculated by the statistical model derived by Macosko and Miller[31,32]. Given the functionalities of the PPO5-epoxy and TETA and their molar ratio, the gel point, defined by an increase in weight-averaged molar mass (M_w) to infinity, is reached at an epoxy conversion of 50 %. Based on this calculation, the reaction time at which the gel point is reached can be estimated from the presented FTIR spectroscopy results, both for neat PPO5-epoxy and for PPO5-epoxy in blends with PCL. This information will be used in a later section, where the phase separation process of the blends is related to the final morphology.

5.3.2. Morphology development

To determine suitable PCL/PPO5-epoxy compositions for the preparation of TPV morphologies (i.e. cross-linked PPO5-epoxy rubber particles dispersed in the PCL matrix), first the late stages of the phase separation process and the morphologies after full curing are studied by OM and SEM, respectively. Based on the OM and SEM results, the earlier stages of the phase separation process of several relevant compositions are studied in more detail by SALS. Fig. 5.4a shows the structure development of a PCL/PPO5-epoxy blend containing 10 wt% PCL. At the

time that phase separation starts to be detectable, relatively large co-continuous structures are observed, which further coarsen with time. This indicates that the composition of 10 wt% PCL is close to the critical composition and that phase separation occurs via spinodal decomposition (SD). Small sub-inclusions are observed in both phases, which indicate the occurrence of secondary phase separation. Comparison of the OM image of Fig. 5.4a at 300 s with the corresponding SEM image of the same sample (Fig. 5.5a) allows for identification of the larger inclusions ($\overline{D_n} \sim 10$ μm) as PPO5-epoxy-rich droplets that develop in the PCL-rich phase, whereas the smaller inclusions ($\overline{D_n} \sim 1$ μm) are identified as PCL-rich droplets formed in the PPO5-epoxy-rich phase.
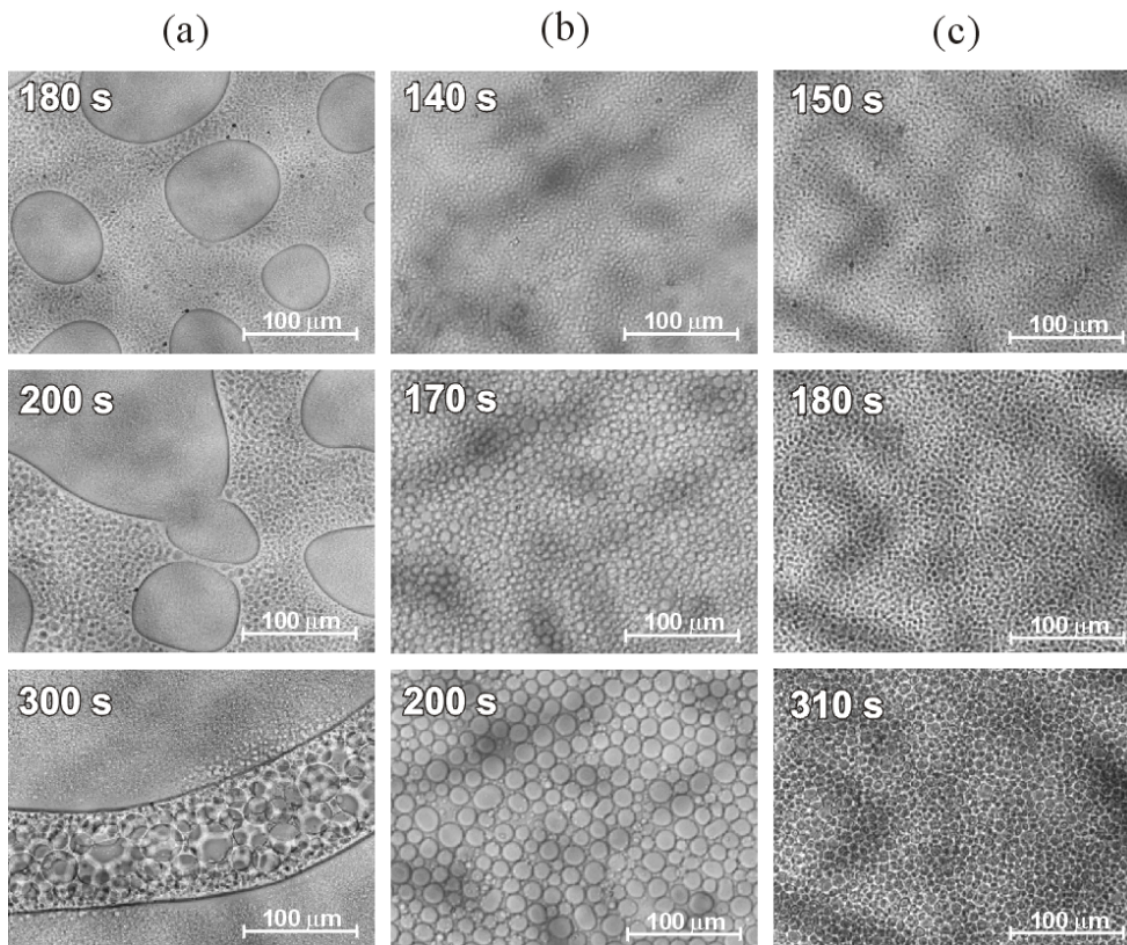
Fig. 5.4. OM images of PCL/PPO5-epoxy blends cured at 120 °C containing (a) 10 wt% PCL, (b) 20 wt% PCL and (c) 30 wt% PCL. The curing times are given in the left top corner of each image.

Compositions with PCL contents of 20 and 30 wt%, i.e. positioned further away from the critical composition, show a different morphology development with time (Figs. 5.4b and c, respectively). In these systems, phase-separated structures are spontaneously formed on a relatively small scale. These structures rapidly grow in size to form spherical particles having $\overline{D_n} \sim 10\text{-}15$ μm for 20 wt% PCL and $\overline{D_n} \sim 3\text{-}7$ μm for 30 wt% PCL. A similar structure development is found at PCL contents of 40 and 50 wt%, although the structural dimensions decrease. Fig. 5.5 is reproduced from Chapter 4 and confirms that TPV morphologies are formed

at PCL contents ≥ 20 wt% and that the rubber particle size decreases with increasing PCL content.
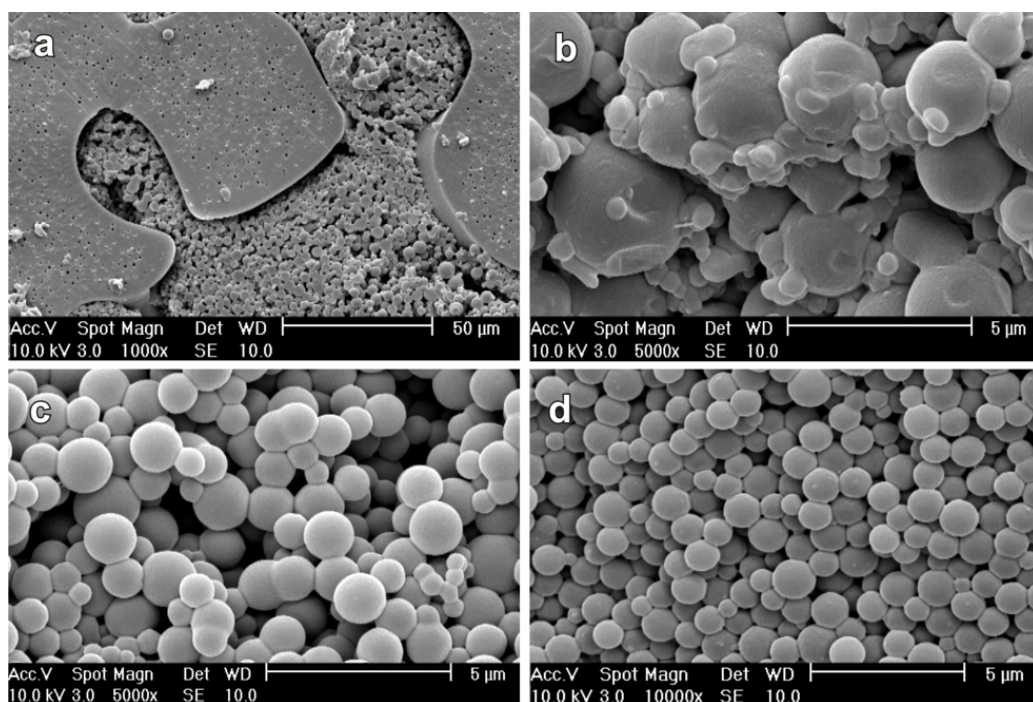
Fig. 5.5. SEM images of PCL/PPO5-epoxy blends containing (a) 10 wt% PCL, (b) 20 wt% PCL, (c) 40 wt% PCL and (d) 60 wt% PCL after full curing at 140 °C. The PCL phase has been extracted with THF, so only the cross-linked rubber phase is visible.

Based on OM and SALS experiments, Vanden Poel *et al.*[15] reported that the phase separation process for miscible blends of PCL with an aromatic epoxy resin with off-critical compositions occurs via the formation of a bi-continuous structure, which breaks up into spherical particles. The formation of bi-continuous structures was not observed for the PCL/PPO5-epoxy systems, which implies that the formation of a bi-continuous structure and its subsequent break-up into spherical particles occurs rapidly and at a relatively small scale. Since the OM and SEM studies show that no typical TPV morphologies are obtained at PCL contents below 20 wt%, the remainder of this paper will only discuss blends with PCL contents of 20 wt% and higher.

Fig. 5.6 shows SEM images of fully cured PCL/PPO5-epoxy blends containing 60 wt% PCL. Clearly, T_{cure} has a significant influence on the final morphology. Spherical rubber particles with little connectivity are obtained at low T_{cure} (80 °C, Fig. 5.6a), whereas a higher T_{cure} (140 °C, Fig. 5.6b) leads to extensive particle connectivity. This phenomenon was previously discussed by Yamanaka and Inoue[33], who introduced the so-called connected-globule structure for RIPS of
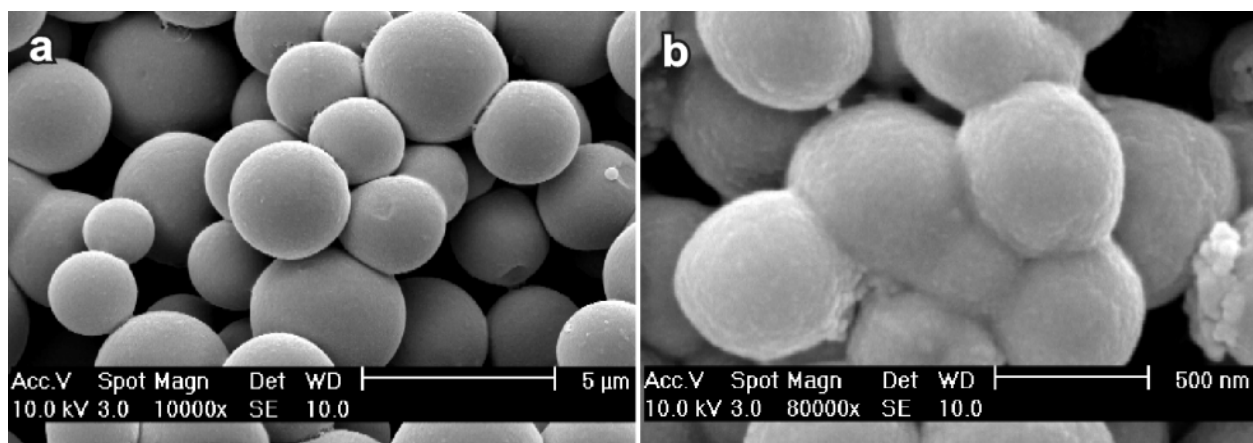
Fig. 5.6. SEM images of PCL/PPO5-epoxy blends containing 60 wt% PCL after full curing at (a) 80 °C and (b) 140 °C. The PCL phase has been extracted with THF, so only the cross-linked rubber phase is visible.

miscible blends of poly(ether sulphone) (PES) and an aromatic epoxy resin. They proposed that, after a periodic increase of the bi-continuous structure formed by SD, the phase connectivity is disrupted by an increase in interfacial tension, eventually leading to a dispersed droplet-like morphology. A connected-globule structure is formed when complete break up of the co-continuous structure cannot be realized, e.g. by gelation or vitrification of the epoxy-rich phase. However, since phase separation of the PES/aromatic epoxy resin was affected by both gelation and vitrification, the actual origin of particle connectivity could not fully be clarified.

5.3.3. Phase separation dynamics

To study the structure development during the early stages of phase separation, light scattering studies were performed on the PCL/PPO5-epoxy blends during curing. Fig. 5.7 shows the evolution of the SALS patterns of a PCL/PPO5-epoxy blend containing 30 wt% PCL upon curing at 100 °C. Typically, no appreciable light scattering is detected for the homogeneous blend during the early stages of the reaction. After ~ 4 min, a maximum in the scattering pattern appears at a certain scattering vector q_{max}, where q is the scattering vector ($q = (4\pi n/\lambda)\sin(\theta/2)$, with λ the wavelength, θ the scattering angle and n the refractive index), indicating the development of a well-correlated, phase-separated structure. Upon further curing, q_{max} shifts to lower values under increasing maximum intensity (I_{max}), which implies coarsening of the phase-separated structure (arrow 1 in Fig. 5.7). These changes in the scattering profile are typical for the late stages of spinodal decomposition (SD)[34-36]. Similar scattering profiles were obtained at PCL contents ranging from 20 to 50 wt% PCL and T_{cure} ranging from 80 to 140 °C. These results suggest that RIPS of the PCL/PPO5-epoxy blends proceeds via reaction-induced spinodal decomposition. Since an aliphatic amine (TETA) is used as the curing agent, the curing reaction is expected to proceed fast in comparison to phase separation. This implies that phase separation

via nucleation and growth (NG) is suppressed and, therefore, SD is indeed the most likely phase separation mechanism to be observed[37]. Yamanaka *et al.*[36,38] actually stated that RIPS can only proceed via SD, since the NG process is too slow to occur. Although this statement is only true for systems with a relatively high interfacial tension (the free energy barrier for nucleation is proportional to the third power of the interfacial tension), SD is generally accepted as the most common phase separation process for RIPS of miscible blends of epoxy resins and thermoplastics[4,39]. Due to the high reaction rate of the PPO5-epoxy/TETA system, the early stages of the SD process, which is characterized by an increasing intensity at a constant q_{max}, cannot be observed here[34].

Fig. 5.7 shows that after a curing time of ~ 7 min, a broad shoulder appears next to the low-angle scattering peak (arrow 2). The position of the shoulder suggests that a structure with a characteristic length scale of 2-3 μm appears in addition to the 4-8 μm-sized structure formed during the initial stages of phase separation. Vanden Poel *et al.*[15] observed a similar scattering profile for off-critical mixtures of PCL and an aromatic epoxy resin. They assigned the appearance of the wide-angle peak to break up of the earlier developed structure into smaller particles. This explanation is also plausible for the shoulder in the scattering profile shown in Fig. 5.7. Since the size of the newly formed particles is relatively small, they are not clearly visible in the OM images presented in Fig. 5.4c. A similar phase separation behavior was observed for this blend composition at all curing temperatures studied. At higher PCL contents the occurrence of the wide-angle shoulder next to the low-angle peak was not observed.
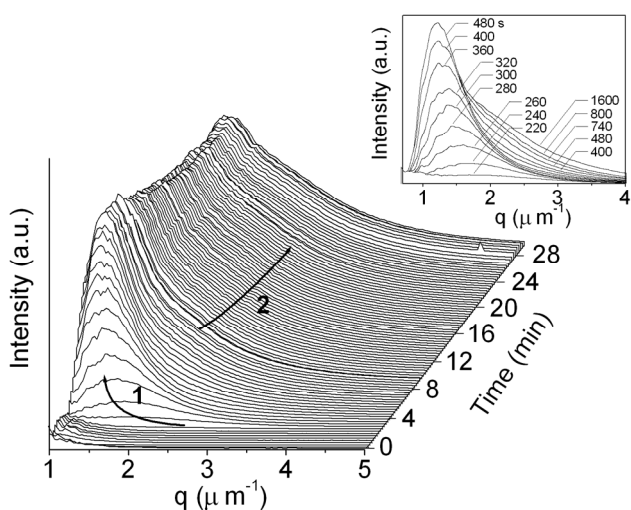
Fig. 5.7. Time-resolved evolution of the SALS pattern of a PCL/PPO5-epoxy mixture with 30 wt% PCL cured at 100 °C.
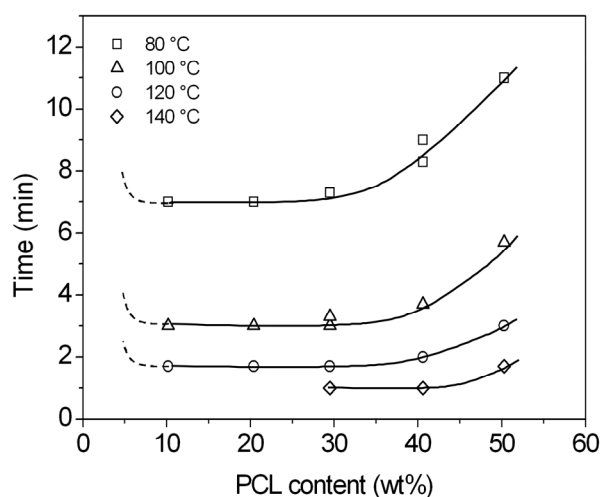
Fig. 5.8. Onset of phase separation for PCL/PPO5-epoxy blends at various T_{cure} as determined by SALS.

Some authors[15,34] reported that the phase separation process in miscible blends of PCL and aromatic epoxy resins changes from SD to NG upon increasing the PCL content. This is due to the decrease in curing rate in the presence of PCL and to a widening of the metastable region

upon deviation from the critical point. In the case of PCL/PPO5-epoxy blends cured with TETA, such a transition from SD to NG upon increasing the PCL content is not observed; SD is the dominating phase separation mechanism up to 50 wt% PCL. As discussed earlier, the absence of NG can be attributed to the relatively high rate of the PPO5-epoxy/TETA reaction[36-38].

The onset of phase separation during isothermal curing of the PCL/PPO5-epoxy mixtures is identified by SALS as the first increase of the scattered intensity (Fig. 5.8). Phase separation sets in earlier with increasing T_{cure} and decreasing PCL content. At very low PCL contents the onset of phase separation should go to infinite values (dotted lines), since the neat PPO5-epoxy will not phase separate.

The growth dynamics in the intermediate and late stages of SD is often described by a power law relation[35,40,41]:

$$q_{max}(t) \propto t^{-\alpha} \qquad (5.2)$$

$$I_{max}(t) \propto t^{\beta} \qquad (5.3)$$

The experimental data of Fig. 5.7 for off-critical PCL/PPO5-epoxy blends can be translated to the variation of q_{max} and I_{max} with time as shown in Fig. 5.9. The maximum of the scattering vector q_{max} fits the power law expression only at the early stages of phase separation. The power law coefficient α is equal to 1.0, indicating that the coarsening process is hydrodynamically controlled[42]. The maximum peak intensity does not follow a power law over any reasonable time interval. This may be attributed to the occurrence of apparent phase dissolution, which originates from the relatively large change in refractive index of the PPO5-epoxy phase upon reaction with TETA. As the curing reaction proceeds, the refractive index of the PPO5-epoxy-rich phase gets close to that of the PCL-rich phase and the total scattered intensity decreases[11,43].

Fig. 5.9. Variation of q_{max} and I_{max} with time of a PCL/PPO5-epoxy mixture with 30 wt% PCL upon curing at 100 °C.

The log(q_{max}) versus log(t) plots obtained at various T_{cure} can be superimposed by horizontal and vertical shifting to form a single mastercurve, with a_T the horizontal and b_T the vertical shift

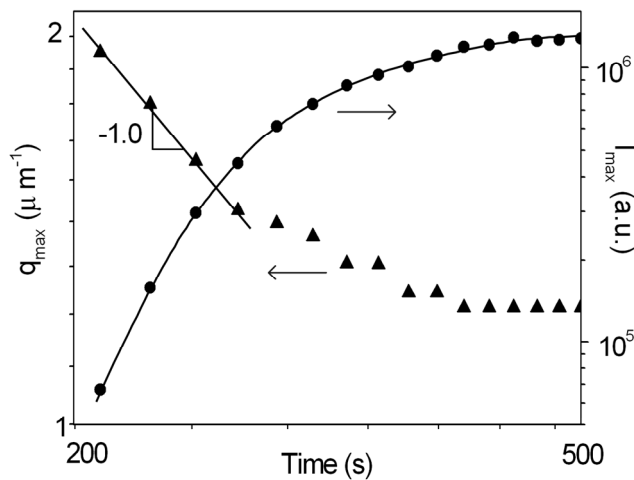factor. This indicates that the time-temperature superposition (TTS) principle is valid. Fig. 5.10 shows the result of TTS of q_{max} to a reference temperature (T_r) of 80 °C for the 30 and 50 wt% PCL blends. The power law coefficient α equals 1.0 for both blends over the whole range of T_{cure} (80 to 140 °C), which indicates similar phase separation dynamics. The inset of Fig. 5.10 gives plots of $1/\log(a_T)$ against $1/(T\text{-}T_r)$, which follow a linear relationship. This demonstrates that a Williams-Landel-Ferry (WLF)-like function, which is typically applied to describe the relaxation time of amorphous polymers controlled by the diffusion of segments[25,44], is valid. The TTS principle is also applicable to the $\log(I_{max})$ versus $\log(t)$ plots obtained at various T_{cure}. Mastercurves were obtained by using similar values for a_T as were used for TTS of the $\log(q_{max})$ versus $\log(t)$ plots. The observation that the intermediate and late-stage SD process obeys the TTS principle and can be described by the WLF-equation suggests that the coarsening process is mainly controlled by viscoelastic flow[41].

It was previously reported by Tanaka that viscoelastic phase separation is a universal phenomenon common to all dynamically asymmetric mixtures[45,46]. The dynamic asymmetry can originate from the difference in size of the component molecules or the existence of specific transitions, such as a T_g[47,48]. Viscoelastic phase separation is characterized by changes of the relevant coarsening mode in time; namely, it switches from an initial diffusive mode to an elastic mode and eventually to a hydrodynamic mode. In the elastic regime, the elastic force balance determines the morphology instead of the interfacial tension. Therefore, fixation of the morphology in the elastic regime (e.g. by gelation or vitrification) leads to connectivity between the PPO5-epoxy domains and to a co-continuous morphology in the extreme case. When the reaction is sufficiently slow, the coarsening process can proceed further into the hydrodynamic
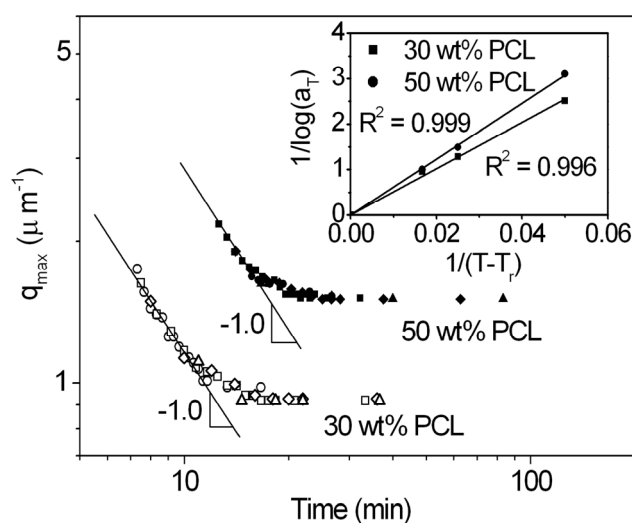

Fig. 5.10. Mastercurves of q_{max} versus time of PCL/PPO5-epoxy blends with 30 wt% and 50 wt% PCL during curing at 80, 100, 120 and 140 °C. The curves are superimposed to a reference temperature (T_r) of 80 °C. The inset shows the relationship between the horizontal shift factor a_T and the relative temperature $T\text{-}T_r$.

regime. In that case the interfacial energy overcomes the elastic energy and the PPO5-epoxy domains change from an anisotropic to a spherical shape. The occurrence of rubber connectivity in our PCL/PPO5-epoxy blends, as observed in Fig. 5.6b, can be explained by a shift in structure fixation by gelation from the hydrodynamic to the elastic regime with increasing T_{cure}.

The scattering vector is related to the characteristic length scale (l_c) by $l_c = 2\pi/q_{max}$, where l_c corresponds to the distance between similar phases, separated by the other phase and measured from centre to centre. The development of l_c at various T_{cure} is shown for blends containing 30 and 50 wt% PCL in Figs. 5.11a and b, respectively. During the first stages of phase separation l_c increases with time, but eventually levels off, which indicates that further structure development is suppressed. An increase in T_{cure} leads to a decrease in l_c, which is consistent with the SEM results presented in Chapter 4.3.1. The arrows shown in Fig. 5.11 indicate the curing times at which gelation sets in. As discussed in the section on the PPO5-epoxy/TETA reaction, the gel points are calculated from FTIR spectroscopy results by using the model proposed by Macosko and Miller[31,32]. It has been shown that the calculated gel point agrees very well with the experimentally determined gel point, both for neat epoxy/amine systems as well as for their miscible blends with thermoplastic polymers[11]. Nevertheless, the position of the gel point should be used with care, since it is based on the combination of experimental and statistical data.
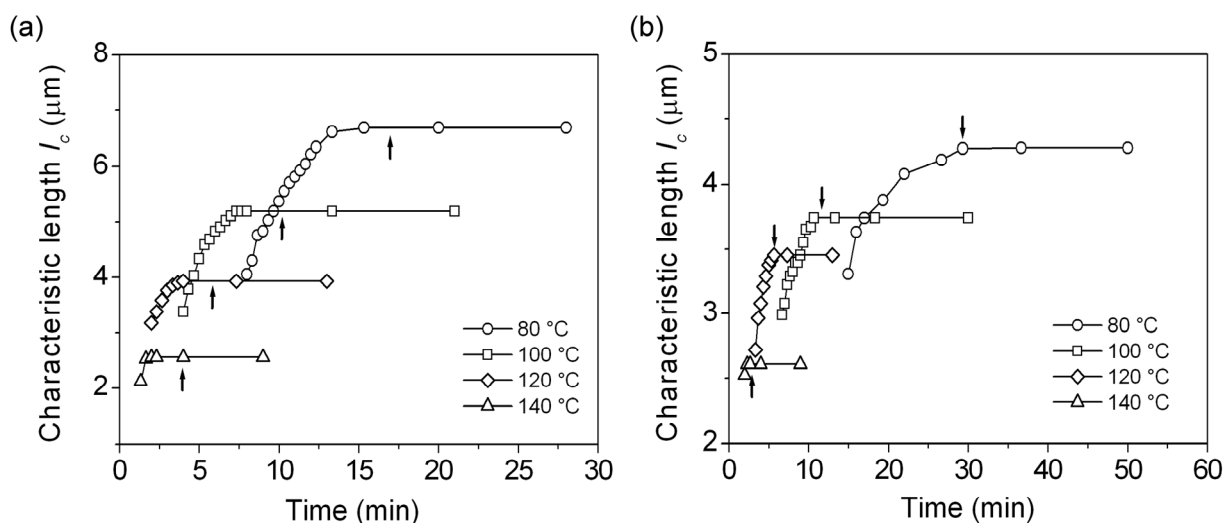
Fig. 5.11. Variation of l_c with T_{cure} for PCL/PPO5-epoxy blends containing (a) 30 wt% PCL and (b) 50 wt% PCL. The arrows indicate the position of the gel point.

Fig. 5.11a shows that for blends with a PCL content of 30 wt%, l_c levels off prior to reaching the gel point. This implies that structure coarsening can proceed up to the hydrodynamic regime, where a decrease in interfacial energy leads to the formation of spherical PPO5-epoxy domains dispersed in the PCL matrix. For blends containing 50 wt% PCL, l_c levels off abruptly after reaching the gel point, which is most profound at high T_{cure} (Fig. 5.11b). This suggests that the phase separation process is hindered by gelation of the PPO5-epoxy-rich phase, thus influencing the final morphology. Under these conditions, the viscoelastic domain formation may not switch

to the hydrodynamic regime and fixation of the morphology shifts towards the elastic regime, leading to the formation of a connected-globule structure as shown in Fig. 5.6b.

Based on these results, the increasing extent of connectivity between the epoxy particles in Figs. 5.6a and b can be explained. The combination of SALS and FTIR spectroscopy showed that PCL/PPO5-epoxy blends with a PCL content of 60 wt% phase separate at an epoxy conversion α of ~ 20 % upon curing at 80 °C. This is far below the calculated epoxy gel content (α = 50 %) and phase separation is, therefore, not severely hindered by gelation (Fig. 5.6a). On the other hand, a curing temperature of 140 °C leads to phase separation at α ~ 70 %, which means that gelation sets in prior to phase separation. A severe hindrance of gelation on the phase separation process is, therefore, expected, which leads to the formation of a connected-globule structure (Fig. 5.6b).

5.3.4. Correlation between morphology and properties

Only the tensile properties of PCL/PPO5-epoxy blends containing 40 wt% PCL and 60 wt% cross-linked rubber will be discussed, since they are most representative for TPVs. Samples with higher PCL contents exhibit a high modulus and inferior elastic behavior and samples with lower PCL contents may lead to (partially) co-continuous morphologies.

Fig. 5.12 shows the tensile properties of PCL/PPO5-epoxy blends containing 40 wt% PCL cured at various temperatures. The rubber particle size decreases from 3.0 to 0.9 μm when T_{cure} is increased from 80 to 160 °C. A decrease in elastic modulus (E), elongation at break (EB) and tensile strength (TS) is observed with decreasing rubber particle size, which is in contrast to the work of Coran et al.[18] and Araghi[19] and the results presented in Chapter 2 on PP/EPDM-based TPVs. This deterioration in tensile properties may be explained by various structural changes of the TPV, such as variations in the crystallinity of PCL, degradation of the PCL phase, different cross-link densities of the PPO5-epoxy rubber phase, incomplete phase separation and/or changes in the morphology. Variations in the crystallinity of the PCL phase were not observed; all samples showed a crystallinity of 40.4 ± 1.5 % as measured by differential scanning calorimetry (DSC) during the second heating run. Degradation of the PCL phase was also not observed; all samples, including the pure PCL, had a M_n of 20 kg/mol and a M_w of 38 kg/mol as measured by size exclusion chromatography (SEC) on the THF-extract of the blends. Dynamic mechanical thermal analysis (DMTA) showed the presence of two T_g's at −53.3 ± 1.1 °C and at 0.4 ± 1.0 °C for all samples (determined as the maxima in the loss moduli), assigned to the PCL phase and the cross-linked PPO5-epoxy phase, respectively. The constant T_g for the cross-linked PPO5-epoxy phase indicates that the cross-link density in all samples is the same. In addition, complete phase separation has occurred, since the observed T_g's are equal to the T_g's of the pure components. The

small differences in gel content and in the amount of grafted PCL as discussed in Chapter 4 can not fully account for the differences in tensile properties as shown in Fig. 5.12. It can, therefore, be concluded that partial connectivity of the rubber particles, which increases with T_{cure} as discussed in detail in the previous section, causes the deterioration in tensile properties. Connection of the rubber particles causes the morphology to shift from a dispersed droplet-like structure towards a co-continuous structure. Consequently, the influence of the soft, cross-linked PPO5-epoxy phase on the tensile properties increases. Since E of the cross-linked PPO5-epoxy is much lower (~ 2 MPa) than E of PCL (~ 280 MPa), interconnection of the PPO5-epoxy particles will decrease E of the TPV. Similarly, EB and TS of the cross-linked PPO5-epoxy are lower than those of PCL, which explains the decrease in EB and TS of the TPVs. So by increasing T_{cure} not only the rubber particle size is reduced, but also the extent of particle connectivity increases. As a result, the positive effect of the particle size reduction on the tensile properties seems to be counteracted by the negative effect of the rubber connectivity.
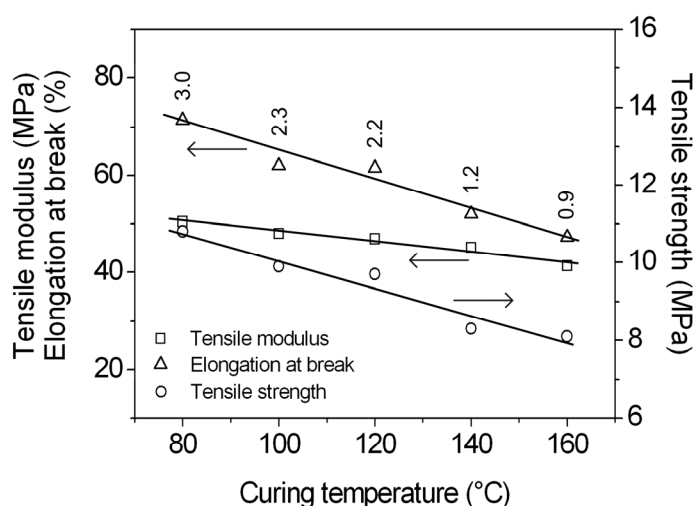
Fig. 5.12. The effect of T_{cure} on tensile properties for PCL/PPO5-epoxy blends containing 40 wt% PCL. The number-averaged rubber particle size is indicated in the figure.

5.4. Conclusions

RIPS of miscible PCL/PPO5-epoxy blends was used to prepare (sub-μm) TPVs with up to 80 wt% of cross-linked PPO5-epoxy rubber dispersed in the PCL matrix (Chapter 4). OM and SALS studies indicate that phase separation of PCL/PPO5-epoxy blends with a composition ranging from 10 to 50 wt% PCL is dominated by SD. Within the applied temperature region, the phase separation behavior follows the TTS principle. The growth-dynamics of the PPO5-epoxy droplets can be described by the WLF-equation, which suggests that the coarsening process is mainly controlled by viscoelastic flow. At relatively low T_{cure}, coarsening proceeds into the hydrodynamic regime, which leads to the formation of spherical rubber particles that are slightly connected to each other. A high T_{cure}, however, leads to fixation of the morphology in the elastic

regime. This explains the extensive particle connectivity as observed by SEM and the consequent deterioration in tensile properties with increasing T_{cure}. Fixation of the morphology is fully determined by gelation of the PPO5-epoxy-rich phase, since vitrification of the PPO5-epoxy-rich phase does not occur in this system. The formation of a connected-globule structure may be prevented by using a less functional curing agent or by applying a dynamic curing process, as was discussed in Chapter 4. Unfortunately, these suggestions to prevent rubber connectivity will result in an increase of the rubber particle size, which is expected to lead to inferior tensile properties[18,19,49]. The application of RIPS to prepare sub-μm TPVs with limited rubber connectivity may be achieved by changing the cross-linking chemistry and, thus, the gelation kinetics and phase separation behavior. An interesting approach would be to change the cross-linking chemistry from the current step-growth mechanism to a chain-growth mechanism, which is discussed in the next chapter.

5.5. References

[1] Sultan, J.; McGarry, F.J. *Polym. Eng. Sci.* **1973**, *13*, 29-34.
[2] Verchère, D.; Pascault, J.P.; Sautereau, H.; Moschiar, S.M.; Riccardi, C.C.; Williams, R.J.J. *J. Appl. Polym. Sci.* **1990**, *41*, 467-485.
[3] Verchère, D.; Pascault, J.P.; Sautereau, H.; Moschiar, S.M.; Riccardi, C.C.; Williams, R.J.J. *J. Appl. Polym. Sci.* **1991**, *42*, 701-716.
[4] Moschiar, S.M.; Riccardi, C.C.; Williams, R.J.J.; Verchère, D.; Sautereau, H.; Pascault, J.P. *J. Appl. Polym. Sci.* **1991**, *42*, 717-735.
[5] Verchère, D.; Pascault, J.P.; Sautereau, H.; Moschiar, S.M.; Riccardi, C.C.; Williams, R.J.J. *J. Appl. Polym. Sci.* **1991**, *43*, 293-304.
[6] Rowe, E.H.; Siebert, A.R.; Drake, R.S. *Mod. Plast.* **1970**, *47*, 110-117.
[7] Bucknall, C.B.; Partridge, I.K. *Polymer* **1983**, *24*, 639-644.
[8] Bucknall, C.B.; Gilbert, A.H. *Polymer* **1989**, *30*, 213-217.
[9] Pearson, R.A.; Yee, A.F. *J. Appl. Polym. Sci.* **1993**, *48*, 1051-1060.
[10] Meijer, H.E.H.; Venderbosch, R.W.; Goossens, J.G.P.; Lemstra, P.J. *High Perform. Polym.* **1996**, *8*, 133-167.
[11] Ishii, Y.; Ryan, A.J. *Macromolecules* **2000**, *33*, 158-166.
[12] Chen, J.; Chang, F. *Macromolecules* **1999**, *32*, 5348-5356.
[13] Chen, J.; Chang, F. *Polymer* **2001**, *42*, 2193-2199.
[14] Chen, J.; Chang, F. *J. Appl. Polym. Sci.* **2003**, *89*, 3107-3114.
[15] Vanden Poel, G.; Goossens, S.; Goderis, B.; Groeninckx, G. *Polymer* **2005**, *46*, 10758-10771.
[16] Remiro, P.M.; Cortazar, M.M.; Calahorra, M.E.; Calafel, M.M. *Macromol. Chem. Phys.* **2001**, *202*, 1077-1088.
[17] Guo, Q.; Groeninckx, G. *Polymer* **2001**, *42*, 8647-8655.
[18] Coran, A.Y.; Patel, R.P. *Rubber Chem. Technol.* **1980**, *53*, 141-150.
[19] Araghi H.H. Proceedings of the International Rubber Conference, Birmingham, United Kingdom, 2001.
[20] Ratna, D. *Polymer* **2001**, *42*, 4209-4218.
[21] Prusty, M.; Keestra, B.J.; Goossens, J.G.P.; Anderson, P.D. *Chem. Eng. Sci.* **2007**, *62*, 1825-1837.
[22] Sivalingam, G.; Madras, G. *Biomacromolecules* **2004**, *5*, 603-609.

5

94

23 ASTM Standard D412 "Standard Test Methods for Vulcanized Rubber and Thermoplastic Elastomers – Tension", 1986.

24 Keenan, M.R. *J. Appl. Polym. Sci.* **1987**, *33*, 1725-1734.

25 Wissanrakit, G.; Gillham, J.K. *J. Appl. Polym. Sci.* **1990**, *41*, 2885-2929.

26 Vyazovkin, S.; Sbirrazzouli, N. *Macromol. Chem. Phys.* **1999**, *200*, 2294-2303.

27 Riccardi, C.C.; Adabbo, H.E.; Williams, R.J.J. *J. Appl. Polym. Sci.* **1984**, *29*, 2481-2492.

28 Kim, M.; Kim, W.; Choe, Y.; Park, J.; Park, I. *Polym. Int.* **2002**, *51*, 1353-1360.

29 Vanden Poel, G. *Ph.D. Thesis*, Catholic University Leuven, Leuven, Belgium, 2003.

30 Bonnet, A.; Pascault, J.P.; Sautereau, H.; Taha, M. *Macromolecules* **1999**, *32*, 8517-8523.

31 Macosko, C.W.; Miller, D.R. *Macromolecules* **1976**, *9*, 199-206.

32 Miller, D.R.; Macosko, C.W. *Macromolecules* **1976**, *9*, 206-211.

33 Yamanaka, K.; Inoue, T. *Polymer* **1989**, *30*, 662-667.

34 Girard-Reydet, E.; Sautereau, H.; Pascault, J.P.; Keates, P.; Navard, P.; Thollet, G.; Vigier, G. *Polymer* **1998**, *39*, 2269-2280.

35 Inoue, T. *Prog. Polym. Sci.* **1995**, *20*, 119-153.

36 Yamanaka, K.; Inoue, T. *J. Mater. Sci.* **1990**, *25*, 241-245.

37 *Rubber-toughened plastics, Advances in Chemistry Series*; Verchère, D.; Sautereau, H.; Pascault, J.P.; Moschiar, S.M.; Riccardi, C.C.; Williams, R.J.J., Eds.; Washington, DC: American Chemical Society, 1993 (p. 335).

38 Yamanaka, K.; Takagi, Y.; Inoue, T. *Polymer* **1989**, *60*, 1839-1844.

39 Williams, R.J.J.; Rozenberg, B.A.; Pascault, J.P. *Adv. Polym. Sci.* **1997**, *128*, 95-156.

40 Gunton, J.D.; San Miguel, M.; Sahni, P.S. In *Phase Transitions and Critical Phenomena*; Domb, C.; Lebowitz, J.L., Eds.; London: Academic, 1983 (pp. 269).

41 Zheng, Q.; Peng, M.; Song, Y.; Zhao, T. *Macromolecules* **2001**, *34*, 8483-8489.

42 Siggia, E.D. *Phys. Rev. A* **1979**, *20*, 595-605.

43 Kim, B.S.; Chiba, T.; Inoue, T. *Polymer* **1995**, *36*, 67-71.

44 Williams, M.L.; Landel, R.F.; Ferry, J.D. *J. Am. Chem. Soc.* **1955**, *77*, 3701.

45 Tanaka, H. *Macromolecules* **1992**, *25*, 6377-6380.

46 Tanaka, H. *Phys. Rev. Lett.* **1993**, *71*, 3158-3164.

47 Tanaka, H. *Phys. Rev. Lett.* **1996**, *76*, 787-790.

48 Gan, W.; Yu, Y.; Wang, M.; Tao, Q.; Li, S. *Macromolecules* **2003**, *36*, 7746-7751.

49 Chapter 2 of this thesis.

Chapter 6

Sub-micrometer thermoplastic vulcanizates obtained by reaction-induced phase separation of miscible poly(ε-caprolactone)/dimethacrylate systems

Reaction-induced phase separation (RIPS) of initially miscible mixtures of poly(ε-caprolactone) (PCL) and elastomer precursors based on difunctional methacrylate resins was applied to prepare thermoplastic vulcanizates (TPVs) with rubber particles ranging from 80 to 900 nm. The radicals formed by the peroxide decomposition initiate the formation of a cross-linked rubber network with gel contents exceeding 90 %, but also abstract hydrogen atoms from the aliphatic moieties in PCL. This leads to the formation of PCL-grafted rubber particles, which show a high nucleating efficiency for crystallization of the PCL matrix. It is demonstrated that the mechanical properties of these TPVs are determined by a complex interplay of the morphology, the type of elastomer precursor, the extent of PCL grafting, the crystallinity and the lamellar thickness. Time-resolved small-angle X-ray scattering (SAXS) measurements during tensile testing indicated that the deformation mechanism of the TPVs is dominated by localized yielding of the PCL matrix. The materials showed a rheological behavior that is typical for TPVs, for which the melt changes from an elastic to a viscous behavior above a critical stress.

6.1. Introduction

A new concept for the preparation of thermoplastic vulcanizates (TPVs) was introduced in Chapters 4 and 5, which is based on the reaction-induced phase separation (RIPS) of initially miscible blends of a semi-crystalline thermoplastic in combination with a low-molar-mass elastomer precursor. Poly(ε-caprolactone) (PCL) in combination with bisepoxide-terminated poly(propylene oxide) (PPOn-epoxy) and triethylene tetramine (TETA) were used as the thermoplastic, the elastomer precursor and the cross-linker, respectively. By using RIPS of homogeneous PCL/PPOn-epoxy/TETA mixtures, up to 80 wt% of μm-sized, cross-linked PPOn-epoxy rubber particles could be dispersed in the thermoplastic PCL matrix without the use of high shear forces, as are typically applied during dynamic vulcanization of TPVs, or the need of additional compatibilization. Although the concept of RIPS was successfully applied for the preparation of TPVs, the correlation length of the concentration fluctuations at the onset of phase separation were found to be in the μm-range, which imposes a severe limit for the preparation of sub-μm morphologies (Chapter 5). The relatively large length scales are related to the continuous increase of the molar mass during the step-growth cross-linking reaction of PPOn-epoxy/TETA. Additionally, partial connectivity between the rubber particles was observed, which explained the relatively low *EB* and *TS* of these PCL/PPOn-epoxy/TETA-based TPVs.

This chapter deals with the preparation of TPVs via RIPS based on miscible PCL/difunctional methacrylate/peroxide systems instead of PCL/PPOn-epoxy/TETA mixtures. The change in cross-linking mechanism from step-growth to chain-growth may allow for the preparation of sub-μm rubber dispersions. First, the cross-linking reaction of the neat elastomer precursors is discussed in terms of the gel content, the degree of swelling and the glass transition temperature (T_g) for different mono- and difunctional methacrylate ratios. Subsequently, the miscibility of the initial mixtures is studied by differential scanning calorimetry (DSC). The morphology of the blends obtained after the *in-situ* reaction is studied by transmission electron microscopy (TEM). Possible side-reactions that may occur during the preparation of the TPVs, such as grafting of PCL onto the rubber particles and cross-linking of PCL, are discussed and are related to the crystallization behavior and mechanical properties of the blends. The micromechanical deformation mechanism of the TPVs is studied by time-resolved small-angle X-ray scattering (SAXS) measurements. Finally, the rheological behavior of the blends is discussed, based on dynamic frequency sweep measurements and creep experiments at various levels of shear stress.

6.2. Experimental

6.2.1. Materials

PCL having M_n = 20 kg/mol and M_w = 37 kg/mol (CAPA 6400) was supplied by Solvay Caprolactones, UK. Two different poly(ethylene oxide)-(PEO)-based dimethacrylate resins (Aldrich) were used, having PEO block lengths of 9 (PEO9, M_n = 550 g/mol) and 14 (PEO14, M_n = 750 g/mol) repeating units. PEO methylether methacrylate (PEO-MA, M_n = 475 g/mol), PPO dimethacrylate (PPO7, M_n = 560 g/mol), the free-radical initiator *tert*-butyl peroxybenzoate, ethanol, methanol, tetrahydrofuran (THF) and sodium hydroxide (NaOH) were obtained from Aldrich and used as received.

6.2.2. Blend preparation

Neat, cross-linked elastomers were prepared by curing the liquid elastomer precursors or mixtures thereof with a varying peroxide content of 0.2 to 4.5 wt% for 90 min at 110 °C. To prepare the blends, PCL was dissolved in ~ 95 wt% of the required amount of liquid dimethacrylate resin at 110 °C in a round bottom flask by using a mechanical stirrer. The peroxide was added as a solution in the remaining ~ 5 wt% of dimethacrylate resin and the solution was mixed at 150 rpm until a homogeneous mixture was obtained (mixing time ~ 4 min). The stirring was stopped during the cross-linking reaction and a nitrogen flow was applied to remove oxygen, which may act as a radical scavenger. Unless stated otherwise, a peroxide content of 0.5 wt% (based on the elastomer precursor content) and a curing time of 90 min were used. An additional curing step of 30 min at 150 °C was applied to all samples to ensure complete decomposition of the peroxide.

TPVs with a constant PCL concentration (40 and 60 wt%) and varying rubber particle size were obtained by the addition or removal of PCL via a solution route. Selected TPVs were dissolved in THF, after which the required amount of PCL was added or removed. The removal of PCL was achieved by centrifuging the TPV solution at 3000 rpm in a Mistral 3000E centrifuge to separate the cross-linked rubber particles from the PCL in solution. The addition of PCL was achieved by dissolving the required amount of PCL in the TPV solution. All samples were dried overnight at 30 °C under vacuum to remove THF and were subsequently extruded for 10 min at 90 °C in a home-built, recirculating, twin-screw micro-extruder with an internal volume of 5 cm³ in order to homogenize the samples.

After separation of the rubber particles from the PCL solution via centrifugation, the PCL grafts were removed by hydrolysis of the grafted PCL chains. Hydrolysis of grafted PCL was achieved by stirring the centrifuged rubber fraction for 3 hours in a 10 wt/vol% NaOH/methanol solution[1]. The rubber fraction was then washed with a 70/30 wt/wt% water/methanol solution to remove residual NaOH and the sodium carboxylate hydrolysis product. Subsequently, the rubber particles were added to a THF solution containing the required amount of PCL, after which the sample was dried and extruded as previously described.

6.2.3. Characterization techniques

Solvent extractions. The gel content (*%gel*) and degree of swelling (*%swell*) of the neat, cross-linked elastomers were determined by extraction with THF for 48 hrs at room temperature. The *%gel* and *%swell* of the rubber phase in the blends with PCL was determined by extraction and swelling with ethanol for 48 hrs.

Size exclusion chromatography (SEC). The molar mass distribution of PCL was determined by using a Waters model 510 pump and a Waters 712 WISP chromatograph with PL-gel mix D columns (300 x 7.5 mm, Polymer Laboratories). THF was used as eluent with a flow rate of 1 mL/min. All samples were diluted to 1 mg/mL and filtered by using 0.2 μm syringe filters. The absolute molar mass of PCL was calculated using poly(styrene) standards, applying the universal calibration principle with the Mark-Houwink parameters K = 0.00109 dL/g and α = 0.6[2].

Transmission electron microscopy (TEM). Morphological investigations were performed on a Tecnai 20 transmission electron microscope operated at 200 kV. Samples were trimmed at -120 °C and subsequently bulk-stained for 24 hrs with a ruthenium tetroxide (RuO_4) solution prepared according to Montezinos *et al.*[3]. Ultrathin sections (70 nm) were obtained at -100 °C by using a Leica UltracutS/FCS microtome. The sections were placed on a 200 mesh copper grid with a carbon support layer. The number-averaged diameter of the rubber particles ($\overline{D_n}$) was determined with the Image Pro Plus 4.5 software. Tilt series for TEM tomography were obtained in an automatic fashion by using the EXPLORE 3D software (Fei Co.). The alignment and reconstruction of the data series was performed by using the INSPEC 3D software (Fei Co.), and visualization of the 3D reconstructed volume was done with the Amira 3.1 software (Mercury Computer Systems, Inc.).

Differential scanning calorimetry (DSC). The miscibility study of PCL/PEO9 mixtures was performed on a Perkin Elmer Pyris 1 calorimeter, while crystallization studies were performed on a TA Instruments Q1000 calorimeter. Hermetically sealed aluminum pans were used with a sample weight of ~ 5 mg. The samples were first heated to 100 °C and equilibrated for 5 min in order to remove the thermal history. Subsequently, they were cooled at a rate of 10 °C/min to -90 °C, where they were kept for 5 min, and then reheated to 100 °C at a rate of 10 °C/min. The offset at the end of the melting endotherm of the second heating run was used to determine the melting temperature (T_m) in the miscibility studies[4], while the maximum of the melting endotherm of the second heating run was used to determine T_m in the crystallization studies. The onset of the crystallization exotherm of the cooling run was used to determine the crystallization temperature (T_c). The crystallinity (X_c) was calculated by using 136 J/g as the heat of fusion of 100% crystalline PCL[5].

Fourier transform infrared (FTIR) spectroscopy. Infrared experiments were performed on a BioRad Excalibur 3000 spectrometer equipped with a diamond Specac Golden Gate attenuated total reflection (ATR) setup over a spectral range of 650 to 5000 cm^{-1}. Fifty spectra at a resolution of 4 cm^{-1} were signal-averaged and the resulting spectra were analyzed by using the BioRad Merlin 3.0 software. The grafted PCL content was determined by evaluating the ratio of the integrated intensities of the C=O

stretching band of PCL at 1721 cm^{-1} and the asymmetric C-O-C stretching band of the ethylene oxide repeat unit of PEO9 positioned at 1095 cm^{-1}.

Dynamic mechanical thermal analysis (DMTA). Compression-molded samples (10.0 x 3.0 x 0.5 mm) were measured on a TA Instruments DMA Q800 with a film tension setup. Temperature sweeps from -100 to 100 °C were performed with a heating rate of 3 °C/min at a frequency of 1 Hz. A pre-load force of 0.01 N, an amplitude of 10 μm and a force track of 110 % were used. The glass transition temperature (T_g) was determined from the maximum in tan δ, since it is often difficult to accurately determine the maximum in the loss modulus (E'')[6].

Tensile testing. Dumbbell-shaped tensile bars (32.0 x 2.0 x 1.0 mm) were punched from compression-molded samples. Tensile tests were performed at 12 mm/min by using a 2.5 kN force cell on a Zwick Z010 tensile tester according to ASTM D412[7]. The equipment was controlled with the TestXpert v7.11 software. Each sample was tested in at least 10-fold and average values are presented.

Small-angle X-ray scattering (SAXS). The mode of microscopic deformation was studied by performing time-resolved SAXS measurements during tensile testing at the Dutch-Belgian (DUBBLE) beamline BM26 of the European Synchrotron Radiation Facility (ESRF) in Grenoble, France. The size of the X-ray beam was approximately 200 x 200 μm[2] with a wavelength of 1.203 Å. A 2D multiwire gas-filled detector was used with 512 x 512 pixels and a horizontal and vertical pixel size of 260 μm at a distance of 3200 mm. For calibration of the SAXS detector, the scattering pattern from an oriented specimen of dry collagen (rat-tail tendon) was used. The experimental data were corrected for background scattering, i.e. subtraction of the scattering from air. The tensile bars (32.0 x 2.0 x 1.0 mm) were stretched using a Linkam tensile device in which both clamps moved in opposite directions at a tensile speed of 12 mm/min. The total beam intensity in front of and behind the sample was recorded by ionization chambers during the drawing process.

Compression set. The compression set (*CS*) was measured on cylindrical samples with a diameter of 13 mm and a thickness of 6 mm for 22 hrs at 10 % or 25 % compressive strain and a subsequent relaxation time of 30 min, according to ASTM D395[8] and ISO 815[9]. The *CS* was calculated as follows:

$$CS = \frac{(t_i - t_o)}{(t_i - t_n)} \times 100\%$$ (6.1)

where t_i is the initial thickness of the sample, t_o the final thickness of the sample and t_n the thickness of the spacer. The relative standard deviation in *CS* is 1-2 %.

Rheological measurements. Dynamic shear measurements were performed on a strain-controlled AR-G2 rheometer (TA Instruments) by using a 8 mm parallel-plate geometry and disk-shaped specimens (8 mm diameter; 0.5 mm thick). Dynamic shear measurements on pure PCL were conducted by using a 25 mm parallel-plate geometry and disk-shaped specimens (25 mm diameter; 1 mm thick). Frequency sweeps from 500 to 0.01 rad/s were performed at 100 °C with a strain of 1 %, which corresponds to the linear viscoelastic regime. Creep measurements were performed on a stress-controlled AR-G2 rheometer (TA Instruments). Shear stresses ranging from 0.1 to 45 kPa were applied for 10 min at 100 °C.

6.3. Results and discussion

6.3.1. Cross-linking of neat elastomers

Cross-linking of mixtures of difunctional and monofunctional (meth)acrylates typically leads to imperfect cross-linked networks with varying levels of dangling chain ends[10,11]. An increase in the monofunctional monomer content causes a significant decrease in the cross-link density, since the monofunctional monomer acts as a chain extender. The gel content (*%gel*), the degree of swelling (*%swell*) and the glass transition temperature (T_g) are commonly used to express the state of cross-linking of rubber networks. Where *%gel* quantifies the amount of rubber that is incorporated into the covalently cross-linked network, *%swell* specifies the ability of the network to swell in the presence of a solvent and decreases with increasing cross-link density. T_g typically increases linearly with increasing cross-link density[12], although a more rapid increase in T_g is often observed at high cross-link densities due to non-Gaussian behavior and steric effects[13]. Figs. 6.1 and 6.2 and Table 6.1 show the *%gel*, *%swell* and T_g as a function of the peroxide content and the monofunctional PEO-MA content. Variations in the peroxide content in a range from 0.2 to 4.5 wt% have no major influence on the cross-link density of the rubber, which is reflected in a constant *%gel*, *%swell* and T_g. Increasing the PEO block length from 9 to 14 units leads to an increase in *%swell* and a decrease in T_g, which indicates a decrease in the cross-link density as a result of diluting the network with longer PEO spacers.
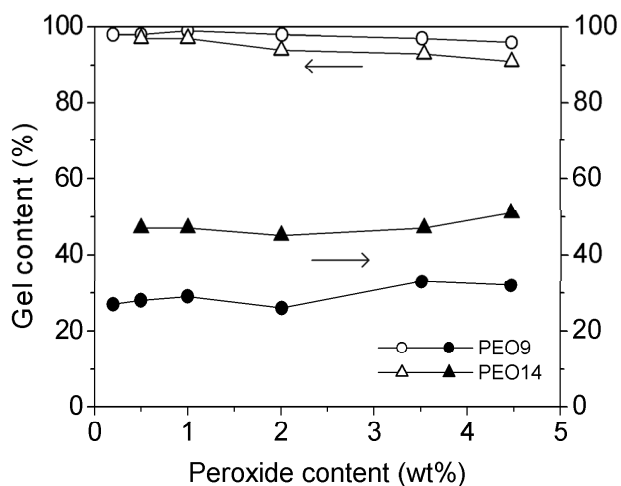
Fig. 6.1. %gel and %swell as a function of the peroxide content at 0 wt% PEO-MA.
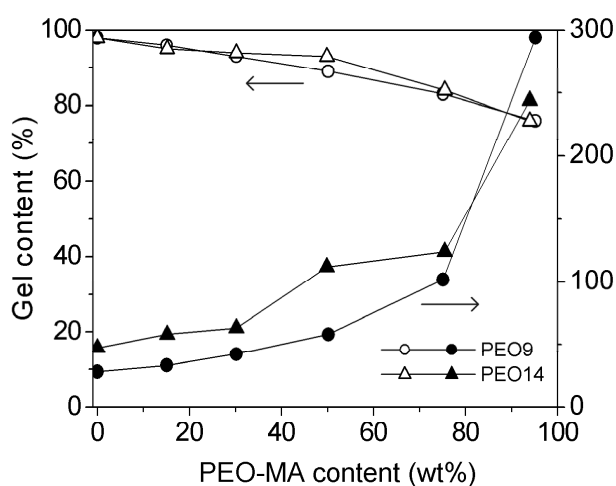
Fig. 6.2. %gel and %swell as a function of the PEO-MA content at 0.5 wt% peroxide.

An increase in the PEO-MA content from 0 to 50 wt% leads to an increase in *%swell*, a small decrease in *%gel* and a decrease in T_g, which is attributed to a decrease in cross-link density by the monofunctional PEO-MA, which acts as a chain extender. At PEO-MA contents exceeding 50 wt%, *%swell* increases drastically and *%gel* drops to values below 90 %, which is attributed to a combined effect of decreasing cross-link density and increasing amount of dangling ends[10].

These results show that the cross-link density of the PEO-based rubbery networks can be controlled by changing the PEO block length and the PEO-MA content, which is useful in tuning the mechanical properties of TPVs containing a cross-linked PEO-based rubbery phase.

It has to be noted that T_g should be determined from the maximum in E'' rather than from the maximum in tan δ[6]. Nevertheless, the maximum in tan δ has been used in this study, since the maximum in E'' is not evident for all samples and significant errors in T_g may, therefore, be induced. This is especially true for the PEO in blends with PCL, where the T_g's of PCL and the cross-linked rubber phases may (partially) overlap. The T_g values presented throughout this chapter should, therefore, be taken as indicative rather than absolute values.

Table 6.1. T_g as a function of peroxide and PEO-MA content for PEO9 and PEO14 elastomer precursors.

Elastomer precursor	Peroxide content (wt%)	PEO-MA content (wt%)	T_g (°C)
PEO9	0.5	0	12
PEO9	2.0	0	13
PEO14	2.0	0	-26
PEO9	0.5	15	-7
PEO9	0.5	30	-12

6.3.2. Miscibility of PCL/PEO9 mixtures

In order to be able to apply RIPS to PCL/PEO9 mixtures, first the miscibility has to be determined. The miscibility of PCL/PEO9 mixtures with varying compositions was studied by evaluating the melting temperature (T_m) of PCL in the mixtures. The extent of the T_m depression of semi-crystalline polymers in mixtures with low-molar-mass species, such as solvents or monomers, provides information on the thermodynamic miscibility of the blend components. In the PCL/PEO9 mixtures, a continuous decrease of T_m and T_c of PCL is observed with increasing PEO9 content (Fig. 6.3). From the T_m depression, the interaction parameter χ_{12} can be calculated based on the modified Flory-Huggins lattice model[14-16]:

$$\frac{1}{T_m} - \frac{1}{T_m^0} = -\frac{RV_2}{\Delta H_2 V_1}\left[\frac{\ln\phi_2}{m_2} + \left(\frac{1}{m_2} - \frac{1}{m_1}\right)\phi_1 + \chi_{12}\phi_1^2\right] \tag{6.2}$$

where subscripts 1 and 2 identify the amorphous PEO9 and the crystalline PCL, respectively. R is the universal gas constant, V is the molar volume of the repeating unit, ΔH_2 is the melting enthalpy of 100 % crystalline PCL, ϕ is the volume fraction and m is the degree of polymerization. T_m^0 and T_m are the melting temperatures of pure PCL and PCL in the mixture, respectively. Taking $T_m^0 = 333$ K, $\Delta H_2 = 136.0$ J/g[5], $V_1 = 469.2$ cm³/mol[17], $V_2 = 98.5$ cm³/mol, m_1

= 1 and m_2 = 187 leads to a value for χ_{12} of -0.28 at 333 K. The negative value of χ_{12} indicates a negative enthalpy of mixing, which means that the system is fully miscible in the molten state. It should be noted that this approach to estimate χ_{12} neglects the effect of any morphological changes of the PCL crystals and assumes that the observed T_m depression is primarily caused by thermodynamic interactions between the crystalline and the amorphous phases.
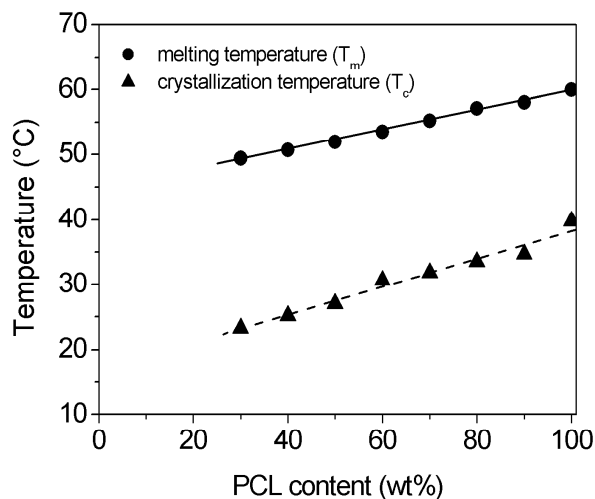
Fig. 6.3. T_m and T_c of PCL/PEO9 mixtures as a function of the composition. The solid line represents the Flory-Huggins fit of T_m. The dashed line represents the best fit through the data points of T_c.

6.3.3. Preparation of PCL/PEO9 blends

A recent study showed that the polymerization of methacrylate monomers in immiscible blends with PCL can lead to grafting reactions of the methacrylate monomer onto the PCL chains, especially at high peroxide concentrations[18]. Homolytic decomposition of the peroxide yields oxyradicals which can abstract hydrogen atoms from the aliphatic moieties in PCL, leading to the formation of PCL macroradicals. These PCL macroradicals may add to the methacrylate monomer or combine with the growing poly(methacrylate) chains, leading to PCL graft formation[18]. Combination of two PCL macroradicals and multiple PCL grafting can, ultimately, lead to cross-linking of PCL. For the preparation of TPVs, partial grafting of PCL onto the reacting PEO9 network may be advantageous, since *in-situ* formed graft copolymers are known to suppress the growth of concentration fluctuations during the early stages of phase separation and to suppress the rate of coarsening at the later stages, thereby reducing the final particle size of the dispersed phase[19]. On the other hand, cross-linking of the PCL matrix must be prevented, since it will severely limit the melt processability of the TPV. Additionally, multiple grafting of a single PCL chain may lead to connectivity between the rubber particles and, ultimately, to cross-linking of the PCL matrix via the rubber particles.

Fig. 6.4 summarizes the influence of the peroxide content on the chemical composition of PCL/PEO9 blends containing 60 wt% PCL after *in-situ* cross-linking of the PEO9. The amount of

PCL that is grafted onto the cross-linked rubber network was determined by removing the non-grafted PCL via THF extraction and subsequent FTIR spectroscopy analysis on the dried residue. The amount of grafted PCL is expressed in wt% based on the total sample weight and increases with the peroxide content, which is caused by an increased extent of PCL macroradical formation. This is also reflected by a slight increase in molar mass of the THF-extracted PCL, which is most profound for the z-averaged molar mass (M_z), since M_z is most sensitive to high-molar-mass species such as graft copolymers. Since the molar mass of the extracted PCL does not increase dramatically, extensive cross-linking of the PCL matrix in these samples can be ruled out. The *%gel* of the PEO9 phase increases with increasing peroxide content and reaches reasonable values of > 90 % over the whole range of applied peroxide contents. During the remainder of this study, a peroxide concentration of 0.5 wt% is applied to prepare the blends, since this leads to a combination of a high *%gel*, a limited extent of PCL grafting and only a slight increase in the molar mass of the PCL matrix (Fig. 6.4), which is expected to be optimal for TPV properties.
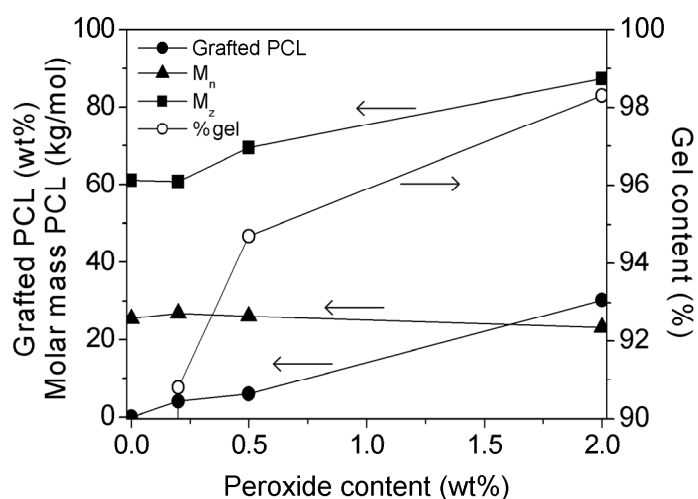
Fig. 6.4. Influence of peroxide content on M_n and M_z of the THF-extracted PCL matrix, the amount of grafted PCL and %gel for cross-linked PCL/PEO9 blends containing 60 wt% PCL.

6.3.4. Morphology of cross-linked PCL/PEO9 blends

The morphology of the phase-separated PCL/PEO9 blends after *in-situ* cross-linking of the PEO9 elastomer precursor was studied by TEM (Fig. 6.5). The rubber phase appears black in the TEM images, since RuO_4 was used to stain the amorphous PCL phase and the rubber phase. A relatively coarse structure ($\overline{D_n} \sim 900 \pm 250$ nm) is found at a PCL content of 20 wt% (Fig. 6.5a), which appears to be partially co-continuous. This indicates that the initial composition is close to the critical concentration, i.e. the concentration where the binodal and spinodal curves intersect. Upon increasing the PCL content to 40 wt% and higher, the cross-linked rubber clearly becomes the dispersed phase and has sub-μm dimensions. Increasing the PCL content leads to a decrease

in $\overline{D_n}$ from 305 ± 90 nm at 40 wt% PCL down to 80 ± 20 nm at 80 wt% PCL. Variations in the peroxide content between 0.2 and 2 wt% did not lead to visible changes in the morphology as studied by TEM.
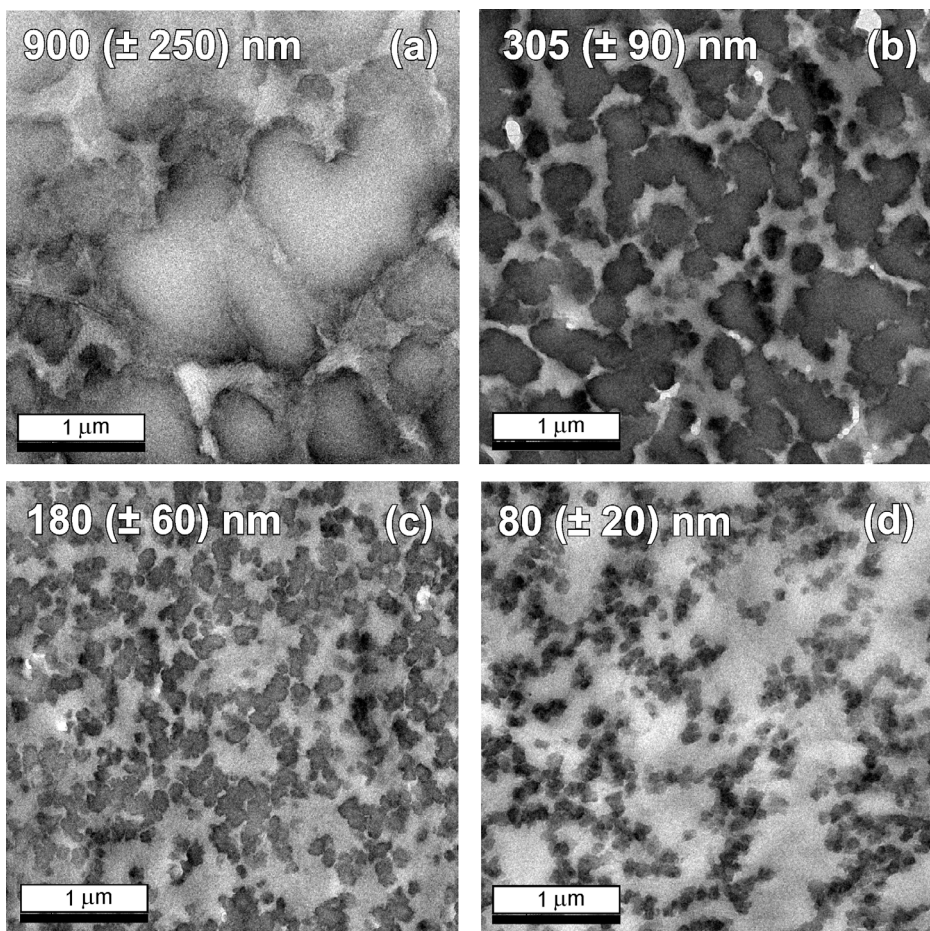
Fig. 6.5. TEM images of PCL/PEO9 blends containing (a) 20 wt%, (b) 40 wt%, (c) 60 wt% and (d) 80 wt% PCL. The number-averaged rubber particle size ($\overline{D_n}$) and its standard deviation are given in the figures.

Generally, the demixing process of initially miscible polymer/monomer systems as induced by free-radical polymerization is rather complex, since the binary system changes into a ternary system during chain polymerization and the thermodynamic quench depth continuously changes during the reaction. In the case of cross-linking polymerization, not only the composition changes during the reaction, but also the cross-link density of the polymerized monomer(s). From studies on the bulk polymerization of mixtures of mono- and divinyl compounds, it is known that gelation occurs in the very early stages of the reaction, typically around 1-2 % conversion, which hardly depends on the divinyl concentration between 10 and 100 wt%[20]. Since in our case a difunctional monomer is used, it is anticipated that gelation occurs in the early stages of the reaction and that it will influence the phase separation process. Gelation may even precede phase separation, i.e. liquid-gel separation rather than liquid-liquid separation may occur[21,22]. Due to the high elasticity of the phase-separating PEO9 phase in comparison to the viscous PCL phase, a

dynamically asymmetric mixture is formed and coarsening may be controlled by viscoelastic flow[23]. Viscoelastic phase separation is characterized by changes of the relevant coarsening mode in time; namely, it switches from an initially diffusive mode to an elastic mode and eventually to a hydrodynamic mode. In the elastic regime, the elastic force balance determines the morphology instead of the interfacial tension. Therefore, fixation of the morphology in the elastic regime of phase separation typically leads to a sponge-like co-continuous structure[23]. During the later stages of phase separation the system approaches its equilibrium state and the deformation rate of the domains slows down as phase separation proceeds into the hydrodynamic regime. The morphology tends to transform into the shape of the lowest interfacial energy (a sphere), so the sponge-like structure becomes unstable and the inter-connectivity breaks up. The results presented in Chapter 5 on RIPS of PCL/epoxy systems showed that the high elasticity of the cross-linking epoxy phase can lead to a significant extent of particle connectivity in the final blend. Although Fig. 6.5 clearly shows that the cross-linked rubber is the dispersed phase, the clustered rubber domains in the TEM images suggest partial rubber connectivity, especially at high rubber contents, which may be attributed to fixation of the phase-separating structure prior to reaching the hydrodynamic regime. The irregular shape of the cross-linked rubber particles is related to the high elasticity of the particles, which influences their shape relaxation during and after phase separation[22,23].

The TEM images presented in Fig. 6.5 are a projection of the three-dimensional (3D) structure of the blend along the direction of the common axis onto a two-dimensional (2D) screen. Therefore, valuable information of the morphology in the third dimension is discarded and the 2D-TEM images introduce some uncertainty as to the true 3D structure of the samples. In the case of polymer blends with a matrix/dispersion morphology, a 2D projection of nearby particles may lead to overlap, which gives the impression of a co-continuous structure in a 2D-TEM image. A previous study showed that a 2D representation of a true TPV morphology can be quite misleading, since the dispersed rubber particles appear to be partially connected or may even appear as a continuous phase in the 2D image[24]. Electron tomography is a relatively new and powerful technique for the reconstruction of a 3D structure from a series of 2D projections taken at various tilt angles. 3D-TEM images of a PCL/PEO9 blend containing 60 wt% PCL obtained at different tilt angles are shown in Fig. 6.6, where the rubber appears as the light phase. The arrows indicate representative areas where the rubber particles appear either separated or connected, depending on the tilt angle. Studying the electron images at various tilt angles allows for a better interpretation of the true 3D structure of the blend and shows that the extent of rubber connectivity is lower than implied by the 2D-TEM images in Fig. 6.5. Connectivity between

particles that originates from the grafting of a single PCL chain on multiple rubber particles cannot be resolved from these TEM studies.
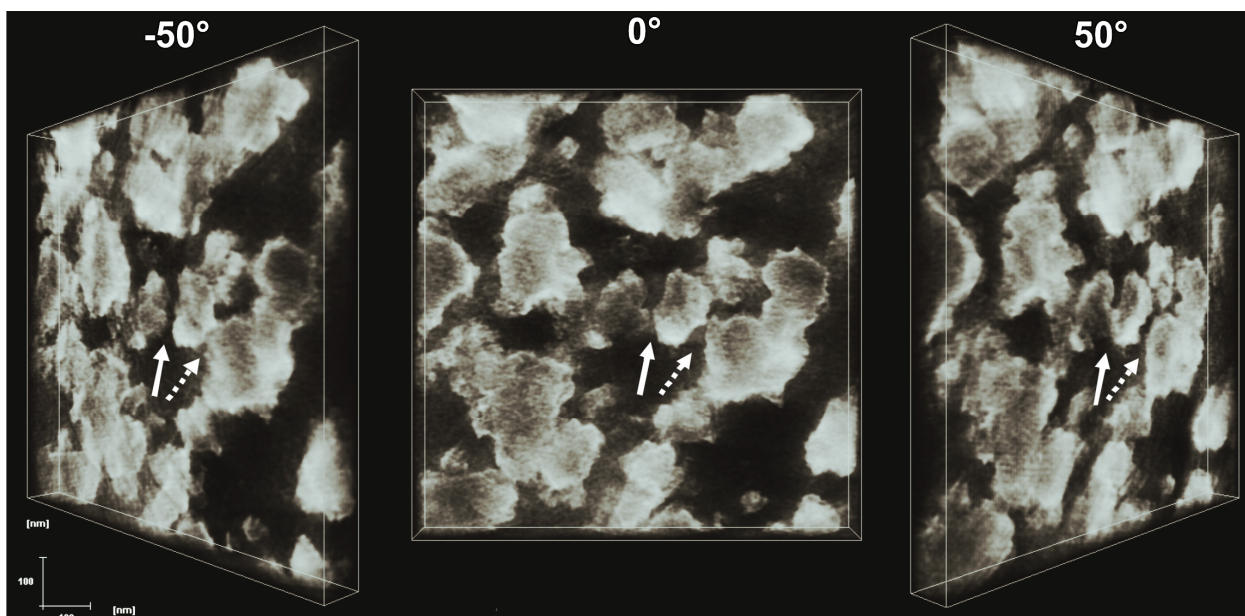
Fig. 6.6. Representative 3D-TEM images of a PCL/PEO9 blend containing 60 wt% PCL at tilt angles of -50, 0 and 50°.

Fig. 6.7 shows an enlargement of Fig. 6.5c, where the amorphous rubber particles and the crystalline PCL lamellae are clearly visible. The image suggests the growth of lamellae from the surface of the rubber particles, which would indicate a nucleating ability of the rubber particles. In order to gain a better insight in the nucleating effect of the rubber particles on the PCL matrix, the next section deals with the thermal properties of the TPVs.
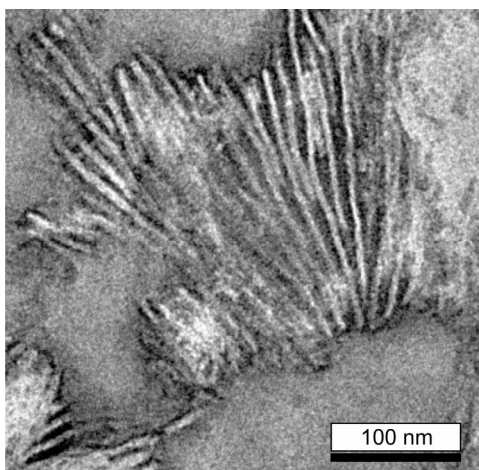
Fig. 6.7. Orientation of crystalline lamellae near the surface of rubber particles.

6.3.5. Thermal properties of PCL/PEO9-based TPVs

Table 6.2 provides an overview of the thermal properties of PCL and the PCL/PEO9-based TPVs with a variation in PCL content, peroxide content, $\overline{D}_n$ and amount of grafted PCL. X_c decreases with increasing rubber content from 46 % for pure PCL to 37 % for TPVs containing

80 wt% of rubber. A similar decrease in Xc was observed for PP/EPDM-based TPVs (Chapter 2.3.2) and is attributed to topological confinements imposed by the presence of the rubber phase[25,26]. No significant changes in T_m are observed. Increasing the peroxide and PEO9 content leads to an increase in the amount of grafted PCL. Where X_c and T_m are hardly affected by increasing the peroxide content, a significant increase in T_c is observed from 33.4 °C at 0.2 wt% peroxide to 37.3 °C at 2.0 wt% peroxide. A strong increase in T_c from 32.7 °C to 38.5 °C is also observed upon increasing the rubber content from 20 to 80 wt% at a constant peroxide content of 0.5 wt%. These results indicate that the rubber particles act as a nucleating agent for PCL. The significant increase in T_c of these blends is remarkable, since amorphous particles are known to have only a limited nucleating ability[27]. Therefore, the nucleating effect of the rubber particles in these TPVs is expected to be related to the grafting of PCL chains on the surface of the rubber particles. Obviously, the best nucleating agent for a semi-crystalline polymer is the polymer itself, due to the epitaxial fit and the low interfacial energy difference.

Table 6.2. Thermal properties of PCL and PCL/PEO9-based TPVs.

PCL (wt%)	Peroxide (wt%)	$\overline{D_n}$ (nm)	Grafted PCL (wt%)	X_c (%)	T_m (°C)	T_c (°C)
100	-	-	-	45.9	55.1	31.3
60	0.2	200 ± 60	4.0	43.0	54.8	33.4
60	0.5	180 ± 60	5.9	42.0	55.1	34.1
60	2.0	140 ± 40	30.3	44.1	55.3	37.3
80	0.5	80 ± 20	3.0	44.0	56.3	32.7
40	0.5	305 ± 90	5.9	39.7	55.6	36.0
20	0.5	900 ± 250	7.3	37.1	54.5	38.5

6.3.6. Mechanical properties of PCL/PEO9-based TPVs

As shown by the THF extraction and TEM results, RIPS of PCL/PEO9 blends yields materials with a fine dispersion of cross-linked rubber particles in a semi-crystalline PCL matrix, which fulfils the structural requirements of a TPV. Variations in the composition, the rubber particle size, the crystallization behavior and the cross-link density of the rubber phase will influence the mechanical properties of the TPVs, which is discussed in this section.

Fig. 6.8 shows that *%gel* of the cross-linked rubber phase in the TPVs decreases slightly upon increasing the PCL content, but remains > 90 % for all samples. The T_g of the rubber phase in the TPVs is lower compared to the T_g of the neat cross-linked rubber (see also Fig. 6.1). Since the T_g of the PCL matrix remains constant at -55 °C, this change in T_g of the rubber phase cannot be

attributed to incomplete phase separation and can, therefore, be ascribed to a decrease in cross-link density. An increase in the rubber content leads to a decrease in the Shore D hardness and an improvement of the elastic recovery, i.e. a decrease in *CS*. According to ASTM D395[8] and ISO 815[9], the compressive strain that is applied during a compression set measurement has to be adjusted to the hardness of the TPV. A compressive strain of 25 % should be used for materials with a hardness lower than 30 Shore D, whereas for TPVs with a hardness above 30 Shore D a strain of 10 % should be used. Fig. 6.8 shows a clear dependence of *CS* on the applied compressive strain. A larger compressive strain increases the extent of plastic deformation during compression and, therefore, leads to less elastic recovery after removal of the strain.
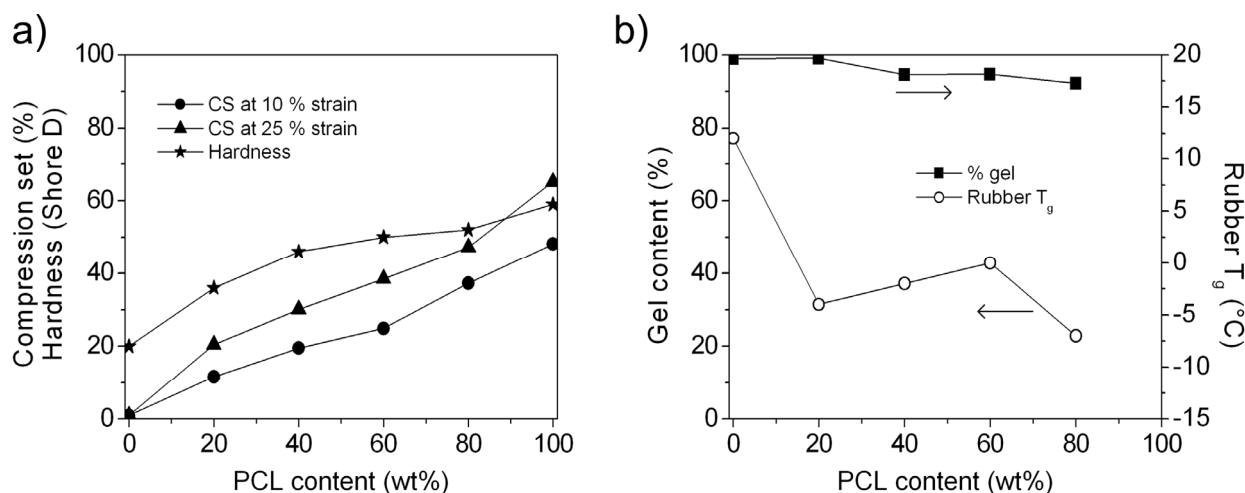
Fig. 6.8. (a) CS and hardness and (b) %gel and rubber T_g of PCL/PEO9-based TPVs as a function of the composition.

Fig. 6.9 shows the tensile properties of the PCL/PEO9-based TPVs with a variation in the PCL content. A decrease in the PCL content leads to a lower elongation at break (*EB*), elastic modulus (*E*) and tensile strength (*TS*), which is a trend typical for TPVs. The PCL/PEO9-based TPVs show a *CS* of ~ 30 % at a PCL content of 50 wt%, whereas the conventional PP/EPDM-based TPVs show a *CS* of ~ 40 % at a PP content of 50 wt% (see Chapter 2.3.5), which indicates that the elastic recovery of the PCL/PEO9-based TPVs is relatively good. However, both *EB* and *TS* of the PCL/PEO9-based TPVs are relatively low, especially at high rubber contents. The combination of a good elastic recovery and a poor *EB* may be related to the relatively high cross-link density of the rubber phase. In the case of full cross-linking, the theoretical molar mass between cross-links (M_c) of the PEO9 phase is calculated to be 550 g/mol, assuming that all methacrylate end groups have reacted. M_c of the rubber phase in commercial PP/EPDM-based TPVs is typically in the order of 2000 g/mol, which includes both chemical cross-links and trapped chain entanglements[28,29]. Although the rubber phase in the PCL/PEO9-based TPVs is not fully cross-linked (Fig. 6.8), M_c of the PEO9-based rubber is expected to be high in comparison to that of EPDM in PP/EPDM-based TPVs. It is known that the elastic recovery of TPVs

improves with decreasing M_c, but eventually levels off to a plateau value which depends only on the total rubber content of the TPV[30]. *EB*, on the contrary, shows a continuous decrease with decreasing M_c. Due to the finite extensibility of the network, a decrease in M_c leads to an increase in the local stress that is experienced by the network chains. Therefore, the critical stress that leads to chain rupture is reached at lower macroscopic elongations, yielding a decrease in the ultimate *EB* of the TPV[31]. This suggests that *EB* of the PCL/PEO9-based TPVs can be increased by decreasing the cross-link density of the rubber phase, without significantly deteriorating the elastic recovery. This enhancement is demonstrated by replacing PEO9 with PEO14 as the elastomer precursor, which increases the theoretical M_c from 550 to 750 g/mol and, consequently, increases *EB* from 125 to 170 % (Fig. 6.9), while *CS* increases only slightly from 39 to 41 % at a compressive strain of 25 % (not shown here).
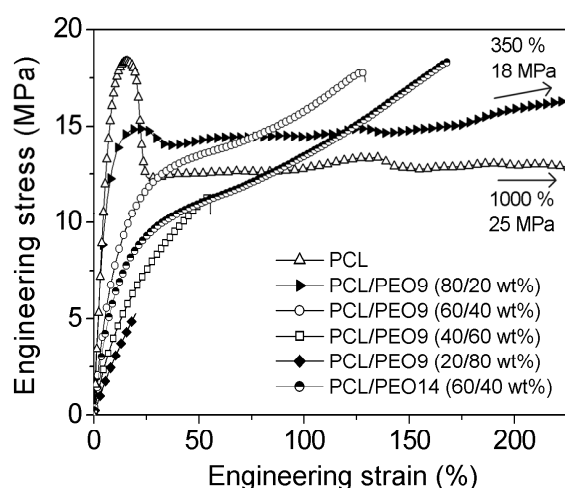
Fig. 6.9. Influence of composition and type of elastomer precursor on tensile properties of PCL/PEO-based TPVs.

6.3.7. Influence of rubber particle size on mechanical properties

As discussed in Chapter 2.3.3, a decrease in rubber particle size from 70 to 1 μm leads to a significant enhancement of the tensile properties of PP/EPDM-based TPVs. Fig. 6.10 shows the influence of $\overline{D_n}$ on *EB* and *TS* for PCL/PEO9-based TPVs containing 60 and 40 wt% PCL prepared by adding/removing PCL via solution routes. A decrease in $\overline{D_n}$ from 520 to 80 nm leads to a significant increase in *EB*, especially for the TPVs containing 60 wt% PCL, while relatively small variations in *TS* are observed. *E* tends to decrease slightly with decreasing $\overline{D_n}$ (not shown here). The increase in *EB* is consistent with the extrapolation of the results presented in Chapter 2.3.3 and can be explained by the more efficient suppression of interlamellar void formation and subsequent coalescence of voids. Additionally, the suppression of rubber particle cavitation and the decreasing probability of reaching the critical crack size upon internal fracture of the rubber particle contribute to the enhanced tensile properties. However, $\overline{D_n}$ is not the only

variable of the PCL/PEO9-based TPVs that influences the mechanical properties. The amount of grafted PCL also varies, which may lead to changes in the interfacial adhesion and the nucleation behavior and, concomitantly, to changes in the lamellar thickness and the size of spherulites. As was already stated by Corté et al.[32], the mechanical properties of rubber-modified blends are largely influenced by changes in the crystalline morphology of the semi-crystalline matrix and the improvement in tensile properties can, therefore, not solely be attributed to the decrease in $\overline{D_n}$. A more detailed study on the crystallization behavior of these TPVs is, therefore, required, which is the subject of the next chapter.
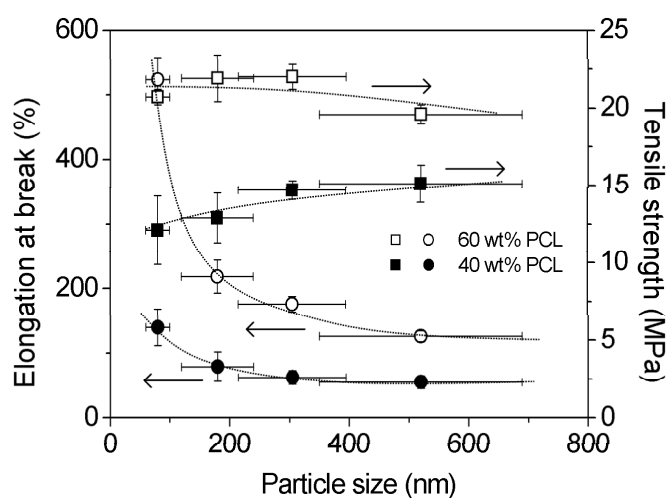
Fig. 6.10. EB and TS as a function of $\overline{D_n}$ for PCL/PEO9-based TPVs containing 60 and 40 wt% PCL.

Fig. 6.11 shows the influence of $\overline{D_n}$ on *CS* for PCL/PEO9-based TPVs containing 60 and 40 wt% rubber. For both rubber contents, decreasing $\overline{D_n}$ leads to an increase in *CS* at both 10 and 25 % compressive strain, i.e. to a deterioration of the elastic recovery. This is in contradiction to the results on PP/EPDM-based TPVs presented in Chapter 2.3.5, which showed an improvement of *CS* with decreasing $\overline{D_n}$. The improved *CS* with increasing $\overline{D_n}$ in Fig. 6.10 may be explained by changes in the crystalline morphology of the PCL matrix. Previous work on PP containing various amounts of nucleating agent showed a direct relationship between T_c, the lamellar thickness (L_c) and the yield stress (σ_y)[33]. A linear increase in L_c was observed with increasing T_c. Additionally, σ_y showed a linear increase with L_c. It was concluded that the frequently observed changes in mechanical properties of nucleated PP are mainly the result of changes in T_c and, concomitantly, L_c and σ_y, rather than of changes in the spherulite size and/or crystallinity. An increase in σ_y of the PCL/PEO9-based TPVs would result in a higher resistance to plastic deformation of the PCL matrix during compression, leading to a decreased *CS*. Fig. 6.12 shows that *CS* of PCL/PEO9-based TPVs decreases linearly with increasing T_c. This indicates that the lower *CS* of the TPVs with higher $\overline{D_n}$ does not originate from a particle size effect, but from the increased nucleating ability of the rubber particles, which increases the lamellar thickness and,

concomitantly, σ_y. The increase in L_c and σ_y with increasing T_c were supported by small-angle X-ray scattering (SAXS) measurements and tensile tests, respectively (not shown here).
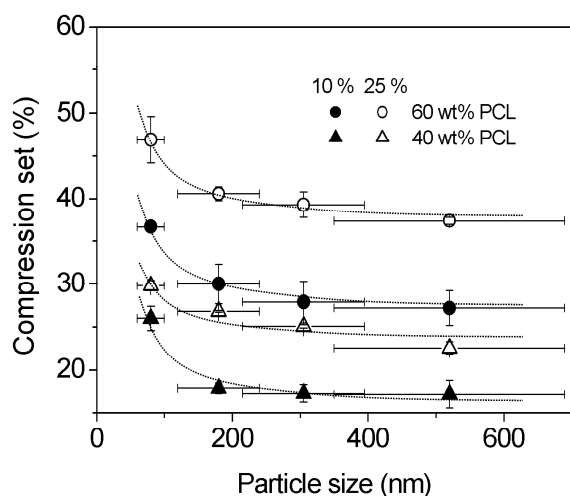

Fig. 6.11. CS as a function of $\overline{D_n}$ for PCL/PEO9-based TPVs containing 60 and 40 wt% PCL at 10 and 25 % compressive strain.
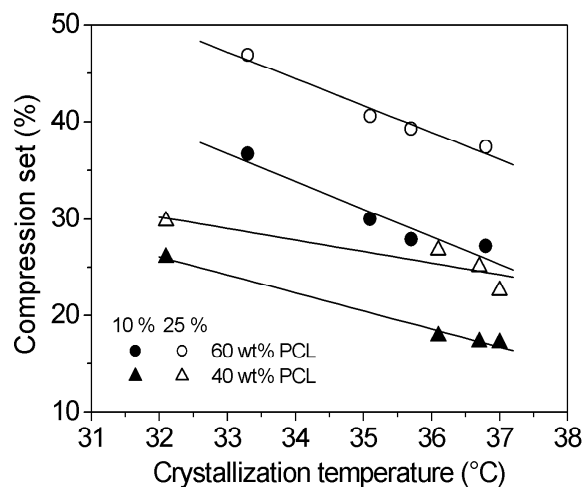
Fig. 6.12. Relation between CS and T_c for PCL/PEO9-based TPVs containing 60 and 40 wt% PCL at 10 and 25 % compressive strain. The solid lines represent the best fits through the data points.

6.3.8. Deformation mechanism of PCL/PEO9-based TPVs

Small-angle X-ray scattering (SAXS) is a non-destructive technique that can be used to study structural changes on the nanometer scale during the deformation of polymers. It is important to note that pure PCL deformed via localized yielding and subsequent necking, while all the TPVs deformed homogeneously, i.e. necking was not observed. Fig. 6.13a shows the development of the SAXS patterns of pure PCL as a function of the applied macroscopic strain (ε_{macro}). These patterns show a large resemblance to the patterns of *in-situ* deformed PP[34] and PE[35], where yielding is the main deformation mechanism and interlamellar void formation occurs during yielding. The initial scattering pattern shows an isotropic scattering ring at $q = 0.459$ nm^{-1}, where q is the scattering vector defined by $q = (4\pi/\lambda)\sin(\theta)$, with λ the wavelength and θ the scattering angle. This scattering pattern originates from the long period of PCL at a *d*-spacing of $d = 2\pi/q = 137$ Å. Upon deformation, the material reaches its yield stress and a neck propagates through the sample. As the neck moves into the X-ray beam, meridional streaks appear close to the beam stop, immediately followed by the formation of intense equatorial streaks. The meridional streaks originate from interlamellar voids oriented perpendicular to the stretching direction[34]. These voids rapidly orient parallel to the stretching direction, giving rise to the formation of equatorial streaks. At small ε_{macro}, the scattering ring originating from the long period shifts to a slightly lower q-value of 0.452 nm^{-1} (or $d = 139$ Å), which indicates that interlamellar separation occurs. Upon yielding, the isotropic scattering ring related to the long period disappears due to disruption

of the lamellar structure and the concomitant loss in lamellar order. After yielding, the SAXS pattern is composed of intense equatorial streaks at low q-values and weak meridional arcs at a q-value of 0.470 nm^{-1} and a d-spacing of 133.7 Å, the latter originating from small crystalline domains oriented with their c-axis parallel to the deformation direction formed after breaking up of the lamellar structure[36]. No changes in the SAXS pattern are observed as the neck propagates throughout the remainder of the sample. The very different morphology development upon deformation of the TPVs is apparent from the SAXS patterns in Figs. 6.13b-d. Except for the observation that a higher ε_{macro} is reached upon decreasing $\overline{D_n}$, no distinct differences in the development of the SAXS patterns are observed with varying $\overline{D_n}$. No distinction can be made between interlamellar void formation in the PCL matrix and orientation of the rubber particles, since both will lead to the formation of equatorial streaks at low q-values. It is evident, however, that the intensity of the equatorial streaks is significantly lower for the TPVs than for pure PCL, which indicates the suppression of void formation in the TPVs. The formation of crazes, as may occur upon deformation of brittle polymers, leads to a SAXS pattern in the form of a cross, with meridional streaks originating from the reflection of the direct X-ray beam from the craze-bulk interface and equatorial streaks originating from the scattering of the fibrils and voids[37]. The SAXS patterns in Fig. 6.13 clearly demonstrate that crazing does not occur in these materials.

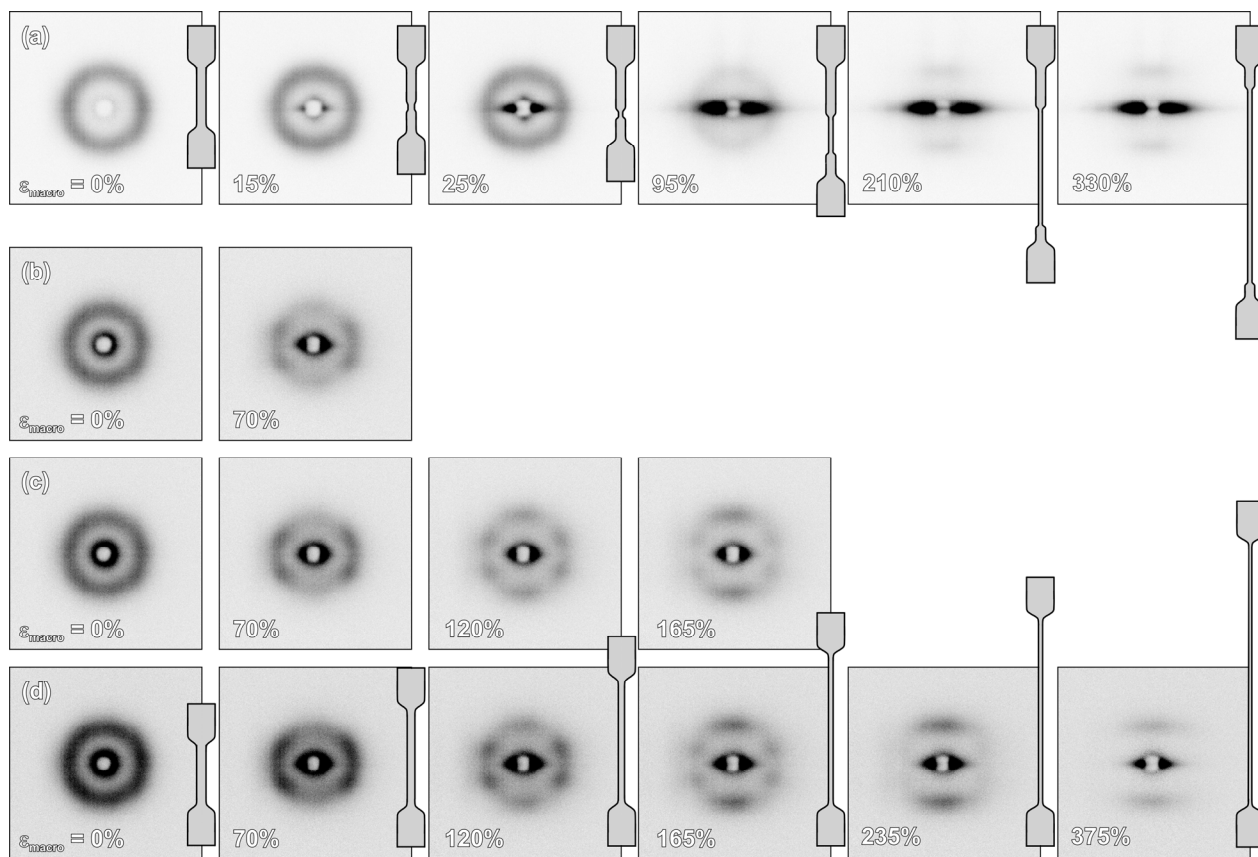*Fig. 6.13. Development of SAXS patterns of in-situ deformed (a) PCL and TPVs containing 60 wt% PCL with (b) $\overline{D_n}$ = 305 nm, (c) $\overline{D_n}$ = 180 nm and (d) $\overline{D_n}$ = 80 nm. The stress is applied in the vertical direction.*

A detailed overview of the SAXS patterns of the TPV with $\overline{D_n}$ = 80 nm is shown in Fig. 6.14, which includes the d-spacings (long periods) and an idealized, schematic representation of the morphology as derived from each of the SAXS patterns. At ε_{macro} = 0 %, the TPVs show an isotropic scattering ring at q-values of 0.449-0.455 nm^{-1} or d-spacings of 138-140 Å, which originate from the long period of PCL. Additionally, a strong isotropic scattering intensity at low q-values is observed, which is mostly covered by the beam stop. Since this profile is not observed for pure PCL, it can be attributed to scattering of the rubber particles. The initial morphology is represented by Fig. 6.14b, where the crystalline PCL lamellae have grown from the rubber particle surface as a result of the nucleation effect (see also Fig. 6.7), leading to an overall isotropic lamellar orientation. Increasing ε_{macro} to 70 % leads to an increase of the d-spacing in the meridional direction from 138.3 to 143.1 Å (Fig. 6.14c), which is caused by separation of the lamellae at the equatorial region of the rubber particles (Fig. 6.14d). Simultaneously, the equatorial q-value increases from 0.454 to 0.464 nm^{-1}, which is indicative for a decrease in the d-spacing of the lamellar stacks at the polar region of the rubber particles from 138.3 to 135.4 Å due to strain compression. Fig. 6.14c shows that the equatorial scattering intensity is significantly higher than the meridional intensity, which means that the structural order of the lamellae at the equatorial region of the rubber particles has partially been disrupted, while the lamellar order at the polar regions is still preserved. This result is in good agreement with the work of Kikuchi *et al.*[38,39], who stated that plastic deformation of the matrix concentrates in the thinnest ligaments at the equatorial regions of the rubber particles, while the ligaments at the polar regions remain below the matrix yielding condition up to high strains.

Close examination of Fig. 6.14c reveals the presence of a symmetric four-point pattern at a d-spacing of 133.1 Å and azimuthal angles of 0° +/- α and 180° +/- α, where α = 33°. This indicates the presence of scattering entities with a preferred average orientation inclined to the tensile direction. This four-point pattern may originate from *(i)* a preferred orientation of lamellae at an angle α with respect to the tensile direction (right hand side of Fig. 6.14d) and/or *(ii)* break-up of long lamellae into shorter pieces that tend to orient in the stress direction, leading to a chevron-type structure[40] (left hand side of Fig. 6.14d). Although such four-point SAXS patterns have not been reported for TPVs, they were previously observed during the deformation of PE[41] and diblock copolymers based on hard and soft segments[42-45] and were generally attributed to the formation of a chevron-type structure[41,44,45]. However, the physical connection of lamellae onto the rubber particles via the grafted PCL makes the orientation and deformation of the lamellae dependent on the deformation of the rubber particle, which could lead to lamellae with a preferred orientation inclined to the tensile direction. Increasing ε_{macro} to 120 % shows the

appearance of the meridional arcs, but at a lower *d*-spacing of 127.2 Å (Fig. 6.14e). The intensity of these meridional arcs becomes stronger with increasing ε_{macro}. This scattering originates from the small crystalline domains that form after break-up of the lamellae at the equatorial regions of the rubber particles, with a smaller interlamellar spacing due to stress relaxation after break-up (Fig. 6.14f). The scattering entities with a preferred orientation inclined to the stress
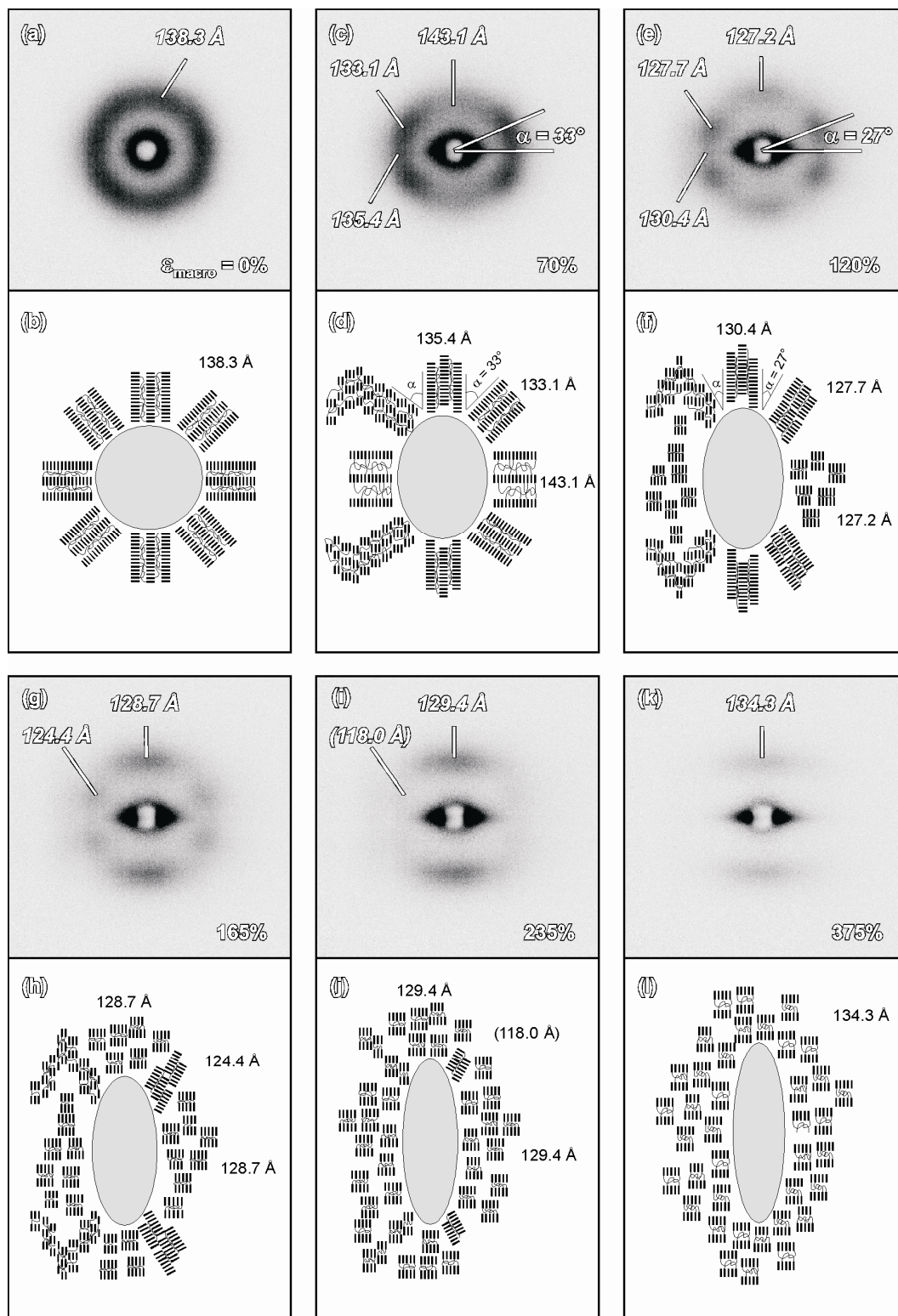

Fig. 6.14. Detailed description of the SAXS patterns in Fig. 6.13d. A schematic drawing of the morphology as derived from each of the SAXS patterns is included.

direction tend to orient in the direction of the applied stress, as deduced from the decrease in α from 33 to 27°. The equatorial scattering has entirely disappeared at ε_{macro} = 165 % (Fig. 6.14g), which indicates that the lamellae oriented parallel to the stress direction have fully broken up (Fig. 6.14h). Upon further stretching, also the scattering entities with a preferred orientation inclined to the stress direction break up (Fig. 6.14j) and only the scattering arcs of the small crystalline domains remain (Fig. 6.14i). The d-spacing of these small domains increases upon further stretching, which is indicative of interlamellar separation or further disruption of the lamellar structure.

6.3.9. Compression set of PCL/PEO and PCL/PPO-based TPVs

The temperature window for TPV applications is typically limited to temperatures between the T_g of the rubber and/or thermoplastic phases and the T_m of the thermoplastic matrix. The temperature window can be enlarged by decreasing the T_g of the cross-linked elastomer, which can be achieved by changing the type of elastomer precursor. Since the molar mass between the methacrylate end groups of the PEO9 and PPO7 rubber precursors is similar ($M_n \sim$ 550 g/mol), they have the same theoretical cross-link density, or M_c, after full cross-linking. The DMTA curves presented in Fig. 6.15 show that the T_g of the cross-linked rubber phase in the corresponding TPVs changes from -32 °C for PEO14 via -1 °C for PEO9 to +21 °C for PPO7, which changes the temperature window for the corresponding TPV.
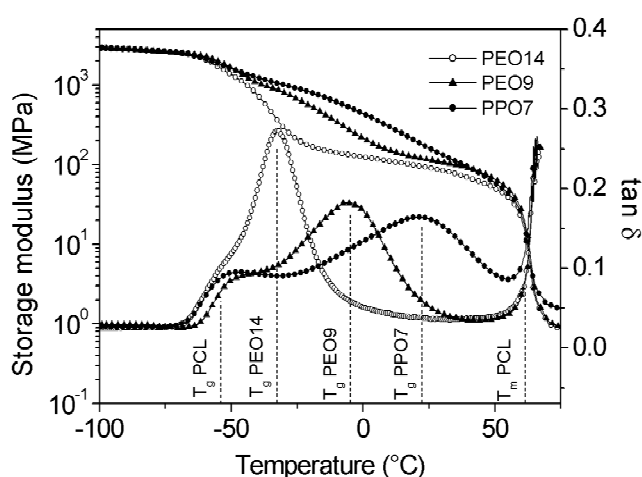
Fig. 6.15. DMTA curves of PCL/PEO14, PCL/PEO9 and PCL/PPO7-based TPVs containing 60 wt% PCL.
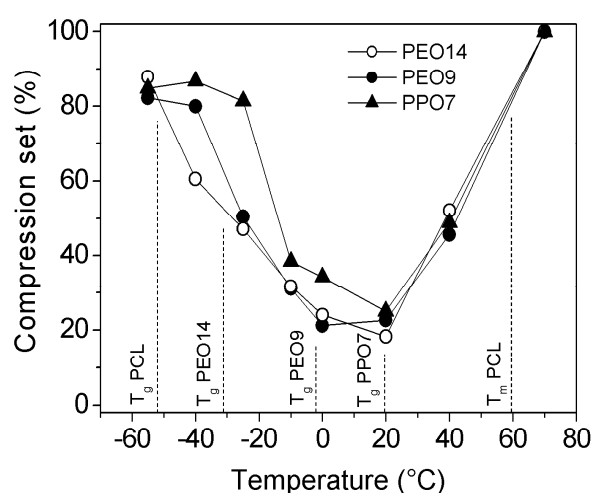
Fig. 6.16. Influence of temperature on the CS of PCL/PEO14, PCL/PEO9 and PCL/PPO7-based TPVs containing 60 wt% PCL. A compressive strain of 10 % was applied.

CS depends on the deformation behavior during compression as well as on the recovery behavior after releasing the compressive strain. Since both the compression and the recovery steps are characterized by a viscoelastic behavior, the measuring temperature and T_g of the matrix

and rubber phases are expected to influence the measured *CS* values. Fig. 6.16 summarizes the influence of the position of the T_g of the rubber phase on *CS* measured at temperatures ranging from -55 to +70 °C. A low *CS* is obtained when little plastic deformation occurs during the compression step and a good recovery occurs after unloading. According to ASTM D395[8] and ISO 815[9], for compression temperatures (T_1) at or above 23 °C the relaxation after unloading was performed at T_2 = 23 °C; for compression at T_1 < 23 °C the relaxation after unloading was performed at the compression temperature T_1 (so $T_2 = T_1$). Starting from 23 °C, increasing the measuring temperature T_1 leads to an increase in *CS* of the TPVs, which eventually reaches 100 % at $T_1 > T_m$ (Fig. 6.16). This increase in *CS* is due to softening and, eventually, melting of the PCL matrix with increasing temperature, which leads to more plastic deformation of the matrix during the compression step. When T_1 is decreased starting from 23 °C, the mobility of the PCL matrix during compression is reduced and an improved *CS* is therefore expected. However, since the relaxation process after unloading is performed at $T_2 = T_1$, the strain recovery is suppressed by the lower mobility of both the rubber and PCL phase. The higher *CS* at temperatures below 23 °C of the TPVs based on PPO7 in comparison to those based on PEO9 can, therefore, be explained by the higher T_g of the former. The TPV based on PEO14 shows a slight deviation from this trend at intermediate T_1, which is due to its lower cross-link density. It can be concluded from Fig. 6.16 that performing compression set measurements at various temperatures (according to ASTM D 395[8] and ISO 815[9]) leads to a minimum *CS* at $T_1 \sim 23$ °C. This is independent of the type of rubber and thermoplastic used in the TPV (assuming that the T_g's of the rubber and thermoplastic are well below 23 °C and the T_m of the thermoplastic is well above 23 °C) and is the result of the prescribed combination of the compression and relaxation temperatures.

6.3.10. Rheological behavior of PCL/PEO9-based TPVs

The TEM images in Figs. 6.5 and 6.6 show that RIPS of initially miscible PCL/PEO9 mixtures leads to typical TPV morphologies over a broad composition range, and Figs. 6.8 and 6.9 show that typical TPV properties are obtained. The thermoplastic PCL forms the matrix and melt processability is thus anticipated, but partial rubber connectivity and the presence of PCL grafts on the cross-linked rubber particles are expected to influence the rheological behavior. Figs. 6.17 and 6.18 show the complex viscosity (η^*) and the storage modulus (G'), respectively, both as a function of the applied frequency (ω). The pure PCL shows terminal flow over a large frequency range, which is indicated by a slope of 0 for $\log(\eta^*)$ versus $\log(\omega)$ and a slope of nearly 2 for $\log(G')$ versus $\log(\omega)$. Upon increasing the rubber content of the TPVs, both η^* and G' rapidly increase. The slope of -1 for the $\log(\eta^*)$ versus $\log(\omega)$ plots indicates that the cross-linked PCL/PEO9-based TPVs behave like ideal elastic networks in the melt, which is typical for

TPVs[48]. The TPVs containing 40 and 60 wt% cross-linked rubber show a η^* of 4000-6000 Pa·s at $\omega = 100$ rad/s and $T = 100$ °C (= T_m + 40 °C). This η^* is higher than that of the conventional PP/EPDM-based TPVs ($\eta^* \sim 3000$ Pa·s at $\omega = 100$ rad/s and $T = 210$ °C (= T_m + 50 °C), see Chapter 2.3.7) and that of the PCL/PPO5-epoxy-based TPVs ($\eta^* = 300-800$ Pa·s at $\omega = 100$ rad/s and $T = 110$ °C (= T_m + 50 °C), see Chapter 4.3.4) at similar rubber contents.
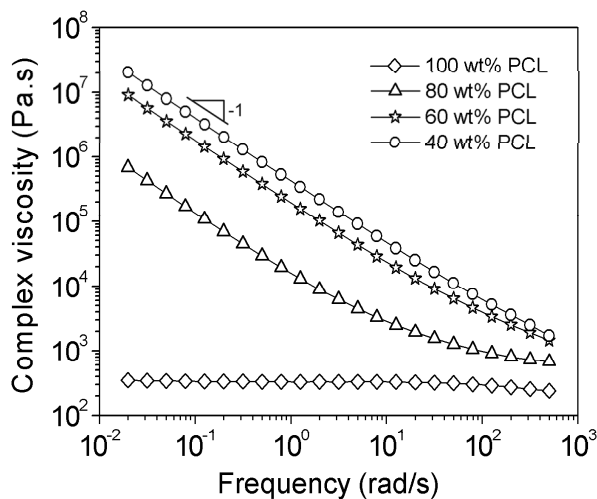
Fig. 6.17. Complex viscosity as a function of frequency ω for PCL/PEO9-based TPVs with varying PCL content at 100 °C.
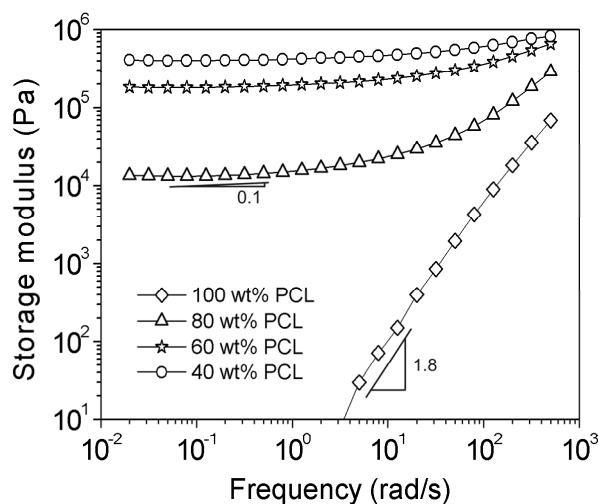
Fig. 6.18. Storage modulus as a function of frequency ω for PCL/PEO9-based TPVs with varying PCL content at 100 °C.

Previous studies on PP/EPDM-based TPVs showed the importance of the applied shear stress on the rheological behavior of TPVs[46-48]. At low stresses, the melt behaves elastically (even at relatively low rubber contents), which is attributed to the presence of a physically interacting network of the cross-linked rubber particles. At a certain critical stress, i.e. the yield stress, the physical network is broken up and the materials behave as a thermoplastic melt filled with rubber particles. Fig. 6.19 shows a typical example of creep curves for the PCL/PEO9-based TPV with 60 wt% PCL, where shear stresses ranging from 5 to 35 kPa were applied. At shear stresses of 5 and 10 kPa, the material shows a limited compliance, which indicates that little stress relaxation occurs in the melt and, thus, that the material displays an elastic behavior. The compliance shows a continuous increase at stresses from 15 kPa and higher, which indicates that the critical stress is exceeded and the melt behavior has changed from elastic to viscous.

The results of the creep measurements on PCL/PEO9-based TPVs with varying PCL content have been summarized in Fig. 6.20, which shows the shear viscosity after 100 s creep at 100 °C as a function of the applied shear stress. At relatively low shear stresses (e.g. as applied during frequency sweep measurements) the viscosity increases with the rubber content, which is consistent with Fig. 6.17. A significant increase in the yield stress, i.e. the critical stress at which

the shear viscosity drops, is observed with increasing rubber content, which is consistent with results reported for PP/EPDM-based TPVs with varying EPDM contents[48].
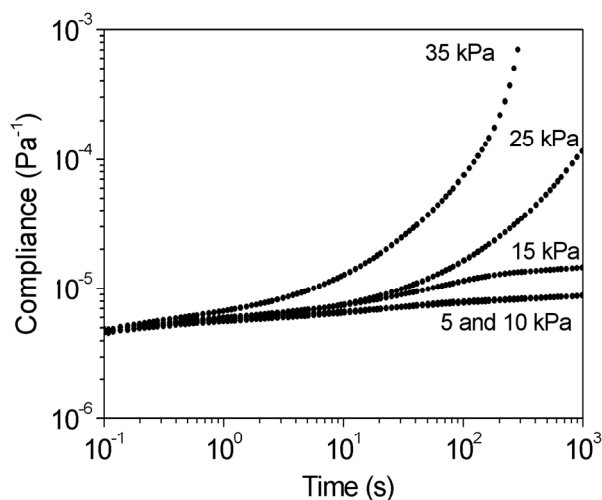
Fig. 6.19. Example of creep curves of a PCL/PEO9-based TPV containing 60 wt% PCL measured at various shear stresses at 100 °C.
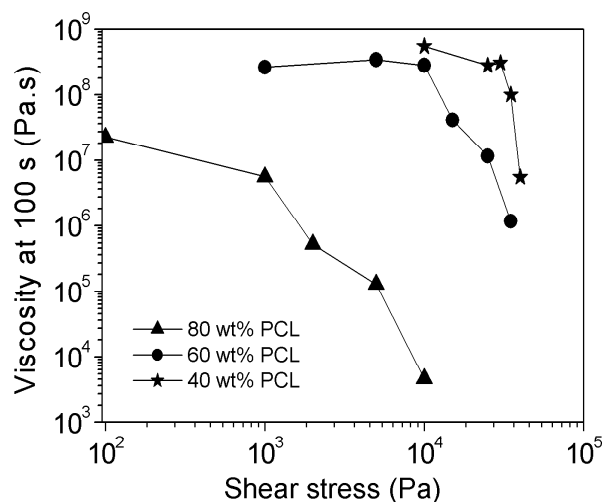
Fig. 6.20. The shear viscosity after 100 s creep of PCL/PEO9-based TPVs at 100 °C as a function of shear stress.

Figs. 6.17-6.20 show that RIPS of PCL/PEO9 mixtures indeed leads to melt processable materials. However, the absolute values of the viscosity and the yield stress are relatively high in comparison to conventional PP/EPDM-based TPVs (Chapter 2.3.7), PCL/PPO5-epoxy-based TPVs prepared via RIPS (Chapter 4.3.4) and oil-extended PP/EPDM-based TPVs[46-48]. There are several reasons for the high viscosity and yield stress for these TPVs. First of all, the PCL/PEO9-based TPVs do not contain any processing oil, which is typically added to commercial TPVs to enhance their melt processability. Secondly, the relatively small size of the rubber particles in the PCL/PEO9-based TPVs increases the viscosity and the yield stress (see also Chapter 2.3.7). At a constant volume fraction of rubber, the amount of interfacial area increases with decreasing rubber particle size, which increases the extent of physical interaction between the particles and, thereby, the viscosity and yield stress. The presence of PCL grafts on the cross-linked rubber particles will also influence the rheological properties. The PCL grafts can form bridges between the rubber particles, either via a direct chemical connection (i.e. multiple grafting of a single PCL chain on various rubber particles) or via chain entanglements with the PCL matrix, both leading to an increased viscosity and yield stress. Additionally, partial connectivity between the rubber particles via the rubber network, i.e. the formation of a connected-globule structure, will significantly limit the melt processability of the TPVs. Rubber connectivity was observed in previous studies on TPVs obtained by RIPS of initially miscible blends (Chapters 4 and 5) and, as discussed previously, partial rubber connectivity in the PCL/PEO9-based TPVs cannot be excluded.

6.4. Conclusions

It is demonstrated that TPVs can be prepared by RIPS of initially miscible mixtures of PCL and elastomer precursors based on difunctional methacrylate resins. Up to 80 wt% of cross-linked rubber particles can be dispersed in the PCL matrix, where the rubber particle size ranges from 80 to 900 nm. The relatively high elasticity of the rubber phase during cross-linking leads to a dynamically asymmetric nature of the phase-separating system, which may explain the occurrence of partial connectivity between the rubber particles. 3D-TEM analysis shows that the extent of rubber connectivity as observed in 2D-TEM images is overestimated.

Peroxide decomposition during the preparation of the TPVs causes hydrogen abstraction of PCL, which leads to partial grafting of PCL chains onto the cross-linked rubber particles. The significant increase in T_c demonstrated that the rubber particles act as an excellent nucleating agent for PCL, where the nucleating ability is believed to originate from the PCL chains that are grafted onto the cross-linked rubber particles. To better understand the origin of the increased T_c and its influence on the crystalline structure and the mechanical properties, a more detailed study on the crystallization behavior of these TPVs is required. Therefore, (non-)isothermal crystallization studies on the PCL/PEO9-based TPVs with varying amounts of PCL grafting are the subject of Chapter 7.

The mechanical and rheological properties of the TPVs are determined by a complex interplay of the type of elastomer precursor, the morphology, the extent of PCL grafting, the crystallinity and the lamellar thickness. Due to the high cross-link density of the PEO9 rubber phase and partial rubber connectivity, PCL/PEO9-based TPVs with a relatively high hardness and a good elastic recovery are obtained, whereas EB and TS are relatively low. The temperature window and the mechanical properties of the TPVs can be controlled by changing the cross-link density and/or the T_g of the rubber phase, which is achieved by using different elastomer precursors.

Decreasing $\overline{D_n}$ from 520 to 80 nm leads to a significant increase in EB, which is attributed to *(i)* a more efficient suppression of interlamellar void formation and subsequent coalescence of voids, *(ii)* an increased interfacial adhesion due to the grafting of PCL chains and *(iii)* changes in the lamellar thickness and spherulite structure of the PCL matrix due to a nucleating effect of the grafted rubber particles (see also Chapter 7). The deformation mechanism of the TPVs under tensile conditions is dominated by yielding of the PCL matrix, which is initially localized at the equatorial regions of the rubber particles and progresses towards the polar regions at higher strains. The increase in lamellar thickness with increasing nucleating efficiency of the rubber particles explained variations in the elastic recovery of the TPVs.

Increasing the rubber content in the TPVs leads to an increased melt viscosity and to an increase in the critical stress, the 'yield stress', which is required for the material to flow. The relatively high viscosity and yield stress are attributed to a combination of grafting of PCL chains, the small rubber particle size and partial rubber connectivity.

6.5. References

[1] Cam, D.; Hyon, S.-H.; Ikada, Y. *Biomaterials* **1995**, *16*, 833-843.

[2] Sivalingam, G.; Madras, G. *Biomacromolecules* **2004**, *5*, 603-609.

[3] Montezinos, D.; Wells, B.G.; Burns, J.L. *J. Polym. Sci., Polym. Lett. Ed.* **1985**, *23*, 421-425.

[4] Stoks, W.; Berghmans, H. *J. Polym. Sci., Part B: Polym. Phys.* **1991**, *29*, 609-617.

[5] Avella, M.; Errico, M.E.; Rimedio, R; Sadocco, P. *J. Appl. Polym. Sci.* **2002**, *83*, 1432-1442.

[6] Rotter, G.; Ishida, H. *Macromolecules* **1992**, *25*, 2170-2176.

[7] ASTM Standard D412 "Standard Test Methods for Vulcanized Rubber and Thermoplastic Elastomers – Tension", 1986.

[8] ASTM Standard D395 "Standard Test Methods for Rubber Property – Compression Set", 1989.

[9] International Standard ISO 815 "Rubber, Vulcanized or Thermoplastic – Determination of Compression Set at Ambient, Elevated or Low Temperatures", 1991.

[10] Okay, O. *Polymer* **1999**, *40*, 4117-4129.

[11] Litvinov, V.M.; Dias, A.A. *Macromolecules* **2001**, *34*, 4051-4060.

[12] Fox, T.G.; Loshaek, S. *J. Polym. Sci.* **1955**, *15*, 371-390.

[13] Hale, A.; Macosko, C.W.; Bair, H.E. *Macromolecules* **1991**, *24*, 2610-2621.

[14] *Principles of Polymer Chemistry*; Flory, P.J.; Cornell University Press, Ithaca, 1953.

[15] Scott, R.L. *J. Chem. Phys.* **1949**, *17*, 279-284.

[16] Nishi, T.; Wang, T.T. *Macromolecules* **1975**, *8*, 909-915.

[17] *Properties of Polymers: Their Correlation with Chemical Structure; Their Numerical Estimation and Prediction from Additive Group Contributions*; van Krevelen, D.W.; Elsevier, Amsterdam, 1997; p 87.

[18] Kim, C.-H.; Cho, K. Y.; Park, J.-K. *Polymer* **2001**, *42*, 5135-5142.

[19] Chen, W.; Kobayashi, S.; Inoue, T.; Ohnaga, T.; Ougizawa, T. *Polymer* **1994**, *35*, 4015-4021.

[20] Maunsky, J.; Klaban, J.; Dušek, K. *J. Macromol. Sci., Part A: Pure Appl. Chem.* **1971**, *5*, 1071-1085.

[21] Boots, H.M.J.; Kloosterboer, J.G.; Serbutoviez, C.; Touwslager, F.J. *Macromolecules* **1996**, *29*, 7683-7689.

[22] Serbutoviez, C.; Kloosterboer, J.G.; Boots, H.M.J.; Touwslager, F.J. *Macromolecules* **1996**, *29*, 7690-7698.

[23] Tanaka, H. *Phys. Rev. Lett.* **1996**, *76*, 787-790.

[24] Sengupta, P.; Noordermeer, J.W.M. *Macromol. Rapid Commun.* **2005**, *26*, 542-547.

[25] D'orazio, L; Mancarella, C.; Martuscelli, E.; Sticotti, G. *J. Mat. Sci.* **1991**, *26*, 4033-4047.

[26] Bieliński, D.M.; Ślusarski, L.; Włochowicz, A.; Ślusarczyk, C.; Douillard, A. *Polym. Int.* **1997**, *44*, 161-173.

[27] Wittmann, J.C.; Lotz, B. *J. Polym. Sci., Part B: Polym. Phys.* **1981**, *19*, 1837-1851.

[28] Orza, R.A.; Magusin, P.C.M.M.; Litvinov, V.M.; van Duin, M.; Michels, M.A.J. *Macromol. Symp.* **2005**, *230*, 144-148.

[29] Litvinov, V.M. *Macromolecules* **2006**, *39*, 8727-8741.

[30] Radar, C.P. In *Handbook of Thermoplastic Elastomers*; Walker, B.M.; Radar, C.P., Eds.; Van Nostrand Reinhold: New York, 1988.

[31] Halpin, J.C. *Rubber Chem. Technol.* **1965**, *38*, 1007-1038.

[32] Corté, L.; Beaume, F.; Leibler, L. *Polymer* **2005**, *46*, 2748-2757.

[33] Kristiansen, M.; Tervoort, T.; Smith, P.; Goossens, H. *Macromolecules* **2005**, *38*, 10461-10465.

[34] Li, X.; Schneider, K.; Kretzschmar, B.; Stamm, M. *Macromolecules* **2008**, *41*, 4371-4379.

[35] Pawlak, A. *Polymer* **2007**, *48*, 1397-1409.

[36] Lee, H.S.; Yoo, S.R.; Seo, S.W. *J. Polym. Sci.: Part B: Polym. Phys.* **1999**, *37*, 3233-3245.

[37] Mills, P.J.; Kramer, E.J.; Brown, H.R. *J. Mat. Sci.* **1985**, *20*, 4413-4420.

[38] Kikuchi, Y.; Fukui, T.; Okada, T.; Inoue, T. *J. Appl. Polym. Sci.: Appl. Polym. Symp.* **1992**, *50*, 261-271.

[39] Kikuchi, Y.; Fukui, T.; Okada, T.; Inoue, T. *Polym. Eng. Sci.* **1991**, *31*, 1029-1032.

[40] Pakula, T.; Saijo, K.; Kawai, H.; Hashimoto, T. *Macromolecules* **1985**, *18*, 1294-1302.

[41] Wilke, W.; Bratrich, M. *J. Appl. Cryst.* **1991**, *24*, 645-650.

[42] Fakirov, S.; Fakirov, C.; Fischer, E.W.; Stamm, M.; Apostolov, A.A. *Colloid Polym. Sci.* **1993**, *271*, 811-823.

[43] Blundell, D.J.; Eeckhaut, G.; Fuller, W.; Mahendrasingam, A.; Martin, C. *Polymer* **2002**, *43*, 5197-5207.

[44] Cohen, Y.; Albalak, R.J.; Dair, B.J.; Capel, M.S.; Thomas, E.L. *Macromolecules* **2000**, *33*, 6502-6516.

[45] Laity, P.R.; Taylor, J.E.; Wong, S.S.; Khunkamchoo, P.; Norris, K.; Cable, M.; Chohan, V.; Andrews, G.T.; Johnson, A.F.; Cameron, R.E. *J. Macromol. Sci., Part B: Polym. Phys.* **2004**, *43*, 95-124.

[46] Han, P.K.; White, J.L. *Rubber Chem. Technol.* **1995**, *68*, 728-738.

[47] Araki, T.; White, J.L. *Polym. Eng. Sci.* **1998**, *38*, 590-595.

[48] Steeman, P.; Zoetelief, W. *ANTEC* **2000**, 3297-3302.

6

Crystallization kinetics and crystalline morphology of poly(ε-caprolactone) in blends with grafted rubber particles

The crystallization behavior of neat PCL and PCL in blends with cross-linked rubber particles was studied under (non-)isothermal crystallization conditions, where the rubber particles were grafted with PCL chains via hydrogen abstraction of the aliphatic moieties in PCL. The crystal growth and the organization of crystals into spherulitic superstructures are significantly influenced by the presence of the grafted rubber particles. According to an Avrami analysis, an increased PCL grafting density leads to an increase in the overall crystallization rate and increases the nucleating rate of PCL. Small-angle light scattering studies showed a significant decrease in the internal order of the spherulites with increasing nucleating efficiency. Favorable thermodynamic interactions lead to a decrease in the equilibrium melting temperature of PCL with increasing rubber content, which is independent of the PCL grafting density.

7.1. Introduction

The previous chapter described the preparation of thermoplastic vulcanizates (TPVs) based on reaction-induced phase separation (RIPS) of initially miscible blends of a semi-crystalline thermoplastic in combination with a low-molar-mass elastomer precursor. Miscible blends of poly(ε-caprolactone) (PCL) and poly(ethylene oxide)-based dimethacrylate resins (PEO9) were used, which led to sub-μm-sized, cross-linked rubber particles dispersed in the PCL matrix over a very broad composition range. The radicals that originate from peroxide decomposition initiate the cross-linking reaction of the difunctional methacrylate resin to form a cross-linked rubber, but also abstract hydrogen atoms from the aliphatic moieties in PCL. The formation of PCL macroradicals leads to grafting of PCL chains onto the cross-linked rubber particles. Non-isothermal crystallization studies showed an increase in crystallization temperature (T_c) of up to 7.0 °C for the TPVs in comparison to neat PCL, which indicates that the rubber particles act as a good nucleating agent for the PCL matrix. Since amorphous particles are known to have only a limited nucleating ability[1], the nucleating effect is believed to originate from the PCL chains that are grafted onto the amorphous particles and not from the particle surface. The nucleating effect of the grafted rubber particles is expected to lead to changes in the crystalline structure of the PCL matrix, such as lamellar thickness and spherulite size, and, consequently, to changes in the mechanical properties.

Several authors reported an increase in T_c after reactive compatibilization of polymer blends consisting of a semi-crystalline thermoplastic and an amorphous phase. Inoue *et al.*[2] prepared TPVs based on PP and EPDM by dynamic vulcanization with a bismaleimide cross-linker. Vulcanization did not alter the morphology of the blends, but led to an enhancement of the interfacial adhesion between the PP matrix and the cross-linked EPDM particles, which was attributed to grafting of PP onto the surface of the vulcanized EPDM particles[3]. Additionally, an increase in T_c from 115 °C prior to vulcanization up to 120 °C after vulcanization was reported[4]. D'orazio *et al.*[5] demonstrated that the small increase in T_c that is sometimes observed for PP/rubber blends prior to cross-linking[6] originates from impurities in the rubber and not from a nucleation effect of the rubber particles. The formation of graft copolymers during dynamic vulcanization and an increase in the nucleating efficiency of the cross-linked rubber particles was later reported by Jain *et al.*[7] and López-Manchado *et al.*[8] for PP/EPDM blends and by Huang *et al.*[9] for nylon/EPDM blends compatibilized with an anhydride-grafted EPDM copolymer. Several studies on blends of PCL with epoxy resins prepared via RIPS showed a significant nucleating effect of the dispersed, amorphous epoxy phase on the PCL matrix[10-12]. Although grafting reactions are not discussed in those studies, the occurrence of PCL-grafting onto the cross-linked

epoxy network is known to occur via *(i)* amidation of PCL with the amine, *(ii)* the hydroxyl end groups of PCL that react with the oxirane rings of the epoxy resin and *(iii)* transesterification[13,14]. Similar results were obtained after compatibilization of incompatible blends by the addition of copolymers in the absence of cross-linking: Tang *et al.*[15] reported an increase in T_c for blends of PP and poly(ethylene oxide) (PEO) by compatibilization with a maleated PP-PEO copolymer, whereas Adewolde *et al.*[16] observed an increase in T_c for PP in blends with poly(styrene) (PS) after the addition of a PP-PS graft copolymer. In the few cases for which the physical origin of the increased T_c is discussed, the nucleation is attributed to the increased surface area of the dispersed phase after dynamic vulcanization and/or (reactive) compatibilization[8,9,16].

This chapter discusses the influence of PCL grafting onto amorphous rubber particles on the crystallization behavior of PCL. Since RIPS of initially miscible PCL/PEO9 blends leads to TPVs with a varying amount of dispersed rubber particles and varying PCL grafting contents, they form a suitable model system for this study. First, the non-isothermal crystallization behavior of the TPVs is discussed. Subsequently, the nucleation and growth of PCL crystals under isothermal crystallization conditions is discussed both qualitatively and quantitatively by optical microscopy studies and an Avrami analysis, respectively. Time-resolved small-angle light scattering (SALS) measurements are used to study the development of crystalline superstructures in more detail.

7.2. Experimental

7.2.1. Materials

PCL having M_n = 20 kg/mol and M_w = 37 kg/mol (CAPA 6400) was supplied by Solvay Caprolactones, UK. Poly(ethylene oxide) dimethacrylate (Sigma Aldrich) with a PEO block length of 9 repeating units (PEO9, M_n = 550 g/mol) was used. The free-radical initiator *tert*-butyl peroxybenzoate, tetrahydrofuran (THF) and sodium hydroxide (NaOH) were obtained from Aldrich and used as received.

7.2.2. Blend preparation

Homogeneous blends were prepared by dissolving PCL in ~ 95 wt% of the required amount of liquid PEO9 at 110 °C in a round bottom flask by using a mechanical stirrer. The peroxide was added as a solution in the remaining ~ 5 wt% of PEO9 and the solution was mixed at 150 rpm until a homogeneous mixture was obtained (mixing time ~ 4 min). The stirring was stopped during the cross-linking reaction and a nitrogen flow was applied in order to remove oxygen, which may act as a radical scavenger. Unless stated otherwise, a peroxide content of 0.5 wt% (based on the PEO9 content) and a curing time of 90 min were used. An additional curing step of 30 min at 150 °C was applied to ensure complete decomposition of the peroxide.

TPVs with a constant PCL concentration (40 and 60 wt%) but with varying rubber particle sizes were obtained by the addition or removal of PCL via a solution route. Selected TPVs were dissolved in THF, after which the required amount of PCL was added or removed. The removal of PCL was achieved by

centrifuging the TPV solution at 3000 rpm in a Mistral 3000E centrifuge to separate the cross-linked rubber particles from the PCL in solution. The addition of PCL was achieved by dissolving the required amount of PCL in the TPV solution. All samples were dried overnight at 30 °C under vacuum to remove THF and were subsequently extruded for 10 min at 90 °C in a home-built, recirculating, twin-screw micro-extruder with an internal volume of 5 cm^3 to homogenize the samples.

After separation of the rubber particles from the PCL solution via centrifugation, the PCL grafts were removed by hydrolysis of the grafted PCL chains. Hydrolysis of grafted PCL was achieved by stirring the centrifuged rubber fraction for 3 hours in a 10 wt/vol% NaOH/methanol solution[17]. The rubber fraction was then washed with a 70/30 wt/wt% water/methanol solution to remove residual NaOH and the sodium carboxylate hydrolysis product. Subsequently, the rubber particles were added to a THF solution containing the required amount of PCL, after which the sample was dried and extruded as previously described.

7.2.3. Characterization techniques

Differential scanning calorimetry (DSC). The thermal behavior of PCL and PCL/PEO9 blends was studied by using a TA Instruments Q1000 calorimeter. Hermetically sealed aluminum pans were used with a typical sample weight of 5 mg. The samples were first heated to 100 °C and equilibrated for 5 min in order to remove the thermal history. Subsequently, they were cooled at a rate of 10 °C/min to -90 °C, where they were kept for 5 min, and then reheated to 100 °C at a rate of 10 °C/min. The maximum of the melting endotherm of the second heating run was used to determine the melting temperature (T_m)[18], whereas the onset of the crystallization exotherm was used to determine the crystallization temperature (T_c). The crystallinity (X_c) was calculated by using 136 J/g as the heat of fusion of 100% crystalline PCL[19].

The nucleating efficiency (*NE*) was determined via the calorimetric efficiency scale proposed by Fillon *et al.*[20,21] and was calibrated according to their procedure based on the 'ideally' nucleated polymer attainable via self-nucleation. Two limits were defined: the lower limit refers to the neat (non-nucleated) PCL and the upper limit to self-nucleated PCL. *NE* is a percentage of the range defined by the two limits and is expressed as:

$$NE = \frac{\left(T_c - T_{c,PCL}\right)}{\left(T_{c,\max} - T_{c,PCL}\right)} \times 100\% \qquad (7.1)$$

where $T_{c,PCL}$ and $T_{c,max}$ are the crystallization temperatures of the neat and self-nucleated PCL, respectively, and T_c is the crystallization temperature obtained in the presence of a nucleating agent. $T_{c,max}$ was determined by *(i)* erasing the thermal history by heating with 10 °C/min to 120 °C and 5 min isothermal at 120 °C, *(ii)* creation of a crystalline 'standard' state by cooling with 10 °C/min to -20 °C and 5 min isothermal at -20 °C, *(iii)* partial melting by heating with 10 °C/min to a temperature T_s and 5 min isothermal at T_s, and *(iv)* recrystallization by cooling with 10 °C/min to -20 °C. $T_{c,max}$ was determined as the onset of the crystallization exotherm after partial melting at T_s, where T_s was chosen as the limit between domain II (large variations in the concentration of remaining crystal fragments due to partial melting) and domain III (incomplete melting and considerable annealing of the unmolten material), as

defined by Fillon *et al.*[20,21]. The transition from domain II to III was determined by the appearance of a second melting peak of the annealed material upon reheating[22].

Polarized optical microscopy (POM). The isothermal crystallization behavior was studied by optical microscopy with crossed polarizers by using a Zeiss Axioplan 2 microscope equipped with a Zeiss Axiocam camera. The images were analyzed with the accompanying AxioVision v3.0.6 software. Samples were sandwiched between two thin glass slides and fixed on a Linkam THMS-600 hot-stage for temperature control.

Fourier transform infrared (FTIR) spectroscopy. Infrared experiments were performed on a BioRad Excalibur 3000 spectrometer equipped with a diamond Specac Golden Gate attenuated total reflection (ATR) setup over a spectral range of 600 to 5000 cm^{-1}. Fifty spectra at a resolution of 4 cm^{-1} were signal-averaged and the resulting spectra were analyzed by using the BioRad Merlin 3.0 software. The grafted PCL content was determined by evaluating the ratio of the integrated intensities of the C=O stretching band of PCL at 1721 cm^{-1} and the asymmetric C-O-C stretching band of the ethylene oxide repeat unit of PEO9 at 1095 cm^{-1}. The grafting density (σ) was calculated by using the following equation:

$$\sigma = \frac{m_{PCL} \times N_{AV} \times \rho_{PEO9} \times \frac{1}{6}\pi \overline{D_n}^3}{M_{PCL} \times m_{PEO9} \times \pi \overline{D_n}^2} \tag{7.2}$$

where m_{PCL} is the amount of grafted PCL as determined by FTIR spectroscopy, N_{AV} is Avegadro's number, ρ_{PEO9} is the density of PEO9 (0.868 g/cm^3), M_{PCL} is the number-averaged molar mass of PCL (24 kg/mol), m_{PEO9} is the mass of the rubber and $\overline{D_n}$ is the number-averaged rubber particle size.

Small-angle light scattering (SALS). The development of crystalline superstructures during isothermal crystallization was studied by small-angle light scattering (SALS) measurements. Fig. 7.1 shows a schematic representation of the used SALS setup. The laser light was guided through a pinhole and then through the sample, which was fixed between two glass slides. The temperature was controlled by a Linkam THMS-600 hot-stage. The scattered light was projected on a semi-transparent PP screen. The scattering patterns were captured with a 16-bit 512x512-CCD camera (Versarray:512B Princeton CCD with a ST-133 controller), equipped with a Rodenstock Rodagon 50mm f 1:2,8 lens with a variable focal distance. The CCD camera was linked to a personal computer for data acquisition and analysis. The scattering angles were calibrated with a 300 lines/mm grid. The usable span of scattering vector (q) magnitudes was in the range of 0.7 µm^{-1} < q < 4 µm^{-1}. The data acquisition time was typically 2500 ms per image and was controlled by a home-made script running under V++ for Windows (version 4.0, Digital Optics Ltd), which also controlled the rotation of the bottom polarizer (number 3 in Fig. 7.1) in order to measure under parallel and cross-polarized conditions.
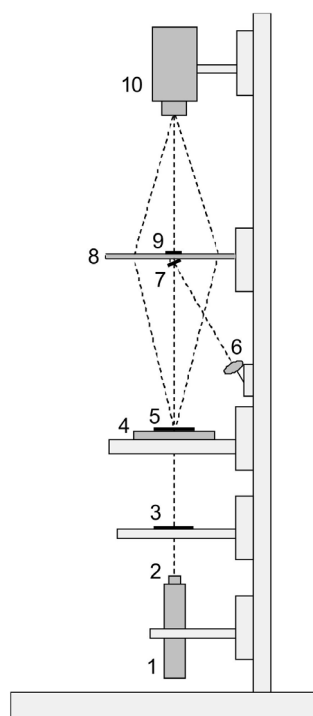
7

Fig. 7.1. Schematic setup of the light scattering apparatus: (1) 1 mW intensity-stabilized HeNe laser (λ = 633 nm), (2) 300 μm pinhole, (3) computer-controlled polarizer, (4) Linkam THMS-600 hot-stage, (5) polarizer, (6) computer-interfaced optical diode, (7) mirror, (8) semi-transparent PP screen, (9) beam stop and (10) CCD camera.

7.3. Results and discussion

The TPVs used in this study were prepared by *in-situ* cross-linking of the PEO9 elastomer precursor in initially miscible blends with PCL, forming cross-linked PEO9 particles dispersed in the PCL matrix (as described in Chapter 6). TPVs were prepared by using rubber contents of 20 to 80 wt% and peroxide contents from 0.2 to 2.0 wt%.

7.3.1. Non-isothermal crystallization

Table 7.1 provides an overview of the thermal properties of PCL and PCL/PEO9-based TPVs prepared with a variation in PCL and peroxide content, as reproduced from Chapter 6. The crystallinity (X_c) decreases with increasing rubber content from 46% for neat PCL to 37% for TPVs containing 80 wt% of rubber. This decrease is attributed to topological confinements imposed by the presence of the rubber phase[5,23,24]. No significant changes in the melting temperature (T_m) are observed. Increasing the peroxide and PEO9 content leads to an increase in the amount of grafted PCL. At a PCL content of 60 wt%, a strong increase in T_c is observed with increasing peroxide content, ranging from 33.4 °C at 0.2 wt% peroxide to 37.3 °C at 2.0 wt% peroxide. An increase in T_c from 32.7 °C to 38.5 °C is also observed upon increasing the rubber content from 20 to 80 wt% at a constant peroxide content of 0.5 wt%. Although the trend is not

consistent over the whole range of grafted PCL contents, the results suggest that the nucleating ability of the rubber particles increases with the amount of grafted PCL.

Table 7.1. Thermal properties of PCL and PCL/PEO9-based TPVs prepared with a variation in PCL and peroxide content.

PCL (wt%)	Peroxide (wt%)	$\overline{D_n}$ (nm)	Grafted PCL (wt%)	X_c (%)	T_m (°C)	T_c (°C)
100	-	-	-	45.9	55.1	31.3
60	0.2	200 ± 60	4.0	43.0	54.8	33.4
60	0.5	180 ± 60	5.9	42.0	55.1	34.1
60	2.0	140 ± 40	30.3	44.1	55.3	37.3
80	0.5	80 ± 20	3.0	44.0	56.3	32.7
40	0.5	305 ± 90	5.9	39.7	55.6	36.0
20	0.5	900 ± 200	7.3	37.1	54.5	38.5

In order to study the influence of PCL grafting on the crystallization behavior in more detail, a series of TPVs was prepared with varying $\overline{D_n}$ at fixed PCL contents of 60 and 40 wt% by adding/removing PCL via a solution route. Besides a variation in $\overline{D_n}$, these TPVs have varying grafted PCL contents and PCL grafting densities (σ). It has to be noted that the dissolution, drying and extrusion steps that were successively applied to prepare these materials may influence the morphology of the samples. However, microscopy studies did not reveal visible morphological changes in these samples in comparison to the samples prior to dissolution, drying and extrusion.

Fig. 7.2 displays the crystallization curves of neat PCL and TPVs containing 60 wt% PCL with varying $\overline{D_n}$ and σ. The nucleating effect of the grafted rubber particles is evident from the increase in T_c, which shifts from 31.3 °C to 36.8 °C with increasing σ. The sample with $\sigma = 0.119$ chains/nm^2 and $\overline{D_n}$ = 520 nm was subjected to a hydrolysis step, by which part of the grafted PCL chains was removed from the rubber particles, leading to a decrease in σ from 0.119 to 0.037 chains/nm^2. Fig. 7.2 shows that T_c of this sample decreases from 36.8 to 33.4 °C, which is similar to T_c of the sample with $\sigma = 0.038$ chains/nm^2 and $\overline{D_n}$ = 80 nm. This demonstrates that the nucleating ability of the rubber particles depends on σ and not on $\overline{D_n}$ and it can, therefore, be concluded that the nucleating ability does not originate from the surface of the rubber particles, but from the PCL chains grafted onto the particles.
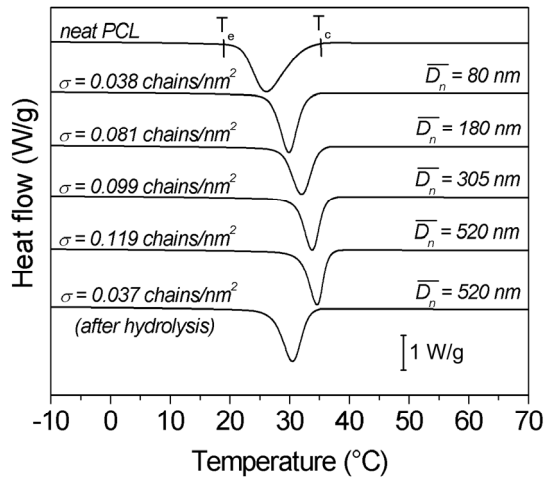
Fig. 7.2. DSC cooling scans of PCL and PCL/PEO9-based TPVs containing 60 wt% PCL with varying grafting density (σ) and rubber particle size ($\overline{D}_n$) at a cooling rate of 10 °C/min.

The non-isothermal crystallization data of neat PCL and the TPVs are summarized in Table 7.2. While T_m remains approximately constant, X_c decreases with increasing rubber content, which is consistent with the results presented in Table 7.1. The overall crystallization time (t_c) was calculated by using the following equation:

$$t_c = \frac{(T_c - T_e)}{\beta_0} \tag{7.3}$$

where β_0 is the cooling rate, T_c is the onset temperature of crystallization and T_e is the offset temperature of crystallization, as indicated in Fig. 7.2. A decrease in t_c from 1.15 min for neat PCL to a minimum value of 0.45 min for the TPVs is observed. The increase in T_c and decrease in t_c are typical characteristics of nucleation-controlled crystallization. The nucleating efficiency (*NE*) of the rubber particles was calculated via equation 7.1 by using $T_{c,max}$ = 45.0 °C as determined from self-nucleation experiments, leading to values for *NE* ranging from 5.8 to 41.6 %. These values for *NE* are high in comparison to those that have been reported in literature, where the use of heterogeneous nucleating agents in PCL led to a maximum *NE* of 39.3 % upon the addition of 5 wt% chitin whiskers[25], 40.0 % in the case of adding 7.5 wt% silica nano-particles[26] and 72.2 % when using 15 wt% boron nitride[27]. The relatively high *NE* of the TPVs originates from the fact that the species responsible for the nucleating effect is the grafted PCL. Obviously, the best nucleating agent for a semi-crystalline polymer is the polymer itself, which is the basis of the earlier described self-nucleation experiments[20,21]. The limited mobility of the PCL chains grafted on the rubber surface leads to a lower loss in entropy upon crystallization and, therefore, to a higher T_c. This small fraction of less mobile PCL acts as the nucleating agent for the bulk PCL. It has to be noted that the presence of cross-linked PCL may also lead to an increased T_c, since the cross-linked polymer network is more difficult to melt and can, therefore, act as a heterogeneous nucleating agent. A previous study on the crystallization behavior of

radiation cross-linked PCL showed that T_c increases with the cross-link density of PCL[28]. A maximum increase in T_c of 3.7 °C was found at a high degree of PCL cross-linking, the latter being represented by a PCL gel content of 46 % as determined by toluene extraction. In contrast to this study, other studies reported a significant decrease of T_c after partial cross-linking of poly[(3-hydroxybutyrate)-*co*-(3-hydroxyvalerate)][29] and poly(ethylene)[30]. Since the extent of PCL cross-linking in our samples is low (see Chapter 6.3.3), its influence on the thermal behavior of the TPVs can be neglected and the nucleating ability of the rubber particles can be attributed to the presence of PCL-grafted rubber particles.

Table 7.2. Thermal properties of PCL and PCL/PEO9-based TPVs with varying PCL content, $\overline{D_n}$, grafted PCL content and σ.

PCL content (wt%)	$\overline{D_n}$ (nm)	Grafted PCL (wt%)	σ (chains/nm²)	t_c (min)	X_c (%)	T_m (°C)	T_c (°C)	NE (%)
100	-	-	-	1.15	45.9	55.1	31.3	-
60	80 ± 20	6.1	0.038	0.62	54.9	55.0	33.3	14.6
60	180 ± 60	5.7	0.081	0.71	47.0	55.8	35.1	27.7
60	305 ± 90	4.0	0.099	0.61	46.0	54.3	35.7	32.1
60	520 ± 170	2.7	0.119	0.47	46.2	53.9	36.8	40.1
60 (*)	520 ± 170	0.9	0.037	0.67	52.9	55.3	33.4	14.9
40	80 ± 20	9.1	0.038	0.51	45.6	53.9	32.1	5.8
40	180 ± 60	8.5	0.081	0.47	43.7	54.3	36.1	35.0
40	305 ± 90	5.9	0.099	0.45	42.7	54.9	36.7	39.4
40	520 ± 170	4.0	0.119	0.59	44.4	55.0	37.0	41.6

(*) After hydrolysis with NaOH/methanol solution.

Although the data presented in Tables 7.1 and 7.2 and Fig. 7.2 clearly demonstrate the nucleating ability of the PCL-grafted rubber particles, no consistent trend was found when relating *NE* to the total amount of grafted PCL in the sample. However, a clear trend is observed upon relating *NE* to σ (Fig. 7.3), showing an exponential dependency of *NE* on σ. This indicates that the nucleating ability of the PCL-grafted rubber particles is mainly determined by the density of the PCL chains on the rubber particle surface and not only by the amount of grafted PCL. From the decreasing slope of *NE* versus σ it is concluded that nucleation of the PCL-grafted rubber particles becomes less efficient at higher σ. The results suggest that the nucleating ability of the polymer chains grafted to the particle surface is highly dependent on the molecular architecture of the grafted surface, such as the number of grafts, the grafting density, the surface coverage, the molar mass of the grafts and the graft/surface interactions[31-33]. A solid conclusion

on the mode of nucleation by the surface grafts would require a more detailed study on the molecular organization of the grafts on the rubber particles, which is outside the scope of this research.
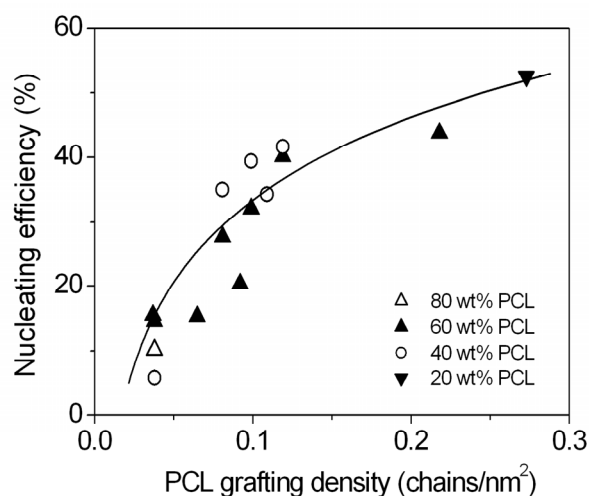

Fig. 7.3. Correlation between NE and σ for PCL/PEO9-based TPVs with varying PCL contents. The solid line represents the best fit through the data points.

7.3.2. Isothermal crystallization

The influence of the grafted rubber particles on the formation of spherulites upon crystallization is clearly observed when comparing polarized optical microscopy (POM) images during isothermal crystallization at 45 °C (Fig. 7.4). Particles with increasing σ decrease the onset time of crystallization (first row of pictures in Fig. 7.4) and decrease the overall crystallization time, which is in agreement with the non-isothermal DSC measurements. The nucleating density increases drastically with increasing σ, which is evidenced by the large number of small spherulites that is formed during the early stages of crystallization. Due to the increasing number of nucleating sites with increasing σ, the size of the spherulites decreases significantly. At $\sigma = 0.081$ and 0.099 chains/nm^2 the nucleating density is so high that the individual spherulites become too small to be clearly visible in the POM pictures (Figs. 7.4c and d).
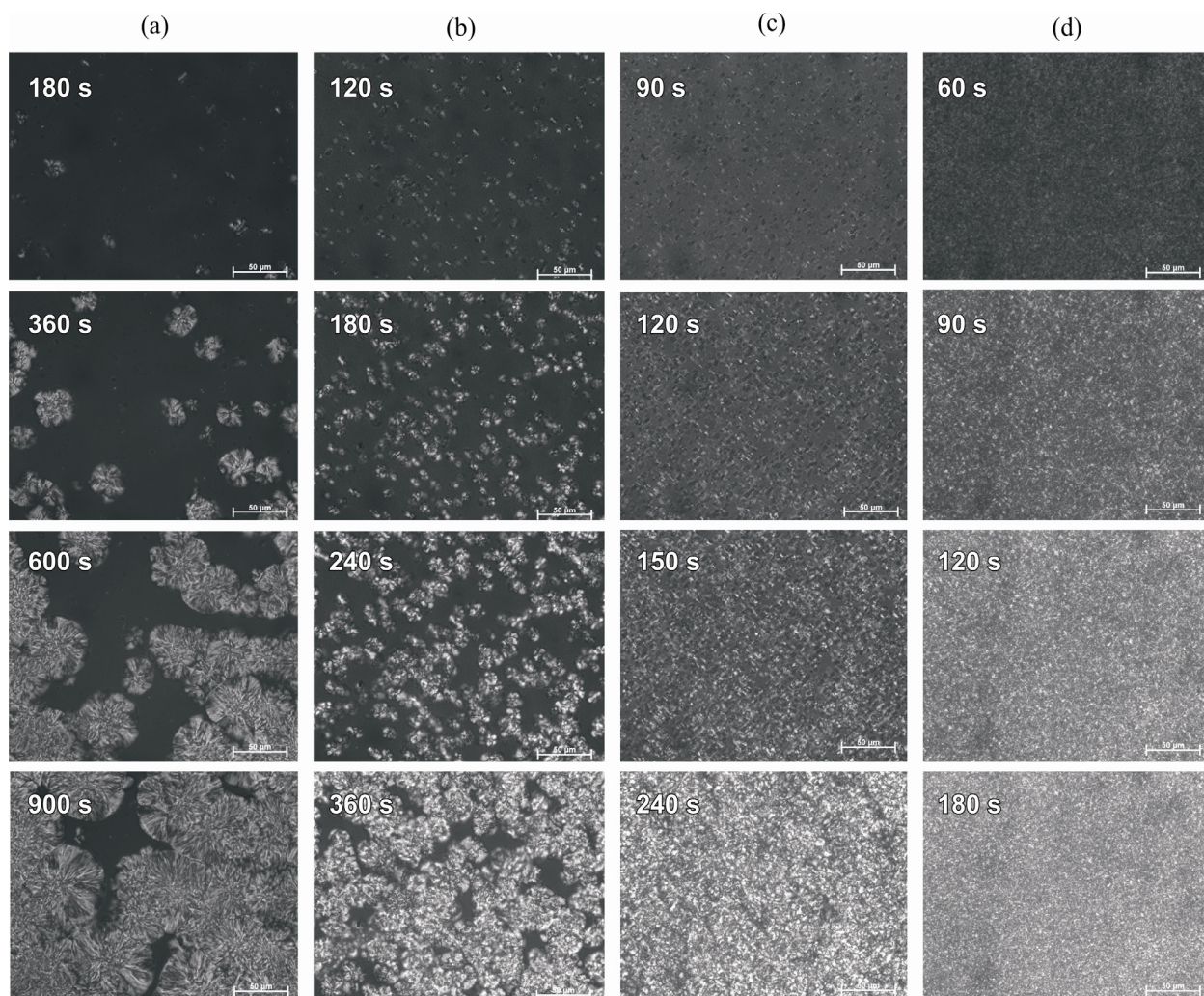
Fig. 7.4. POM images taken during isothermal crystallization of (a) neat PCL and PCL/PEO9-based TPVs containing 60 wt% PCL with (b) $\sigma = 0.038$, (c) $\sigma = 0.081$ and (d) $\sigma = 0.099$ chains/nm^2 at 45 °C.

The crystallization kinetics of polymers under isothermal conditions for various modes of nucleation and growth can be described by the Avrami equation[34,35]. The general form of the Avrami equation is

$$X(t) = 1 - \exp[-K(T)t^n] \qquad (7.4)$$

where $X(t)$ is the relative crystallinity at crystallization time t, n is a constant depending on the mechanism of nucleation and the geometry of crystal growth, and $K(T)$ is a rate constant related to nucleation and growth parameters. $X(t)$ can be calculated according to equation 7.5:

$$X(t) = \frac{Q_t}{Q_\infty} = \frac{\int_0^t (dH/dt)dt}{\int_0^\infty (dH/dt)dt} \qquad (7.5)$$

where Q_t and Q_∞ are the integrated heat flows generated at time t and infinite time, respectively, and dH/dt is the heat flow rate. The half-time of crystallization ($\tau_{1/2}$) is defined as the time at which $X(t)$ reaches 50 % and is often used to characterize the rate of crystallization, which is the

product of the growth rate and the nucleation rate. $\tau_{1/2}$ is calculated from the Avrami parameters according to:

$$\tau_{1/2} = \left(\frac{\ln 2}{nK(T)}\right)^{1/n} \qquad (7.6)$$

The development of $X(t)$ as a function of time for neat PCL and PCL/PEO9-based TPVs is shown in Fig. 7.5 for various isothermal crystallization temperatures ($T_{c,i}$). The inverse of $\tau_{1/2}$ is a measure for the overall rate of crystallization, which increases with decreasing $T_{c,i}$ and increasing σ (Fig. 7.6).
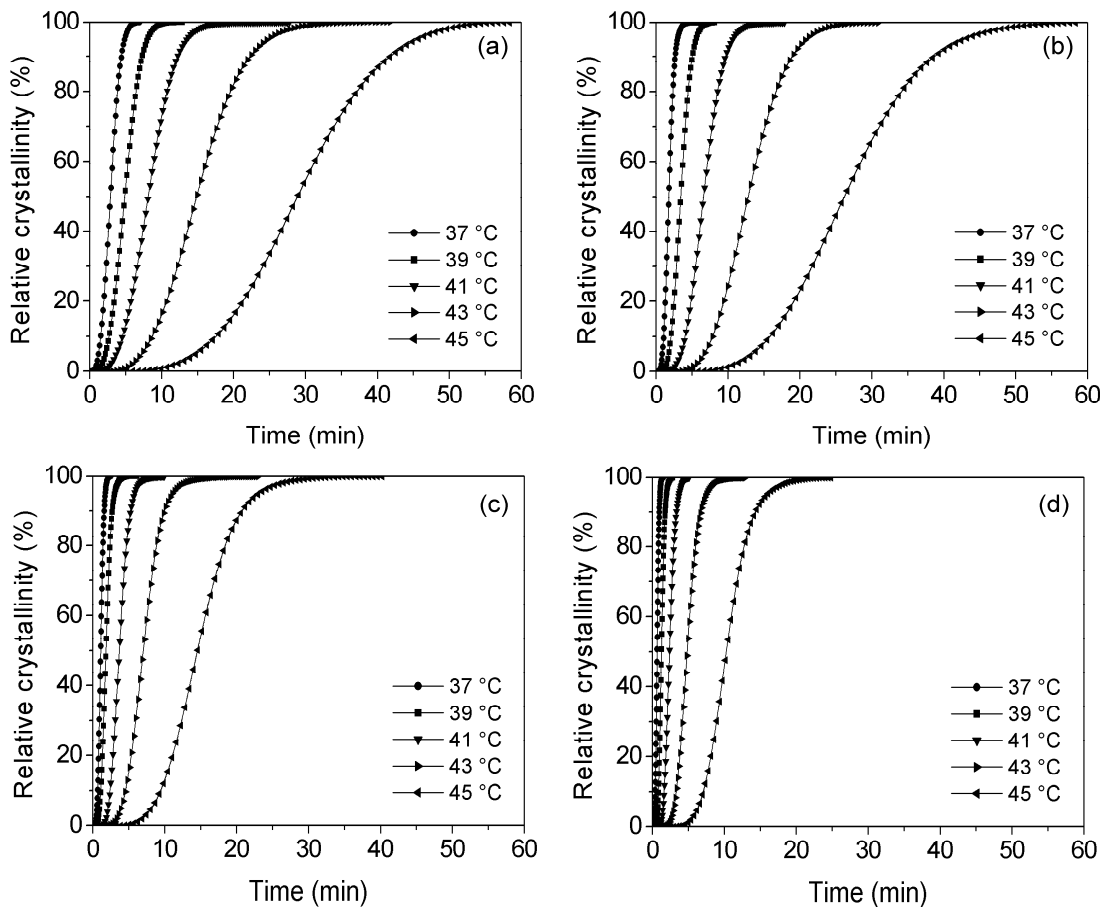
Fig. 7.5. Development of relative crystallinity X(t) with time of (a) neat PCL and PCL/PEO9-based TPVs containing 60 wt% PCL with (b) σ = 0.038, (c) σ = 0.081 and (d) σ = 0.099 chains/nm² at various $T_{c,i}$.

The Avrami equation can be rewritten to:

$$\log\{-\ln[1 - X(t)]\} = n\log(t) + \log\{K(T)\} \qquad (7.7)$$

From a graphic representation of $\log\{-\ln[1-X(t)]\}$ versus $\log(t)$, the constants n and $K(T)$ can be obtained. Fig. 7.7 shows the Avrami plots of $\log\{-\ln[1-X(t)]\}$ versus $\log(t)$ at various isothermal crystallization temperatures over a range of $X(t)$ from 3 to 100%. The linear part of the plots (where $X(t)$ typically ranges from 3 to 35 %) represents the stage of primary crystallization, i.e.
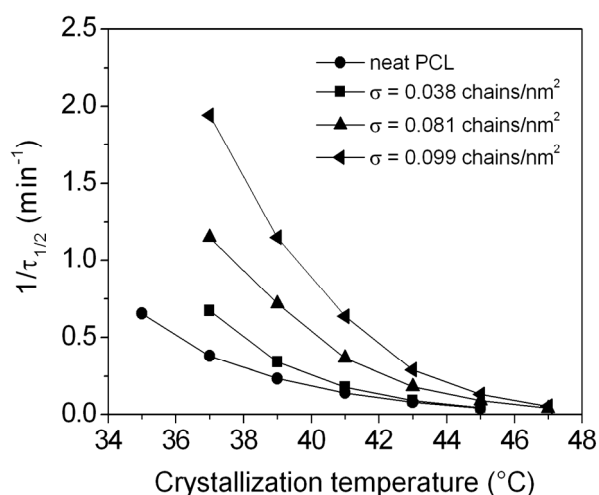
Fig. 7.6. Correlation between the inverse of the crystallization half time (1/τ₁/₂) and the isothermal crystallization temperature (Tc,i) for neat PCL and PCL/PEO9-based TPVs containing 60 wt% PCL.

the formation of nuclei of the critical size and their subsequent growth[36], and can be fitted by a straight line with R > 0.9996. The occurrence of secondary crystallization (e.g. impingement of the spherulites and/or insertion of new crystals in between the already existing ones) is characterized by a deviation from linearity in the log{–ln[1–$X(t)$]} versus log(t) plots. Based on the Avrami plots it is difficult to determine the exact $X(t)$ at which secondary crystallization

Fig. 7.7. Avrami plots of (a) neat PCL and PCL/PEO9-based TPVs containing 60 wt% PCL with (b) σ = 0.038, (c) σ = 0.081 and (d) σ = 0.099 chains/nm² at various Tc,i.

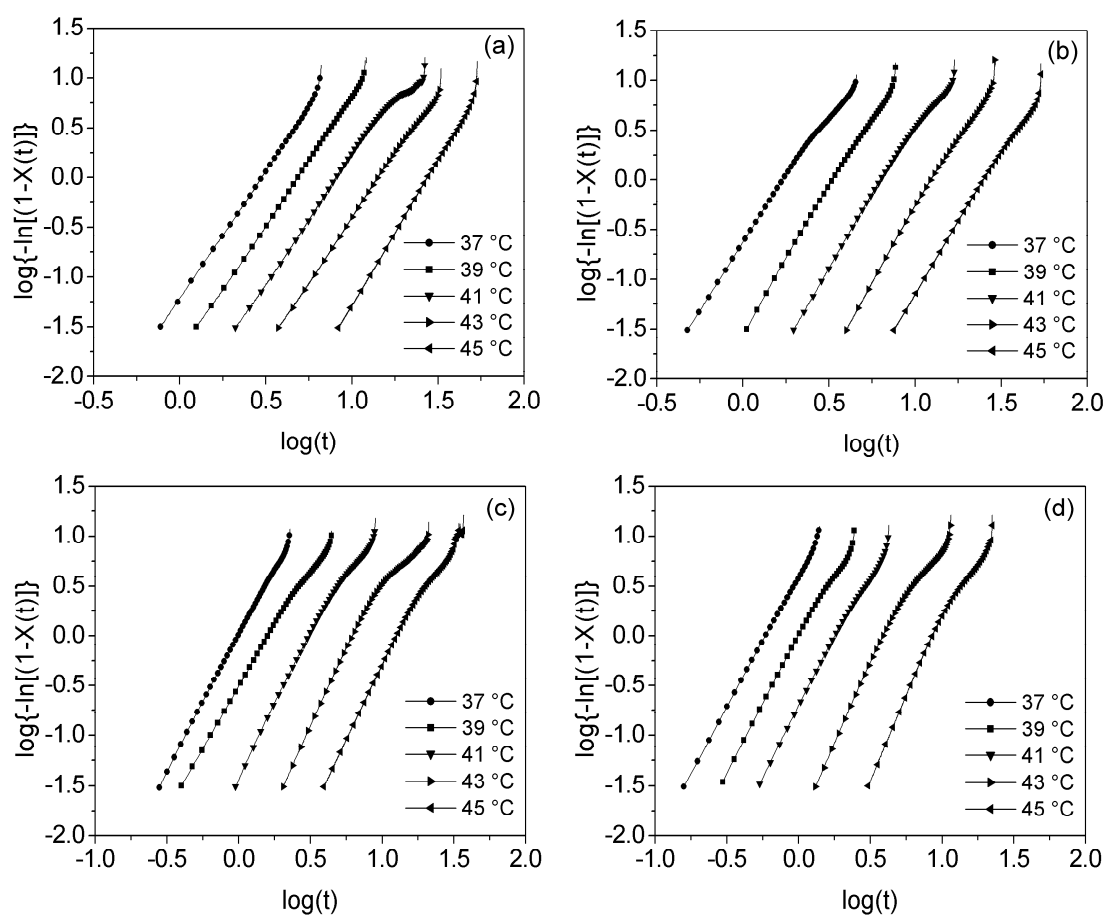starts. However, the presence of the rubber particles with increasing σ leads to a shift in the onset of the secondary crystallization process to lower $X(t)$ (Fig. 7.7), which is more enhanced at a rubber content of 60 wt% (not shown here).

The obtained kinetic parameters n, $K(T)$ and $\tau_{1/2}$ as determined from the Avrami plots are summarized in Table 7.3. Neat PCL shows values for n in the range of 2.5 to 2.9, which suggests that the PCL chains crystallize via three-dimensional growth following a heterogeneous nucleation mode. Although a large variation in the values of n have been reported for PCL[12],

Table 7.3. Kinetic parameters for neat PCL and PCL/PEO9-based TPVs obtained from the Avrami analysis of crystallization experiments at various $T_{c,i}$.

σ (chains/nm^2)	$T_{c,i}$ (°C)	100 wt% PCL					
		n	$K(T)$	$t_{1/2}$ (min)	n	$K(T)$	$t_{1/2}$ (min)
-	37	2.54	6.0×10^{-2}	2.62			
	39	2.52	1.7×10^{-2}	4.25			
	41	2.56	4.5×10^{-3}	7.07			
	43	2.61	9.5×10^{-4}	12.31			
	45	2.93	6.0×10^{-5}	24.2			
		60 wt% PCL			40 wt% PCL		
0.038	37	2.74	2.3×10^{-1}	1.49	-	-	-
	39	3.08	2.8×10^{-2}	2.92	2.93	1.0×10^{-1}	1.99
	41	3.03	4.0×10^{-3}	5.56	2.89	1.0×10^{-2}	4.33
	43	3.15	4.0×10^{-4}	10.88	2.78	1.3×10^{-3}	9.65
	45	2.96	7.6×10^{-5}	21.85	2.79	1.3×10^{-4}	21.64
0.081	37	2.79	1.1×10^{0}	0.87	2.75	3.5×10^{0}	0.58
	39	2.50	3.1×10^{-1}	1.39	2.95	7.4×10^{-1}	1.01
	41	3.00	3.7×10^{-2}	2.72	3.17	7.6×10^{-2}	2.05
	43	3.16	3.2×10^{-3}	5.50	3.28	7.6×10^{-3}	3.99
	45	3.01	4.9×10^{-4}	11.09	3.27	5.9×10^{-4}	8.72
0.099	37	2.67	4.2×10^{0}	0.52	2.81	5.4×10^{0}	0.49
	39	2.79	1.0×10^{0}	0.87	2.80	1.2×10^{0}	0.83
	41	2.87	2.0×10^{-1}	1.57	3.41	1.4×10^{-1}	1.67
	43	3.28	1.3×10^{-2}	3.43	3.29	1.2×10^{-2}	3.46
	45	3.42	6.8×10^{-4}	7.62	3.39	7.1×10^{-4}	7.61

the obtained values of 2.5 to 2.9 are in good agreement with the values reported elsewhere for isothermal crystallization of PCL in a similar temperature range[37,38]. As expected, the overall crystallization rate $K(T)$ decreases with increasing isothermal crystallization temperature $T_{c,i}$. Additionally, an increase in $K(T)$ is observed with increasing σ and increasing rubber content, which is attributed to the increased NE. The values for n in the PCL/PEO9-based TPVs are slightly higher in comparison to the values for neat PCL and vary between 2.7 and 3.4.

Plots of T_m versus $T_{c,i}$ are presented in Fig. 7.8, which show that T_m increases linearly with $T_{c,i}$. The experimental data can be described by the Hoffman-Weeks equation[39]:

$$T_m = \xi T_{c,i} + (1-\xi)T_m^0 \tag{7.8}$$

where T_m^0 is the equilibrium melting temperature and $\xi =1/\gamma$ is a stability parameter that depends on the crystal thickness, where γ is the ratio of the lamellar thickness l to the lamellar thickness of the critical nucleus l^* at T_c. In equation 7.8, ξ may have values between 0 and 1, where $\xi = 0$ implies $l \gg l^*$ and $T_m = T_m^0$, whereas $\xi = 1$ implies $l = l^*$ and $T_m = T_{c,i}$. Consequently, the crystals are most stable for $\xi = 0$ and are inherently unstable for $\xi = 1$. As shown in Fig. 7.8, the values of T_m^0 can be evaluated by extrapolation of the experimental data according to equation 7.8 to intersect the line of $T_m = T_{c,i}$, whereas the ξ parameters can be determined from the slope of these fitted lines. The values of T_m^0 and ϕ for neat PCL and the PCL/PEO9-based TPVs are summarized in Table 7.4. For neat PCL, values of 63.1 °C and 0.255 are obtained for T_m^0 and ξ, respectively, which are in good agreement with the values of 61.7 °C and 0.167 as reported by Zheng et al.[40] for PCL. A depression in T_m^0 is observed with increasing PEO9 content; T_m^0 decreases by 1 °C at a rubber content of 40 wt% and by approximately 3 °C at a rubber content of 60 wt%. Variations in σ do not influence T_m^0 and ξ. This indicates that the depression in T_m^0 is not related to the nucleating effect of the rubber particles, but to the amount of rubber present in
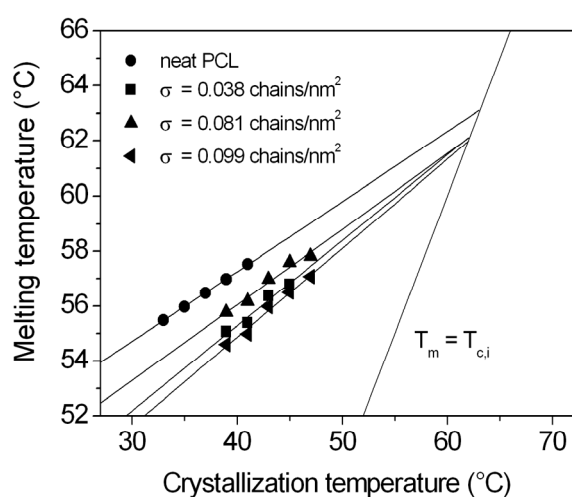

Fig. 7.8. Hoffman-Weeks plots for neat PCL and PCL/PEO9-based TPVs containing 60 wt% PCL.

the TPV. It is, therefore, most likely that the decrease in T_m^{0} originates from a T_m depression induced by favorable thermodynamic interactions between the PCL crystals and the cross-linked PEO9 particles. The small amount of residual, non-cross-linked PEO9, which is in the order of 2-4 wt%, may contribute to the T_m depression. The values of the stability parameter ϕ are relatively constant within the range of 0.248 to 0.324, which indicates that the crystals are fairly stable.

Table 7.4. Values of T_m^{0} and ξ for neat PCL and PCL/PEO9-based TPVs.

PCL content (wt%)	σ (chains/nm^2)	T_m^{0} (°C)	ξ
100	-	63.1	0.255
60	0.038	62.2	0.311
60	0.081	62.1	0.276
60	0.099	62.0	0.324
40	0.038	59.3	0.248
40	0.081	59.3	0.251
40	0.099	60.3	0.258

7.3.3. Small-angle light scattering (SALS)

Several studies demonstrated that time-resolved, polarization-dependent small-angle light scattering (SALS) is very sensitive to micrometer-scale density and orientation fluctuations arising during polymer crystallization[41-45]. In this study, SALS is used to follow the changes in the shape, the size and the internal order of superstructures formed during the course of crystallization of neat PCL and PCL/PEO9-based TPVs.

SALS under cross-polarized optical alignment (Hv) measures mean-square fluctuations in the anisotropy ($\langle\delta^2\rangle$) arising from the arrangement of crystalline aggregates. SALS under parallel-polarized optical alignment (Vv) measures mean-square fluctuations in anisotropy as well as in polarizability ($\langle\eta^2\rangle$), the latter originating from density fluctuations. The total scattered intensity, or the invariant, Q, is defined by:

$$Q = \int_{q=q_{min}}^{q=q_{max}} I(q)q^2 dq \tag{7.9}$$

where q is the scattering vector defined by $q = (4\pi n/\lambda)\sin(\theta)$ with λ the wavelength, 2θ the scattering angle and n the refractive index, and $I(q)$ is the intensity of scattered light at q. The Hv and Vv invariants can then be generalized as:

$$Q(Hv) \propto \langle \delta^2 \rangle = \phi_S (\delta_{cr}^0 x_{CS} P_2)^2 \qquad (7.10)$$

$$Q(Vv) \propto \langle \eta^2 \rangle + Q(Hv) = \phi_S (1 - \phi_S)(\alpha_d - \alpha_0)^2 + \phi_S (\delta_{cr}^0 x_{CS} P_2)^2 \qquad (7.11)$$

where ϕ_S is the volume fraction of spherulites, x_{CS} is the crystallinity with the spherulites, δ_{cr}^{0} is the intrinsic anisotropy of a pure crystal, P_2 is the Hermans-type orientation function, α_d is the average polarizability of the crystals and α_0 is the average polarizability of the surrounding amorphous phase.

A series of Hv and Vv light scattering patterns during isothermal crystallization from the melt for neat PCL and PCL/PEO9-based TPVs is shown in Fig. 7.9. It is well known that isothermal crystallization of PCL gives the usual type of spherulite with a Maltese cross along the direction of polarizers when viewed under a cross-polarized microscope. Such spherulites show a four-leave-clover scattering pattern with maxima occurring at azimuthal angles (α) at odd multiples of 45° when a cross-polarized optical alignment (Hv) is used. An increase in the radius of the spherulites leads to a decrease in the scattering angle 2θ and, consequently, to an increase in the scattering vector q. The average radius of the spherulites (R_{sph}) is directly related to the maximum scattering vector (q_{max}) in the Hv pattern via $R_{sph} = 4.08/q_{max}$[46]. Upon crystallization from the melt the typical four-leaf-clover pattern is observed in the Hv scattering profiles (Fig. 7.9). Since the size of the spherulites of neat PCL increases up to relatively large dimensions (in the order of 50-100 μm after reaching $X(t) > 50$ %, see Fig. 7.4a), the maxima in the scattering patterns of neat PCL are mostly covered by the beam stop. The Hv patterns of the TPVs, however, clearly show the formation of a four-leaf-clover pattern, where the average radius of the spherulites decreases with increasing σ. Upon crystallization, the Vv scattering pattern is initially circularly symmetrical. This scattering profile can already be observed before any scattering in the Hv pattern is visible. This circular contribution originates from the development of small aggregates that induce fluctuations in the polarizability. The intensity of the circularly symmetrical scattering pattern increases as the small aggregates grow in size and number and, according to equation 7.11, passes through a maximum at $\phi_S = 0.5$. At about this stage, a two-fold symmetrical contribution with respect to the polarization direction grows as the crystalline regions become more anisotropic, while the circularly symmetrical contribution diminishes in intensity as the spherulites become space-filling ($\phi_S = 1$).
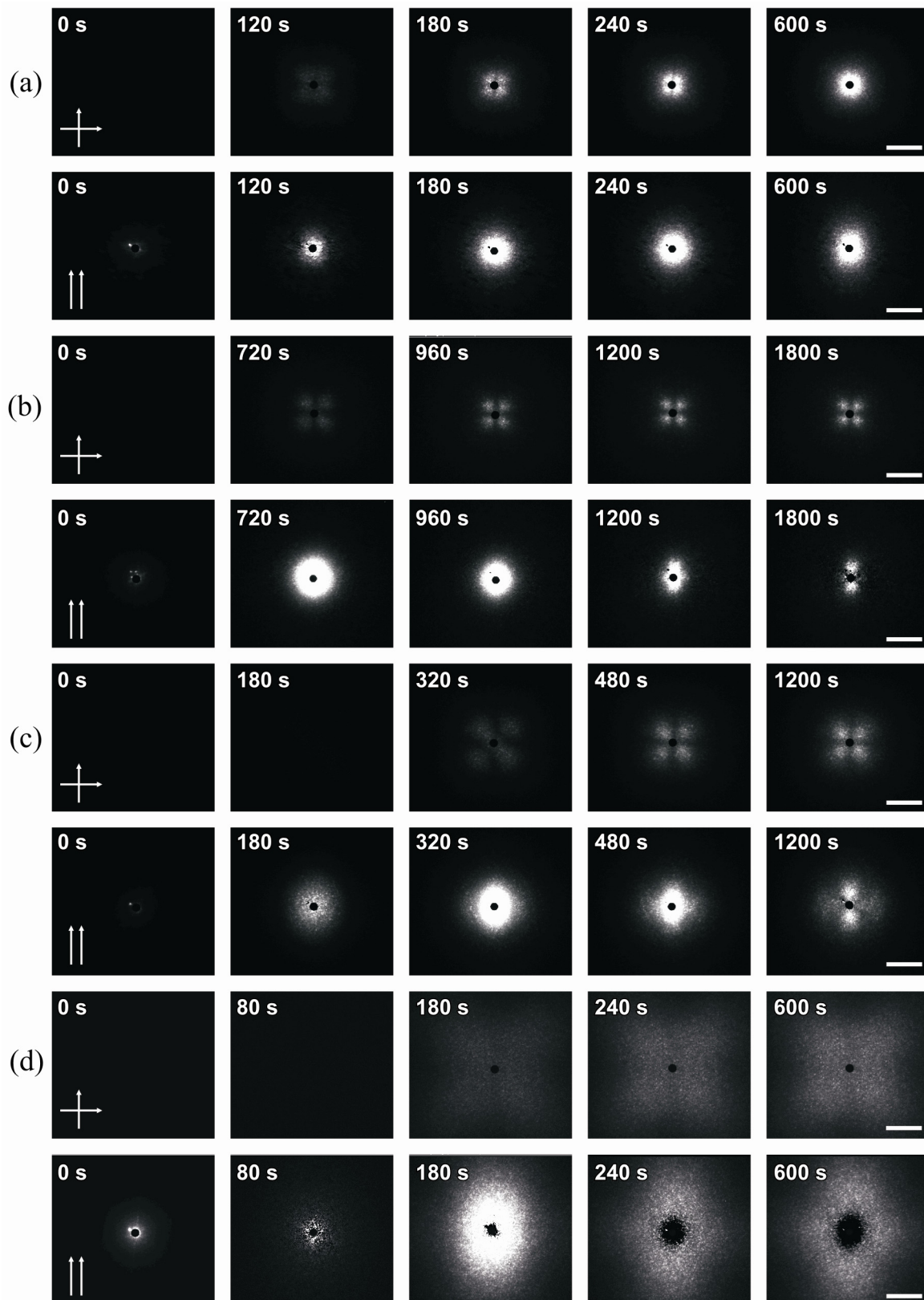
Fig. 7.9. Changes in SALS Hv and Vv patterns during isothermal crystallization of (a) neat PCL at 43 °C and PCL/PEO9-based TPVs containing 60 wt% PCL at 47 °C with (b) σ = 0.038 chains/nm², (c) σ = 0.081 chains/nm² and (d) σ = 0.099 chains/nm². The arrows indicate the direction of the polarizers and the scale bar is equivalent to a scattering angle of θ = 13°.

As shown in Fig. 7.10a, the normalized $Q(Hv)$ and $Q(Vv)$ for neat PCL gradually increase with time. However, the development of these invariants is not representative for the

crystallization process of neat PCL, since most of the scattered light is blocked by the beam stop due to the relatively large size of the spherulites. In contrast to neat PCL, the normalized invariants of the PCL/PEO9-based TPVs show the typical behavior that is expected on the basis of equations 7.10 and 7.11. After an induction time, the formation of small crystals leads to an increase in density fluctuations during the early stages of crystallization, which is reflected in an increase in $Q(Vv)$. The orientation fluctuations that arise from the optical anisotropy of these small crystals develop at later stages, causing $Q(Hv)$ to increase after $Q(Vv)$ has already reached a significant value. The difference in onset time of $Q(Vv)$ and $Q(Hv)$ is caused by the development of weakly anisotropic domains as the precursors of spherulites[41,42]. These weakly anisotropic domains are loosely structured spherulites, causing $Q(Vv)$ to increase, for which the crystalline parts are too small to cause a measurable anisotropy by themselves, i.e. no visible scattering in the Hv pattern. With ongoing crystallization, the internal structure of these spherulites matures and orientation fluctuations caused by the growing anisotropic entities start to increase, leading to an increase in $Q(Hv)$. With time, $Q(Vv)$ increases as the small crystalline regions grow in size and number and $Q(Vv)$ passes through a maximum when the spherulites occupy 50% of the volume, following equation 7.11. A subsequent decrease in $Q(Vv)$ is observed during the later stages of crystallization, when the crystalline phase becomes dominant ($\phi_S > 0.5$). $Q(Hv)$ shows a sigmoidal increase, where the changes in $Q(Hv)$ parallel those in $Q(Vv)$ during the later stages of crystallization[47]. The exact position of the maximum in $Q(Vv)$ relative to the sigmoidal increase in $Q(Hv)$ is believed to be polymer specific and depends on the crystallization temperature and the sensitivity of the camera used for the scattering experiments[45].

As proven by the (non-)isothermal DSC and POM studies, the grafted rubber particles act as a good nucleating agent for the PCL matrix, where NE increases with σ. The nucleating ability of the particles is also evident from the Hv and Vv scattering patterns shown in Figs. 7.9b-d and the corresponding invariants in Figs. 7.10b-d. The onset of crystallization shifts to shorter times and the time required to reach the maximum $Q(Hv)$ is significantly shortened. The increase in the scattering angle with increasing σ indicates a reduced average size of the formed spherulites, which is in agreement with the POM images presented in Fig. 7.4. The symmetry in the four-leaf-clover patterns in the Hv scattering indicates a randomized growth of the spherulites, i.e. the crystalline structures are not oriented.
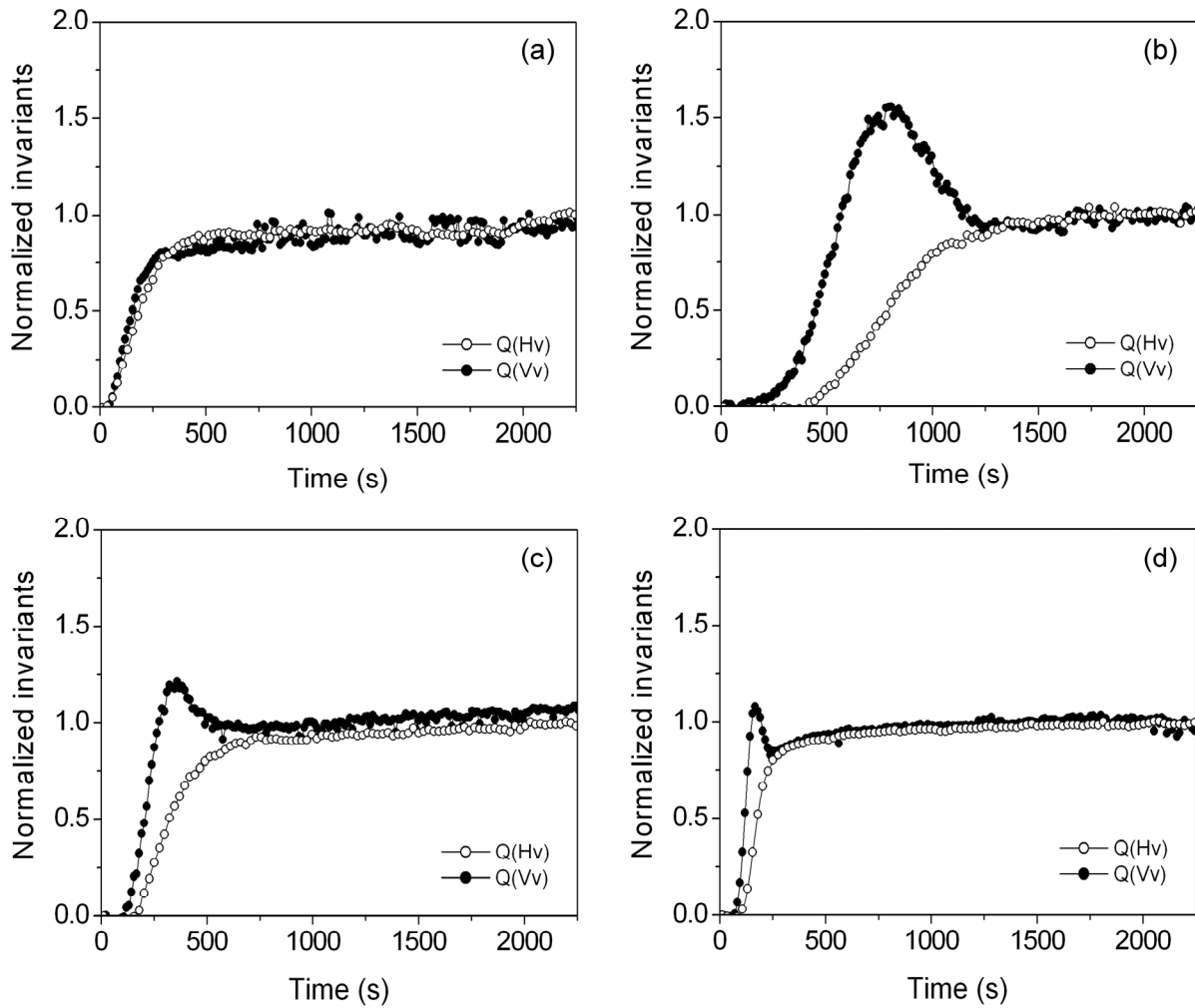
Fig. 7.10. Changes in normalized Q(Hv) and Q(Vv) during isothermal crystallization of (a) neat PCL at 43 °C and PCL/PEO9-based TPVs containing 60 wt% PCL at 47 °C with (b) $\sigma = 0.038$ chains/nm^2, (c) $\sigma = 0.081$ chains/nm^2 and (d) $\sigma = 0.099$ chains/nm^2.

For most semi-crystalline polymers the experimental SALS patterns deviate significantly from the ideal patterns, which mainly originates from the internal disorder of the spherulites[48]. According to equation 7.11, the ideal Vv scattering pattern is composed of an anisotropic ($\langle\delta^2\rangle$) contribution only, since scattering from density fluctuations ($\langle\eta^2\rangle$) diminishes at $\phi_S = 1$. Comparison of the Vv scattering patterns at high crystallinity (last column in Figs. 7.9b-d) shows that the $\langle\delta^2\rangle$ contribution relative to $\langle\eta^2\rangle$ decreases with increasing σ. This indicates that the anisotropy of the crystals decreases (i.e. P_2 in equation 7.10 and 7.11 decreases), suggesting that more defective spherulites are formed with increasing σ. An increased internal disorder leads to a decrease in the maximum intensity of the Hv scattering pattern at an azimuthal angle (α) of 45° and to an increase in the scattering intensity at all other angles[49]. The extent of disorder in the spherulites can, therefore, be determined by evaluation of the ratio of the maximum intensity in the Hv scattering pattern at $\alpha = 0°$ and $\alpha = 45°$:

$$\frac{I(\alpha = 0°, q = q_{max})}{I(\alpha = 45°, q = q_{max})} \tag{7.12}$$

The value of these intensity ratios ranges from 0 (for perfect spherulites) to 1 (for a random correlation). Table 7.5 shows the calculated disorder parameters for the PCL/PEO9-based TPVs. Due to the relatively large size of the spherulites, the disorder parameter of the neat PCL could not be determined from the SALS patterns. The extent of disorder in the spherulites increases drastically with increasing σ and $\overline{D_n}$. It is known that an increase in the crystallization rate (e.g. by decreasing the crystallization temperature or increasing the amount of nucleating agent) leads to smaller and less perfectly formed spherulites[50]. The increase in the disorder parameter can, therefore, be attributed to the increasing *NE* of the rubber particles with increasing σ. Additionally, the growth of spherulites will be influenced by the topological confinement that is imposed by the rubber particles. This confinement will depend on $\overline{D_n}$ and the interparticle distance (*ID*), where *ID* is defined by:

$$ID = \overline{D_n} \left[\left(\frac{k\pi}{6\phi} \right)^{1/3} - 1 \right] \tag{7.13}$$

with ϕ the volume fraction of rubber and k = 2 assuming a body-centred cubic (BCC) lattice[51]. Table 7.5 shows that the formed spherulitic superstructures are at least one order of magnitude larger than *ID*, from which it can be concluded that the rubber particles are incorporated in the spherulites and will, therefore, influence the growth of the spherulites.

Table 7.5. Spherulite sizes and disorder parameters for PCL/PEO9-based TPVs.

PCL content (wt%)	σ (chains/nm^2)	$\overline{D_n}$ (nm)	ID (nm)	R_{sph} (μm)	$\dfrac{I(\alpha = 0°, q = q_{max})}{I(\alpha = 45°, q = q_{max})}$
100	-	-	-	50-100[a]	-
60	0.038	80	30	3.1	0.32
60	0.081	180	70	2.4	0.50
60	0.099	305	120	1.9	0.81

[a]*As determined from the POM image taken after the SALS measurement.*

7.4. Conclusions

The crystallization behavior of neat PCL and PCL in blends with cross-linked rubber particles was studied under (non-)isothermal crystallization conditions. Hydrogen abstraction from the PCL chains during the preparation of the TPVs leads to the formation of PCL grafts on the cross-linked rubber particles. These grafted rubber particles form an excellent nucleating agent for PCL, where the nucleating efficiency *NE* shows an exponential dependency on the grafting density σ. The rubber particle size does not influence *NE*. The increased *NE* leads to *(i)* an

increase in overall crystallization rate, *(ii)* a decrease in the size of the spherulites and *(iii)* a decrease in the internal order of the spherulites.

Favorable thermodynamic interactions between the PCL crystals and the cross-linked rubber particles lead to a decrease in the equilibrium melting temperature with increasing rubber content.

Several authors have reported an increase in the crystallization temperature after dynamic vulcanization and/or (reactive) compatibilization of polymer blends consisting of a semi-crystalline thermoplastic matrix and an dispersed amorphous phase[2-11]. The results presented here indicate that the formation of graft copolymers on the interface of the amorphous dispersed phase and the matrix is the major reason for the increased crystallization temperature.

A more detailed study on the molecular organization of the surface grafts is required in order to fully understand their mode of nucleation. Since the surface grafts in the PCL/PEO9-based TPVs originate from hydrogen abstraction occurring randomly in the sample during the preparation of the TPVs, the amount of surface grafts and their molecular organization in the TPVs is difficult to control. Therefore, future work should focus on a well-defined system where the length, the amount and the density of the surface grafts can be controlled.

7.5. References

[1] Wittmann, J.C.; Lotz, B. *J. Polym. Sci., Part B: Polym. Phys.* **1981**, *19*, 1837-1851.
[2] Inoue, T.; Suzuki, T. *J. Appl. Polym. Sci.* **1995**, *56*, 1113-1125.
[3] Inoue, T. *J. Appl. Polym. Sci.* **1994**, *54*, 723-733.
[4] Inoue, T.; Suzuki, T. *J. Appl. Polym. Sci.* **1996**, *59*, 1443-1450.
[5] D'orazio, L; Mancarella, C.; Martuscelli, E.; Sticotti, G. *J. Mat. Sci.* **1991**, *26*, 4033-4047.
[6] Martuscelli, E.; Silvestre, C.; Abata, G. *Polymer* **1982**, *23*, 229-237.
[7] Jain, A.K.; Nagpal, A.K.; Singhal, R.; Gupta, N.K. *J. Appl. Polym. Sci.* **2000**, *78*, 2089-2103.
[8] López-Manchado, M.A.; Kenny, J.M.; Quijada, R.; Yazdani-Pedram, M. *Macromol. Chem. Phys.* **2001**, *202*, 1909-1916.
[9] Huang, H.; Liu, X.; Ikehara, T.; Nishi, T. *J. Appl. Polym. Sci.* **2003**, *90*, 824-829.
[10] Zheng, S.; Zheng, H.; Guo, Q. *J. Polym. Sci., Part B: Polym. Phys.* **2003**, *41*, 1085-1098.
[11] Guo, Q.; Zheng, H. *J. Appl. Polym. Sci.* **1999**, *74*, 322-327.
[12] Guo, Q.; Groeninckx, G. *Polymer* **2001**, *42*, 8647-8655.
[13] Chen, J.; Chang, F. *Macromolecules* **1999**, *32*, 5348-5356.
[14] Chen, J.; Huang, H.; Li, M.; Chang, F. *J. Appl. Polym. Sci.* **1999**, 71, 75-82.
[15] Tang, T.; Huang, B. *J. Polym. Sci., Part B: Polym. Phys.* **1994**, *32*, 1991-1998.
[16] Adewole, A.A.; Denicola, A.; Gogos, C.G.; Mascia, L. *Adv. Polym. Techn.* **2000**, *19*, 180-193.
[17] Cam, D.; Hyon, S.-H.; Ikada, Y. *Biomaterials* **1995**, *16*, 833-843.
[18] Stoks, W.; Berghmans, H. *J. Polym. Sci., Part B: Polym. Phys.* **1991**, *29*, 609-617.
[19] Avella, M.; Errico, M.E.; Rimedio, R.; Sadocco, P. *J. Appl. Polym. Sci.* **2002**, *83*, 1432-1442.
[20] Fillon, B.; Wittmann, J.C.; Lotz, B.; Thierry, A. *J. Polym. Sci., Part B: Polym. Phys.* **1993**, *31*, 1383-1393.
[21] Fillon, B.; Lotz, B.; Thierry, A.; Wittmann, J.C. *J. Polym. Sci., Part B: Polym. Phys.* **1993**, *31*, 1395-1405.
[22] Balsamo, V.; Müller, A.J.; Stadler, R. *Macromolecules* **1998**, *31*, 7756-7763.

[23] Bieliński, D.M.; Ślusarski, L.; Włochowicz, A.; Ślusarczyk, C.; Douillard, A. *Polym. Int.* **1997**, *44*, 161-173.

[24] Svoboda, P.; Svobodova, D.; Slobodian, P.; Ougizawa, T.; Inoue, T. *Polym. Test.* **2009**, *28*, 215-222.

[25] Castillo, V.; Matos, M.; Müller, A.J. *Rev LatinAm. Met. Mat.* **2003**, *23*, 12-25.

[26] Vassiliou, A.A.; Papageorgiou, G.Z.; Achilias, D.S.; Bikiaris, D.N. *Macromol. Chem. Phys.* **2007**, *208*, 364-376.

[27] Balsamo, V.; Sánchez, A.; Aguilera, E.; Müller, A.J.; Ronca, G. *Rev. Fac. Ing. UCV* **2006**, *21*, 105-119.

[28] Zhu, G.; Xu, Q.; Qin, R.; Yan, H.; Liang, G. *Rad. Phys. Chem.* **2005**, *74*, 42-50.

[29] Fei, B.; Chen, C.; Chen, S.; Peng, S.; Zhuang, Y.; An, Y.; Dong, L. *Polym. Int.* **2004**, *53*, 937-943.

[30] Khonakdar, H.A.; Morshedian, J.; Mehrabzadeh, M.; Wagenknecht, U.; Jafari, S.H. *Eur. Polym. J.* **2003**, *39*, 1729-1734.

[31] Elzein, T.; Brogly, M.; Schultz, J. *Surf. Interface Anal.* **2003**, *35*, 231-236.

[32] Elzein, T.; Brogly, M.; Schultz, J. *Polymer* **2002**, *43*, 4811-4822.

[33] Beigbeder, A.; Bruzaud, S.; Spěváček, J.; Brus, J.; Grohens, Y. *Macromol. Symp.* **2005**, *222*, 225-231.

[34] Avrami, M. *J. Chem. Phys.* **1939**, *7*, 1103-1112.

[35] Avrami, M. *J. Chem. Phys.* **1940**, *8*, 212-224.

[36] Lorenzo, A.T.; Arnal, M.L.; Albuerne, J.; Müller, A.J. *Polym. Test.* **2007**, *26*, 222-231.

[37] Cheng, E.-C.; Wu, T.-M. *Polym. Degrad. Stab.* **2007**, *92*, 1009-1015.

[38] Remiro, P.M.; Cortazar, M.M.; Calahorra, M.E.; Calafel, M.M. *Macromol. Chem. Phys.* **2001**, *202*, 1077-1088.

[39] Hoffman, J.D.; Weeks, J.J. *J. Chem. Phys.* **1962**, *37*, 1723-1741.

[40] Zheng, S.; Lü, H.; Guo, Q. *Macromol. Chem. Phys.* **2004**, *205*, 1547-1558.

[41] Okada, T.; Saito, H.; Inoue, T. *Macromolecules* **1992**, *25*, 1908-1911.

[42] Pogodina, N.V.; Siddiquee, S.K.; van Egmond, J.W.; Winter, H.H. *Macromolecules* **1999**, *32*, 1167-1174.

[43] Stein, R.S. In *Crystallization of Polymers*; Dosiere, M., Ed.; Kluwer Academic Publishers: Dordrecht, 1993.

[44] Akpalu, Y.; Kielhorn, L.; Hsiao, B.S.; Stein, R.S.; Russell, T.P.; van Egmond, J.; Muthukumar, M. *Macromolecules* **1999**, *32*, 765-770.

[45] Baert, J.; van Puyvelde, P. *Macromol. Mat. Eng.* **2008**, *293*, 255-273.

[46] Stein, R.S.; Misra, A.; Yuasa, T.; Khambatta, F. *Pure Appl. Chem.* **1977**, *49*, 915-928.

[47] Tabar, R.J.; Leite-James, P.; Stein, R.S. *J. Polym. Sci., Part B: Polym. Phys.* **1985**, *23*, 2085-2107.

[48] *Physico-Chemical Approaches to the Measurement of Anisotropy and Orientation*; Stein, R.S.; Wilkes, G.L. In *Structure and Properties of Oriented Polymers*; Ward, I.M., Ed.; Applied Science Publishers: London, 1975; p. 75.

[49] Akpalu, Y.A.; Lin, Y. *J. Polym. Sci., Part B: Polym. Phys.* **2002**, *40*, 2714-2727.

[50] *Macromolecular Physics, Vol. 2: Crystal Nucleation, Growth, Annealing*; Wunderlich, B., Ed.; Academic Press: New York, 1976.

[51] Wu, S. *J. Appl. Polym. Sci.* **1988**, *35*, 549-561.

7

Chapter 8[*]

Sub-micrometer thermoplastic vulcanizates obtained by reaction-induced phase separation of miscible mixtures of poly(ethylene) and alkyl methacrylates

Sub-μm thermoplastic vulcanizates (TPVs) with cross-linked rubber particles with sizes ranging from 70 to 500 nm were prepared by reaction-induced phase separation (RIPS) of initially miscible blends of poly(ethylene) (PE), lauryl methacrylate (LMA) and divinylbenzene (DVB). Cross-linking under static conditions led to (partial) connectivity of the rubber particles via chemical bridging of grafted PE chains. Dynamic preparation conditions caused the connected structure to break up, which led to a significant enhancement of the mechanical properties and the melt processability. The addition of 25 to 80 wt% extender oil resulted in a reduced complex viscosity and yield stress in the melt, without deteriorating the mechanical properties. The relatively good elastic recovery and excellent ultimate properties of these high-hardness TPVs may be explained by the sub-μm rubber dispersions. It was demonstrated that the preparation of TPVs via RIPS of polyolefins and alkyl methacrylates is a versatile approach, where variations in the thermoplastic, the elastomer precursor, the cross-linker and the preparation conditions can be used to control the morphology and the properties of the resulting TPVs.

8.1. Introduction

Chapter 2 demonstrated a significant improvement of the tensile properties of TPVs based on poly(propylene) (PP) and ethylene-propylene-diene (EPDM) rubber upon decreasing the rubber particle size from 70 to 1 μm, which is in good agreement with the work presented by Coran *et al.*[1] and Araghi[2]. Additionally, an improvement of the elastic recovery and an increase in the melt viscosity was observed with decreasing particle size. Chapters 4-7 showed that reaction-induced phase separation (RIPS) of miscible blends based on a semi-crystalline thermoplastic in combination with a low-molar-mass elastomer precursor is a promising route to prepare TPVs with very fine rubber dispersions over a very broad composition range. Although the concept of RIPS was successfully applied for the preparation of TPVs, several things have to be taken into account. Cross-linking of the elastomer precursor via a step-growth reaction, e.g. an epoxy resin cross-linking with a multifunctional amine, leads to relatively coarse, μm-sized morphologies, where the final gel content is highly dependent on the stoichiometric epoxy/amine ratio (Chapter 4). Changing the cross-linking mechanism from step-growth to chain-growth, e.g. peroxide-initiated cross-linking of (meth)acrylate resins, leads to sub-μm-sized rubber dispersions and high gel contents (Chapter 6). However, the relatively high cross-link density of the elastomer precursors during cross-linking leads to the interference of gelation with the phase separation process, which leads to connectivity between the rubber particles and inferior tensile properties and melt processability (Chapters 5 and 6). An additional disadvantage of the systems studied in Chapters 4-7 is the relatively low melting temperature (T_m) of the poly(ε-caprolactone) matrix.

The aim of this chapter is to apply the knowledge obtained from the previous chapters in order to prepare TPVs with sub-μm morphologies over a very broad composition range and to prevent the occurrence of significant particle connectivity. Additionally, a semi-crystalline thermoplastic with a relatively high T_m is used in order to broaden the temperature window for applications of the TPVs. In this study, the simultaneous polymerization and cross-linking of alkyl methacrylates with divinylbenzene (DVB) in initially miscible blends with poly(ethylene) (PE) is used for the preparation of TPVs. After initiation of the reaction, high-molar-mass macromolecules are rapidly formed at relatively low conversions. As a result, phase separation is induced in the early stages of the cross-linking reaction. Additionally, both phases will contain large amounts of the reactive monomer, which lowers the interfacial tension between the phase-separated domains. These factors are expected to reduce the particle size of the cross-linked poly(alkyl methacrylate) rubber, potentially into the sub-μm range.

In-situ polymerization and cross-linking of initially homogeneous blends of PE and vinyl monomers was previously applied to synthesize (semi-)interpenetrating polymer networks

(IPNs)[3-9]. In general, the *in-situ* approach is useful for reactive processing of (in)tractable polymers[10-14] and for the reactive compatibilization of incompatible polymer blends[15-18]. The materials obtained by *in-situ* polymerization cannot be described by a simple three-component system, i.e. PE, polymerized/cross-linked monomer and residual monomer. Side reactions may occur due to the free-radical character of the polymerization reaction. Radical transfer reactions can lead to the formation of PE macroradicals, which are able to react with the monomer to yield grafted PE[3,4,8,15,16,18]. Additionally, termination reactions of PE macroradicals via disproportionation may lead to chain branching and cross-linking of PE[3-5,9]. In the case of TPVs, partial grafting of the monomer onto PE may be advantageous, since the graft copolymers may compatibilize the two phases and suppress diffusive and hydrodynamic coarsening of the morphology during phase separation, thereby decreasing the rubber particle size. However, cross-linking of the PE matrix is highly undesirable, since it will severely limit the melt processability of the final material. Although these side reactions are expected to have a significant influence on the physical properties of the materials, a quantitative analysis of the grafting and cross-linking reactions was only presented by Lazár *et al.*[4].

Previous research in our group has focused on the processing of PE by applying a reactive solvent approach, where both styrene and LMA were used as reactive solvent[10,11]. It was shown that liquid-liquid (L-L) phase separation is induced during the early stages of the *in-situ* polymerization of the reactive solvent. Upon slow polymerization of styrene in miscible PE/styrene mixtures at temperatures close to the melting temperature (T_m) of PE, small-angle X-ray scattering (SAXS) and wide-angle X-ray diffraction (WAXD) studies revealed that L-L phase separation proceeds via the nucleation and growth (NG) mechanism[10,11]. Due to the higher reaction rate of LMA compared to styrene, the demixing behavior may change from NG to spinodal decomposition (SD) in PE/LMA blends, although no direct evidence for this was found in the SAXS/WAXD studies. It was shown for both styrene and LMA as the reactive solvent that the addition of 1-3 wt% DVB as cross-linking monomer did not alter the morphology development. No evidence was found that gelation occurs prior to L-L phase separation with the used monomer/cross-linker ratios. This suggests that gelation does not limit full structure development and particle connectivity is, therefore, not expected to occur in these systems.

To our knowledge, the concept of RIPS of poly(olefin)/alkyl (meth)acrylate systems has never been applied to produce TPVs. This paper discusses the possibilities of *in-situ* polymerization and cross-linking of initially miscible blends of PE and alkyl methacrylates to prepare TPVs with sub-μm rubber dispersions. Based on differential scanning calorimetry (DSC) measurements, the influence of the length of the alkyl chain on the miscibility of PE/alkyl methacrylate blends is discussed. The morphology obtained after the *in-situ* reaction is elucidated

by transmission electron microscopy (TEM). Selective extractions combined with Fourier transform infrared (FTIR) spectroscopy are used to study the influence of the cross-linker concentration, peroxide content and cross-linking temperature on the chemical composition of the final products. The mechanical and rheological properties of the TPVs are related to the changes in chemical composition. Most commercial TPVs contain a significant amount of extender oil to enhance the melt processability and to lower the hardness and material costs. The application of oil extension to these TPVs is discussed in terms of their mechanical and rheological behavior. Finally, the versatility of the approach is demonstrated by changing the reactants and the preparation conditions.

8.2. Experimental

8.2.1. Materials

High-density PE (MFI = 4.0 g/10 min and ρ = 0.953 g/cm^3) was supplied by Sabic Europe, the Netherlands. Butyl methacrylate (BMA), lauryl methacrylate (LMA), octadecyl methacrylate (ODMA), divinylbenzene (DVB; mixture of isomers), the free-radical initiator *tert*-butyl peroxybenzoate, methanol, methyl ethyl ketone (MEK) and xylene were acquired from Aldrich and used as received. BMA, LMA and ODMA contained monomethyl ether hydroquinone as the inhibitor, while DVB contained *p-tert*-butylcatechol. The paraffinic oil (Sunpar 2280) was supplied by Sunoco, the Netherlands.
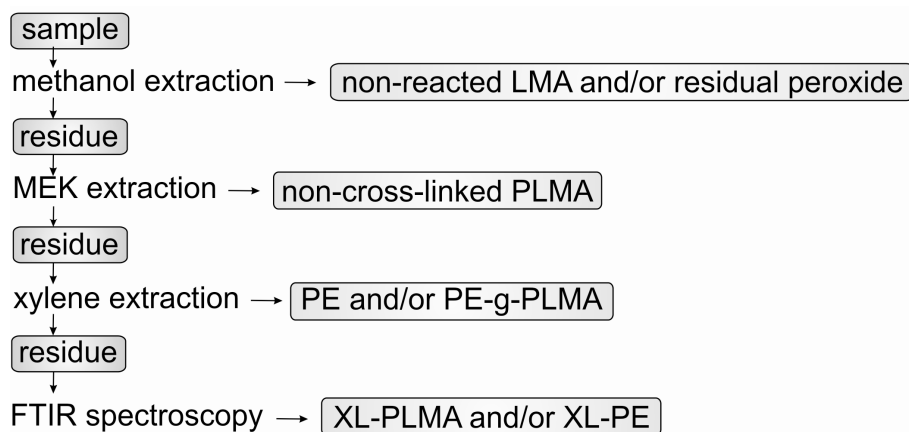
8.2.2. Blend preparation

First, LMA/DVB mixtures with varying compositions were prepared. PE and ~ 95 % of the required LMA/DVB solution were mixed in a home-built, recirculating, twin-screw micro-extruder with an internal volume of 5 cm^3, which is equipped with a pressure sensor. The peroxide was added in combination with the remaining ~ 5 % of LMA/DVB solution and the system was mixed at 150 rpm until a homogeneous mixture was obtained (mixing time ~ 3 min). During the remainder of the cross-linking process, the mixing was stopped (static conditions) or continued at 100 rpm (dynamic conditions). Cross-linking times of 12, 60 and 90 min were applied at the respective cross-linking temperatures of 150, 135 and 125 °C, where the half-life time of the peroxide is 3, 13 and 40 min, respectively. Oil-extended samples were obtained by further extrusion of the statically or dynamically-prepared TPVs with the required amount of oil in the micro-extruder for an additional 10 min at 100 rpm and 150 °C. The amounts of DVB and oil are expressed in wt% and are related to the LMA content.

8.2.3. Characterization techniques

Differential scanning calorimetry (DSC). DSC experiments were performed on a Perkin Elmer Pyris 1 Calorimeter. High-pressure, aluminum sample pans were used with a typical sample weight of 10 mg. The samples were first heated to 140 ^{o}C and equilibrated for 5 min in order to remove the thermal history. Subsequently, they were cooled at a rate of 10 ^{o}C/min to 30 ^{o}C, where they were kept for 5 min, and then

they were reheated to 140 $^{\circ}$C at a rate of 10 $^{\circ}$C/min. The offset at the end of the melting peak of the second heating run was used to determine the T_m depression[19].

Solvent extractions. Extractions were carried out with boiling solvents under reflux by using cellulose extraction thimbles in a Soxlet HT2 1045 extraction unit. The extraction procedure is shown in Scheme 8.1.

sample
↓
methanol extraction → non-reacted LMA and/or residual peroxide
↓
residue
↓
MEK extraction → non-cross-linked PLMA
↓
residue
↓
xylene extraction → PE and/or PE-g-PLMA
↓
residue
↓
FTIR spectroscopy → XL-PLMA and/or XL-PE

Scheme 8.1. Extraction scheme used to determine the chemical composition of PE/LMA-based TPVs.

Non-reacted LMA and other low-molar-mass species (e.g. residual peroxide and decomposition products) were extracted with methanol, whereas the free PLMA homopolymer was extracted with MEK. The selectivity of the methanol and MEK extractions was verified by FTIR spectroscopy on the extracts. PE and PE grafted with PLMA (PE-*g*-PLMA) were extracted with xylene. The total amount of PLMA grafted onto PE was calculated from the overall mass balance of the extracts. The insoluble residue of the xylene extraction is regarded as cross-linked (XL) product, consisting of cross-linked PLMA (XL-PLMA), cross-linked PE (XL-PE) and/or cross-linked PE-*g*-LMA. The weight fractions of PLMA and PE in the residue were determined by means of FTIR spectroscopy. However, no distinction can be made between grafted and cross-linked PE in the residue. The gel content (*%gel*) of the PLMA rubber phase was defined as:

$$\%gel = \frac{m_{LMA,in} - m_{LMA,free} - m_{PLMA,free}}{m_{LMA,in}} \times 100\% \tag{8.1}$$

where $m_{LMA,in}$ is the amount of LMA used to prepare the TPV, $m_{LMA,free}$ is the non-reacted LMA monomer as determined by methanol extraction and $m_{PLMA,free}$ is the free PLMA polymer as determined by MEK extraction.

Fourier transform infrared (FTIR) spectroscopy. Infrared studies were performed on a BioRad Excalibur 3000 spectrometer equipped with a diamond Specac Golden Gate attenuated total reflection (ATR) setup over a spectral range of 600 to 5000 cm^{-1}. Fifty spectra at a resolution of 4 cm^{-1} were signal-averaged and the resulting spectra were analyzed using the BioRad Merlin 3.0 software. The LMA content was determined by evaluating the ratio of the integrated intensities of the C=O stretching band at 1725 cm^{-1} and the CH$_2$ and CH$_3$ stretching bands at 2800-3000 cm^{-1}.

Transmission electron microscopy (TEM). Morphological investigations were performed with a Tecnai 20 transmission electron microscope operated at 200 kV. Samples were trimmed at -120 °C and

subsequently bulk-stained for 24 hrs with a ruthenium tetroxide (RuO$_4$)-solution prepared according to Montezinos *et al.*[20]. Ultrathin sections (70 nm) were obtained at -100 °C by using a Leica UltracutS/FCS microtome. The sections were placed on a 200 mesh copper grid with a carbon support layer. The number-averaged size of the rubber particles was determined with the Image Pro Plus 4.5 software.

Tensile testing. Films with a thickness of 1 mm were compression molded at 100 bar and 160 °C from which dumbbell-shaped tensile bars (32 x 2 x 1 mm) were punched. Tensile tests were performed at 12 mm/min using a 2.5 kN force cell on a Zwick Z010 tensile tester according to ASTM D412[21]. The equipment was controlled with TestXpert v7.11 software. Each sample was tested in at least 7-fold and average values are presented.

Compression set. The compression set (*CS*) was measured on cylindrical samples with a diameter of 13 mm and a thickness of 6 mm at 25 % compressive deformation for 22 hrs at 23 °C or 70 °C and a relaxation time of 30 min at room temperature, according to ASTM D395[22]. The *CS* was calculated as follows:

$$CS = \frac{(t_i - t_o)}{(t_i - t_n)} \times 100\% \tag{8.2}$$

where t_i is the initial thickness of the sample, t_o the final thickness of the sample and t_n the thickness of the spacer.

Dynamic mechanical thermal analysis (DMTA). Compression-molded samples (10 x 3 x 1 mm) were measured on a DMA Q800 (TA Instruments) with a film tension setup. A temperature sweep from -150 to 200 °C was performed with a heating rate of 3 °C/min at a frequency of 1 Hz. A pre-load force of 0.01 N, an amplitude of 10 μm and a force track of 110 % were used.

Rheological measurements. Dynamic shear measurements were performed on a strain-controlled AR-G2 rheometer (TA Instruments) by using a 8 mm parallel-plate geometry and disk-shaped specimens (8 mm diameter; 0.5 mm thick). Frequency sweeps from 10^2 to 10^{-1} rad/s were performed at 160 °C with a strain of 1 %, which is in the linear viscoelastic regime. Time-temperature superposition (TTS) was applied by horizontal shifting of *G'* to a reference temperature of 160 °C. Creep measurements were performed on a stress-controlled AR-G2 rheometer (TA Instruments). A range of shear stresses was applied to the samples for 10 min at 160 °C.

8.3. Results and discussion

8.3.1. PE/(alkyl methacrylate) miscibility

To explore the applicable temperature-composition window for the preparation of TPVs via RIPS, the miscibility of PE/(alkyl methacrylate) mixtures was studied by evaluating the T_m depression of PE. The length of the alkyl chain of the alkyl methacrylate was varied from 3 (BMA) via 11 (LMA) to 17 (ODMA) methyl units. The T_m analysis of mixtures of semi-crystalline polymers and low-molar-mass species, such as solvents or monomers, provides information on the miscibility of the blend components. With increasing monomer contents a T_m

depression of PE is observed for all three monomers, with an increased slope in the order ODMA < LMA < BMA (Fig. 8.1). The decrease in T_m indicates favorable interactions between PE and the monomers, which suggests miscibility at temperatures above the measured T_m over the studied composition range. The miscibility increases with decreasing length of the alkyl chains, which is attributed to the decrease in molar volume (V) of the alkyl methacrylate. The polarity of the alkyl methacrylate hardly varies with the length of the alkyl group, i.e. the solubility parameter as calculated from the group contribution theory[23] is more or less constant. The T_m depression can be described by the Flory-Huggins (FH) lattice theory[24] (solid lines in Fig. 8.1) with values for the solubility parameter (δ) and V as presented in Table 8.1 and $\delta = 17.4$ $(J/cm^3)^{1/2}$, $V = 16.1$ cm^3/mol[23] and $\Delta H_m = 293$ J/g[25] for PE.
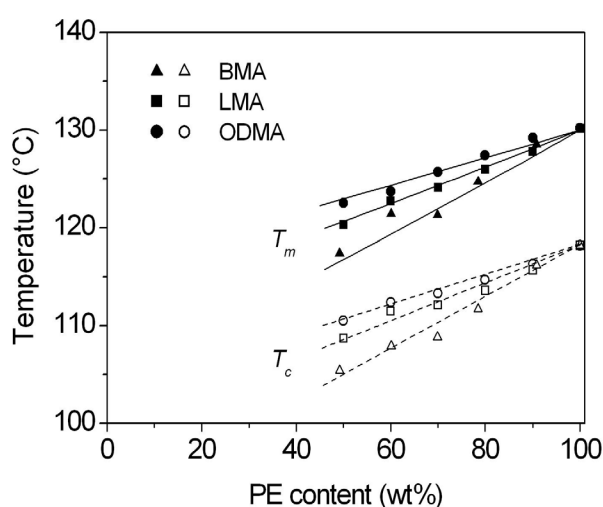
Fig. 8.1. Phase diagram of PE/(alkyl methacrylate) solutions (symbols indicate DSC data; solid lines represent calculated T_m based on the FH lattice theory; dashed lines serve as guides to the eyes for T_c).

Table 8.1. Physical properties of alkyl methacrylate monomers and corresponding polymers.

Material	Monomer			Polymer	
	δ^{23} $(J/cm^3)^{1/2}$	V^{23} (cm^3/mol)	T_b^{25} $(°C)$	T_m^{25} $(°C)$	T_g^{25} $(°C)$
BMA	17.0	156.3	162	–	20
LMA	17.1	285.1	272	-34	-65
ODMA	17.2	381.7	> 300	38	-100

The temperature window to apply RIPS is limited to temperatures between T_m of the thermoplastic and the boiling point (T_b) of the monomer (Table 8.1). Additionally, the glass transition temperature (T_g) of the poly(alkyl methacrylate) should be well below room temperature in order to generate a broad application window for the produced TPVs. Table 8.1 indicates that BMA is unsuitable for the RIPS approach, as it has a relatively low T_b and a high T_g. ODMA has a T_m of 38 °C, which is related to crystallization of the relatively long alkyl side

chains. This makes ODMA also less suitable for the preparation of TPVs, since crystallization of the side chains will limit the elastic properties of the TPVs at room temperature. In conclusion, LMA appears to be the most suitable monomer for the preparation of PE-based TPVs by RIPS and is, therefore, used throughout the main part of this chapter.

8.3.2. Morphology after *in-situ* polymerization/cross-linking

The phase-separated morphologies of the PE/LMA/DVB samples were studied by TEM. Samples were prepared by *in-situ* polymerization and cross-linking of miscible PE/LMA blends with 1 wt% DVB and 0.5 wt% peroxide at a cross-linking temperature (T_{XL}) of 125 °C under static conditions. The PLMA rubber phase appears black in the TEM images, since RuO_4 was used to stain the amorphous PE phase and the PLMA rubber phase. For PE concentrations of 20, 40 and 60 wt%, the TEM images show two distinct phases (Fig. 8.2). The TEM images clearly show that very fine rubber dispersions are obtained, where $\overline{D_n}$ increases from 70 nm at 60 wt% PE via 200 nm at 40 wt% PE up to 500 nm at 20 wt% PE. The crystalline PE lamellae are clearly visible in all the samples, especially at higher magnifications (Fig. 8.2d). It has to be noted that TEM analysis on these samples is not straightforward. The long alkyl chain of the monomer results in a high chemical similarity between the PE phase and the rubber phase. This makes the quality of the staining procedure crucial for a good contrast between the two phases, which explains the relatively poor contrast of the sample containing 20 w% PE (Fig. 8.2a). The TEM images clearly show the absence of particle connectivity, which implies that L-L phase separation precedes gelation of the rubber phase. This conclusion is supported by the spherical nature of the rubber particles, which suggests that phase separation occurs at low conversions of the LMA/DVB mixture. It should be noted that previous studies on RIPS of mixtures of diacrylates and liquid crystals showed that phase separation during chain cross-linking is driven by liquid-gel demixing rather than L-L demixing[26,27]. The occurrence of gelation prior to phase separation in those systems is related to the relatively high cross-linker contents in the range of 5 to 20 wt%. The absence of severe particle connectivity of the PE/LMA-based TPVs was supported by disintegration of the samples in boiling toluene.
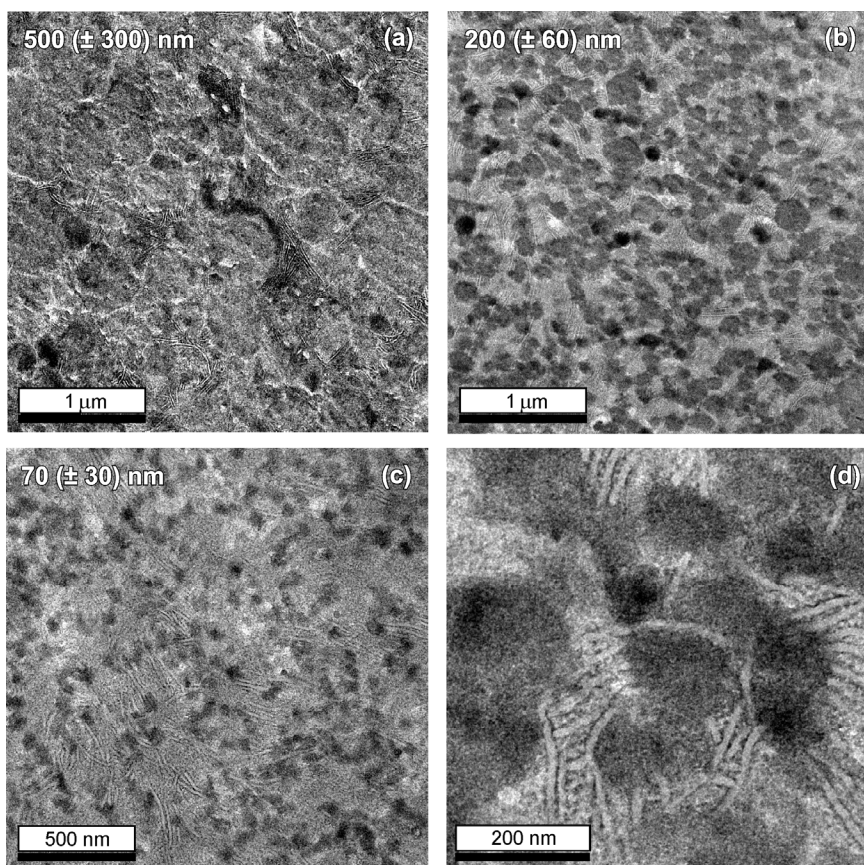
Fig. 8.2. TEM images of PE/LMA-based TPVs after in-situ cross-linking under static conditions at T_{XL} = 125 °C, containing (a) 20 wt% PE, (b) 40 wt% PE, (c) 60 wt% PE and (d) magnification of (b). The number-averaged rubber particle size ($\overline{D}_n$) and its standard deviation are shown in the figures.

8.3.3. Chemical composition after *in-situ* polymerization/cross-linking

Previous studies on blends consisting of PE and vinyl monomers prepared by *in-situ* free-radical polymerization showed that several side reactions may occur during polymerization[3-5,8,9,15,16,18]. Therefore, it is important to study the chemical composition of the prepared materials in order to establish structure-property relations. In this section the influence of the DVB content, the peroxide content and T_{XL} on the chemical composition is discussed for statically-prepared TPVs containing 40 wt% PE. As discussed in the experimental section, the chemical composition is investigated by a combination of solvent extractions and FTIR spectroscopy.

Fig. 8.3 shows that by increasing the DVB content from 0.5 to 2.0 wt%, the overall composition is hardly affected. The amount of cross-linked PLMA (XL-PLMA) and cross-linked PE (XL-PE) is slightly increased, while the amount of grafted PLMA decreases. In all cases, hardly any free LMA (< 5 wt%) and PLMA (< 2 wt%) is present; the methacrylate gel content (*%gel*) of the blends exceeds 90 % under these conditions. At T_{XL} = 135 °C and a DVB content of 2 wt%, no significant influence of the peroxide concentration on the chemical composition was observed in the range of 0.5 to 2 wt% peroxide. This is consistent with the observations of Lazár

et al.[4], who found only a slight increase in free BMA with peroxide concentrations ranging from 0.05 to 2 wt% for interpenetrating networks based on PE and BMA.
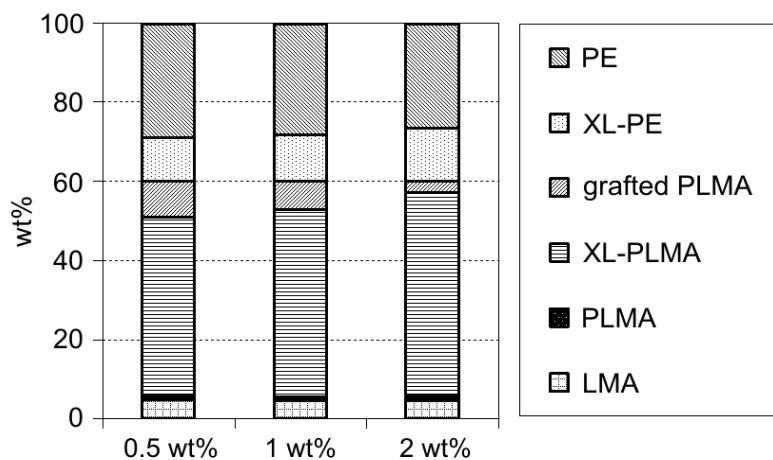

Fig. 8.3. Influence of DVB content on the chemical composition of statically-prepared PE/LMA containing 40 wt% PE cross-linked with 0.5 wt% peroxide at T_{XL} = 135 °C.

Fig. 8.4 shows that T_{XL} does have a significant influence on the chemical composition of the blends. By increasing T_{XL} from 125 to 150 °C, both the amount of non-reacted LMA and free PLMA as well as the amount of XL-PE increases significantly. At T_{XL} = 125 °C hardly any residual monomer and XL-PE are present, indicating that a close to ideal TPV composition is achieved, i.e. non-reacted LMA and cross-linked PE are not present. Elevated temperatures lead to partial degradation of the poly(alkyl methacrylate) by alkoxy radicals that originate from peroxide decomposition[4] and to thermal degradation of poly(alkyl methacrylate) due to the presence of unstable head-to-head linkages[28]. Additionally, the ceiling temperature of alkyl methacrylates is known to be close to 200 °C, which limits full conversion of alkyl methacrylates at elevated temperatures[28,29]. The extent of grafting of PLMA onto PE increases with increasing T_{XL}, which is consistent with the results published by Lazár *et al.*[4]. The increase in grafting efficiency is responsible for the increasing amount of XL-PE with T_{XL}, since PE becomes part of the XL-PLMA network after multiple grafting reactions of a single PE chain. Additionally, the extent of chain branching and cross-linking of PE by the formation of alkyl radicals from the peroxide primary alkoxy radicals is known to increase with increasing reaction temperature[30].

Compression molding of the blends for 15 min at 160 °C does not lead to a significant increase in the amount of low-molar-mass material (Fig. 8.4), which suggests that the applied molding conditions do not lead to a noticeable degradation of PLMA and XL-PLMA. However, the applied cross-linking times are relatively short compared to the peroxide half-life times, as mentioned in the experimental section, which leads to small amounts of residual peroxide in the blends. Decomposition of this residual peroxide during compression molding is responsible for the small increase of grafted PLMA and XL-PE. The influence of the DVB content, peroxide

content and T_{XL} on the chemical composition was similar at an initial composition of 60 wt% PE and 40 wt% LMA.
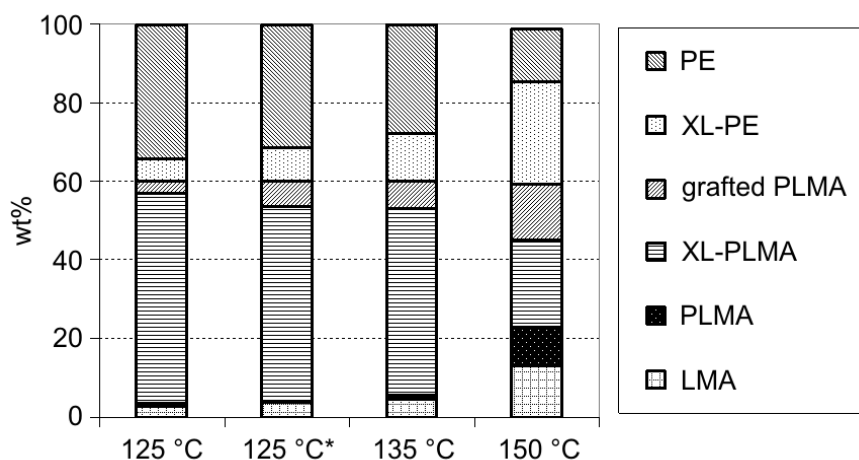

Fig. 8.4. Influence of T_{XL} on chemical composition of statically-prepared PE/LMA blends containing 40 wt% PE cross-linked with 1 wt% DVB and 0.5 wt% peroxide, where * indicates that the sample was compression molded for 15 min at 160 °C.

8.3.4. Properties of statically-prepared TPVs

TEM studies and fractionation results showed that RIPS of PE/LMA blends yields materials with a very fine dispersion of cross-linked PLMA rubber particles in a semi-crystalline PE matrix, which fulfills the structural requirements of a TPV. Therefore, the *in-situ* cross-linked PE/LMA blends are expected to provide melt-processable materials with good elastic properties. It is important to study the influence of variations in the final chemical composition, that are induced by changes in the preparation conditions, on the TPV properties, since knowledge of the appropriate preparation conditions will allow for optimization of the properties. The sample preparation of PE/LMA-based TPVs is typically done by compression molding at 160 °C for 15 min. To prevent possible changes in the chemical composition as induced by decomposition of the residual peroxide in the TPVs, the samples were first extracted with methanol at room temperature for 48 hrs to remove any residual peroxide. It should be kept in mind that by methanol extraction also the residual non-reacted LMA is removed. Compression molding of the material that was *in-situ* cross-linked at T_{XL} = 150 °C was impossible, because the material did not flow sufficiently to form smooth films. This is related to the large extent of PLMA grafting and cross-linking of the PE matrix. Therefore, only the properties of the samples cross-linked at T_{XL} = 125 and 135 °C are discussed.

Table 8.2 presents an overview of some solid state properties for a number of statically-prepared TPVs. After methanol extraction, the statically-prepared TPVs were compression molded to prepare smooth films. The crystallinity (X_c) of the PE matrix of the TPVs is not significantly influenced by varying the rubber or DVB content; X_c varies between 57 and 63 %

and is similar to that of the pure PE (60 %). Increasing the DVB concentration leads to an increase in the cross-link density of the rubber phase, which is reflected in an increased elastic modulus (E), tensile strength (TS) and hardness, while the elongation at break (EB) and the compression sets values at 23 °C (CS_{23}) and 70 °C (CS_{70}) decrease. Such trends are typically observed for cross-linked rubbers and TPVs[31] and show that, similar to traditional TPVs prepared by dynamic vulcanization, the mechanical properties of these PE/LMA-based TPVs prepared via RIPS can be tuned by varying the cross-link density of the rubber phase. Tensile tests show that an increase of T_{XL} from 125 to 135 °C causes the elastic modulus (E) and, correspondingly, the hardness to increase (Table 8.2), which is attributed to the increased content of XL-PE. Additionally, EB and TS decrease with increasing T_{XL}. Partial cross-linking of the PE matrix limits the occurrence of plastic yielding during static compression of the TPV, which leads to an improved elastic recovery (lower CS values).

Table 8.2. Properties of statically-prepared TPVs.[a]

PE (wt%)	DVB (wt%)	Peroxide (wt%)	T_{XL} (°C)	X_c (%)	E (MPa)	EB (%)	TS (MPa)	Hardness (Shore D)	CS_{23} (%)	CS_{70} (%)
40	0.5	0.5	135	61	45	115	4.9	35	33	34
40	1.0	0.5	135	60	51	95	6.4	38	30	32
40	2.0	0.5	135	62	60	85	8.4	41	26	31
20	1.0	0.5	125	57	16	70	3.2	23	12	16
40	1.0	0.5	125	63	44	105	7.0	36	31	33
60	1.0	0.5	125	61	143	250	9.7	49	41	43

[a] *The relative standard deviation is 5-10 % for E, 10-30 % for EB, 10-30 % for TS, 1-5 % for hardness and 1-2 % for CS.*

In the previous sections, the preparation and processing conditions were optimized to limit the occurrence of side reactions. Unless stated otherwise, cross-linking at T_{XL} = 125 °C with 1 wt% DVB and 0.5 wt% peroxide and subsequent methanol-extraction at room temperature will be used throughout the rest of this chapter. These conditions were applied to prepare additional TPVs with a variation in the PE content, which were compression molded for further evaluation. TPVs with a PE content of 80 wt% could not be prepared under these conditions, since the initial mixture is immiscible at 125 °C (see Fig. 8.1). Fig. 8.5 shows representative tensile curves for statically-prepared TPVs with 20, 40 and 60 wt% PE and Table 8.2 provides a full overview of the properties. Decreasing the soft rubber content in the TPVs in this series leads to an increase in E, EB, TS, hardness and CS, which are the trends typical for TPVs[31]. CS_{70} values are only slightly higher than CS_{23} values, although the measurement temperature comes relatively close to T_m of PE (130 °C). In relation to the relatively high hardness of these TPVs, their elastic recovery is

quite good. The very low *CS* values of the sample containing 20 wt% PE suggest a (partial) co-continuous morphology.
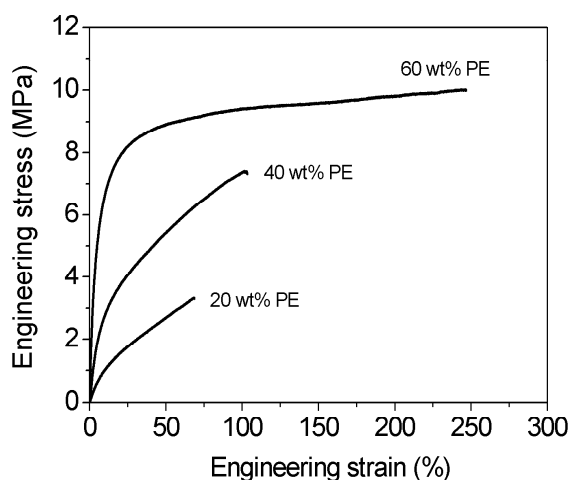

Fig. 8.5. Influence of PE content on the tensile behavior of statically-prepared TPVs cross-linked with 1 wt% DVB and 0.5 wt% peroxide at T_{XL} = 125 °C.
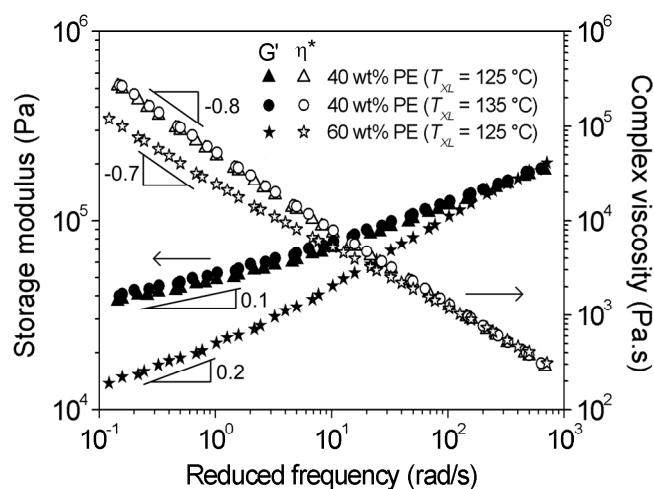
Fig. 8.6. Storage modulus and complex viscosity mastercurves at 160 °C of PE/LMA-based TPVs with a variation in PE content and T_{XL}.

Fig. 8.6 shows the mastercurves of the complex viscosity (η^*) and the storage modulus (G') for the PE/LMA-based TPVs, which were obtained by horizontal shifting of G' to a reference temperature of 160 °C. The slope of log(η^*) versus log(ω_r) (where ω_r is the reduced frequency) approaches -1, which indicates that the materials behave almost like an ideal elastic network. The small increase in the amount of XL-PE (caused by increasing T_{XL} from 125 to 135 °C, see Fig. 8.4) has only a minor effect on the rheological behavior; both G' and η^* increase only slightly. Increasing the PE content from 40 to 60 wt% leads to a decrease in G' and η^* over the whole frequency range due to the increased volume of the processable matrix. These results suggest that a three-dimensional network is present in the melt at high rubber contents. This observation is consistent with previous work on PP/EPDM-based TPVs, in which it was suggested that physical clustering of the rubber particles at low shear rates leads to rheological co-continuous behavior, whereas high shear rates lead to break-up of the clusters, resulting in rheological behavior typical for a matrix/dispersion morphology[32-35]. True chemical connectivity between the rubber particles would also contribute to an increased elastic behavior, both in the melt and in the solid state. Interconnection between the rubber particles was observed for the TPVs based on PCL/PPOn-epoxy (Chapters 4 and 5) and PCL/PEO9 (Chapter 6). However, TEM and extraction studies performed on the PE/LMA-based TPVs suggest that rubber connectivity is not present in these materials. The rheological properties of the PE/LMA-based TPVs will be discussed in more detail in a later section, which deals with the addition of oil to the TPVs to improve their melt processability.

8.3.5. Morphology and properties of dynamically-prepared TPVs

Compared to static cross-linking conditions, dynamic cross-linking is more practical because it can more easily be applied in a continuous process and is, consequently, favorable for the industrial production of TPVs via RIPS. Therefore, this section deals with the influence of dynamic preparation conditions on the morphology and properties of PE/LMA-based TPVs. First, statically-prepared TPVs were subjected to an extrusion step of 10 min at 100 rpm and 150 °C to have the correct reference samples, which did not lead to any noticeable change in the morphology; TEM images similar to the ones presented in Fig. 8.2 were obtained. This indicates that stable morphologies are obtained by static cross-linking, i.e. break up and coalescence of the rubber particles do not occur in the subsequent extrusion step. Alternatively, the TPVs were prepared by dynamic cross-linking in the micro-extruder at 100 rpm. The pressure profile in the micro-extruder during dynamic cross-linking was recorded and is shown in Fig. 8.7. The increase in pressure between 5-15 min is related to an increase in the viscosity of the system, which originates from a combination of cross-linking of the LMA phase and phase separation of the mixture.
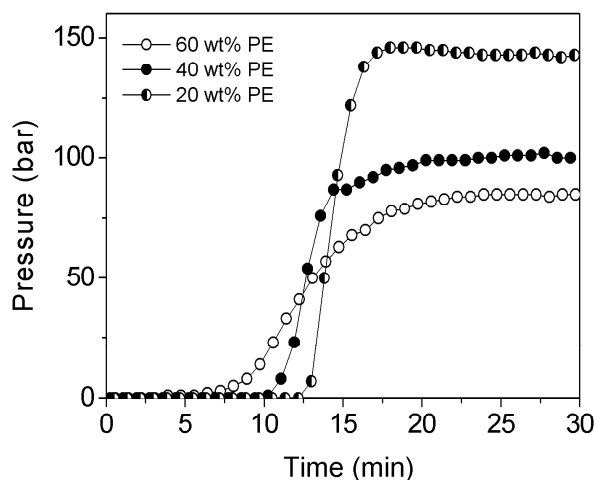
Fig. 8.7. Pressure profile as a function of reaction time during dynamic cross-linking of PE/LMA mixtures at T_{XL} = 135 °C.

Fig. 8.8 shows representative TEM images of the TPVs prepared by dynamic cross-linking with a variation in rubber content. In comparison to static cross-linking conditions (see Fig. 8.2), dynamic cross-linking leads to larger rubber particles with a broader size distribution. This can be attributed to coalescence of the phase-separating rubber domains during the extrusion process.

Fig. 8.9 and Table 8.3 show the influence of dynamic cross-linking on the mechanical properties of the TPVs in comparison to static cross-linking. The crystallinity of the PE phase (X_c) is not affected by applying dynamic preparation conditions, while *EB* and *TS* increase substantially at all compositions and *E* remains approximately constant. Generally, the elastic
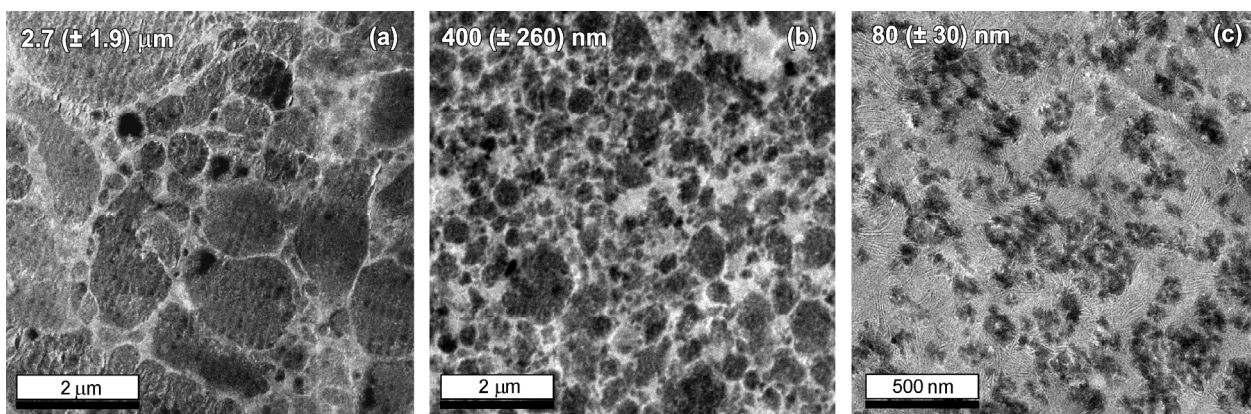
Fig. 8.8. TEM images of PE/LMA-based TPVs after in-situ cross-linking under dynamic conditions at T_{XL} = 125 °C with 1 wt% DVB and 0.5 wt% peroxide, containing (a) 20 wt% PE, (b) 40 wt% and (c) 60 wt% PE. The number-averaged rubber particle size ($\overline{D}_n$) and its standard deviation are shown in the figures.

recovery of the materials decreases slightly, i.e. the values of CS_{23} and CS_{70} increase. Very similar results were obtained for the statically-prepared TPVs subjected to an extrusion step. The enhanced tensile properties and decreased elastic recovery suggest that the rubber particles are partially connected to each other in the case of statically-prepared TPVs. Since true rubber connectivity was not observed in the TEM images (Fig. 8.2), the connectivity of the rubber particles is assumed to originate from bridging of the rubber particles by grafted PE chains. This rubber connectivity in statically-prepared TPVs is disrupted by the shear forces that are applied during extrusion, explaining the increase in *EB* and the decrease in *CS*. Since very similar properties are obtained for the dynamically-prepared samples and the extruded statically-prepared samples, it can be concluded that rubber connectivity is fully disrupted by the extrusion step.
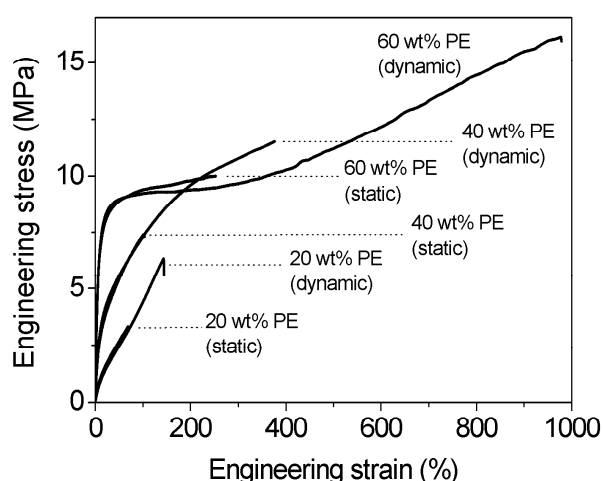
Fig. 8.9. Tensile behavior of PE/LMA-based TPVs with varying PE content prepared by static and dynamic cross-linking conditions.

Another reason for the observation of rubber connectivity may be related to diffusional processes during phase separation in the micro-extruder. The different interactions of PE and LMA with the metal screws and walls of the extruder may lead to diffusion of one of the components towards the metal surface. Under static conditions, this will lead to an enrichment of

one of the phases near the metal surface. This may lead to the formation of a very thin layer with a high concentration of cross-linked rubber at or close to the metal surface, which will lead to defective samples after compression molding and, consequently, to inferior tensile properties. This hypothesis could not be unambiguously proven by TEM analyses due to uncertainties in the contrast of the images that are induced by the staining process.

Table 8.3. Properties of PE/LMA-based TPVs with varying PE content prepared by (I) static cross-linking, (II) static cross-linking and subsequent extrusion and (III) dynamic cross-linking.[a]

PE (wt%)	Preparation Method	X_c (%)	E (MPa)	EB (%)	TS (MPa)	Hardness (Shore D)	CS_{23} (%)	CS_{70} (%)
60	I	61	143	250	9.7	49	41	43
60	II	63	121	920	15.0	46	39	43
60	III	64	122	980	16.1	48	40	49
40	I	63	44	105	7.0	36	31	33
40	II	58	44	270	10.6	38	33	37
40	III	61	49	340	11.2	39	34	38
20	I	57	16	70	3.2	23	12	16
20	II	67	20	170	6.9	25	21	25
20	III	53	15	140	6.2	21	23	25

[a] The relative standard deviation is 5-10 % for E, 10-30 % for EB, 10-30 % for TS, 1-5 % for hardness and 1-2 % for CS.

8.3.6. Influence of oil extension on morphology and properties

The properties-processing balance of commercial PP/EPDM-based TPVs is typically tuned by the addition of processing oils and fillers. In particular the addition of processing oil is attractive, since it improves the melt processability of TPVs and lowers their formulation costs[36-38]. As stated earlier, the large amount of cross-linked rubber particles and their physical interaction typically leads to rheological co-continuous-like behavior in the melt, with the viscosity being hardly dependent on temperature and generally too high for standard melt-processing techniques. Therefore, the addition of oil is often a requisite to produce TPVs that are processable on standard processing equipment for thermoplastic polymers. In this section, the applicability of extension of PE/LMA-based TPVs with a paraffinic oil is discussed, where a statically-prepared TPV containing 60 wt% PE is used as the starting material. After preparation of the TPV, the oil was added via an additional extrusion step. The reference sample, without oil, was subjected to the extra extrusion step as well.

The storage and loss moduli (E' and E'', respectively) of the oil extended TPVs are shown in Fig. 8.10. The loss modulus shows a weak maximum at -120 °C, which corresponds to the T_g of the amorphous PE phase. This transition broadens or even disappears upon increasing oil contents. This is attributed to a decrease in the overall PE content in the samples and to a plasticizing effect of the oil. DSC experiments showed that the T_m of PE is also affected by the presence of the oil; the offset of the melting endotherm of the second heating run decreases from 132.9 °C at 0 wt% oil to 131.5 °C at 80 wt% oil. The PLMA phase in the sample prior to the addition of oil shows a broad transition between -65 and -35 °C, which originates from the overlapping T_g and T_m, respectively. These values suggest that complete phase separation has occurred, since the T_g's of PE and cross-linked PLMA in the TPVs are similar to those of the pure components[7,25]. The overlapping transition of the PLMA phase narrows and shifts to lower temperatures with increasing oil content. Consistent with the DMTA results, a decrease in T_m of the PLMA phase from -36 °C at 0 wt% oil to -42 °C at 80 wt% oil is also observed by DSC measurements. These results indicate that in the solid state the paraffinic oil is located in both the PLMA and PE phases, which is in agreement with studies performed on PP/EPDM/oil-based TPVs, where the oil was found to reside in the cross-linked EPDM phase and in the amorphous phase of PP[36,39].
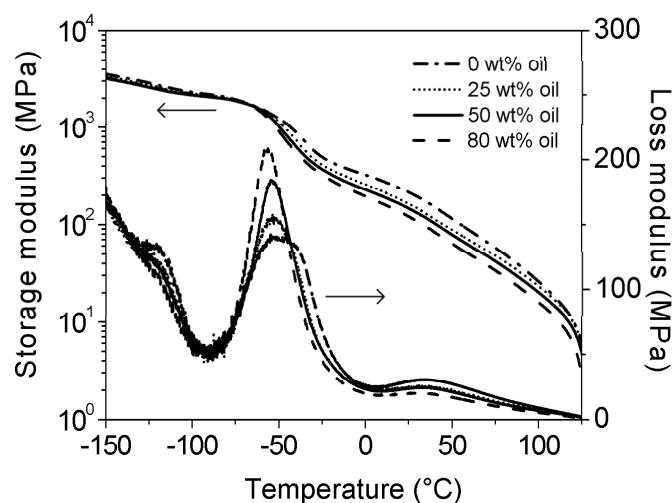

Fig. 8.10. Storage and loss moduli as a function of temperature for statically-prepared PE/LMA-based TPVs with 60 wt% PE and varying oil contents.

Fig. 8.11 shows the TEM images of PE/LMA-based TPVs containing 40 wt% PE, both before and after oil extension. The morphologies of the statically-prepared TPV (Fig. 8.11a) and the statically-prepared TPV extended with 25 wt% oil (Fig. 8.11b) appear to be identical. Fig. 8.11c shows that the rubber particle size and the particle size distribution are larger for the oil-extended dynamically-prepared TPV, which is in agreement with the results presented in the previous section. Due to the relatively small amounts of oil that are used in this study, swelling of the rubber particles is not evident from the TEM images.
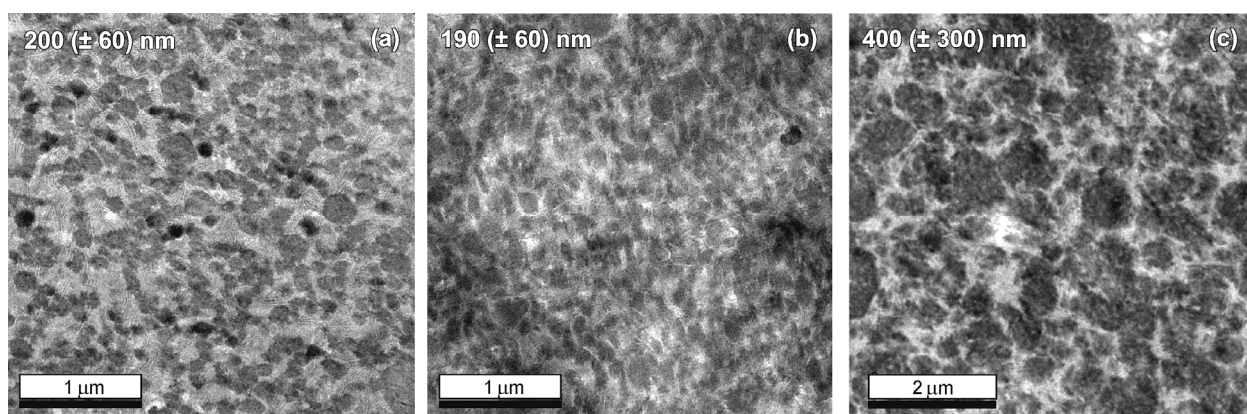
Fig. 8.11. TEM images of PE/LMA-based TPVs with 40 wt% PE after (a) static cross-linking, (b) oil extension of the statically-prepared TPV with 25 wt% oil and (c) oil extension of the dynamically-prepared TPV with 25 wt% oil. The number-averaged rubber particle size ($\overline{D_n}$) and its standard deviation are shown in the figures.

Although in the solid state the oil is excluded from the crystalline PE phase, it was shown for PP/EPDM/oil-based TPVs in the melt state that the oil is redistributed over both the rubber and the molten thermoplastic phase, leading to a reduced viscosity and improved melt processability[37,38,40]. Fig. 8.12 shows the *G'* and *η** for the oil-extended TPVs and the reference TPV, which were obtained by horizontal shifting of *G'* to a reference temperature of 160 °C. With increasing amount of oil, the curves of *G'* and *η** shift to lower values without changing their power law coefficient, indicating an improved melt processability of the oil-extended TPVs over the whole frequency range. The relative decrease in *η** upon the addition of 80 wt% oil is low compared to the decrease in *η** upon adding 25 wt% oil. This suggests that the amount of oil that is present in the molten PE matrix is limited, and that a further increase of the oil content does not lead to a significant enhancement of the melt processability of the TPV.
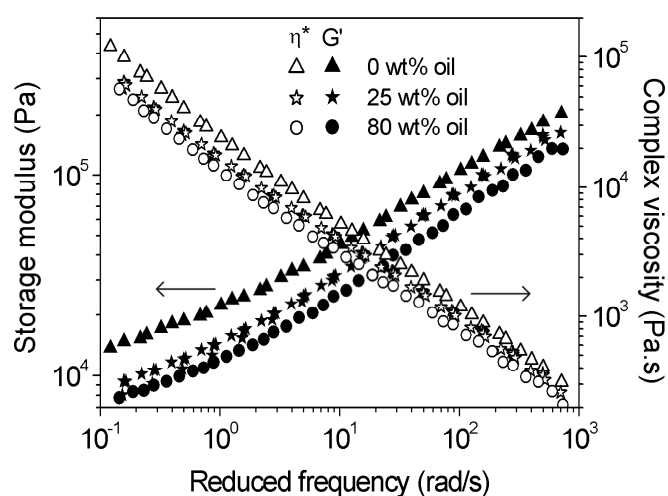

Fig. 8.12. Storage modulus and complex viscosity mastercurves at 160 °C for PE/LMA-based TPVs with 60 wt% PE and varying amounts of oil.

The absolute values of η^* of the PE/LMA-based TPVs are very similar to those of the conventional PP/EPDM-based TPVs. Where the PE/LMA-based TPVs containing 40 and 60 wt% cross-linked rubber show a η^* of 1000-1500 Pa·s at $\omega = 100$ rad/s and $T = 180$ °C (= T_m + 50 °C), the PP/EPDM-based TPVs show a η^* of ~ 3000 Pa·s at $\omega = 100$ rad/s and $T = 210$ °C (= T_m + 50 °C, see Chapter 2.3.7). Previous studies on PP/EPDM-based TPVs showed the importance of the applied shear stress on the rheological behavior of the TPVs[33-35]. At low stresses the melt behaves elastically, which is attributed to the presence of a physically interacting network of chemically cross-linked rubber particles. However, upon increasing the applied shear stress the physical network is broken up and the material behaves as a melt of PP filled with rubber particles. The critical stress to break up the physical network, i.e. the yield stress, increases with increasing rubber content. Fig. 8.13 shows creep curves of a statically-prepared TPV containing 60 wt% PE after the extrusion step, where shear stresses of 100 Pa up to 15 kPa have been applied at a temperature of 160 °C. At stresses up to 1 kPa the material shows a limiting compliance, which indicates elastic behavior. However, at stresses exceeding 1 kPa the material shows a continuous increase in the compliance. Apparently, the yield stress is ~ 3 kPa, which changes the material behavior from highly elastic to viscous.
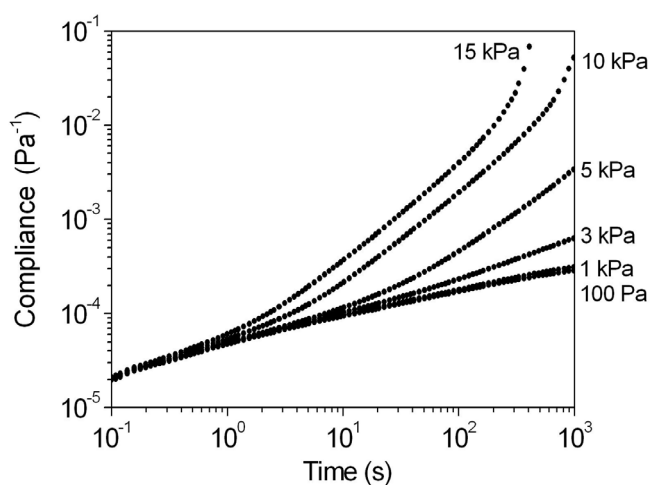

Fig. 8.13. Compliance as a function of time of a statically-prepared TPV containing 60 wt% PE after extrusion, measured at various shear stresses at 160 °C.
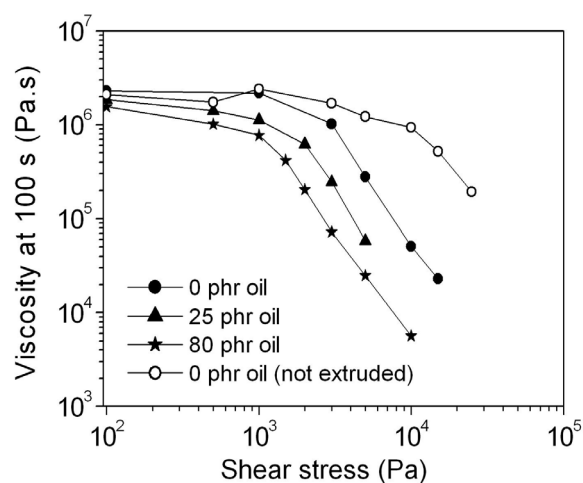
Fig. 8.14. The shear viscosity after 100 s creep of statically-prepared TPVs with 60 wt% PE before and after oil extension at 160 °C.

Creep experiments were also performed on the oil-extended TPVs. The results are summarized in Fig. 8.14, which shows the (non-steady) shear viscosity of the material after 100 s creep as a function of the applied shear stress. At low shear stresses, e.g. as applied during the frequency sweeps presented in Figs. 8.5 and 8.12, the viscosities of the samples are very similar. However, the curves show a sharp decrease in the viscosity when a critical stress is passed, which indicates the presence of a yield stress in all the samples. The yield stress of the statically-prepared TPV prior to the extrusion step is significantly higher compared to the same TPV after

extrusion. This supports the hypothesis that the rubber connectivity, which may originate from bridging of the rubber particles by grafted PE, is broken-up by the extrusion step, thereby allowing the material to flow at lower stresses. The yield stress decreases upon increasing the oil content, which can be attributed to a lower overall concentration of rubber particles in the system, i.e. an increased interparticle distance and decreased interaction.

As discussed in the previous section, extrusion of the statically-prepared TPVs leads to a significant increase in *EB* and *TS*. Fig. 8.15 shows that the addition of oil to the TPV with a PE content of 60 wt% causes *EB* to increase further to a value of ~ 1200 %, independent of the amount of oil. As expected, *E*, *TS* and the hardness decrease with increasing amount of oil. Table 8.4 shows that the elastic recovery remains constant or even improves, i.e. the values of CS_{23} and CS_{70} remain constant or decrease with increasing oil content. Upon the addition of oil, a decrease in elastic recovery may be anticipated, since the decrease in the total amount of cross-linked rubber in the sample is expected to lead to more plastic deformation of the sample in the compressed state. The improved elastic recovery upon increasing oil content may be explained by a facilitation of the recovery process after releasing the compressive stress on the sample, caused by an increased mobility of the plasticized matrix. Similar trends on tensile properties and *CS* were obtained for oil-extended TPVs containing 40 and 20 wt% PE (Table 8.4). Oil extension of dynamically-prepared samples gave identical tensile curves and *CS* values. It has to be noted that, as for the TPVs without oil, the CS_{70} is surprisingly close to CS_{23}.
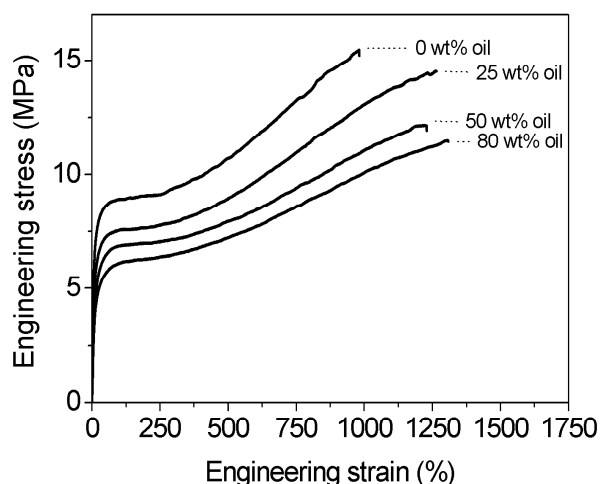

Fig. 8.15. Tensile behavior of oil-extended TPVs with 60 wt% PE and varying oil content.

Table 8.4. Mechanical properties of oil-extended TPVs at varying oil content.[a]

PE (wt%)	Oil content (wt%)	X_c (%)	E (MPa)	EB (%)	TS (MPa)	Hardness (Shore D)	CS_{23} (%)	CS_{70} (%)
60	0	63	121	920	15.0	46	39	43
60	25	65	109	1220	14.5	41	38	40
60	50	63	74	1110	11.3	37	38	40
60	80	65	63	1160	10.7	34	38	39
40	0	58	44	270	10.6	39	33	37
40	25	62	33	460	9.5	31	30	36
20	0	67	26	170	6.9	25	21	25
20	25	57	11	180	4.8	14	18	20

[a] *The relative standard deviation is 5-10 % for E, 10-30 % for EB, 10-30 % for TS, 1-5 % for hardness and 1-2 % for CS.*

8.3.7. Application of *in-situ* polymerization/cross-linking to other systems

In order to demonstrate the versatility of the RIPS approach based on *in-situ* polymerization and cross-linking of alkyl methacrylate monomers, some variations to the PE/LMA system are shortly discussed in this section, where the influence on the properties of the TPVs is summarized in Table 8.5.

To limit grafting and cross-linking reactions involving the matrix material, PP would be preferred over PE as the thermoplastic matrix, since it is less susceptible to grafting and cross-linking via hydrogen abstraction. As an example, syndiotactic PP (sPP) is used, since the T_m of ~ 135 °C allows for similar preparation conditions as were used for the PE/LMA systems. Fig. 8.16 shows the obtained morphologies after dynamic (Figs. 8.16a-c) and static cross-linking (Fig. 8.16d) at 135 °C, which are very similar to the morphologies obtained for the PE/LMA systems (Figs. 8.2 and 8.8). Sub-μm rubber dispersions are obtained over the whole composition range. The morphology is hardly dependent on the shear rate during the dynamic cross-linking process, since the rubber particle size decreased only slightly upon increasing the screw speed from 50 to 200 rpm (Table 8.5).
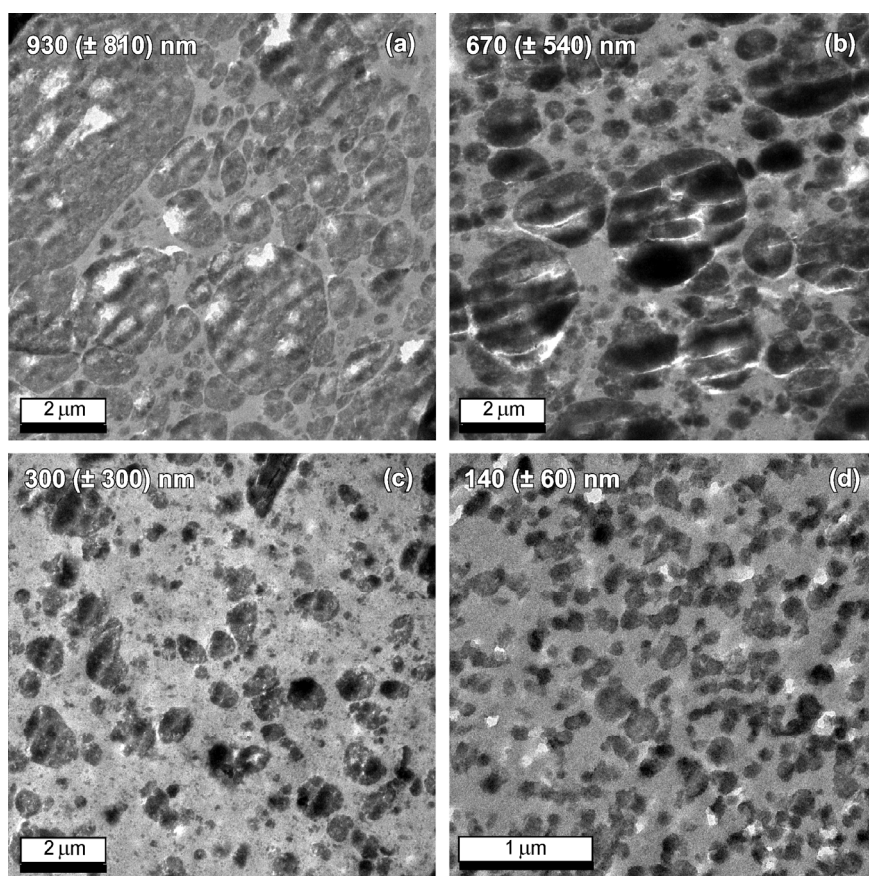
8

Fig. 8.16. TEM images of sPP/LMA-based TPVs after in-situ cross-linking under static conditions at T_{XL} = 135 °C, containing (a) 20, (b) 40 and (c) 60 wt% sPP, all prepared by dynamic cross-linking at 100 rpm and (d) 60 wt% sPP prepared by static cross-linking. The number-averaged rubber particle size ($\overline{D}_n$) and its standard deviation are shown in the figures.

Commercial PP/EPDM-based TPVs are sometimes based on EPDM rubber with a high ethylene content, which leads to a partially crystalline EPDM rubber. Partial crystallinity of the rubber phase in the sPP-based TPVs can be introduced by increasing the alkyl chain length from 11 (LMA) to 17 (ODMA) repeating CH_2 units (see also Table 8.1). The use of ODMA leads to a significant increase in *E, EB* and *TS*, while the elastic recovery is deteriorated. In order to study the influence of the type and reactivity of the cross-linker on the morphology of the TPVs, 1.5 wt% ethylene glycol dimethacrylate (EGDM) was used instead of 1 wt% DVB, where both amounts represent a similar molar amount of functional groups. The use of EGDM under static cross-linking conditions at a sPP content of 60 wt% led to a very similar morphology as presented in Fig. 8.16d, with a rubber particle size of ~ 120 nm.

An overview of the preparation conditions and the properties of the sPP-based TPVs is shown in Table 8.5. The relatively low *%gel* in comparison to the PE/LMA-based TPVs is attributed to the higher cross-linking temperature (T_{XL} = 135 °C), at which the LMA is closer to its ceiling temperature, leading to lower LMA conversions. The relatively low *E, TS* and *CS* of the sPP-based TPVs is attributed to the low gel content and the low crystallinity of the sPP matrix, which is 14.9 ± 0.8 % for all the TPVs as determined from DSC measurements.

Table 8.5. Mechanical properties of TPVs based on sPP and alkyl methacrylates prepared by (I) static cross-linking and (II) dynamic cross-linking.[a]

sPP (wt%)	Method	Elastomer precursor	Cross-linker	Screw speed (rpm)	$\overline{D}_n$ (nm)	%gel (%)	E (MPa)	EB (%)	TS (MPa)	CS$_{23}$ (%)
60	II	LMA	DVB	100	300	80.6	75	482	8.8	49
40	II	LMA	DVB	100	670	85.7	46	204	8.1	43
20	II	LMA	DVB	100	930	88.2	28	120	5.0	32
60	I	LMA	DVB	–	140	83.9	77	452	10.4	n.m.
60	II	LMA	DVB	50	410	n.m.	91	570	9.6	n.m.
60	II	LMA	DVB	200	270	n.m.	81	565	8.6	n.m.
60	II	ODMA	DVB	100	n.m.	n.m.	134	746	12.8	74
60	I	LMA	EGDM	–	120	78.0	n.m.	n.m.	n.m.	n.m.

[a] *The relative standard deviation is 5-10 % for E, 5-30 % for EB, 5-15 % for TS and 1-2 % for CS. n.m. = not measured.*

8.4. Conclusions

It has been demonstrated that TPVs can be prepared by *in-situ* polymerization/cross-linking of initially miscible blends of PE, LMA and DVB, where LMA is the rubber precursor and DVB is the cross-linker. Very fine rubber dispersion of 70-500 nm are obtained over a very broad composition range, i.e. > 80 wt% of cross-linked rubber can easily be dispersed in the PE matrix. Side reactions, such as cross-linking of the PE matrix, can be suppressed by applying a cross-linking temperature close to the T_m of PE in the miscible blend.

The application of static cross-linking conditions appears to induce (partial) rubber connectivity. However, this interconnectivity is not caused by the influence of gelation on the phase separation behavior, as was discussed in Chapter 5 for PCL/PPOn-epoxy mixtures, but probably originates from chemical bridging of the rubber particles by grafted PE chains or from enrichment of the cross-linked rubber phase at or close to the surface.

The application of dynamic shear forces during extrusion leads to full break-up of the rubber connectivity and, consequently, leads to a significant improvement of the tensile properties and the melt processability. The very fine rubber dispersions may explain the relatively good elastic recovery and the excellent ultimate properties (*EB* > 1000 %) of these TPVs. The materials are melt processable and a critical stress for flow is observed, where the absolute values of the melt viscosity and the critical stress are lower than those measured for the PP/EPDM-based TPVs in Chapter 2.3.7. The addition of oil to the TPVs reduces the melt viscosity without deteriorating the tensile properties and the elastic recovery.

The versatility of the preparation of sub-µm TPVs via RIPS based on mixtures of polyolefins and alkyl methacrylates is demonstrated by studying the influence of several variations in the reactants and the preparation conditions on the morphology and properties after *in-situ* polymerization/cross-linking.

8.5. References

[1] Coran, A.Y.; Patel, R.P. *Rubber Chem. Technol.* **1980**, *53*, 141-150.

[2] Araghi, H.H. Proceedings of the International Rubber Conference, Birmingham, United Kingdom, 2001.

[3] Borsig, E; Fiedlerová, A.; Haüsler, K.G.; Sambatra, R.M.; Michler, G.H. *Polymer* **1993**, *34*, 4787-4792.

[4] Lazár, M.; Hrcková, L.; Schulze, U.; Pionteck, J.; Borsig, E. *J. Macromol. Sci. Pure Appl. Chem. A* **1996**, *33*, 261-273.

[5] Hu, J.; Schulze, U.; Pionteck, J.; Borsig, E. *J. Macromol. Sci. Pure Appl. Chem. A* **1998**, *35*, 1285-1297.

[6] Donatelli, A.A.; Sperling, L.H.; Thomas, D.A. *Macromolecules* **1976**, *9*, 671-675.

[7] Huelck, V.; Thomas, D.A.; Sperling, L.H. *Macromolecules* **1972**, *5*, 340-347.

[8] Wycisk, R.; Trochimczuk, W.M. *J. Polym. Sci., Polym. Lett. Ed.* **1989**, *27*, 321-324.

[9] Schulze, U.; Pompe, G.; Meyer, E.; Janke, A.; Pionteck, J.; Fiedlerová, A.; Borsig, E. *Polymer* **1995**, *36*, 3393-3398.

[10] Goossens, J.G.P.; Rastogi, S.; Meijer, H.E.H.; Lemstra, P.J. *Polymer* **1998**, *39*, 6577-6588.

[11] Goossens, J.G.P. Processing of tractable polymers using reactive solvents, PhD Thesis, 1998, Eindhoven University of Technology, The Netherlands.

[12] Sutton, D.; Stanford, J.L.; Ryan, A.J. *J. Macromol. Sci., Part B: Phys.* **2004**, *43*, 219-232.

[13] Sutton, D.; Stanford, J.L.; Ryan, A.J. *J. Macromol. Sci., Part B: Phys.* **2004**, *43*, 233-251.

[14] Klosiewicz, D.W.; Shih, K.S. EP Patent 0453999 A2 1991, to Hercules Incorporated.

[15] Bryjak, M.; Trochimczuk, W.M. *Angew. Makromol. Chem.* **1983**, *116*, 221-224.

[16] Bryjak, M.; Trochimczuk, W.M. *Angew. Makromol. Chem.* **1983**, *118*, 191-195.

[17] Koning, C.; van Duin, M.; Pagnoulle, C.; Jerome, R. *Prog. Polym. Sci.* **1998**, *23*, 707-757.

[18] Ten, J.W.; Rudin, A. *Polym. Eng. Sci.* **1992**, *32*, 1678-1686.

[19] Stoks, W.; Berghmans, H. *J. Polym. Sci., Part B: Polym. Phys.* **1991**, *29*, 609-617.

[20] Montezinos, D.; Wells, B.G.; Burns, J.L. *J. Polym. Sci., Polym. Lett. Ed.* **1985**, *23*, 421-425.

[21] ASTM Standard D412 "Standard Test Methods for Vulcanized Rubber and Thermoplastic Elastomers – Tension", 1986.

[22] ASTM Standard D395 "Standard Test Methods for Rubber Property – Compression Set", 1989.

[23] *Properties of Polymers: Their Correlation with Chemical Structure; Their Numerical Estimation and Prediction from Additive Group Contributions;* van Krevelen, D.W., Ed.; Elsevier: Amsterdam, 1997 (p. 87 and 195).

[24] *Principles of Polymer Chemistry*; Flory, P.J., Ed. Ithaca: Cornell University Press: New York, 1953.

[25] *Polymer Handbook*; Brandrup, J.; Immergut, E.H., Eds.; Wiley-Interscience: London, 1989.

[26] Boots, H.M.J.; Kloosterboer, J.G.; Serbutoviez, C.; Touwslager, F.J. *Macromolecules* **1996**, *29*, 7683-7689.

[27] Serbutoviez, C.; Kloosterboer, J.G.; Boots, H.M.J.; Touwslager, F.J. *Macromolecules* **1996**, *29*, 7690-7698.

[28] *The Chemistry of Free Radical Polymerization*; Moad, G.; Solomon, D.H., Eds.; Pergamon: Oxford, 1995 (Chapter 4 and 7).

[29] *Principles of Polymerization*; Odian, G., Ed.; Wiley-Interscience: New Jersey, 2004 (Chapter 3).

[30] Hinsken, H.; Moss, S.; Pauquet, J.R.; Zweifel, H. *Polym. Degrad. Stab.* **1991**, *34*, 279-293.

[31] *Science and Technology of Rubber*; Coran, A.Y., Ed.; Academic Press: New York, 1978.

[32] Goharpey, F.; Nazockdast, H.; Katbab, A.A. *Polym. Eng. Sci.* **2005**, *45*, 84-94.

[33] Han, P.K.; White, J.L. *Rubber Chem. Technol.* **1995**, *68*, 728-738.

[34] Araki, T.; White, J.L. *Polym. Eng. Sci.* **1998**, *38*, 590-595.

[35] Steeman, P.; Zoetelief, W. *ANTEC* **2000**, 3297-3302.

[36] Ellul, M.D. *Rubber Chem. Technol.* **1998**, *71*, 244-276.

[37] Sengers, W.G.F.; Sengupta, P.; Noordermeer, J.W.M.; Picken, S.J.; Gotsis, A.D. *Polymer* **2004**, *45*, 8881-8891.

[38] Sengers, W.G.F.; Wübbenhorst, M.; Picken, S.J.; Gotsis, A.D. *Polymer* **2005**, *46*, 6391-6401.

[39] Winters, R.; Lugtenburg, J.; Litvinov, V.M.; van Duin, M.; de Groot, H.J.M. *Polymer* **2001**, *42*, 9745-9752.

[40] Gessler, A.M.; Kresge, E.N. US Patent 4132698 1979, to Exxon Research & Engineering Co.

8

Commercial thermoplastic vulcanizates (TPVs) are typically based on isotactic poly(propylene) (iPP) and ethylene-propylene-diene (EPDM) rubber and are prepared by dynamic vulcanization, where the rubber is selectively cross-linked during melt mixing with the thermoplastic. The conventional dynamic vulcanization process of immiscible thermoplastic/rubber blends restricts the minimum rubber particle size to ~ 1-3 μm, since the applicable magnitude of shear rates and melt viscosities during the industrial production of TPVs is limited. Additionally, high rubber fractions (ϕ) of > 0.5 lead to larger rubber particles and often to a (partially) co-continuous morphology due to incomplete phase inversion.

The objective of this study was (*i*) to obtain a more fundamental understanding of the correlation between the properties of TPVs and the rubber particle size and (*ii*) to explore the potential of reaction-induced phase separation (RIPS) as a new route for the preparation of (sub-μm) TPVs. In the first part of this thesis the influence of the rubber particle size on the mechanical and rheological properties of iPP/EPDM-based TPVs, prepared via traditional dynamic vulcanization of immiscible blends, was studied. The second part of the thesis assessed the feasibility of the production of TPVs via RIPS and evaluated the morphology and properties of these TPVs.

Chapter 2 of this thesis confirmed the trends observed by Coran *et al.*[1] and Araghi[2] for iPP/EPDM-based TPVs, where a decrease in the rubber particle size leads to an enhancement of the ultimate tensile properties. Since it was found that internal particle cavitation is not the main mechanism behind the improvement of the tensile properties, no limitations on the minimum rubber particle size of TPVs are expected, which is in sharp contrast to conventional, rubber-toughened thermoplastics. The elastic recovery of the TPVs improves with decreasing particle size, while the melt viscosity shows an undesirable increase. Although sub-μm-sized rubber particles are expected to lead to enhanced mechanical properties, the concomitant increase in the melt viscosity may limit melt processing of sub-μm TPVs. These results indicate that the balance between the mechanical properties and melt processability of TPVs can be shifted by varying the rubber particle size. For industrial applications this balance can be further optimized by oil extension of the TPVs.

Chapter 3 of this thesis dealt with dynamic vulcanization of highly compatible, yet immiscible thermoplastic/rubber blends based on iPP and atactic PP (aPP) rubbers. Although the used aPP rubbers are not commercially available, they are produced by a well-studied

metallocene catalysis system and, therefore, their production could relatively easily be commercialized. The high compatibility between the iPP and aPP phases leads to refined TPV morphologies (< 1 μm) and improved mechanical properties, although co-continuity persists at ϕ > 0.5. The relatively high glass transition temperature (T_g) of the aPP rubbers (~ 5 °C) limits the application of the corresponding TPVs to elevated temperatures. The decrease in T_g via oil extension of the TPVs is, therefore, a requisite for commercial applications. This study demonstrated the lower limit of the rubber particle size (~ 0.5 μm) that is attainable via dynamic vulcanization of immiscible blends, since a further increase in blend compatibility would lead to initially miscible systems.

Since sub-μm rubber dispersions are aspired for TPVs but are not attainable via dynamic vulcanization of immiscible blends, a new route for the preparation of TPVs was developed. This route is based on RIPS of initially miscible blends of semi-crystalline thermoplastics and low-molar-mass elastomer precursors, where phase separation is induced by the increase in molar mass during selective cross-linking of the elastomer precursor. This approach indeed resulted in products with a TPV morphology, i.e. a cross-linked rubber dispersion, and properties typical for TPVs. In addition, RIPS enabled the preparation of TPVs with very small rubber particles ranging from 50 nm up to several μm's, without the use of expensive compatibilizers. To evaluate the potential of RIPS for the preparation of sub-μm TPVs, several model systems were explored in this thesis, which are all based on commercially available materials. Initially miscible blends of poly(ε-caprolactone) (PCL) and polyether-based rubbers as well as miscible mixtures of poly(ethylene) (PE) and alkyl methacrylates were successfully used to produce TPVs. Since the used thermoplastics and elastomer precursors cover a very broad spectrum of polarities, TPVs with a high resistance against either water or organic solvents can be produced, as well as TPVs with a good adhesion to either polar or apolar substrates. Due to restrictions of the laboratory experiments to atmospheric pressure and, thus, relatively low temperatures in order to prevent evaporation of the elastomer precursor, the exploration was not extended to the preparation of TPVs based on thermoplastics with a higher T_m, such as iPP instead of PE or poly(hydroxybutyrate) (PHB), poly(lactic acid) (PLA), poly(oxymethylene) (POM) and poly(butylene terephthalate) (PBT) instead of PCL. A higher T_m of the thermoplastic matrix is beneficial, since it increases the heat resistance of the TPVs and, thereby, broadens the temperature window for applications. The application of RIPS to prepare TPVs based on these high-melting thermoplastics is expected to be feasible, since several (partially) miscible combinations were found, such as iPP with alkyl methacrylates and PLA, PHB, POM and PBT with polyether-based elastomer precursors. It has to be noted that the relatively high T_g of PLA and PBT (T_g > room temperature) limits the applicability of the corresponding TPVs to elevated

temperatures, although oil extension broadens the temperature window due to a decrease in T_g. The relatively low ceiling temperature of most (meth)acrylates complicates their use in combination with high-melting thermoplastics such as PBT. Multi-functional vinyl or allyl-terminated monomers may be a suitable replacement for the (meth)acrylates.

The approach of RIPS for producing TPVs as described in this thesis can be used to prepare TPVs with sub-μm morphologies and/or a very high dispersed rubber content, which shifts the properties-processing balance of TPVs into a range that is not attainable with the currently available TPVs. The sub-μm rubber dispersions allow for the production of high-hardness TPVs without deteriorating the elastic recovery and melt processability. For example, sub-μm TPVs based on PE and alkyl methacrylates with $\phi = 0.4$ were produced with compression set values of ~ 40 % and melt viscosities of 1000-3000 Pa·s. These values are similar to conventional TPVs with $\phi = 0.5$, but the sub-μm TPVs have a higher hardness (Shore D range) and elongation at break (> 1000 %). An intrinsic feature of the used route is the very high fraction of cross-linked rubber particles that can be dispersed in the thermoplastic matrix (which exceeds > 0.8 for most systems) without the formation of a co-continuous structure. Therefore, melt-processable TPVs with a very high rubber content and, consequently, a low hardness and a very high elasticity can be produced. Again, oil extension will enable further optimization of the properties-processing balance.

Though the starting materials and the details of the procedure for TPVs produced via RIPS of miscible systems are different than the actual dynamic vulcanization procedure of immiscible blends, still very similar equipment can be used. The production process of TPVs via RIPS includes an additional step, viz. the dissolution of the thermoplastic in the elastomer precursor. However, since fully miscible blends of for example poly(styrene) and poly(2,6-dimethyl-1,4-phenylene oxide) are prepared via extrusion at a commercial scale, no critical issues are envisioned for the dissolution of thermoplastics in low-molar-mass elastomer precursors. The remainder of the process cycle time for TPVs produced via RIPS will mainly be determined by the rate of the cross-linking reaction, which can be controlled by the choice of the reaction mechanism (e.g. step-growth or chain-growth) and the reactivity of the cross-linking agents (e.g. type of elastomer precursor, curing agent and/or initiator).

Another interesting approach for the preparation of TPVs with sub-μm-sized rubber particles is via multi-layer co-extrusion, which is a single-step process starting with two or more polymers that are simultaneously extruded through an assembly of static mixers. This technique leads to well-defined structures consisting of many alternating layers with a controlled thickness ranging from < 50 nm up to several μm's. Since the very thin layers are inherently unstable, they can easily be broken up into sub-μm-sized particles[3,4]. Cross-linking of the structure via the addition

of a suitable cross-linking agent to the elastomer phase may allow for the preparation of sub-µm TPVs. Additionally, reactive compatibilization of polymer blends during multi-layer co-extrusion is a very attractive approach to control the characteristic length scale of the final morphology, since the amount of interface and, thus, the extent of compatibilization, can be controlled and may be driven up to very high conversions.

References

[1] Coran, A.Y.; Patel, R. P. *Rubber Chem. Technol.* **1980**, *53*, 141-150.
[2] Araghi H.H. Proceedings of the International Rubber Conference, Birmingham, United Kingdom, 2001.
[3] Jin, Y.; Hiltner, A.; Baer, E. *J. Polym. Sci., Part B: Polym. Phys.* **2007**, *45*, 1138-1151.
[4] Chirranjeevi, B.G.; Abinandanan, T.A.; Gururajan, M.P. *Acta Mater.* **2009**, *57*, 1060-1067.

Samenvatting

Rubbers (elastomeren) zijn zachte en flexibele materialen die worden gekenmerkt door een hoge mate van elasticiteit. De bouwstenen van rubbers zijn, evenals bij andere plastics, lange moleculen. In het geval van rubbers zijn dit flexibele ketens die onderling chemisch met elkaar zijn vernet om afglijding tijdens mechanische belasting te voorkomen. Een belangrijk nadeel van deze chemische vernetting is dat smeltverwerking van rubbers niet mogelijk is. Thermoplastische elastomeren (TPEs) zijn een speciaal soort rubbers waarbij fysische interacties in plaats van chemische interacties aanwezig zijn tussen de ketens, waardoor TPEs zowel elastisch als smeltverwerkbaar zijn. Een aparte subgroep binnen de TPEs wordt gevormd door de zogenaamde thermoplastische vulkanisaten (TPVs), welke bestaan uit vernette rubberdeeltjes gedispergeerd in een thermoplastische matrix. Commerciële TPVs zijn over het algemeen gebaseerd op isotaktisch poly(propeen) (iPP) als matrix en etheen-propeen-dieen (EPDM) rubber als disperse fase en worden geproduceerd via dynamische vulkanisatie, waarbij de rubber selectief vernet wordt tijdens mengen met de thermoplast in de smelt. De verhoging van de viscositeit van de rubberfase tijdens het dynamisch vulkanisatie proces beïnvloedt de continuïteit van de fasen en bevordert fase-inversie, wat ervoor zorgt dat de vernette rubber de disperse fase wordt met afmetingen op de μm-schaal. De dispersie van een grote hoeveelheid vernette rubberdeeltjes in de thermoplastische matrix resulteert in zachte, elastische materialen, waarbij de continue thermoplastische matrix zorgt voor verwerkbaarheid in de smelt.

De belangrijkste doelstelling van het eerste deel van dit proefschrift was het verkrijgen van een meer fundamenteel begrip van de invloed van de grootte van de rubberdeeltjes op de mechanische en reologische eigenschappen van commerciële TPVs gebaseerd op iPP en EPDM. Kleine-hoek Röntgenverstrooiing (SAXS) metingen tijdens trektesten lieten zien dat het deformatiemechanisme van de TPVs wordt gedomineerd door vloei van de PP matrix. De vorming van microscheurtjes tussen de lamellen, zoals gebeurt tijdens het deformeren van ongevuld PP, wordt efficiënter onderdrukt bij kleinere rubberdeeltjes. Crazing van de matrix, interne rubbercavitatie en loslating van de deeltjes en de matrix werden niet waargenomen. De significante verbetering van de trekeigenschappen bij afnemende grootte van de rubberdeeltjes kan grotendeels worden toegeschreven aan de onderdrukking van zowel de vorming van interlamellaire microscheurtjes evenals mogelijke coalescentie van de scheurtjes. De kans dat bij falen van een rubberdeeltje de kritische scheurgrootte wordt bereikt daalt met afnemende deeltjesgrootte. De kleinere deeltjes leiden ook tot een verbetering van de elasticiteit, aangezien

een afname van de ligamentdikte tussen de deeltjes het terugbuigen van de plastisch gedeformeerde ligamenten na verwijdering van de compressie-spanning vergemakkelijkt. De afname van de ligamentdikte tussen de rubberdeeltjes en de toename van het totale oppervlak van de rubberfase vergroot de fysische interacties tussen de rubberdeeltjes, hetgeen leidt tot een verhoogde smeltviscositeit bij een afname van de deeltjesgrootte. Deze resultaten laten de mogelijkheden van TPVs met sub-μm rubberdispersies zien, aangezien de grootte van de rubberdeeltjes gebruikt kan worden om de balans tussen de eigenschappen en de verwerkbaarheid te sturen.

De ondergrens van de deeltjesgrootte van traditionele iPP/EPDM-gebaseerde TPVs geproduceerd via dynamische vulkanisatie is gelimiteerd tot 1-3 μm. Daarom werden alternatieve methoden voor het produceren van sub-μm TPVs onderzocht, welke gebaseerd zijn op een verhoogde compatibiliteit van de thermoplastische fase en de rubber fase. De mogelijkheden van zeer compatibele, niet mengbare thermoplast/rubber mengsels voor de productie van sub-μm TPVs werd onderzocht door middel van dynamische vulkanisatie van copolymeren gebaseerd op ataktisch polypropeen (aPP) en 5-ethylideen-2-norborneen (ENB) (aPP-*co*-ENB) in combinatie met iPP. De iPP/aPP-*co*-ENB mengsels vertonen een zeer hoge compatibiliteit, wat leidt tot een verfijning van de morfologie (zowel voor als na dynamische vulkanisatie) in vergelijking tot traditionele mengsels gebaseerd op iPP en EPDM. De TPVs gebaseerd op aPP-*co*-ENB vertonen een verbetering van de trekeigenschappen, maar de relatief hoge glasovergangstemperatuur (T_g) van de rubberfase vertraagt het elastisch herstel na deformatie op kamertemperatuur. Het toevoegen van olie is daarom noodzakelijk, aangezien de olie zorgt voor een verlaging van de T_g van 10 naar -40 °C waardoor de elasticiteit van de TPVs significant wordt verbeterd. Deze studie toont de ondergrens van de dimensies van de rubberdeeltjes die bereikt kan worden via dynamische vulkanisatie van niet-mengbare mengsels (~ 0.5 μm), aangezien een verdere verhoging van de compatibiliteit zou leiden tot een initieel mengbaar systeem. Hoge rubberfracties van > 0.5 leiden tot grotere rubberdeeltjes en tot een (gedeeltelijk) co-continue morfologie bij onvolledige fase-inversie, wat resulteert in een verslechtering van de trekeigenschappen en de smeltverwerkbaarheid.

De doelstelling van het tweede deel van dit proefschrift was het onderzoeken van de mogelijkheden van reactie-geïnduceerde fasescheiding (RIPS) als een nieuwe route voor de productie van sub-μm TPVs. De mengbare systemen die werden bestudeerd waren voornamelijk gebaseerd op poly(ε-caprolacton) en poly(etheen) als thermoplastische fasen in combinatie met een laag-moleculaire rubber-precursor met epoxy of methacrylaat eindgroepen, welke alle commercieel beschikbaar zijn. Fasescheiding werd geïnduceerd door de verhoging van de

molecuulmassa tijdens het selectief polymeriseren en vernetten van de rubber-precursor, wat resulteerde in producten met een typische TPV morfologie en eigenschappen. Deze aanpak heeft een aantal duidelijke voordelen in vergelijking tot de traditionele dynamische vulkanisatie van niet-mengbare systemen. De belangrijkste voordelen zijn (*i*) de kleine rubberdeeltjes die verkregen worden (van 50 nm tot een aantal μm's) over (*ii*) een heel breed samenstellingsgebied (80-90 gewichtsprocent vernet rubber kon gedispergeerd worden in de thermoplastische matrix) en (*iii*) de veelzijdigheid van de methode. Dit laatste blijkt uit de verschillende vernettings-mechanismen die gebruikt kunnen worden (bijv. stap of keten-groei reacties), de variatie aan rubber-precursors die gekozen kunnen worden (volledig amorf of gedeeltelijk kristallijn, hoge/lage T_g en hoge/lage functionaliteit) en de verschillende thermoplast/rubber combinaties die gebruikt kunnen worden (bijv. hoog polaire of apolaire TPVs kunnen worden geproduceerd). Er werd aangetoond dat connectiviteit tussen de rubberdeeltjes (wat het gevolg is van de invloed van de start van het vormen van een macroscopisch netwerk van de rubber-precursor op het fasescheidingsproces onder statische vernettingscondities) een negatieve invloed heeft op de mechanische en reologische eigenschappen. Verder zorgen zijreacties tijdens het vernettingsproces (zoals enting en/of vernetting van de matrix) voor veranderingen in het kristallisatiegedrag van de matrix en de mechanische en reologische eigenschappen van de TPV. De sub-μm TPVs vertonen een interessante combinatie van hoge hardheid (Shore D gebied), goede elasticiteit (compressie set waarden variëren van 10 tot 40 %) en goede trekeigenschappen. Hoewel de smeltviscositeit van TPVs toeneemt met afnemende deeltjesgrootte zorgt de afwezigheid van co-continuïteit in de sub-μm TPVs bij hoge rubbergehalten voor smeltverwerkbare materialen met een viscositeit die vergelijkbaar is met de commercieel beschikbare TPVs gebaseerd op iPP en EPDM. De balans tussen de eigenschappen en de verwerkbaarheid kan verder geoptimaliseerd worden door het toevoegen van olie.

De mechanische eigenschappen en de smeltverwerkbaarheid van TPVs hangen sterk af van de grootte van de rubberdeeltjes en de connectiviteit tussen de rubberdeeltjes. De productie van sub-μm TPVs via RIPS maakt het mogelijk om de balans tussen de eigenschappen en de verwerkbaarheid te verschuiven naar een gebied dat niet haalbaar is met de op dit moment beschikbare supra-μm TPVs.

Dankwoord

Deze laatste pagina's wil ik gebruiken om iedereen die een bijdrage heeft geleverd aan dit proefschrift te bedanken. Allereerst wil ik prof. Piet Lemstra bedanken voor de mogelijkheid om dit project binnen de vakgroep SKT uit te voeren. Han Goossens wil ik bedanken voor zijn grote betrokkenheid bij dit project en de prettige samenwerking. De vrijheid die je me hebt gegeven om mijn onderzoek naar eigen inzicht te sturen werd zeer gewaardeerd. Ondanks deze vrijheid heb je er toch voor gezorgd dat het onderzoek goed verliep door op het juiste moment een nieuw idee aan te dragen of een kritische opmerking te plaatsen. Veel dank ben ik ook verschuldigd aan Martin van Duin, voor de nuttige discussies en kritische correcties. Je enthousiasme en je onuitputbare bron van ideeën heeft me enorm gemotiveerd. Ik vind het jammer dat ik een hoop van die ideeën uiteindelijk onaangeroerd heb moeten laten. Ook wil ik de overige leden van mijn promotiecommissie bedanken: prof. Gabriël Groeninckx, prof. Han Meijer, prof. Jacques Noordermeer and prof. Jean-Pierre Pascault, thank you for the discussions, the corrections of my thesis and the participation in my defense committee.

De begeleiding van vier studenten (Marloes Verbruggen, Rick Bercx, Bardo Bruijnaers en Tamara Vissers) tijdens mijn promotietijd was een erg waardevolle en leerzame ervaring. Marloes, je was de eerste afstudeerster die ik begeleidde en bent verantwoordelijk geweest voor het grootste deel van de resultaten in hoofdstuk 6. Ik heb onze samenwerking erg plezierig gevonden en was blij dat je direct na je afstuderen bij PTG aan de slag kon, zodat we elkaar nog regelmatig zagen en ik je af en toe lastig kon vallen met vragen over hoe je dat ene sample nou precies had gemaakt. Rick, jij besloot om je afstudeerproject van de Fontys bij ons in de groep uit te voeren. Jouw bijdrage is belangrijk geweest voor de ontwikkeling van de 'high-throughput experimentation' setup, wat een onderdeel werd van vervolgonderzoek binnen SKT. Je bleek al snel een slimme kerel die erg handig was op het lab, dus het verbaast me niet dat je direct na je afstuderen aan de verkorte opleiding op de TU/e bent begonnen. Bardo, ook jij kwam vanaf de Fontys voor een korte stage naar onze groep. Toen je begon leek je wat onzeker over je eigen kunnen, maar je hebt zeer goed werk afgeleverd wat uiteindelijk de basis is geworden van hoofdstuk 2. Tamara, jij hebt gewerkt aan een exploratief onderzoek aan de extrusie van multi-laags systemen, waarbij het uiteindelijke doel eigenlijk niet echt duidelijk was toen je begon. Je kreeg daardoor erg veel vrijheid, maar door je zelfstandigheid, je nauwkeurige manier van werken en je plezierige omgang met je collega's heb je het onderzoek succesvol afgesloten. Ik wens je heel veel plezier en succes met jouw promotieonderzoek binnen SKT.

De laatste regels van dit dankwoord wil ik gebruiken om mijn familie te bedanken. In het bijzonder mijn ouders: ik ben jullie enorm dankbaar voor de steun en de opvoeding die jullie me meegegeven hebben, zonder dat had ik dit alles nooit bereikt. Ook nog een extra bedankje voor Anouk voor de fantastische hulp bij het maken van de layout!

Chciałbym podziękować również mojej Kasiuni. Nasze spotkanie rozpoczęło się jak wyzwanie, które przekształciło się we wspólną przyszłość. Nie mówię tego wystarczająco często, ale jestem ogromnie dumny z tego, co udało nam się osiągnąć w ciągu tych lat. Dziękuje za Twoje wsparcie, zrozumienie i cierpliwość, także w chwilach ekscytacji lub uskarżania się na moje „cząsteczki kauczuku". Nie muszę Ci mówić jak wiele dla mnie znaczysz, przekonasz się 5 września!

Curriculum Vitae

The author of this thesis was born on March 25th 1980 in Breda, The Netherlands. After completing his secondary education (VWO) at 'Onze Lieve Vrouwe Lyceum' in Breda in 1998, he started his study Chemical Engineering and Chemistry at the Eindhoven University of Technology. In 2005 he obtained his Master's degree with prof.dr. P.J. Lemstra in the Polymer Technology group on the topic 'Thermoreversible cross-linking of maleic anhydride-grafted ethylene-propylene copolymers'. As part of his study, he performed a 4 months internship at GE Plastics in Bergen op Zoom and an additional 3 months in Cartagena, Spain.

In 2005 he started his PhD at the Eindhoven University of Technology in the Polymer Technology group with prof.dr. P.J. Lemstra under supervision of dr.ir. J.G.P. Goossens and dr.ir. M. van Duin, leading to the publication of this thesis. During his PhD study, he completed five modules of the course 'Registered Polymer Scientist' (RPK, 'Register Polymeerkundige') organized by the 'National Dutch Research School' (PTN, 'Polymeertechnologie Nederland'), which include Polymer Chemistry, Polymer Physics, Polymer Properties, Polymer Processing and Polymer Innovations.

List of publications

Publications from this thesis:

o R.M.A. l'Abee, J.G.P. Goossens, M. van Duin and A.B. Spoelstra, "Sub-micrometer thermoplastic vulcanizates obtained by reaction-induced phase separation of miscible mixtures of poly(ethylene) and alkyl methacrylates", *Eur. Polym. J.* **2009**, *45*, 503-514.

o R.M.A. l'Abee, J.G.P. Goossens and M. van Duin, "Thermoplastic vulcanizates by reaction-induced phase separation of a miscible poly(ε-caprolactone)/epoxy system", *Rubber Fibres Plastics* **2008**, *5*, 280-286.

o R.M.A. l'Abee, J.G.P. Goossens and M. van Duin, "Thermoplastische Vulkanisate durch reaktionsinduzierte Phasenentrennung eines mischbaren Poly(ε-Caprolacton)/Epoxid-systems", *GAK Gummi Fasern Kunstst.* **2008**, *61*, 298-305.

o R.M.A. l'Abee, J.G.P. Goossens and M. van Duin, "Thermoplastic vulcanizates obtained by reaction-induced phase separation: interplay between phase separation dynamics, final morphology and mechanical properties", *Polymer* **2008**, *49*, 2288-2297.

o R.M.A. l'Abee, J.G.P. Goossens and M. van Duin, "Thermoplastic vulcanizates by reaction-induced phase separation of a miscible poly(ε-caprolactone)/epoxy system", *Rubber Chem. Techn.* **2007**, *80*, 311-323.

Other publications:

o W. Li, R.M.A. l'Abee, J.G.P. Goossens, "The effect of silica nanoparticles on the phase behavior of polymer blends using a high-throughput experimentation approach", *Anal. Chim. Acta* **2009**, submitted.

o R.M.A. l'Abee, A.M.J.T. Vissers, J.G.P. Goossens, A.B. Spoelstra, M. van Duin, "Characterization of the morphology of co-extruder, thermoplastic/rubber multi-layer tapes", *Anal. Chim. Acta* **2009**, submitted.

o M.A.J. van der Mee, R.M.A. l'Abee, G. Portale, J.G.P. Goossens and M. van Duin, "Synthesis, structure and properties of ionic thermoplastic elastomers based on maleated ethylene/propylene copolymers", *Macromolecules* **2008**, *41*, 5493-5501.

o R.M.A. l'Abee, W. Li, J.G.P. Goossens and M. van Duin, "Application of FTIR microscopy in combinatorial experimentation on polymer blends", *Macromol. Symposia.* **2008**, *265*, 281-289.

o R.M.A. l'Abee, L.L.J.M Cornelissen, M.C. Diaz, D.A.J.M. Ligthart, M.J. de la Mar, S. Wijnans, B.G.G. Lohmeijer and U.S. Schubert, "High-throughput screening and combinatorial methods: The future for polymer research and academia?", *e-Polymers* **2003**, *T_001*, 1-30.